**TECHNISCHE
UNIVERSITÄT
DRESDEN**

# Strong-Field QED Processes in Short Laser Pulses

One- and Two-Photon Compton Scattering

Dissertation
zur Erlangung des akademischen Grades
Doctor rerum naturalium

vorgelegt von
## Daniel Seipt
geboren am 5. Oktober 1981 in Marienberg

Institut für Theoretische Physik
Fachrichtung Physik
Fakultät Mathematik und Naturwissenschaften
der Technischen Universität Dresden

Dresden 2012

*Für meine Eltern*

Eingereicht am 05.09.2012

1. Gutachter: Prof. Dr. B. Kämpfer
2. Gutachter: Prof. Dr. M. Marklund

Verteidigt am 20.12.2012

# Abstract

The purpose of this thesis is to advance the understanding of strong-field QED processes in short laser pulses. The processes of non-linear one-photon and two-photon Compton scattering are studied, that is the scattering of photons in the interaction of relativistic electrons with ultra-short high-intensity laser pulses. These investigations are done in view of the present and next generation of ultra-high intensity optical lasers which are supposed to achieve unprecedented intensities of the order of $10^{24}$ W/cm$^2$ and beyond, with pulse lengths in the order of some femtoseconds.

The ultra-high laser intensity requires a non-perturbative description of the interaction of charged particles with the laser field to allow for multi-photon interactions, which is beyond the usual perturbative expansion of QED organized in powers of the fine structure constant. This is achieved in strong-field QED by employing the Furry picture and non-perturbative solutions of the Dirac equation in the presence of a background laser field as initial and final state wave functions, as well as the laser dressed Dirac-Volkov propagator.

The primary objective is a realistic description of scattering processes with regard to the finite laser pulse duration beyond the common approximation of infinite plane waves, which is made necessary by the ultra-short pulse length of modern high-intensity lasers. Non-linear finite size effects are identified, which are a result of the interplay between the ultra-high intensity and the ultra-short pulse length. In particular, the frequency spectra and azimuthal photon emission spectra are studied emphasizing the differences between pulsed and infinite laser fields. The proper description of the finite temporal duration of the laser pulse leads to a regularization of unphysical infinities (due to the infinite plane-wave description) of the laser-dressed Dirac-Volkov propagator and in the second-order strong-field process of two-photon Compton scattering. An enhancement of the two-photon process is found in strong laser pulses as compared to the corresponding weak-field process in perturbative QED.

# Kurzdarstellung

Der Zweck der vorliegenden Arbeit ist es das Verständnis von Starkfeld-QED Prozessen in kurzen Laserpulsen zu erweitern. Dazu werden nichtlineare Einphotonen- und Zweiphotonen-Comptonstreuprozesse untersucht, das heißt die Streuung von Photonen bei der Wechselwirkung relativistischer Elektronen mit ultrakurzen intensiven Laserpulsen. Diese Untersuchungen sind notwendig im Hinblick auf die gegenwärtige und nächste Generation von optischen Hochintensitätslasern mit Pulslängen von einigen Femtosekunden, welche eine Feldintensität von $10^{24}$ W/cm$^2$ und höher anstreben.

Die ultrahohe Laserintensität erfordert eine nichtperturbative Beschreibung der Wechselwirkung geladener Teilchen mit dem Laserfeld um Mehrfachphotonenwechselwirkungen korrekt zu berücksichtigen. Diese Prozesse gehen über eine perturbativen Entwicklung nach Potenzen der Feinstrukturkonstanten hinaus. Solch eine Beschreibung wird durch den Übergang in das Furry-Bild erreicht, in dem nichtperturbative Lösungen der Dirac Gleichung in einem Hintergrundfeld als asymptotische Zustände, sowie der lasermodifizierte Dirac-Volkov-Propagator verwendet werden.

Das primäre Ziel ist eine realistische Beschreibung von Streuprozessen in Bezug auf die endliche zeitliche Pulsdauer im Gegensatz zur üblichen Näherung unendlich ausgedehnter ebener Wellen. Diese Beschreibung wird durch die ultrakurzen Pulslängen moderner Hochintensitätslaser notwendig. Nichtlineare Kurzpulseffekte, die sich aus einem Wechselspiel der ultrahohen Intensität und der ultrakurzen Pulsdauer ergeben, werden identifiziert. Insbesondere werden Frequenzspektren und azimuthale Photonemissionsspektren unterusct, wobei die Unterschiede zwischen gepulsten und unendlich ausgedehnten Laserfeldern hervorgehoben werden. Die exakte Beschreibung der endlichen Pulsdauer regularisiert unphysikalische Divergenzen des Dirac-Volkov-Propagators die durch unendlich ausgedehnte Laserfelder hervorgerufen werden. Dementsprechend werden auch die Divergenzen in den Spektren der Zweiphotonen Comptonstreuung regularisiert, der ein Prozess zweiter Ordnung ist. Es ergibt sich eine Verstärkung des Zweiphotonen Comptoneffekts in starken Laserpulsen im Vergleich mit dem entsprechenden Prozess in schwachen Feldern in perturbativer QED.

# Contents

# 1

# Introduction

T HE ELECTROMAGNETIC FORCE — besides the weak and strong nuclear interactions and gravity — is one of the four known fundamental forces of nature. While the nuclear forces are essential for a microscopic understanding of the properties of subatomic and subnuclear particles and their interactions, as well as the existence of stable nuclei or their radioactive decay, gravity is a dominant force on macroscopic scales. The electromagnetic force is responsible for many phenomena on both macroscopic and microscopic scales, including the electromotive force, chemical binding, different phases of matter, such as gases, liquids and solids, and the whole spectrum of electromagnetic radiation from long-wavelength radio waves to short-wavelength gamma rays, to name a few.[1]

The quantized theory of electromagnetic interactions, quantum electrodynamics (QED), is one of the pillars of the modern standard model of particle physics [Hal84, Pes95, Nak10]. Within the standard model, QED is found as the unbroken part of the spontaneously broken Glashow-Salam-Weinberg model of electro-weak interactions. QED is a precise theory with an incredible agreement between theory and experiment. For example, for the electromagnetic fine structure constant[2] $\alpha$ the experimental and theoretical values[3] are quoted as

$$\alpha_{\mathrm{exp}}^{-1} = 137.035\,999\,037(91)\,, \qquad\qquad [\mathrm{Bou11}]\,,$$
$$\alpha_{\mathrm{th}}^{-1} = 137.035\,999\,084(51)\,, \qquad\qquad [\mathrm{Han08}]\,.$$

These numbers show the excellent agreement of theory and experiment on the level of 10 significant digits (for this particular quantity). This is a great success of perturbative QED. Many experiments, in particular accelerator and spectroscopic experiments aim at pushing forward the frontiers in the perturbative high-precision and high-energy domain. However, in the presence of strong background fields, QED acquires novel non-perturbative features and one enters a completely new and interesting field of physics: strong-field or high-intensity QED. The strong-field regime of QED is a completely new area of physics with new phenomena

---

[1] The electromagnetic spectrum is often subdivided into radio waves (1 m ... 1 km wavelength), microwaves (1 mm ... 10 cm), infrared radiation (780 nm ... 1 mm), visible light (380 nm ... 780 nm), UV light (1 nm ... 380 nm), X-rays (10 pm ... 1 nm) and gamma rays ($< 1$ pm).

[2] Taken at zero momentum transfer $\alpha \equiv \alpha(Q^2 = 0)$.

[3] The theoretical determination of $\alpha$ is based on a four loop calculation of the anomalous magnetic moment $a_e$ of the electron [Kin06, Aoy07] and a comparison with experimental values $a_e^{\mathrm{th}}(\alpha) = a_e^{\mathrm{exp}}$. For the most precise experimental determination of $a_e$ see [Han08]. Thus, QED (plus weak and strong corrections) predicts a certain relation between the two dimensionless numbers $\alpha$ and $a_e$ which is confirmed experimentally.
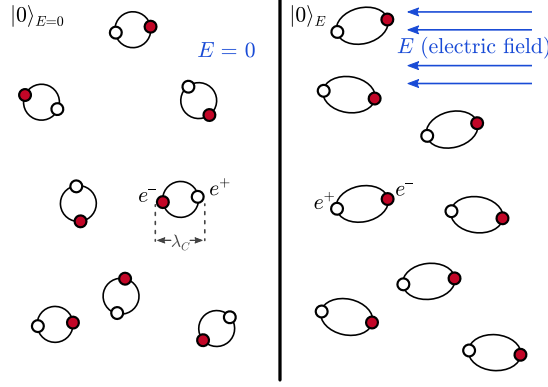
**Figure 1.1:** Visualization of the vacuum state without ($|0\rangle_{E=0}$, left) and with ($|0\rangle_E$, right) an external electric field. An applied electric field leads to an alignment of the virtual vacuum fluctuation dipoles.

to be tested, employing high-intensity lasers as versatile tools to achieve ultra-high field strengths in the laboratory [Mar09].

## Quantum Electrodynamics

QED as a renormalizable gauge theory is formulated in terms of charged fermionic matter fields $\Psi$ (electrons and positrons) with mass $m$, and a $U(1)$ gauge field $\mathcal{A}_\mu$ describing massless gauge bosons (photons). The Lagrangian density defining the theory on the classical level is

$$\mathcal{L} = \bar{\Psi}(i\slashed{D} - m)\Psi - \frac{1}{4}\mathcal{F}_{\mu\nu}\mathcal{F}^{\mu\nu}\,. \tag{1.1}$$

The coupling between fermions and photons is realized in a gauge invariant manner via the covariant derivative $\mathcal{D}_\mu = \partial_\mu + ie\mathcal{A}_\mu$, where $e$ denotes the conserved charge of the fermion fields. The antisymmetric electromagnetic field strength tensor $\mathcal{F}_{\mu\nu} = \frac{1}{ie}[\mathcal{D}_\mu, \mathcal{D}_\nu]$ is the commutator of the covariant derivatives. The classical theory is invariant under Lorentz transformations and local $U(1)$ gauge transformations. The quantization of the theory requires a gauge fixing, i.e. the selection of a representative from the gauge orbit. This can be achieved by adding a gauge fixing term $\frac{1}{2\xi_g}(\partial \cdot \mathcal{A})^2$ to the Lagrangian (1.1). By fixing the gauge one explicitly breaks the classical gauge symmetry in the quantum theory, which is, however, replaced by the Becchi-Rouet-Stora-Tyutin (BRST) symmetry [Pes95]. When considering processes in strong electromagnetic fields it is often useful to separate the electromagnetic field as $\mathcal{F} = \mathcal{F}^{\text{rad}} + F$ into a classical strong-field part $F$ and a radiating part $\mathcal{F}^{\text{rad}}$ which is quantized. Quantization of the theory leads to a definition of a vacuum state $|0\rangle_F$ as a state of minimum energy, which is free of real particles but contains virtual quantum fluctuations. These vacuum fluctuations are always present, also in the absence of an external field. They consist of virtual electron positron pairs forming virtual dipoles, which are oriented statistically, see Figure 1.1. In the presence of a background field, e.g. a static electric field $E$, these virtual dipoles are aligned in the direction of the field, leading to an anisotropy in the vacuum polarization (Figure 1.1, right). The typical spatial size of these vacuum fluctuations is given by the Compton wavelength[4] $\lambda_C = \frac{\hbar c}{mc^2} = 3.86 \times 10^{-13}$ m which is the inherent length scale of QED. Based on that, one defines a *critical* field strength

---

[4]Here, the quantities $\hbar$ and $c$ are written out explicitly. In general, the so-called natural units with $\hbar = c = 1$ are employed.
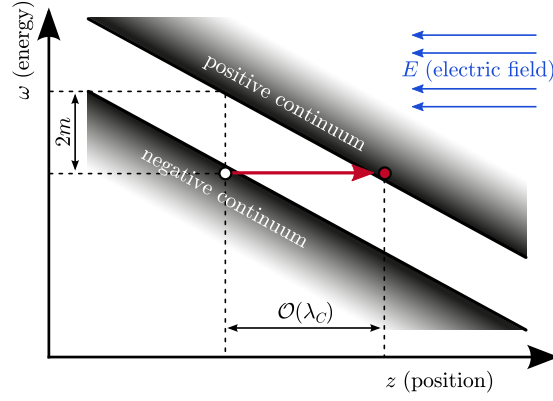
**Figure 1.2:** The pair production via the Schwinger mechanism in a strong electric field can be imagined as the tunnelling of an electron from the negative energy continuum to the positive continuum through the mass gap without energy. This is the separation of the virtual vacuum fluctuations over a distance larger than $\lambda_C$ to produce pairs of real fermions.

(Sauter-Schwinger field strength) as $E_s = m^2/e$ with the meaning that a particle under the influence of an electric field of strength $E_s$ acquires the energy $mc^2$ over a distance of its Compton wavelength. The electric field strength has a value of $E_s = 1.32 \times 10^{18}$ V/m or equivalently the magnetic field strength[5] is $B_s = 4.41 \times 10^9$ T. The field intensity associated to the critical field is $I_s = 2.32 \times 10^{29}$ W/cm$^2$. If the field strength reaches the order of $E_s$, the field is strong enough to separate the virtual charge fluctuations leading to the production of real particle-antiparticle pairs and an instability of the vacuum state which refers to the electric field and virtual pairs only [Sau31, Sch51]. In the intuitive hole picture this means that the positive and negative continua are deformed in such a way that particles from the negative continuum can tunnel through the mass gap to the positive continuum (see Figure 1.2).

The strength of an electromagnetic field can be characterized by the dimensionless scalar and pseudoscalar invariants

$$\mathcal{F} = \frac{e^2}{4m^4} F_{\mu\nu} F^{\mu\nu} \, , \qquad\qquad \mathcal{G} = \frac{e^2}{4m^4} F_{\mu\nu} {}^\star F^{\mu\nu} \, , \qquad\qquad (1.2)$$

with the field strength tensor $F_{\mu\nu}$ and its dual tensor ${}^\star F_{\mu\nu} = \frac{1}{2}\epsilon_{\mu\nu\alpha\beta}F^{\alpha\beta}$. Electromagnetic fields with $\mathcal{F}, \mathcal{G} \sim 1$ are called QED-strong fields; they are capable of producing pairs from the vacuum via the above mentioned Sauter-Schwinger mechanism. This pair production process is a non-perturbative effect and has features of a phase transition [Gre85]. The particle production probability is related to the imaginary part of the vacuum persistence amplitude $\langle 0_{\text{in}}|0_{\text{out}}\rangle$. The leading order result in a constant electric field for the production probability $p$ is [Hei36, Sch51]

$$p = \frac{\alpha^2 E^2}{\pi^2} \exp\left\{-\pi \frac{E_s}{E}\right\} \, . \qquad\qquad (1.3)$$

Pair production is an electric effect; pure magnetic fields can not produce pairs since the invariants obey the relations $\mathcal{F} < 0$ and $\mathcal{G} = 0$; for crossed fields $\mathcal{F} = \mathcal{G} = 0$.

---

[5]The critical magnetic field $B_s$ means that the Landau levels of electrons have an energy distance equal to their rest mass.

Today it is believed that Bohr's conjecture [Som78] — that the electric field with the field strength $E_s$ can never be produced — holds true since at much lower field strengths, corresponding to intensities of $10^{24} \dots 10^{25}$ W/cm$^2 \ll I_s$, a QED cascade will be triggered by a single seed particle consuming most of the energy of the electric field [Bel08, Fed10, Sok10, Elk11, Ner11].

## Sources of strong fields

Sources of strong electromagnetic fields are:

1. Pulsars, i.e. rotating neutron stars that periodically emit electromagnetic radiation, have surface magnetic fields of the order of $10^8$ T, which is almost on the order of the critical magnetic field $B_s$ [Hew70, Har91, Käm75, Her79].

2. Magnetars are special pulsars which are driven by magnetic energy; they have magnetic fields $100 \dots 1000$ times stronger than usual pulsars on the order of $10^{11}$ T, which is much larger than the critical field [Kou98, Mer08].

3. Heavy nuclei with large charge number $Z$ have ultra-strong Coulomb fields in their vicinity. For instance, the $1s$ state *dives* into the negative continuum for charge numbers $Z_c \approx 173$. Since not a single stable nucleus with such a high charge number is known, the critical charge number $Z_c$ was believed to be achievable in deep-inelastic heavy-ion collisions, where the electron dynamics is much faster than the collision dynamics of the nuclei allowing for the formation of quasi molecules with $Z > Z_c$ and possible pair production [Gre85].

4. Optical lasers can provide strong electromagnetic wave fields. The present world record is $I = 2 \times 10^{22}$ W/cm$^2$ [Yan08], which is, however, several orders of magnitude below the critical intensity $I_s$. Novel petawatt, multi-petawatt and even exawatt laser facilities which could reach even higher intensities, exceeding $10^{25}$ W/cm$^2$, are planned for commission in the foreseeable future. These ultra-high intensity laser system are seen today as the most promising tool for experimental studies of strong-field QED in the laboratory. Most of the present and future high-intensity lasers are short pulse lasers with pulse lengths of a few femtoseconds up to tens of femtoseconds.

5. X-ray free electron lasers (XFELs), i.e. coherent light sources with wavelengths in the X-ray regime, are another possibility to produce strong electromagnetic fields. Although the output power of free electron lasers does not exceed the GW level [Rin01] at the present day, and is, therefore, several orders of magnitude lower than for optical lasers, the short wavelength of the radiation allows for a much smaller diffraction limited focus and, therefore, the possibility for higher peak fields. The optimistic "goal" for the European XFEL was given as field strength of the order of $10^{17}$ V/m [Rin01].

## Lasers

Since the first successful demonstration of the laser (light amplification by stimulated emission or radiation) in 1960 [Mai60], exploiting the principle of stimulated emission of radiation first described by Einstein [Ein17], it was in particular the development of chirped pulse amplification (CPA) [Str85, Mou06] which allowed for a huge increase of the achievable laser power. Nowadays, one has achieved peak powers of a petawatt,[6] mostly by compressing

---

[6]The first petawatt laser was realized in 1999 at LLNL [Per99, Sau07].

moderate amounts of energy of a few Joule to ultra-short pulse lengths of a few femtoseconds: 1 PW ≡ 1 J/1 fs.

As state of the art, focused laser intensities as high as $2 \times 10^{22}$ W/cm$^2$ have been reported [Yan08] using the HERCULES laser; that experiment was also the first demonstration of a multi 100 TW laser operating at a high repetition rate of 0.1 Hz. Currently, various PW and multi PW laser systems are in the state of planning and building. To mention a few: The PFS project at the MPQ aims at building a PW laser with high repetition rate of 10 Hz by decreasing the pulse energy to 5 J in 5 fs pulses. Also other PW laser projects are designed for high repetition rates in the order $1 \ldots 10$ Hz such as PEnELOPE (30 J in 30 fs) at the HZDR. The ELI project is a planned high-intensity laser facility, where a multiple laser infrastructure is supposed to deliver the unprecedented peak power of 200 PW in pulses of 15 fs [Kor11]. This is the strong-field physics pillar of ELI, which will be complemented by three more laser facilities belonging to ELI with peak powers of 10 to 20 PW. The ILE APOLLON project, which is supposed to be the single-beamline prototype for ELI and other future high intensity laser facilities, has the objective of creating a laser with the peak power of 10 PW (150 J in 15 fs), which would allow to achieve a maximum intensity of $10^{24}$ W/cm$^2$ [Kor11]. Further envisaged laser projects are XCELS and IZEST, both attempting to break the exawatt ($10^{18}$ W) frontier.

Somewhat contrary to these short pulse high-intensity laser facilities are laser projects like NIF [NIF] and HiPER [HIP] envisaging to deliver a large amount of energy to a small spatial volume over "long" times of a few picoseconds, permitting a few shots per day only. In particular, NIF is designed for a total of 4 MJ energy in 192 beamlines with 20 kJ each over 3 ps. A review on petawatt lasers with a comprehensive list of laser systems with output power exceeding 100 TW can be found in the review [Kor11].

The driving force for the development of strong short pulse lasers are fascinating applications such as laser driven inertial fusion (HiPER, NIF) [Nak04, Atz09]; the acceleration of electrons [Fau04, Fau06, Puk03], protons or ions [Sch06c, Heg06] to relativistic energies (see also the review [Led10]); Thomson backscattering of optical laser light off relativistic electrons from either a linac, a synchrotron or even in an all optical set-up using laser accelerated electrons bunches to produce brilliant X-rays [Sch96, Sch06b, Har07]; other laser driven X-ray sources [Bra09] such as tabletop XFELs [Grü07]; nuclear physics [Led03]; laboratory astrophysics [Bul09]; strong-field QED studies [Mar06, DP12] and physics beyond the standard model [Gie09].[7]

### Dimensionless parameters of non-linearity for lasers

In many cases, in particular for electromagnetic field generated by lasers, both invariants $\mathcal{F}$ and $\mathcal{G}$ [cf. Eq. (1.2)] vanish (since they represent plane electromagnetic waves) or almost vanish (for focused laser beams [Hei11]). Field configurations for which both invariants vanish are called null-fields. Null-fields are not capable to produce pairs via the Schwinger mechanism; only in the presence of a thermal background pairs can be produced [Kin12].

For such fields one needs further physical quantities to form non-vanishing dimensionless invariants, such as the momenta of probe particles propagating in these field configurations. For a probe particle with momentum $p$ one defines the quantum non-linearity parameter [Rit85]

$$\chi = \frac{e}{m^3} \sqrt{(F_{\mu\nu} p^\nu)^2} \,, \tag{1.4}$$

---

[7]The topical complex of ultra-fast strong-field atomic and molecular physics including the phenomena of high harmonic generation, above threshold ionization etc. is not discussed in this thesis. The interested reader is referred to the reviews [Pop04, Mil06a, DP12, Koh12] for an overview on that topic.

describing the importance of non-linear quantum effects for the propagation of the probe particle in the field. For massive probe particles $p^2 = m^2 > 0$, the parameter $\chi$ is the value of the electric field experienced by the particle in its rest frame (rf), i.e. $\chi_p = E_{\text{rf}}/E_s$ in units of the Sauter-Schwinger field strength $E_s$; it represents the work done by the field over the Compton wavelength in the particle rest frame. This means that $\chi$ can be large for ultra-relativistic particles, although the electric field in the laboratory frame is much weaker than $E_s$ due to the Lorentz transformation of the transverse electric field $E_{\text{rf}} = e^\zeta E_{\text{lab}}$, where $\zeta$ is the rapidity of the probe particle. Probe photons with momentum $k$ do not possess a rest frame, due to $k^2 = 0$. One can consider a frame where the probe photon is counterpropagating the laser and the probe photon frequency $\omega'$ equals the laser frequency $\omega$; in that frame $\chi_k = 2\frac{\omega'}{m}\frac{E}{E_s}$. The relevance of the parameters $\chi_p$ and $\chi_k$ is that they measure the non-linear quantum effects for massive and massless probe particles, respectively. According to [Nar80] the expansion parameter of perturbation theory in strong-field quantum electrodynamics is $\alpha\chi^{2/3}$ for $\chi \gg 1$, not $\alpha$ itself. That means, for $\alpha\chi^{2/3} \sim 1$ radiative corrections are of the same magnitude as tree level results. Thus, the applicability of perturbation theory is restricted to parameters obeying $\alpha\chi^{2/3} \ll 1$. Fourth-order and second-order radiative corrections have comparable magnitude for $\alpha\chi^{1/3}\ln\chi \sim 1$, thus, second-order results are valid only for $\alpha\chi^{1/3}\ln\chi \ll 1$ [Rit72].

Another relevant quantity is the dimensionless amplitude of the laser vector potential

$$a_0 \equiv \frac{eA_0}{m} \tag{1.5}$$

with the electric field strength amplitude $E_0 = \omega A_0$, where $\omega$ is again the laser frequency. The definition of $a_0$ can be made explicitly Lorentz and gauge invariant [Hei09b]. The parameter $a_0$ represents the work done by the field in one wavelength $\lambda$ of the wave in units of the electron mass

$$a_0 = \frac{eE_0\lambda}{m} \, . \tag{1.6}$$

From a classical point of view, if $a_0 \sim 1$ or larger, a charged particle with mass $m$ and charge $e$ becomes relativistic within one cycle of the wave. This justifies the nomenclature of the regime $a_0 \sim 1$ as relativistic optics [Mou06]. This means that for such fields the $\boldsymbol{v} \times \boldsymbol{B}$ term in the Lorentz force equation $\boldsymbol{F} = e(\boldsymbol{E} + \boldsymbol{v} \times \boldsymbol{B})$ becomes relevant. A different interpretation of the quantity $a_0$ in the quantum picture is achieved by rewriting

$$a_0 = \frac{eE_0\lambda_C}{\omega} \, , \tag{1.7}$$

that is, $a_0$ describes the number of laser photons with energy $\omega$ absorbed in one Compton wavelength $\lambda_C$ of the electron [Mac11]. Therefore, the parameter $a_0$ also controls multi-photon effects in the quantum picture, and the regime $a_0 \sim 1$ is referred to as multi-photon regime. The parameter $a_0$ is related to the inverse Keldysh parameter known from atomic physics [Pop04]. One can relate $a_0$ to the laser intensity $I$ as

$$a_0^2 = 7.309 \times 10^{-19} I[\text{W/cm}^2]\lambda^2[\mu\text{m}] \, . \tag{1.8}$$

Thus, the experiment [Yan08] with $I = 2 \times 10^{22}$ W/cm$^2$ achieved a value of $a_0 = 100$. The limit $a_0 \to \infty$, refers to both the limit of infinite intensity at fixed frequency and the static limit $\omega \to 0$ ($\lambda \to \infty$) at fixed intensity. For $a_0 \gg 1$ the laser field can be approximated as a constant crossed field in many cases. The regime $a_0 \gg 1$ is referred to as "quasi-static" or "tunnelling" regime.

## Calculation methods

A variety of calculation techniques have been developed and applied to solve problems in strong-field QED. To name a few, there are the semi-classical operator technique [Baĭ68, Baĭ69], Schwinger's proper time method [Sch51, Dit00] and effective action approaches [Hei36, Bur07], world line Monte Carlo and instanton methods [Gie05, Dun06], relativistic quantum wavepacket dynamics [Moc09, SR00, Pea08, Ruf09], kinetic equations [Bla06, Bla09, Heb08, Sok10, Elk11], particle in cell (PIC) simulations for plasma problems [Daw83, Puk03, Fon09], and the semi-classical method of Reiss-Nikishov-Ritus, where exact solutions of the Dirac equation in a given classical background field potential in combination with the Furry picture are used. The latter method is comprehensively reviewed in [Rit85], where the focus is on infinite plane waves and constant crossed fields. This method was first described in [Sen52], but hardly recognized. It was later introduced by Reiss [Rei62] and Nikishov and Ritus [Nik64b] (see [Rei05] for a historical overview). It is applied throughout this thesis to processes in pulsed laser fields.

The results of the the Reiss-Nikishov-Ritus method are valid only for null-fields, where all field-invariants vanish, in particular $\mathcal{F} = \mathcal{G} = 0$, which are highly symmetric field configurations. In the general case, observables such as emission probabilities $W$ will depend on $a_0$, $\chi$ and further invariants $f_i$ (including $\mathcal{F}$ and $\mathcal{G}$), which can be constructed from the field strength tensor, its dual tensor and the momenta of participating particles $W = W(a_0, \chi, \{f_i\})$. Under the conditions $f_i \ll 1$ and $f_i \ll a_0^2, \chi^2$ one expects that up to the lowest order in terms of a series expansion [Rit85, Ber80, Her72]

$$W(a_0, \chi, \{f_i\}) = W(a_0, \chi, \{0\}) + \mathcal{O}(\{f_i\}). \tag{1.9}$$

## Scattering processes with probe particles

The use of probe particles allows to be sensitive to vacuum polarization and other strong-field effects far below the regime of QED-strong fields where the invariants $\mathcal{F}, \mathcal{G} \sim 1$. Furthermore, also in null-fields, where both field invariants vanish, $\mathcal{F} = \mathcal{G} = 0$, strong-field QED effects can be observed. For example, for low frequency probe photons with $\omega \ll m$, non-linear interactions among these degrees of freedom are mediated by anisotropies of the vacuum polarization tensor $\Pi_{\mu\nu}[A]$ [Bec75], which can be calculated using the famous effective Euler-Heisenberg Lagrangian [Hei36]

$$\mathcal{L}_{\text{EH}} = \frac{m^4}{360\pi^2}(4\mathcal{F}^2 + 7\mathcal{G}^2). \tag{1.10}$$

In the presence of a strong background field $A_\mu$, the vacuum acts as a polarized material medium on probe photons, which acquire a modified light-cone condition with two different indices of refraction $n_\pm$ for photon polarizations parallel and perpendicular to the background field. This can lead to birefringence and dichroism effects in suitable scattering geometries [Hei09b, Koc04], see Figure 1.3 (a). Small but measurable experimental signatures of these processes are expected for intensities of the order of $10^{22}$ W/cm$^2$ [Hei09b]. An experimental verification of this process, termed "vacuum birefringence", can be envisaged using a combination of a PW laser with the European XFEL X-ray beam. Besides the possibility to observe modifications of the polarization state of a probe photon, a more direct approach to observe the vacuum polarization based on a "matterless double slit" was proposed [Kin10b, Kin10a]. Since the probe photons couple to any charge fluctuations in the vacuum via the polarization tensor, this can be used as a probe for exotic particles [Kar12], such as axions, axion-like particles [Mai86] and minicharged particles [Gie09], as well as other theories beyond the standard model, such as non-commutativity of spacetime [Ild10, Lan97] and hidden gauge
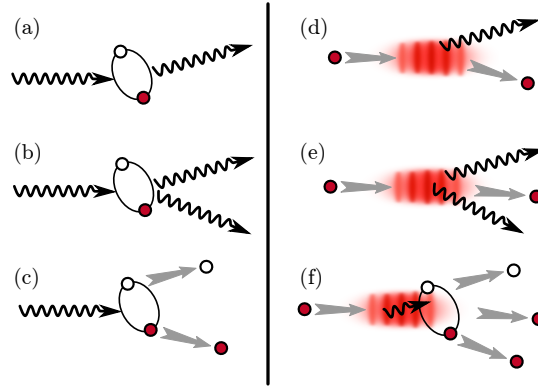
**Figure 1.3:** Visualization of several strong-field processes. Left: probing the vacuum
polarization via (a) vacuum birefringence, (b) photon splitting or (c) Breit-
Wheeler type pair production. Right: Interaction of relativistic electrons
with strong laser pulses resulting in one-photon Compton scattering (d), and
two-photon Compton scattering (e), or trident pair production (f). Photons
are depicted as wavy arrows. Red and white circles stand for electrons and
positrons, respectively, and the laser pulse is depicted as red shaded area.

sectors [Ahl08]. Furthermore, the polarization tensor induces non-linear interactions among
the probe photons leading to photon splitting ($\gamma \to \gamma\gamma$) and photon merging ($\gamma\gamma \to \gamma$)
processes [Adl71, Akh02, DP07], see Figure 1.3 (b).

Just as the propagation of photons is modified by the existence of the vacuum polarization
$\Pi_{\mu\nu}[A]$, also the propagation of electrons is modified by strong background fields via the
mass operator $\Sigma[A]$ [Sch51, Rit72, Rit85, Meu11]. The unitarity of quantum field theory
dictates that the imaginary parts of the photon polarization tensor $\Pi_{\mu\nu}$ and the electron
mass operator $\Sigma$ be related to particle production probabilities via the optical theorem, also
known as Cutkosky rules (see Figure 1.4). For instance the imaginary part of the photon
polarization tensor leads to an imaginary refractive index, which means absorption. A photon
which is *absorbed* in this way emerges as electron positron pair. The probe photon provides
enough energy to separate the virtual vacuum fluctuations [see Figure 1.3 (c)].

In ultra-strong laser fields, charged particles experience violent accelerations, which allows
to reach regimes where the radiation reaction force becomes relevant [DP09, Har11b]. In the
recent years great progress has been achieved in a theoretical understanding of the radiation
reaction force [Spo00], providing both exact analytic and numeric solutions [DP08, Har11a].
Radiation reaction is also seen to be important for ion acceleration schemes at laser intensities
exceeding $5 \times 10^{22}$ W/cm$^2$ [Zhi02, Tam11].

The pioneering studies of strong-field QED processes considered both strong-field pair
creation [Rei62] and the crossed process, electron photon scattering [Nik64b, Nik64a, Nik65,
Gol64, Nar65, Bro64, Kib65], also denoted as high-intensity Compton scattering, non-linear
Compton scattering or one-photon Compton scattering, which is related to the cut (one-loop)
mass operator (see Figure 1.4). Furthermore, the laser assisted pair creation process in
the field of a nucleus has been considered [Mit87, Mül03, Mil06b, Kuc07, Kam06]. Several
second-order processes which are related to two-loop self energies have been discussed,
including laser assisted Mott scattering [Szy97, Pan02a], laser assisted Møller scattering
[Ole67, Ros96, Pan04], laser assisted Compton scattering [Ole68, Bel77] and laser assisted
Bremsstrahlung [Löt07, Sch07] and two-photon Compton scattering [Mor75, Löt09b]. The
modification of weak interaction processes by strong laser fields has been considered, such
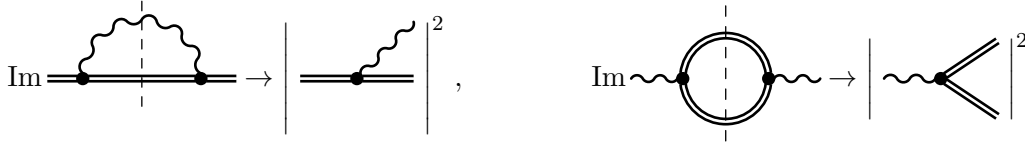
**Figure 1.4:** The imaginary part of the (one-loop) electron mass operator $\Sigma$ is related to the total probability of non-linear Compton scattering via the Cutkosky-rule/the optical theorem. Likewise, the imaginary part of the photon polarization operator $\Pi_{\mu\nu}$ is related to the electron-positron pair production [Hei09a].

as muon decay in a laser field [Dic09] and neutrino production [Tit11]. For a further overview of the literature on strong-field processes, the reader is referred to the reviews [Rit85, McD86, Fer89, Lau03, Sal06, Mar06, Ehl09, DP12].

Of particular interest in this thesis are the photon emission processes when colliding an ultrarelativistic electron — either from a synchrotron, a linac or from a laser acceleration set-up — with a high-intensity short laser pulse, one-photon and two-photon Compton scattering, where one or two photons are emitted in the interaction [see Figure 1.3 (d) and (e)]. The focus will be on a realistic description of the finite temporal extent of the laser pulse and on signatures thereof in the emission spectra.

A description of these processes in strong laser fields requires a non-perturbative treatment of the latter, which is based on the Furry picture [Fur51] and one utilizes laser dressed Volkov states [Vol35] as basis for the perturbative expansion of the $S$ matrix. It turns out that the parameter $a_0$ is the effective coupling strength between the strong laser pulse and the charged particles. In this picture, for instance the one-photon (two-photon) Compton scattering process appears as the one-photon (two-photon) *decay* of these quasi-particle Volkov states.

### One-photon Compton scattering

In view of the present and upcoming generation of high-intensity lasers, which are essentially short pulse lasers, the finite temporal envelope will have to be considered in the theoretical description of strong-field QED processes. The seminal works on non-linear one-photon Compton scattering [Nik64b, Nik64a, Nik65, Nar65, Gol64] did not consider the case of finite laser pulses; they considered either infinite plane waves or constant crossed fields which allow for easier analytic results. Newer studies on intensity effects in infinite plane waves have appeared, e.g. in [Kry94, Har09, Hei10b]. A complete description of non-linear Compton scattering in infinite plane waves has been given with respect to the electron spin and photon polarization properties in [Iva04]. (The same has also been achieved for the cross channel process of pair production [Iva05].)

It is known that non-linear Compton scattering has as a classical limit the non-linear Thomson scattering, which is attained in the limit $\varrho \ll 1$, where

$$\varrho = \frac{k \cdot p}{m^2} \tag{1.11}$$

with the electron momentum $p$ and the laser four-vector $k$. The parameter $\varrho$ is a measure for the electron recoil due to the momentum transfer in the photon emission process. The classical limit of Thomson scattering corresponds to the recoil-free low energy limit of the quantum description. The classical Thomson scattering as the one-photon emission in strong-laser

fields has been described in infinite plane wave fields [Sar70], as well as in box-shaped pulses [Esa93, Rid95] and in smooth laser pulses [Har96b, Gao04, Kra04, Kra05, Hei10b, Boc11c]. In particular for smooth laser pulses, serious modifications of the differential photon emission spectra have been obtained in comparison with the case of infinite plane waves.

The first studies of finite pulse effects in the quantum theory of non-linear Compton scattering and the cross channel process of pair production can be found in [Nar96b, Nar96a], where the analysis was restricted to long laser pulses with $\Delta\phi \gg 1$. In view of the new experimental possibilities with the new generation of short-pulse high-intensity lasers, the discussion of non-linear Compton scattering in pulsed strong fields was quite active in the last few years. Starting with [Boc09], several papers on that topic have appeared [Mac10, Sei11b, Mac11, Sei11a, Boc11b, Kra12, Din12], focusing on different aspects of the photon emission spectra, and also on the electron distributions [Boc12] after the electron-laser interaction. Also the scattering of a high-intensity laser pulse off electron wavepackets was discussed [Cor11b, Cor11a]. Furthermore, the cross channels of Compton scattering, which are non-linear Breit-Wheeler pair production [Hei10a, Nou11, Tit12, Nou12], and one-photon annihilation of a electron-positron-pair [Joh11, Ild11b] have been discussed in pulsed laser fields. A discussion of strong-field effects in short laser pulses using the Wigner formalism can be found in [Heb11b, Heb11a].

The spectrum of non-linear Compton scattering has been observed in several experiments colliding laser and electron beams, such as low-intensity laser photons ($a_0 = 0.01$) with low-energy ($\sim 1$ keV) electrons from an electron gun [Eng83], $a_0 = 2$ photons with plasma electrons from a gas jet [Che98] and, more recently, sub-terawatt photons ($a_0 = 0.35$) from a $CO_2$ laser with 60 MeV electrons from a linac at the BNL-ATF [Bab06]. Using linearly polarized photons the latter two experiments [Che98, Bab06] have analysed the characteristic azimuthal intensity distributions confirming quadrupole and sextupole patterns for the second and third harmonics, respectively. Recently, the energy spectrum of the scattered radiation has been measured in an all-optical set-up using laser accelerated electrons [Sch06b]. While this "all-optical table-top" set-up is certainly attractive as it does not require a linac or a synchrotron, the electron beam has a rather broad and random energy distribution which in turn is inherited by the scattered photons. As a result, the $\gamma$ spectrum recorded in [Sch06b] is rather difficult to analyse theoretically.

Probably the best known experiment is SLAC E-144 probing strong-field QED using a (by now moderately) intense laser beam in conjunction with high-energy electrons [Bam99]. Colliding a laser of intensity $10^{18}$ W/cm$^2$ with the 46.6 GeV electron beam of the SLAC the observation of the non-linear Compton scattering process has been reported in [Bul96], see Figure 1.3 (d). Here, the absorption of several laser photons induces the production of a high-energy (30 GeV) $\gamma$ quantum which thus takes away a large fraction of the incoming electron energy. This high-energy photon has then been used to produce electron-positron pairs [Bur97] via collision with the laser, employing the multi-photon Breit-Wheeler reaction [Bre34], see Figure 1.3 (c). Hence, using a high-energy setting with a large linac, SLAC E-144 has produced "matter from light" for the first time [Bur97]. While the SLAC data can be well described within this two-step model of pair creation [Bur97, Hu10], there is also the possibility for a direct one-step process, which is termed trident-process [see Figure 1.3 (f)]. In this one-step process, which is a second-order strong-field process, the photon that triggers the production of the pair is a virtual intermediate particle. In contrast to the case of first-order strong-field processes discussed above, the literature on second-order processes in pulsed laser fields is yet quite scarce.
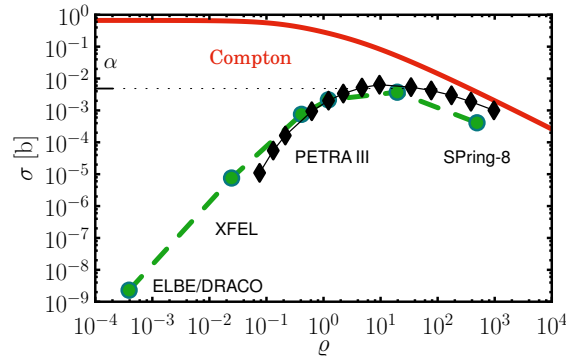
## Two-photon Compton scattering

In the two-photon Compton process, an electron emits two-photons coherently. In the low energy limit of the weak field process, the two photons share the energy of the incoming photon $\omega = \omega_1 + \omega_2$. In this sense, the process can be considered as the splitting of a photon. The theoretical description of the two-photon Compton process (also termed double Compton scattering) in the perturbative (weak-field) regime had been accomplished first in [Hei34, Man52] and was verified experimentally soon afterwards [Bra56] and more recently in [Sek88, San00] using 662 keV $\gamma$ rays from a $^{137}$Cs radioactive source incident on an aluminium foil scatterer. The double Compton effect was observed via coincidence measurements in two detectors. The perturbative double Compton effect is expected to become the main source of soft photons in astrophysical plasmas at low baryon density and can be seen as a dominant mechanism for the thermalization of perturbations of the cosmic microwave background [Lig81, Chl06]. While the one-photon Compton process has a classical analogue in the limit $\varrho \to 0$, this is not true for two-photon Compton scattering, which is a pure quantum process. For low energy, $\varrho \ll 1$, the cross section $\sigma_2$ for two-photon Compton scattering scales as $\sigma_2 \sim \alpha \varrho^2 \sigma_1$, where $\sigma_1$ is the one-photon cross section (see Figure 1.5).

The strong-field two-photon Compton process has been analysed in a constant crossed field [Mor75] and in an infinite plane wave [Löt09b, Löt09a]. The related process of two-photon synchrotron radiation in a strong magnetic field was also considered [Sok76]. It was found that the two photons which are emitted in the two-photon Compton scattering process have a certain degree of entanglement, such that this process could be used as a source for high-energy entangled photons in the keV or MeV regime [Sch08, Löt09b].

Recently, experiments on two-photon emission by electrons in an intense laser field have been proposed [Che99, Thi09]. The motivation of such experiments is seen in [Sch06a, Sch08] in an attempt to verify the Unruh radiation [Unr84] which is related to the physical vacuum experienced by accelerated observers in a flat space-time and manifests as the emission of entangled photon pairs off accelerated charges. The Unruh radiation in turn is related to Hawking radiation off a horizon in curved space-time [Unr76]. These issues concern the concepts of quantum field theory, of vacua and of particles in non-inertial frames [Cri08]. The relation between the two-photon Compton process and Unruh radiation has been analysed further in [Sch09].

In second-order strong-field processes (e.g. [Löt09b, Löt07, Kra10, Hu10]), intermediate particles can become real (i.e. go on their mass shell) due to the presence of the background field. In infinite plane wave fields, the on-shell contributions diverge as Oleinik resonance singularities [Ole67, Ole68, Ros96]. A regularization procedure is necessary in this case. One possibility, which is used in several papers on second-order strong-field QED processes is the inclusion of an imaginary mass contribution to propagator pole in order to screen the Oleinik resonances [Ole67, Ole68]. This imaginary mass contribution is related to the imaginary part of the electron self-energy $\Sigma[A]$ in the case of two-photon Compton scattering, and via the correspondence discussed in Figure 1.4 also to the total probability of one-photon Compton scattering. The relation of the on- and off-shell processes, i.e. the relative importance of the one-step and two-step processes, in the case of a photon propagator has been analysed recently in [Hu10, Ild11a] for finite laser pulses. The two-photon emission probability is infrared divergent if one of the two emitted photons is soft, $\omega_{1,2} \to 0$. The cancellation of such divergences is ensured by the Bloch-Nordsieck theorem [Blo37]. An explicit calculation, where the cancellation between the infrared divergence of double Compton scattering and radiative corrections to one-photon Compton scattering is shown for the weak-field process can be found in [Bro52]. Similar cancellations occur in the strong field process. Parts of the electron mass operator $\Sigma[A]$ are required for the cancellation of the infrared divergent

**Figure 1.5:** The cross section of perturbative double Compton scattering (green dashed
curve and circles) in comparison with single-photon Compton scattering (red
solid curve) as a function of $\varrho = k \cdot p / m^2$, which is a measure for the centre-of-
mass energy. The green circles and dashed curve correspond to a calculation
employing the formula for the perturbative double Compton cross section
from [Jau76]. The black diamonds and black solid curve correspond to data
taken from [Ram71]. The employed parameters include possible experimental
set-ups at ELBE/DRACO [Deb09], XFEL [XFE], PETRA III [PET] and
SPring-8 [SPR].

parts of the two-photon Compton emission probability (see Chapter 4 and, in particular,
Appendix E for some details on that topic).

## Outline of the thesis

The structure of this thesis is as follows: In Chapter 2, the theory of strong field QED is
presented, starting with a discussion of the classical dynamics of charged particles in strong
electromagnetic fields. The relation of coherent photon states and classical background fields
is discussed and the transition to the Furry picture, where Volkov states, i.e. solutions of the
Dirac equation in the presence of a plane wave background field, are employed. The properties
of the Volkov wave functions, as well as of the laser dressed Dirac-Volkov propagator, in
pulsed plane wave laser fields are studied. A close relation between the classical trajectory
solutions and the Volkov wave functions is found.

Chapter 3 contains the discussion of one-photon Compton scattering in high-intensity
short laser pulses. After the calculation of a general expression for the $S$ matrix and the
emission probability, using the methods provided in Chapter 2, the weak-field limit is concisely
discussed. (A detailed discussion of the weak-field limit and the limit of infinite plane waves
for one-photon Compton scattering is presented in Appendix C.) In a numerical study of the
emission probability the frequency spectra are exhibited. Different regimes for ultra-short
pulses and for longer pulses are identified, a bandwidth dominated regime and a ponderomotive
regime, respectively. In the ponderomotive regime, the emergence of sub-peaks is discussed,
as well as the transition between these two regimes. Azimuthal distributions are considered
for the case of single-cycle laser pules, where the polarization and carrier envelope phase
effects are studied.

The relation of non-linear Compton scattering to the classical limit of non-linear Thomson
scattering is emphasized. A scaling relation between the classical and quantum emission
probability are found, which is based on the longitudinal light-front kinematics and the
different phase spaces in the classical and quantum theory. Analytic approximations are

presented employing a slowly varying envelope approximation and an expansion of the one-photon Compton amplitude into a series of partial amplitudes which can be related to the harmonics in infinite plane waves. Using a stationary phase analysis the emergence of sub-peaks is set into relation with the accumulated phase shift of the Volkov wave functions during the interaction with the laser. For a special pulse envelope, a completely analytic result for the emission spectra is presented. In the case of ultra-high intensity $a_0 \gg 1$, an averaging method based on the stationary phase approximation is presented to calculate the total emission probability in pulsed laser fields in comparison to results in constant crossed fields.

In Chapter 4, the second-order QED process of two-photon Compton scattering is presented. The $S$ matrix for the process end the emission probability are calculated in the strong-field regime. The weak-field limit of the $S$ matrix is obtained and it is shown that it coincides with the previous result from perturbative QED. A detailed discussion of the on- and off-shell contributions to the emission probability is given with a factorization of the on-shell part into two successive one-photon Compton $S$ matrix elements. It is shown by an explicit calculation that in the the on-shell contributions, which are finite in a pulsed laser field, develop Oleinik resonance singularities in the limit of an infinite plane wave. Numerical results for differential spectra are presented, the inclusive two-photon spectrum calculated and compared to the emission probability of one-photon Compton scattering. For a box-shaped pulse, an analytic expression for the pulse-length dependence of the on-shell and off-shell parts of the emission probability is given.

A summary of the main results and an outlook is given in Chapter 5.

In Appendix A, general relations are collected concerning the conversion of units, conventions for the Minkowski metric, light-front coordinates, Dirac matrices, collections of important integrals and details of the description of the vector potential that describes the laser pulse. The basic field theoretic relations in the Furry picture are presented in Appendix A including the commutation relations of particle creation and annihilation operators, the eigenmode decomposition of the field operators and the calculation of $S$ matrix elements from the general perturbative expansion of the scattering operator $\hat{S}[A]$ in the Furry picture. In Appendix B, the Furry picture in the path integral approach is discussed. A derivation of the Volkov matrix functions is presented together with a new and easy proof of their orthogonality and completeness relations. As stated above, in Appendix C the weak-field and monochromatic limit of the one-photon Compton scattering are discussed. Additionally, some remarks on the relation between long laser pulses and infinite plane waves can be found there. The gauge invariance of the one-photon and two-photon matrix elements is proven in Appendix D, which serves as a definition for numerically divergent parts of the corresponding matrix elements. Appendix E is devoted to the discussion of the infrared divergence of the two-photon matrix element, where the cancellation of the infrared divergent parts with radiative corrections of one-photon Compton scattering is shown explicitly. In the final Appendix F, the issues of realistic conditions, such as spatial focusing of the laser and finite electron distributions are considered for one-photon Compton scattering. The robustness of the sub-peaks in the frequency spectra is tested.

Parts of the work presented in this thesis have been published in [Hei10b, Sei11b, Sei11c, Sei11a, Sei12, Nou12], see also the listing on page I at the end of this thesis.

# 2

# The theory of strong-field QED

I N this chapter, the theory of quantum electrodynamics (QED) in strong external fields is presented. Before discussing the quantized theory, it is instructive to inspect the classical theory first. Therefore, the classical dynamics of charged particles in strong background fields is briefly reviewed. Many concepts, such as the quasi-momentum, can be introduced much clearer in the realm of classical electrodynamics. Thereafter, the relation between classical background fields and coherent quantum states for laser pulses of arbitrary spectral content is established. Strong-field QED is formulated in the Furry picture, where the interaction of electrons and positrons with the background wave field is taken into account exactly and non-perturbatively. Volkov wave functions are utilized as one-particle basis for the mode expansion of the electron field operators. The properties of these wave functions and the corresponding Green's function are discussed in the last part of this chapter, emphasizing the differences between pulsed plane wave (PPW) and infinite plane wave (IPW) laser fields. A close connection between the momentum space properties of Volkov states in PPW and the classical trajectory solutions is found.

## 2.1 The classical theory

In the classical theory of electrodynamics, without the radiation reaction force[1], the dynamics of point-like charged particles in a given external field configuration, described by the field strength tensor $F_{\mu\nu} = \partial_\mu A_\nu - \partial_\nu A_\mu$, is governed by the Lorentz force equation [Jac83]

$$\frac{du^\mu}{d\tau} = \frac{e}{m} F^{\mu\nu} u_\nu \,, \tag{2.1}$$

where $e$ ($m$) is the charge (mass) of the particle and $u^\mu = dx^\mu/d\tau$ denotes the four-velocity of the particle, where $\tau$ is the proper time. In general this is a non-linear differential equation as the field strength has to be taken along the trajectory to be solved for $F^{\mu\nu} = F^{\mu\nu}(x(\tau))$. The equations of motion (2.1) follow from the relativistic Lagrangian [Sch68]

$$L = m u^\mu u_\mu + e A^\mu u_\mu \tag{2.2}$$

---

[1] Radiation reaction is not discussed in this thesis. The interested reader is referred to the recent papers [Spo00, DP08, Har11a] and the review [DP12] for a survey on the topic.

by means of the variational principle with Euler-Lagrange equations

$$\frac{\partial L}{\partial x^\mu} - \frac{d}{d\tau}\left\{\frac{\partial L}{\partial u^\mu} - \left(\frac{\partial L}{\partial u^\nu}u^\nu - L\right)u_\mu\right\} = 0\,. \tag{2.3}$$

This form of the Euler-Lagrange equations implements already the normalization of the four-velocity, $u_\mu u^\mu = 1$. Equation (2.3) can be derived by adding the constraint to (2.2) via a Lagrangian multiplier $\lambda$, $L \to L + \lambda(\tau)(u_\mu u^\mu - 1)$ and solving for $\lambda$. If the external field $F_{\mu\nu}$ or the potential $A_\mu$ depends only on one Lorentz-invariant phase $\phi = k \cdot x$, as for a transverse plane wave field, the equation of motion (2.1) possesses an analytic solution [Har02, Mey71] due to the existence of an additional constant of motion $\kappa = d\phi/d\tau$. The quantity $\kappa$, which is referred to as light-cone variable in [Har02], is the longitudinal velocity, i.e. the projection of $u^\mu$ onto the laser four-momentum, $\kappa = k^\mu u_\mu = k \cdot u = const$. The time evolution of the light-cone variable

$$\frac{d\kappa}{d\tau} = \frac{e}{m}\left[(k \cdot k)(u \cdot A') - (\partial \cdot A)(k \cdot u)\right] = 0 \tag{2.4}$$

proves that it is a constant of motion, indeed. The first term vanishes because $k \cdot k = 0$, and the second term is zero due to the Lorenz gauge $\partial \cdot A = k \cdot A' = 0$; the prime denotes the derivative with respect to the laser phase $\phi$. Throughout this thesis, the real transverse plane wave field

$$A^\mu(\phi) = A_0\, g(\phi)\, \mathrm{Re}\left[\epsilon_+^\mu \exp\left\{-i(\phi + \hat\phi)\right\}\right] \tag{2.5}$$

will be utilized, where $g(\phi)$ describes the pulse envelope, $\epsilon_+^\mu$ is a complex transverse polarization vector and $\hat\phi$ denotes the carrier envelope phase. A detailed description of the laser vector potential is provided in Appendix A.3. As a consequence of the constancy of the light-cone variable $\kappa$ the proper time $\tau$ can be replaced by the laser phase $\phi = \kappa\tau = k \cdot u_0\tau$ in the equations of motion, where $u_0^\mu = u^\mu(\tau_0)$ denotes the initial value of the velocity at the initial proper time $\tau_0$. Thus, Eq. (2.1) becomes fully integrable,

$$\frac{du^\mu}{d\phi} = \frac{e}{m\kappa}F^{\mu\nu}(\phi)u_\nu(\phi)\,. \tag{2.6}$$

The solution for the particle velocity reads

$$u^\mu(\tau) = u_0^\mu - a^\mu + \frac{a \cdot u_0}{\kappa}k^\mu - \frac{a \cdot a}{2\kappa}k^\mu\,, \tag{2.7}$$

where a dimensionless vector potential $a_\mu = eA_\mu/m$ was defined. Another integration over proper time yields the particle's orbit

$$x^\mu(\tau) = x^\mu(\tau_0) + u_0^\mu(\tau - \tau_0) - \int_{\tau_0}^{\tau} d\tau' a^\mu + \frac{k^\mu}{2\kappa}\int_{\tau_0}^{\tau} d\tau'(2a \cdot u_0 - a \cdot a)\,. \tag{2.8}$$

These are the exact solutions for particle orbits in a plane wave field with arbitrary spectral composition, as the one defined in Eq. (A.24). The fields are such that there is no net acceleration, i.e. $u^\mu(\tau \to \infty) = u^\mu(\tau \to -\infty)$.

Alternatively, one could solve the relativistic Hamilton-Jacobi equation, which is a nonlinear differential equation [Ebe69, Bag90, Löt08]

$$(\partial_\mu S + eA_\mu)(\partial^\mu S + eA^\mu) = m^2\,, \tag{2.9}$$

for the Hamilton-Jacobi action

$$S_p(x) = -p_0 \cdot x - \frac{1}{2p_0 \cdot k} \int^\phi d\phi' [2ep_0 \cdot A - e^2 A \cdot A] , \tag{2.10}$$

with initial momentum $p_0 = mu_0$. The particle's canonical momentum $P^\mu = mu^\mu + eA^\mu$ is the negative gradient of the Hamilton-Jacobi action $P_\mu = -\partial_\mu S$ [Bag90]. Evaluating the kinetic momentum $p^\mu = mu^\mu = -\partial^\mu S - eA^\mu$ with (2.10) gives the same result as (2.7). The physical significance of the Hamilton-Jacobi action is the fact that it also appears below as the phase of the quantum states.

Having found the particle orbits in a plane wave field, a concise discussion of this solution is necessary. Of particular interest is the average motion of the charged particle, by averaging the velocity $u$ over the laser phase

$$\langle u^\mu \rangle = u_0^\mu - \langle a^\mu \rangle + \frac{\langle a \rangle \cdot u_0}{\kappa} k^\mu - \frac{\langle a \cdot a \rangle}{2\kappa} k^\mu . \tag{2.11}$$

For periodic fields $A_\mu$, in particular in the limit of infinite monochromatic plane waves, one would average over one period of the phase with $\langle a^\mu \rangle = 0$ and $\langle u^\mu \rangle = u_0^\mu - \frac{\langle a \cdot a \rangle}{2\kappa} k^\mu$, which defines the average longitudinal momentum $q^\mu = m\langle u^\mu \rangle$ named quasi-momentum. The square of this quasi-momentum gives rise to an effective, intensity dependent mass[2]

$$m_\star^2 = q \cdot q = m^2 \langle u \rangle \cdot \langle u \rangle = m^2 (1 - \langle a \cdot a \rangle) . \tag{2.12}$$

For the special choice of the vector potential (2.5) which is used throughout this thesis, for $g \to 1$ the average of $a \cdot a$ is independent of the polarization state of the background field and one has the unique effective mass $m_\star^2 = m^2(1 + a_0^2/2)$. This effective mass can be attributed to the relativistic mass increase due to the transverse quiver-motion [McD86]. In pulsed laser fields, there are two time scales where one is given by the carrier frequency $\omega$ and the other one is related to the length $\Delta\phi$ of the pulse envelope $g$. A particular possibility for the definition of the averaging procedure for long pulses $\Delta\phi \gg 1$ would include a separation of fast (carrier wave) and slow (envelope) time scales, averaging over the fast time scales only [Nar96b]. Then, the quasi-momentum and effective mass depend on the phase via the square of the envelope function

$$q^\mu(\phi) = p^\mu + k^\mu \frac{ma_0^2}{2\kappa} g^2(\phi) , \qquad\qquad m_\star^2(\phi) = m^2 \left( 1 + \frac{a_0^2}{2} g^2(\phi) \right) . \tag{2.13}$$

This separation of scales is inadequate for single cycle laser pulses where the pulse length is $\Delta\phi = \mathcal{O}(1)$. For generally pulsed, non-periodic fields, where $\langle a^\mu \rangle \neq 0$, one can define

$$\mathfrak{M}^2 = m^2(1 + \langle a \rangle \cdot \langle a \rangle - \langle a \cdot a \rangle) = m^2(1 - \Delta a^2) , \tag{2.14}$$

with the variance of the laser field $\Delta a^2$. However, the definition of the average is not unique. A certain possibility is to use floating averages [Bro64, Kib75, Har12]

$$\langle a \rangle (\phi, \phi') \equiv \frac{1}{\phi' - \phi} \int_\phi^{\phi'} d\phi'' a(\phi'') , \tag{2.15}$$

---

[2]Note that $u \cdot u = 1$, as is required by the normalization of the relativistic velocity. Thus, averaging $\langle u \cdot u \rangle = 1$ would not give rise to an effective mass.
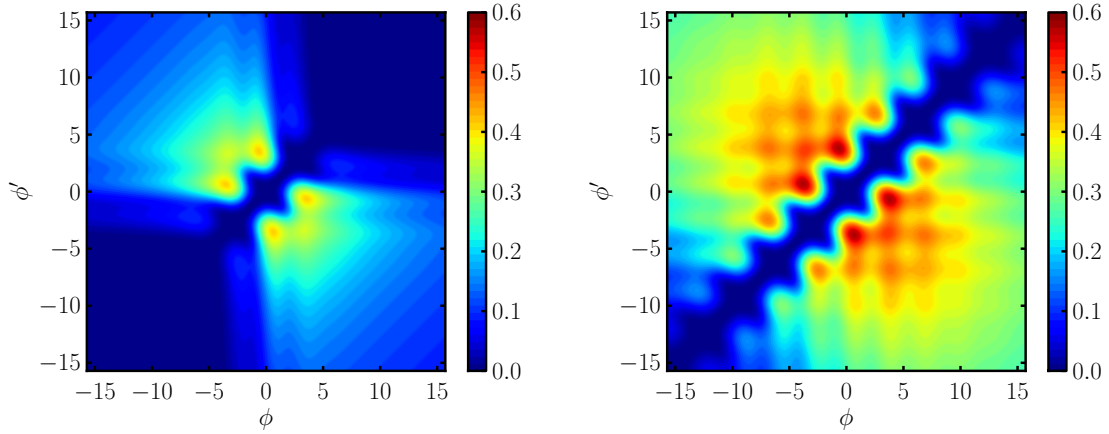
**Figure 2.1:** The effective mass $\mathfrak{M}^2(\phi, \phi')$ as a function of $\phi$ and $\phi'$. The normalized value $(\mathfrak{M}^2 - m^2)/a_0^2$ is plotted for the pulse length $\Delta\phi = \pi$ ($\Delta\phi = 3\pi$) in the left (right) panel for a Gaussian shape function $g(\phi) = \exp{-\{\frac{\phi^2}{2\Delta\phi^2}\}}$ (see also Appendix A.3).

which does not allow for such a simple interpretation of $\mathfrak{M}(\phi, \phi')$ as an effective mass since it depends on two phase variables. The quantity $\mathfrak{M}$ was used in [Bro64, Kib75] in the discussion of the electron Green's function in a strong laser field (cf. Section 2.9). In Figure 2.1, contour plots of the normalized effective mass $(\mathfrak{M}^2 - m^2)/a_0^2$ are shown as a function of the two phase variables $\phi$ and $\phi'$, evidencing the strong dependence of the effective mass $\mathfrak{M}^2(\phi, \phi')$ on the averaging interval. For an infinite interval $|\phi' - \phi| \to \infty$ the effective mass approaches the free mass $\mathfrak{M}^2 \to m^2$. The appearance of the variance $\Delta a^2$ instead of $\langle a^2 \rangle$ in the definition of $\mathfrak{M}^2$ ensures that $\mathfrak{M}^2 \to m^2$ for the interval length $|\phi' - \phi| \to 0$. Thus, for ultra-short pulses the effective mass is expected to play no role. The usual definition of the average in periodic fields is reobtained from the expression (2.15) by specifying the averaging interval as $|\phi' - \phi| = 2\pi$. The existence and experimental detection of the mass shift is still a debated subject. For a recent discussion in the literature see [Har12].

When considering a monochromatic plane-wave field (i.e. $g = 1$) which is periodic in $\phi$, the solutions for the particle orbits can be specified further on. Going to the co-moving inertial frame where $\langle u^\mu \rangle = 0$, the spatial components of the quasi-momentum vanish, $q^\mu = (m_\star, 0, 0, 0)$. In that frame the dynamics in linearly and circularly polarized waves can be easily seen to have very different characteristics. For circularly polarized waves, the electron moves in a circle in the plane spanned by the two polarization vectors $\boldsymbol{\epsilon}_i$ of the laser. Since $A \cdot A = \langle A \cdot A \rangle$, there is no longitudinal velocity component in that inertial system, i.e. $u_\parallel = \boldsymbol{n} \cdot \boldsymbol{u} = 0$ with $\boldsymbol{n} = \boldsymbol{k}/\omega$. The motion resembles that of a micro-scale synchrotron.

On the other hand, for linear laser polarization, the motion is in a plane spanned by the polarization vector and the longitudinal beam direction of the laser, forming a Lissajous curve with frequency ratio $1 : 2$, usually termed "figure-8 motion" [Sar70]. The longitudinal component of the velocity, $u_\parallel \propto A \cdot A - \langle A \cdot A \rangle \propto \cos 2\phi$, has twice the frequency of the transverse motion and vanishes on average $\langle u_\parallel \rangle = 0$. In this situation, the motion resembles the trajectory in an undulator. In fact, the radiation produced has similar properties as undulator radiation such that the notion "optical undulator" is often used in the literature when referring to the radiation process in laser fields [Deb10]. In a pulsed laser field, the co-moving frame is not an inertial frame; it is accelerated and therefore inadequate for describing the dynamics in a Poincaré invariant formalism.

## 2.2   Coherent photon states and classical fields

The usual formulation of quantum electrodynamics where the complete electromagnetic field, including the laser pulse, is described as a Fock space state of individual photons is inadequate for the description of strong-field QED [Nev76]. In the interaction of strong laser pulses with charged particles, one has to deal with a huge amount of photons present in the laser pulse. A proper quantum mechanical treatment based on usual perturbation theory, organized solely in powers of the fine structure constant $\alpha$, would require a tremendously large number of diagrams to be taken into account, describing the absorption and re-emission of laser photons, and resummations of certain classes of diagrams [Fri64, Ebe66]. Such a formulation of the theory where the laser is described by a set of photons is inappropriate, as one has to incorporate the coherence of the laser field [Nev76]. For example, a laser pulse with a total energy of 1 J and a wavelength of $\lambda = 800$ nm consists of $4 \times 10^{18}$ individual photons; a laser strength of $a_0 = 1$ corresponds to a photon density of $10^{14}$ photons/$\mu m^3$.

Coherent states are useful as idealizations of the quantum state of a laser beam in scattering theory [Ebe69]. The treatment of the laser field as coherent state instead of a quantized multi-photon Fock space state is appropriate as long as the number of photons which is scattered out of the coherent part is much smaller than the number of photons present in the laser pulse, i.e. the depletion of the laser pulse is negligible.

Coherent states were first recognized as eigenstates of the quantum harmonic oscillator [Sch26] and later used for the description of laser fields in quantum optics [Gla63b, Gla63a, Man95]. They are quantum states that posses the minimum uncertainty and therefore behave as classical as possible, in particular, the field strength operators of the electromagnetic field do have non-vanishing expectation values in coherent states. A single-mode coherent state $|v_{\boldsymbol{k},\lambda}\rangle$ is defined as an eigenstate of the annihilation operator $\hat{a}_{\boldsymbol{k},\lambda}$ of a certain mode of the photon field with (three-)momentum quantum number $\boldsymbol{k}$ and polarization quantum number $\lambda$

$$\hat{a}_{\boldsymbol{k},\lambda}|v_{\boldsymbol{k},\lambda}\rangle = v_{\boldsymbol{k},\lambda}|v_{\boldsymbol{k},\lambda}\rangle \,. \tag{2.16}$$

In analogy with (2.16), multi-mode coherent states $|C\rangle$ describing an electromagnetic field are defined as eigenstates of the positive-frequency part of the field operator $\hat{\mathcal{A}}_\mu(x)$,

$$\hat{\mathcal{A}}_\mu^{(+)}(x)|C\rangle = C_\mu(x)|C\rangle \,, \tag{2.17}$$

with complex eigenvalue $C_\mu(x)$ [Fra65, Kib65]. The positive-frequency part of the field operator

$$\hat{\mathcal{A}}_\mu^{(+)}(x) = \sum_\lambda \int \frac{d^3\boldsymbol{k}}{(2\pi)^3 2k^0} e^{-ik \cdot x} \epsilon_{\mu,\lambda}(\boldsymbol{k})\, \hat{a}_{\boldsymbol{k},\lambda} \tag{2.18}$$

is a superposition of the annihilation operators $\hat{a}_{\boldsymbol{k},\lambda}$ with the commutation relations of photon creation and annihilation operators

$$[\hat{a}_{\boldsymbol{k},\lambda}, \hat{a}_{\boldsymbol{k}',\lambda'}^\dagger] = -(2\pi)^3 2k^0 g^{\lambda\lambda'} \delta^3(\boldsymbol{k} - \boldsymbol{k}') \,. \tag{2.19}$$

The complete field operator is a sum of positive and negative frequency parts $\hat{\mathcal{A}}_\mu(x) = \hat{\mathcal{A}}_\mu^{(+)}(x) + \hat{\mathcal{A}}_\mu^{(-)}(x)$ with $\hat{\mathcal{A}}_\mu^{(-)}(x) = [\hat{\mathcal{A}}_\mu^{(+)}(x)]^\dagger$ [see also Appendix A.6, in particular Eq. (A.83)]. The coherent state $|C\rangle$ can be generated as a displaced vacuum state $|C\rangle = \hat{D}|0\rangle$ with the unitary displacement operator

$$\hat{D} = \exp\left\{\sum_\lambda \int \frac{d^3\boldsymbol{k}}{(2\pi)^3 2k^0} \left[C_\lambda(\boldsymbol{k})\hat{a}_{\boldsymbol{k},\lambda}^\dagger - C_\lambda^*(\boldsymbol{k})\hat{a}_{\boldsymbol{k},\lambda}\right]\right\} \,, \tag{2.20}$$

which fulfils $\hat{D}(-C_\lambda) = \hat{D}^\dagger(C_\lambda)$. The unitarity of $\hat{D}$ can be shown by employing the Baker-Campbell-Hausdorff relation. Using the unitarity of $\hat{D}$ one easily shows that the coherent states are normalized as $\langle C|C\rangle = \langle 0|0\rangle = 1$. The quantities $C_\lambda(\boldsymbol{k})$ define the momentum and polarization distribution of photons in the coherent state and are related to the Fourier transform of the eigenvalue $C_\mu(x)$. The commutation relations of the photon creation and annihilation operators with the displacement operator read

$$[\hat{a}_{\boldsymbol{k},\lambda}, \hat{D}] = C_\lambda(\boldsymbol{k})\,\hat{D}\,, \tag{2.21}$$

$$[\hat{a}^\dagger_{\boldsymbol{k},\lambda}, \hat{D}] = C^*_\lambda(\boldsymbol{k})\,\hat{D}\,, \tag{2.22}$$

$$[\hat{\mathcal{A}}^{(+)}_\mu(x), \hat{D}] = \sum_\lambda \int \frac{d^3k}{(2\pi)^3 2k^0} e^{-ik\cdot x}\epsilon_{\mu,\lambda}(\boldsymbol{k})C_\lambda(\boldsymbol{k})\,\hat{D} \equiv C_\mu(x)\,\hat{D}\,. \tag{2.23}$$

The unitary displacement operator $\hat{D}$ "shifts" the photon field operator according to

$$\hat{D}^\dagger\hat{\mathcal{A}}^{(+)}_\mu\hat{D} = \hat{\mathcal{A}}^{(+)}_\mu + C_\mu(x)\,, \tag{2.24}$$

$$\hat{D}^\dagger\hat{\mathcal{A}}^{(-)}_\mu\hat{D} = \hat{\mathcal{A}}^{(-)}_\mu + C^*_\mu(x)\,, \tag{2.25}$$

such that the expectation value of the photon field operator $\hat{\mathcal{A}}_\mu$ in a coherent state is

$$\langle C|\hat{\mathcal{A}}_\mu(x)|C\rangle = C_\mu(x) + C^*_\mu(x) \equiv A_\mu(x)\,, \tag{2.26}$$

thus yielding the real classical background field configuration $A_\mu(x)$. That is, there exists a certain correspondence between coherent states $|C\rangle$ and classical background fields [Kib68]. Both approaches are equivalent if radiative corrections are neglected [Gla63b, Kib65, Ole68]. To make contact with the usual description of the laser field (A.24) used in this thesis, one identifies

$$C^\mu(x) = \frac{A_0}{2}g(k\cdot x)\epsilon^\mu_+ e^{-i(k\cdot x+\hat{\phi})}\,. \tag{2.27}$$

Thereby, each coherent $|C\rangle$ state corresponds uniquely to a classical solution of the wave equation $\Box A_\mu = 0$ where the vector potential $A_\mu$ fulfils the Lorenz gauge condition $\partial_\mu A^\mu = 0$; it is the quantum state which most closely approximates this classical field [Kib65]. In order to describe scattering processes in a background field, a slight generalization of coherent states is required, where the displacement operator $\hat{D}$ acts on a $N$-photon Fock space state

$$|N\rangle = |\{n_{\boldsymbol{k},\lambda}\}\rangle = \prod_{k,\lambda}\frac{(\hat{a}^\dagger_{\boldsymbol{k}\lambda})^{n_{\boldsymbol{k},\lambda}}}{\sqrt{n_{\boldsymbol{k},\lambda}!}}|0\rangle\,, \tag{2.28}$$

instead of the Fock vacuum $|0\rangle$. These states $|N;C\rangle = \hat{D}|N\rangle$ are termed "semi-coherent" states in [Fra91] with the expectation values

$$\frac{\langle N;C|\hat{\mathcal{A}}_\mu(x)|N;C\rangle}{\langle N|N\rangle} = A_\mu(x)\,, \tag{2.29}$$

$$\frac{\langle N;C|\hat{n}_{\boldsymbol{k},\lambda}|N;C\rangle}{\langle N|N\rangle} = |C_\lambda(\boldsymbol{k})|^2 + n_{\boldsymbol{k},\lambda} \tag{2.30}$$

and the photon number operator $\hat{n}_{\boldsymbol{k},\lambda} = \hat{a}^\dagger_{\boldsymbol{k},\lambda}\hat{a}_{\boldsymbol{k},\lambda}$. Thus, in semi-coherent states, there exists a part of the electromagnetic field which can be described using the classical potential $A_\mu(x)$, or the Fourier transforms $C_\lambda(\boldsymbol{k})$. Moreover, a number of $N$ photons is excited over this classical background with occupation numbers $n_{\boldsymbol{k},\lambda}$ in Fock space [Fra91]. For a scattering

matrix element consisting of coherent parts $C$ describing the laser pulse and Fock space parts for the excitations above the background field in the initial ($i$) and final ($f$) states one may note the relations [Kib65, Fra65]

$$\langle f; C|\hat{S}|\, i\, ; C\rangle \equiv \langle f; C|\hat{S}[\hat{\Psi}, \hat{\bar{\Psi}}, \hat{\mathcal{A}}]|\, i\, ; C\rangle = \langle f\, |\hat{S}[\hat{\Psi}, \hat{\bar{\Psi}}, \hat{\mathcal{A}} + A]|\, i\, \rangle \equiv \langle f\, |\hat{S}[A]|\, i\, \rangle , \quad (2.31)$$

where $\hat{S}[A]$ denotes the scattering operator in the presence of the background field [Kib65, Mit75, Har09] which is specified in the next subsection.

## 2.3  Strong-field QED in the Furry picture

The Lagrangian for a system of electrons/positrons ($\bar{\Psi}$, $\Psi$) and the electromagnetic field, decomposed into the radiation field $\mathcal{A}_\mu$ and an external background field $A_\mu$, reads

$$\mathcal{L} = \bar{\Psi}(i\slashed{\partial} - m)\Psi - \frac{1}{4}\mathcal{F}^{\mu\nu}\mathcal{F}_{\mu\nu} - \frac{1}{2\xi_g}(\partial \cdot \mathcal{A})^2 - e\bar{\Psi}(\slashed{\mathcal{A}} + \slashed{A})\Psi \qquad (2.32)$$

with the electromagnetic field strength tensor $\mathcal{F}_{\mu\nu} = \partial_\mu \mathcal{A}_\nu - \partial_\nu \mathcal{A}_\mu$ of the radiation field and gauge fixing parameter $\xi_g$.[3] Note that there is no dynamical kinetic term involving the external background field $A_\mu$. The external field $A_\mu$ is a solution of Maxwell's equations without the current of the quantized charged particles. Thus, there is no back-reaction of the currents of the theory on the dynamics of the background field.

The Furry picture [Fur51], is a special case of the interaction picture describing the time-evolution of a quantum system. In the Furry picture, a certain part of the interaction, related to the background field is considered to be part of the "free" fermionic Lagrangian, such that the single-particle states related to $\bar{\Psi}$ and $\Psi$ are to be considered as solutions of the Dirac equation in the background field, see (2.40) below. The prototypical example for the Furry picture is the interaction of an electron in a Coulomb field, where bound electron states have to be treated properly.[4]

Absorbing the interaction with the background field into the fermionic Lagrangian, the reorganized fermionic (f), gauge field (g) and interaction (int) Lagrangians read

$$\mathcal{L}_{\mathsf{f}} = \bar{\Psi}(i\slashed{\partial} - e\slashed{A} - m)\Psi , \qquad (2.33)$$

$$\mathcal{L}_{\mathsf{g}} = -\frac{1}{4}\mathcal{F}_{\mu\nu}\mathcal{F}^{\mu\nu} - \frac{1}{2\xi_g}(\partial_\mu \mathcal{A}^\mu)^2 , \qquad (2.34)$$

$$\mathcal{L}_{\mathsf{int}} = -e\bar{\Psi}\slashed{\mathcal{A}}\Psi . \qquad (2.35)$$

This means, the interaction of the electrons and positrons with the background field is treated completely non-perturbatively. The interaction of the charged particles with the radiation field $\mathcal{A}_\mu$ can be described within perturbation theory. The perturbative series for the scattering operator $\hat{S}$ in the Furry picture is obtained in the form [Mit75]

$$\hat{S}[A] = \mathsf{T}\exp\left\{-i\int d^4x\, \mathscr{H}_{\mathsf{int}}(x)\right\}$$

$$= \mathsf{T}\exp\left\{-ie\int d^4x : \hat{\bar{\Psi}}_{(F)}(x)\gamma^\mu \hat{\mathcal{A}}_\mu(x)\hat{\Psi}_{(F)}(x) :\right\} . \quad (2.36)$$

---

[3]Further on, the Feynman-'t Hooft gauge with $\xi_g = 1$ will be used.
[4]Therefore, the Furry picture is also also called "bound interaction picture"

The subscript $(F)$ specifies the electron operators in the Furry picture. The symbol $\mathsf{T}$ is the time ordering operation and $: \cdots :$ denotes normal ordering of the enclosed operators. The eigenmode decomposition of the electron field operator in the Furry picture reads [MP09]

$$\hat{\Psi}_{(F)}(x) = \sum_{\alpha} \Psi_{\alpha}^{(+)}(x)\hat{c}_{\alpha} + \Psi_{\alpha}^{(-)}\hat{d}_{\alpha}^{\dagger}, \qquad (2.37)$$

where $\Psi_{\alpha}^{(\pm)}(x)$ denote the positive and negative energy single-particle wave functions, which are discussed in the next section for the case of Volkov wave functions in plane wave background fields. The operators $\hat{c}_{\alpha}$ $(\hat{d}_{\alpha}^{\dagger})$ annihilate (create) an electron (positron) in the one-particle state $\alpha$. The fermionic anti-commutation relations for these operators can be found in Appendix A.6, where important relations concerning the formulation of quantum field theory in the Furry picture are presented. Since the background field $A_{\mu}$ depends explicitly on the laser phase $\phi = k_{+}x^{+}$, which is a light-like coordinate, it seems necessary to work in light-front QED, or null-plane QED, where the initial conditions for the solution of the single particle wave equations are specified on a null-plane [Nev71b], and also the (anti-)commutation relations of the field operators are defined on light-like hypersurfaces which have a light-like normal vector. In the light-front formulation of the theory, one has to use the $S$ operator in light-front QED [Nev76]

$$\hat{S} = \mathsf{X}^{+} \exp\left\{ -i \int dx^{+} : P_{+}^{\mathsf{int}}(x^{+}) : \right\} \qquad (2.38)$$

instead of (2.36). This particular $S$ operator transforms the in states at $x^{+} = -\infty$ to out states at $x^{+} = +\infty$, where $P_{+}^{\mathsf{int}}$ denotes the interaction part of the $x^{+}$ translation operator, which serves as a Hamiltonian in this case [Nev76]. For details on the subject, the reader is referred to [Kog70, Nev71a, Nev76]. The ambiguity of choosing the time evolution parameter in a relativistic theory is related to a reparametrization invariance of the classical action, which is generated by the mass shell constraint $p^2 = m^2$ (or $u^2 = 1$). One needs to single out a specific parametrization, i.e. to choose a specific time parameter. A distinct choice of the time variable (e.g. $t$ or $x^{+}$) defines the corresponding Hamiltonian, which is the generator of time translations and specifies a corresponding surface of constant "time" where the initial conditions for the solution of the equations of motion can be specified and the "equal-time" commutators are formulated [Hei01].

The equivalence of the usual instant form of field theory, quantized on spacelike surfaces $t = const$, and light-front field theory, quantized on null-planes $\phi = const$ and $x^{+} = const$, was shown in [Cha73a, Cha73b, Yan73a, Yan73b] by proving the equivalence of the two perturbative series [Hei07]

$$\mathsf{T} \exp\left\{ -i \int dt : H_{\mathsf{int}}(t) : \right\} = \mathsf{X}^{+} \exp\left\{ -i \int dx^{+} : P_{+}^{\mathsf{int}}(x^{+}) : \right\}. \qquad (2.39)$$

Another proof of the equivalence of light-front and the instant formulation of QED is due to [Roh73, TE74]. The crucial point in this formulation of light-front field theory is related to the definition of the basic commutation relations on light-fronts, $\{\Psi(x), \bar{\Psi}(x')\}_{x'^{+}=x^{+}}$, instead of defining equal time commutators $\{\Psi(x), \bar{\Psi}(x')\}_{t'=t}$ in the instant form field theory. This refers to boundary conditions and initial values for the solution of the equations of motion which are given on a light-front hypersurface in the case of light-front field theory instead of a space like hypersurface.

An alternative approach to light-front field theory [Cha69, Hei07] is used throughout this thesis: One uses the instant form of the commutation relations for the field operators $\{\Psi(x), \bar{\Psi}(x')\}_{t'=t}$, based on the adiabatic decoupling of the laser pulse and the fermions

at infinite past and future and consequently the representation of the $S$ operator (2.36).[5] The light-front structure is introduced automatically. Spacetime integrations are performed in light-front coordinates where the coordinate $\phi$ is singled out by the dependence of the background field $A_\mu(\phi)$ on the latter. The light-front structure of the theory becomes manifest in expression involving the electron propagator, i.e. starting in second order perturbation theory.

The Feynman rules for strong-field QED in the Furry picture, based on a perturbative expansion of the $S$ operator in (2.36), i.e. the Dyson series (A.93), can be summarized as follows [Mit75]:

1. $S$ matrix elements are calculated in coordinate space.

2. External incoming or outgoing fermions are translated into the laser dressed Volkov wave function $\Psi(x)$ or $\bar\Psi(x)$, see Section 2.4.

3. An internal fermion line corresponds to the Dirac-Volkov propagator $\mathcal{G}(x, y|A)$, cf. Section 2.9.

4. Internal and external photon lines are translated into the free photon propagator and the free photon wave functions, respectively, just as in ordinary QED without background fields.

5. Each fermion-fermion-photon vertex corresponds to a factor of $-ie\gamma^\mu$ and an integration over spacetime $d^4x$.

6. Symmetry factors for identical particles etc. are the same as in usual QED.

## 2.4   Volkov states

The single-particle wave functions $\Psi_\alpha(x)$ in the electromagnetic background field $A_\mu$ are solutions of the Dirac equation

$$(i\slashed{\partial} - e\slashed{A}(x) - m)\Psi_\alpha(x) = 0 \tag{2.40}$$

following from the Lagrangian $\mathcal{L}_\mathsf{f}$ in Eq. (2.33). For background fields in the form of plane waves $A_\mu(\phi)$, as in Eq. (A.24), closed solutions of (2.40) can be found, named Volkov wave functions [Vol35]. The one-particle Volkov states are classified by the quantum numbers of momentum $p$ and spin $r$.[6] The Volkov wave functions have a representation as

$$\Psi_{p,r}(x) = E_p(x)u_{p,r}\,, \tag{2.41}$$

where $u_{p,r}$ is the free Dirac spinor for (on-shell) momentum $p$ which fulfils $(\slashed{p} - m)u_{p,r} = 0$ and $E_p$ are $4 \times 4$ matrices to be specified below. Throughout this thesis, the normalization $\bar{u}_{p,r}u_{p,r'} = 2m\delta_{rr'}$ is utilized for spinors (see Appendix A.5 for further details). The wave functions (2.41) represent the positive energy solutions $\Psi_{p,r} \equiv \Psi_{p,r}^{(+)}$ of (2.40). The negative energy solutions are obtained from (2.41) via the transformation $p \to -p$, i.e. $\Psi_p^{(-)}(x) \equiv$

---

[5] In fact, the description of the laser as a finite, pulsed field provides these conditions: At $t \to \pm\infty$ the background field vanishes for any finite spatial position $|\boldsymbol{x}| < \infty$.

[6] Non-Volkov solutions for a charge in a plane wave have been found [Bag05], where the transverse quantum numbers $\boldsymbol{p}_\perp$ are different from the Volkov states.

$\Psi_{-p}(x)$, where the notation for negative energy spinors is as usual $u_{-p} \equiv v_p$. The Volkov matrices $E_p(x)$ carry the information on the laser-electron interaction. They are given by[7]

$$E_p(x) = \Gamma_p(\phi) \exp\{iS_p(x)\} \,, \tag{2.42}$$

$$\Gamma_p(\phi) = 1 + \frac{e}{2k \cdot p} \slashed{k}\slashed{A}(\phi) \,. \tag{2.43}$$

The phase is the classical Hamilton Jacobi action [see Eq. (2.10)]

$$S_p(x) = -p \cdot x - \frac{1}{2k \cdot p} \int\limits_0^\phi d\phi' [2ep \cdot A(\phi') - e^2 A^2(\phi')] \equiv -p \cdot x - f_p(\phi) \,, \tag{2.44}$$

defining the non-linear part $f_p(\phi)$. In the limit of vanishing laser field, $A_\mu \to 0$, the Volkov matrices correspond to plane waves $E_p(x) \to e^{-ip \cdot x}$. The adjoint wave function $\bar{\Psi}_{p,r} = \bar{u}_{p,r} \bar{E}_p(x)$ involves the Dirac-adjoint matrix $\bar{E}_p(x) = \gamma^0 E_p^\dagger(x)\gamma^0$, which is also the inverse matrix $E_p(x)\bar{E}_p(x) = \bar{E}_p(x)E_p(x) = 1$. For later use, the following abbreviations are defined

$$d_p = \frac{ma_0}{4k \cdot p} \,, \tag{2.45}$$

$$\alpha_{p,i} = ma_0 \frac{\epsilon_i \cdot p}{k \cdot p} \,, \quad \text{for } i \in \{1, 2, +, -\} \,, \tag{2.46}$$

$$\beta_p = \frac{m^2 a_0^2}{4k \cdot p} = ma_0 d_p \,, \tag{2.47}$$

such that

$$f_p(\phi) = \text{Re} \left( \alpha_{p,-} \int\limits_0^\phi d\phi' g(\phi') e^{i(\phi' + \hat{\phi})} \right) + \beta_p \int\limits_0^\phi d\phi' g^2(\phi') \left[ 1 + \cos 2\xi \, \cos 2(\phi' + \hat{\phi}) \right] \,. \tag{2.48}$$

These parameters are of the order $d_p \sim a_0/\omega_\star$, $\alpha_{p,i} \sim a_0 m/\omega_\star$ and $\beta_p \sim a_0^2 m/\omega_\star$, where $\omega_\star = k \cdot p/m$ denotes the laser frequency boosted to the electron rest frame. In particular, $\alpha_{p,i}$ and $\beta_p$ can be very large also for small $a_0$ as the laser frequency is in general much smaller than the electron rest mass when considering lasers in the optical regime $\omega \sim 1$ eV. Only for high-energy electrons with energies $E \sim 50$ GeV colliding almost head-on with the laser pulse, the boosted frequency becomes $\omega_\star \sim m$.

The scalar product for the fermion wave functions is defined in a Lorentz covariant manner as [Bag90]

$$(\Psi_1, \Psi_2) = \int\limits_\sigma d\sigma_\mu \bar{\Psi}_1(x)\gamma^\mu \Psi_2(x) \,, \tag{2.49}$$

where $\sigma$ is an arbitrary hypersurface in Minkowski space and $d\sigma^\mu$ is the infinitesimal normal vector thereupon. The hypersurface can be expressed with general curvilinear coordinates $\xi^\mu(x)$, where $\xi^0 = const$, defines the hypersurface and $\xi^1, \xi^2, \xi^3$ parametrize $\sigma$. Employing this notation, one has $d\sigma^\mu = \frac{\partial \xi^0(x)}{\partial x_\mu} \sqrt{-g} d^3\xi$, where $g$ denotes the determinant of the metric tensor

---

[7]For spin-0 and spin-1 particles, the corresponding Volkov wave functions are known [Bro83, Bro84]. The difference is in the function $\Gamma_p(\phi)$, which is e.g. $\Gamma_p = 1$ for spin-0 particles. Furthermore, the generalization of spin-1/2 Volkov states to background wave fields with general tensor structure (e.g. pseudoscalar, tensor etc.) has been accomplished [Shi91a, Shi91b].
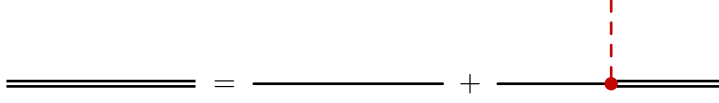
**Figure 2.2:** Diagrammatic representation of the Lippmann-Schwinger equation for the Volkov state (double line). The red dashed lines denote the external laser field and the black solid lines depict free electrons/positrons.

in the coordinates $\xi^\mu$. The scalar product between Volkov states is evaluated most conveniently by using a light-front hypersurface defined by the laser four-vector $n^\mu = k^\mu/\omega$ with the only non-vanishing component $n^- = 2$, i.e. on a plane of constant phase $\phi \propto \xi^0 = n \cdot x$, yielding

$$(\Psi_1, \Psi_2) = \frac{1}{2} \int d^2\boldsymbol{x}^\perp dx^- \bar{\Psi}_1(x) \not{n} \Psi_2(x) . \tag{2.50}$$

Thus,

$$(\Psi_{p,r}, \Psi_{p',r'}) = \frac{1}{2} \int d^2\boldsymbol{x}^\perp dx^- \, \bar{u}_{p,r}(1 + d_p \not{A}\not{k}) \not{n} (1 + d_{p'} \not{k}\not{A}) u_{p',r'} \, e^{i(S_{p'}(x) - S_p(x))} \tag{2.51}$$

$$= \frac{1}{2} \int d^2\boldsymbol{x}_\perp dx^- \, \bar{u}_{p,r} \not{n} u_{p',r'} \, \exp\left\{ i(p'^+ - p^+)\tfrac{x^-}{2} - i(\boldsymbol{p}'_\perp - \boldsymbol{p}_\perp)\cdot\boldsymbol{x}_\perp \right\}$$

$$\times \exp\left\{ i(p'^- - p^-)\tfrac{x^+}{2} + if_p(\phi) - if_{p'}(\phi) \right\} \tag{2.52}$$

$$= (2\pi)^3 \, 2p^+ \, \delta^3(\mathsf{p}' - \mathsf{p}) \delta_{rr'} = (2\pi)^3 \, 2p^0 \, \delta^3(\boldsymbol{p}' - \boldsymbol{p}) \delta_{rr'} . \tag{2.53}$$

The equality in (2.53) holds since for on-shell momenta $p'$ and $p$ one has[8] $2p^0\delta^3(\boldsymbol{p} - \boldsymbol{p}') = 2p^+\delta^3(\mathsf{p} - \mathsf{p}')$. When considering off-shell momenta $p^2 \neq m^2$ instead, the Volkov matrix functions $E_p$ have the properties of orthogonality (2.54) and completeness (2.55) in the form [Mit75, Löt08]

$$\int d^4x \bar{E}_p(x) E_{p'}(x) = (2\pi)^4 \delta^4(p - p') , \tag{2.54}$$

$$\int d^4p E_p(x) \bar{E}_p(x') = (2\pi)^4 \delta^4(x - x') . \tag{2.55}$$

A proof of the orthogonality can be found in [Rit85, Zak05], and the completeness was rigorously proven only recently in [Löt08]. A new simple and elegant proof of the above equalities is presented in Appendix B.3 employing the analytical light-front properties of the Volkov matrix functions $E_p(x)$.

## 2.5   Lippmann-Schwinger equation

The Dirac equation in the external field (2.40) can be reformulated as an integral equation in the form of a Lippmann-Schwinger equation as

$$\Psi_p(x) = \psi_p(x) + \int d^4y \, G_0(x - y) \Sigma_0(y) \Psi_p(y) , \tag{2.56}$$

---

[8]This can be shown by considering $\delta(p^+ - p'^+) = \delta(p^0 - p'^0 + p^3 - p'^3) = \delta(p^3 - p'^3 + \sqrt{(p^3)^2 + \boldsymbol{p}_\perp^2 + m^2} - \sqrt{(p'^3)^2 + \boldsymbol{p}'^2_\perp + m^2}) = \frac{p^0}{p^+}\delta(p^3 - p'^3)$.
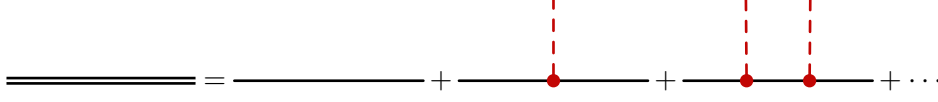
**Figure 2.3:** Perturbative expansion of the Volkov states (double line) in powers of the
coupling to the background field (red dashed line) and free electron states
(black solid lines).

where $\psi_p(x)$ and $G_0(x-y)$ are the free wave function and Green's function in the absence
of a background field as solutions of the homogeneous and inhomogeneous field-free Dirac-
equations,

$$(i\not\partial - m)\psi_p(x) = 0 \qquad \text{and} \qquad (i\not\partial - m)G_0(x-y) = \delta(x-y)\,, \qquad (2.57)$$

respectively; $\Sigma_0(y) = e\not A(y)$ denotes the (irreducible) self-energy part of the interaction with
the background vector potential, which is by definition the only contribution since the classical
background field $A_\mu$ is incapable of forming loops.[9] The Lippmann-Schwinger equation (2.56),
which is visualized diagrammatically in Figure 2.2, represents a proper starting point for a
perturbative expansion of the Volkov states via an iterative solution of the former equation,
which is depicted diagrammatically in Figure 2.3. The $N$th order term is given by

$$\Psi_p^{(N)} = \psi_p + G_0\Sigma_0\psi_p + G_0\Sigma_0 G_0\Sigma_0\psi_p + \ldots = \sum_{n=0}^{N} \left(G_0\Sigma_0\right)^n \psi_p\,, \qquad (2.58)$$

using a symbolic notation, where

$$\left(G_0\Sigma_0\right)^n \psi_p \equiv \int d^4y_1 \cdots d^4y_n G_0(x-y_1)\Sigma_0(y_1)\cdots G_0(y_{n-1}-y_n)\Sigma_0(y_n)\psi_p(y_n)\,. \quad (2.59)$$

Since the background field vector potential $A_\mu(\phi)$ in (A.24) is a real quantity, it contains
the amplitudes for the absorption ($e^{-i\phi}$) and emission ($e^{i\phi}$) of laser photons via $A^\mu(\phi) =$
$A_0\epsilon_+^\mu g(\phi)e^{-i(\phi+\hat\phi)}/2 + c.c.$ where $c.c.$ denotes the complex conjugate of the former expression.
Consequently, the red dashed lines in Figures 2.2 and 2.3 represent both the absorption and
emission of laser photons. The $N$th order term $\Psi^{(N)}$ contains $N$ powers of the interaction
with the background field $\Sigma_0$ (times a free propagator $G_0$) and is therefore of the order
$(eA_0/m)^N = a_0^N$. Thus, the perturbative expansion of the Volkov state in Figure 2.3 via the
iterative solution of the Lippmann-Schwinger equation is an expansion in powers of $a_0$. This
means that such a perturbative series is meaningful only in the limit of $a_0 \ll 1$. The full
non-perturbative Volkov solution $\Psi_p(x)$ has to be employed for $a_0$ of the order of unity or
larger. The probability for the absorption or emission of a single photon from the laser field
is comparable to the probability for the absorption or emission of many laser photons for
$a_0 > 1$.

## 2.6   Properties of Volkov states in finite laser pulses

In order to characterize the Volkov wave function, it is sufficient to consider the Volkov matrix
function $E_p(x)$, instead of $\Psi_p$, as it contains all the information on the interaction with the

---

[9]That means, radiative quantum corrections, i.e. the mass operator $\Sigma$ of the electron, are not included in
(2.56).
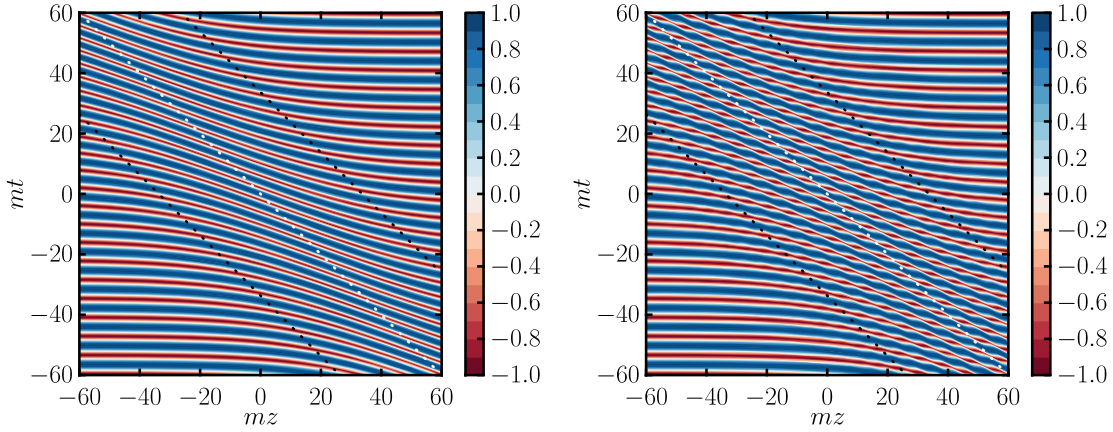
**Figure 2.4:** Contour plot of the scalar projection $\mathcal{S}[E_p(x)]$ in position space in the $z - t$ plane. The laser pulse with hyperbolic secant profile $g(\phi) = \cosh^{-1}\phi/\Delta\phi$ is located between the two black dotted lines. The white dotted line depicts the propagation of the centre of the laser pulse along the light-cone with $\phi = 0$. Left (right) panel: Circularly (linearly) polarized laser pulse with $a_0 = 1.5$ and $\Delta\phi = 20$.

laser field. Since $E_p(x)$ is a $4 \times 4$ matrix it is reasonable to study the different projections onto the basis elements of the Clifford algebra (see Appendix A.5 for the definitions), of which only the scalar and anti-symmetric tensor projections are non-zero

$$\mathcal{S}[E_p] = \frac{1}{4}\operatorname{tr} E_p(x) = \exp\{iS_p(x)\}\,,  \tag{2.60}$$

$$\mathcal{T}^{\mu\nu}[E_p] = \frac{1}{4}\operatorname{tr} \sigma^{\mu\nu} E_p(x) = \frac{ie}{2k\cdot p}(A^\mu k^\nu - A^\nu k^\mu)\exp\{iS_p(x)\}\,.  \tag{2.61}$$

The real part of the scalar projection $\mathcal{S}[E_p]$ is exhibited in Figure 2.4 in the frame where the electron is initially at rest. In that frame, the free electron wave function outside the laser pulse behaves as $\propto \exp\{-ip\cdot x\} = \exp\{-imt\}$. The scalar projection is essentially equivalent to probing the state $\Psi_{p,r}$ with $\bar{u}_{p,r}$ and an average over the spins $r$

$$\frac{1}{2}\sum_r \bar{u}_{p,r}\Psi_{p,r}(x) = \frac{1}{2}\sum_r \bar{u}_{p,r}E_p(x)u_{p,r}(x) = m\mathcal{S}[E_p(x)]\,.  \tag{2.62}$$

The effect of the laser pulse is a local deformation of the electron wave fronts which can be considered as the build-up of an effective, time dependent quasi-momentum $q^\mu(\phi) = p^\mu + g^2(\phi)\beta_p k^\mu$, which takes its maximum at the centre of the laser pulse $\phi = 0$, depicted as white dotted line in Figure 2.4, where it coincides with the usual definition of the quasi-momentum in infinite plane waves.[10] Thus, inside the laser pulse, especially for $\phi = 0$, the fully dressed electron wave function behaves as $\propto \exp\{-iq\cdot x\} = \exp\{-i(m + \beta_p\omega_\star)t + i\beta_p\omega_\star z\}$, i.e. the electron wavelength changes and the wave fronts become tilted in the $t - z$ plane. Both effects are proportional to the ponderomotive potential $U_p \propto ma_0^2 \propto \beta_p$. In Figure 2.4, the situation is such that an electron with an energy of 50 GeV propagates head-on through a strong laser pulse with $a_0 = 1.5$ and a pulse length $\Delta\phi = 20$. The frequency of the laser is $\omega = 1.55$ eV which gives in the electron rest frame $\omega_\star = 300$ keV $\sim m$.

---

[10]Here, $\Delta\phi \gg 1$ is assumed to allow for a separation of fast and slow time scales as discussed above in Eq. (2.13).
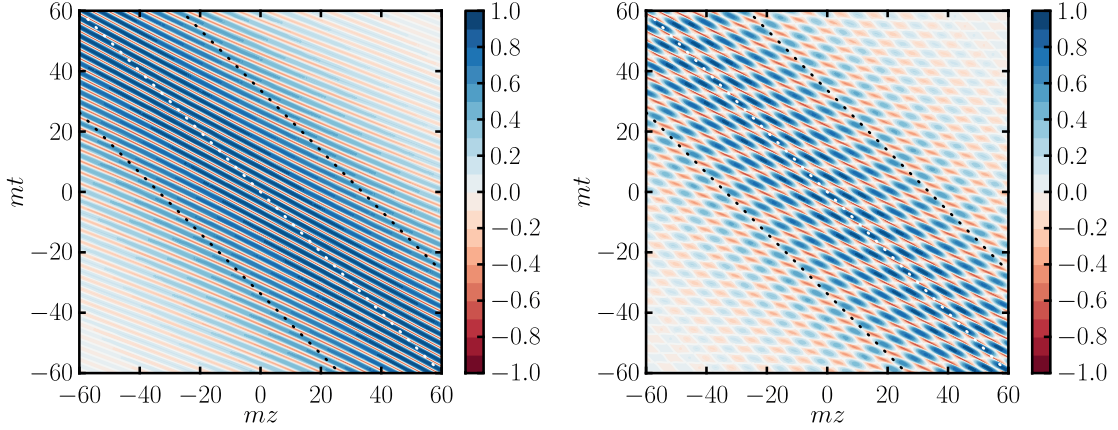
**Figure 2.5:** Normalized contour plot of the tensor projection $\mathcal{T}^{13} - i\mathcal{T}^{23}$. The same parameters as in Figure 2.4 are used.

By a closer inspection one sees that the plane waves in the remote future, when the laser pulse has passed, and the remote past, before the laser pulse arrives, differ by a finite phase shift $\Delta f_p = f_p(\infty) - f_p(-\infty)$, such that $\Psi_{\text{future}} \sim \Psi_{\text{past}} e^{-i\Delta_p}$. For longer pulses $\Delta\phi \gg 1$ the dominant source of this phase shift is the ponderomotive term in the non-linear phase, $\propto \beta_p g^2(\phi)$, which is also responsible for the build-up of the quasi-momentum. For ultra-short pulses there are also contributions to the phase shift coming from the oscillating terms as $\langle A \rangle \neq 0$ and the line integral $\int_{-\infty}^{\infty} dx_\mu A^\mu \neq 0$ can be of the same order of magnitude as the ponderomotive integral in that case. The phase shift $\Delta f_p$ turns out to be responsible for the appearance of substructures in the spectra of strong-field QED processes in short laser pulses.

The antisymmetric tensor projections $\mathcal{T}^{\mu\nu}$ allow for a further characterization of the Volkov wave function. These tensor projections are non-zero only in regions where the laser pulse is present. They mix contributions with different spin orientation and are therefore proportional to a combination of $\bar{u}_{p,\uparrow}\Psi_{p,\downarrow}(x)$ and $\bar{u}_{p,\downarrow}\Psi_{p,\uparrow}(x)$, i.e. the spin-up wave function contains contributions with spin-down and vice versa. From the structure of the Pauli interaction term $\sigma^{\mu\nu}F_{\mu\nu}$ with the field strength tensor $F_{\mu\nu}$, one can infer that $\mathcal{T}^{01}$ ($\mathcal{T}^{02}$) corresponds to the interaction of the electron with the $x$ ($y$) component of the electric field, and $\mathcal{T}^{13}$ ($\mathcal{T}^{23}$) corresponds to the $y$ ($x$) component of the magnetic field. From this correspondence and by inspecting (A.24) it is easy to understand why some projections are zero for linear polarization while they are non-zero for circular polarization. As an example, the tensor projection $\mathcal{T}^{13} - i\mathcal{T}^{23}$ is shown in Figure 2.5.

## 2.7   Construction of Volkov wave packets

Wave packets can be constructed from Volkov wave functions using light-front coordinates. To demonstrate the close connection between these wave packets and the classical trajectories of a charged particle in the same background field it suffices to study the scalar part of the Volkov wave function, which is indeed identical to the Volkov wave function of a point-like, spinless charged boson. According to [Nev71a] scalar wave packets are constructed as

$$\Phi(x) = \int \frac{d^3\mathsf{p}}{(2\pi)^3\, 2p^+} h(p^1, p^2, p^+) \mathcal{S}[E_p(x)] \tag{2.63}$$
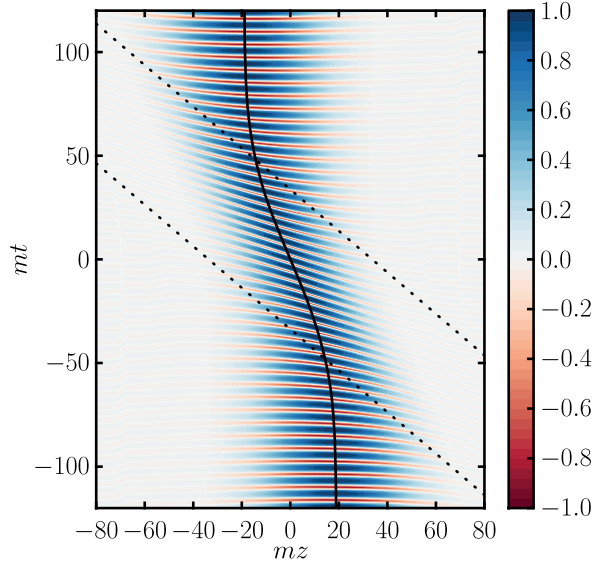
**Figure 2.6:** Contour plot of a normalized scalar Volkov wave packet in the $t - z$ plane. For comparison, the classical trajectory is depicted as solid black curve. The laser pulse propagates between the two black dotted lines. For parameters see the text.

with the Lorentz-invariant integration measure $d^3\mathsf{p}/(2\pi)^3 2p^+$ and the mass shell condition $p^- = (\boldsymbol{p}_\perp^2 + m^2)/p^+$. Since the dynamics in the transverse variables is trivial, it suffices to construct a one-dimensional wave packet by means of the momentum distribution $h(p^1, p^2, p^+) = (2\pi)^3 \delta(p^1)\delta(p^2)h_+(p^+)$, which leads to

$$\Phi(x) = \int \frac{dp^+}{2p^+} h_+(p^+)\mathcal{S}[E_p(x)], \tag{2.64}$$

where $h_+$ is taken as Gaussian distribution $h_+ \propto e^{-p_z^2/2D^2}$ with $p_z = (p_+^2 - m^2)/2p_+$, $\boldsymbol{p}_\perp = 0$ and Gaussian width $D = 0.05\,m$. This construction provides a localized wave packet in the $t - z$ plane with a minimum Gaussian size at $t = z = 0$. The normalized wave packet is exhibited in Figure 2.6 in the $t - z$ plane. The laser pulse parameters are the same as for Figures 2.4 and 2.5. For comparison, the trajectory for a classical particle in a hyperbolic secant laser pulse, projected to the $t - z$ plane is given parametrically by

$$t(\phi) = \frac{1}{\omega_\star}\left[\phi + \frac{a_0^2}{4}\Delta\phi\tanh\frac{\phi}{\Delta\phi}\right], \qquad z(\phi) = -\frac{1}{\omega_\star}\frac{a_0^2}{4}\Delta\phi\tanh\frac{\phi}{\Delta\phi} \tag{2.65}$$

for initial conditions $z(0) = t(0) = 0$. The centre of the wave packet follows the classical trajectory, which shows the close correspondence between the classical trajectory solutions and the Volkov wave functions. Note that $\omega_\star[t(\phi) + z(\phi)] = \phi$ consistently holds for the classical trajectory.

## 2.8   Momentum space properties

The Fourier transformation of the Volkov matrix $E_p(x)$ is defined by

$$\tilde{E}_p(p') = \int d^4x e^{-ip'\cdot x}E_p(x). \tag{2.66}$$

Employing the explicit form of $E_p(x)$ given in (2.42), it can be shown that the Fourier transform $\tilde{E}_p(p')$ has the following representation

$$\tilde{E}_p(p') = (2\pi)^4 \int \frac{ds}{2\pi} \delta(p' - p - sk) \mathcal{E}_p(s) \,. \tag{2.67}$$

Transforming Eq. (2.67) back to position space, the Volkov matrix $E_p(x)$ can be written as a superposition of plane waves

$$E_p(x) = \int \frac{ds}{2\pi} \exp\{-i(p + sk) \cdot x\} \mathcal{E}_p(s) \tag{2.68}$$

with the reduced Volkov matrices

$$\mathcal{E}_p(s) = \mathscr{K}_0(s) + d_p \slashed{k} \left[ \slashed{\epsilon}_- \mathscr{K}_-(s) + \slashed{\epsilon}_+ \mathscr{K}_+(s) \right] \,. \tag{2.69}$$

The functions $\mathscr{K}_n(s)$ are the occupation numbers of the different modes contributing to the Volkov wave function. They are given by

$$\begin{Bmatrix} \mathscr{K}_0(s) \\ \mathscr{K}_\pm(s) \end{Bmatrix} = \int d\phi \begin{Bmatrix} 1 \\ g(\phi) e^{\mp i(\phi + \hat{\phi})} \end{Bmatrix} \exp\{is\phi - i f_p(\phi)\} \,. \tag{2.70}$$

The variable $s$ parametrizes the amount of longitudinal momentum which is exchanged between the electron and the background field. Upon evaluating the integral in (2.67) the value of $s$ is related to $p$ and $p'$ as $s = (p'^- - p^-)/k^-$. It can be interpreted as a continuous analogue to the number of exchanged laser photons [Ild11a]. For a spin-$\frac{1}{2}$-particle, the function $\mathscr{K}_0(s)$ represents the scalar part (which is also relevant for spin-0 Klein-Gordon particles), and $\mathscr{K}_{\pm 1}(s)$ correspond to the spin dynamics in the background field which can be related to the tensor projection $\mathcal{T}^{\mu\nu}[E_p]$.

Some caution is needed for the function $\mathscr{K}_0$, which is an infinite integral over a pure phase as it contains no pulse shape function in the pre-exponential and is therefore numerically non-convergent. Analytically, $\mathscr{K}_0(s) \to 2\pi\delta(s)$ holds if the background field is switched off $A_\mu \to 0$, such that $E_p(x) \to e^{-ip \cdot x}$. Using a suitable regularization [Boc09, Sei11b] a delta distribution can be separated off the integral, corresponding to the free electron motion outside of the laser pulse

$$\mathscr{K}_0(s) = 2\pi\delta(s) + \frac{1}{s} \int d\phi \frac{df_p}{d\phi} \exp\{is\phi - i f_p(\phi)\} \equiv 2\pi\delta(s) + \mathscr{K}_0^R(s) \,, \tag{2.71}$$

with a now finite integral due to the derivative of $f_p$ appearing in the pre-exponential. This makes apparent that this divergence is associated to the interaction with $s = 0$ laser photons, i.e. zero energy exchange with the laser beam. Using this rewritten version of $\mathscr{K}_0$ in the Fourier representation of the Volkov matrix functions $E_p$, one sees that

$$E_p(x) = e^{-ip \cdot x} + \int \frac{ds}{2\pi} e^{-i(p + sk) \cdot x} \mathcal{E}_p^R(s) \,, \tag{2.72}$$

where the first part stemming from the integration of the delta distribution produces indeed a free plane electron wave. For the regularized reduced Volkov matrix $\mathcal{E}_p^R(s)$ it is understood that $\mathscr{K}_0(s) \to \mathscr{K}_0^R(s)$ in the definition in Eq. (2.69).

In the limit of IPW background fields, i.e. for $g \to 1$, the Floquet theorem [Flo83] applies to the Volkov wave functions: Given a differential equation with periodic external source with period $2\pi$, the solution has the form

$$\Psi_p(\phi) = e^{-iq \cdot x} \Phi(\phi) \,, \tag{2.73}$$
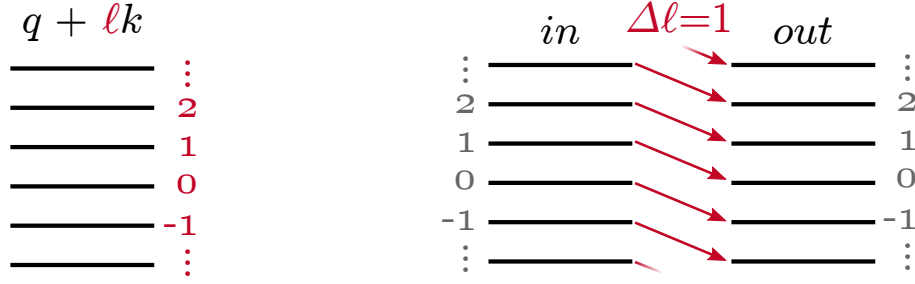
**Figure 2.7:** In an IPW background field, the Volkov wave function is given by a superposition of discrete Zel'dovich levels (left figure). Strong-field QED processes can be interpreted as transitions between Zel'dovich levels (right figure) [Löt08].

where $\Phi(\phi+2\pi) = \Phi(\phi)$ is periodic with the same period as the source. The quasi-momentum $q^\mu = p^\mu + \beta_p k^\mu$ appears here in the spirit of the Floquet theorem. The Fourier-zero mode, i.e. the non-periodic part of the non-linear phase $f_p$, has been absorbed into the definition of the quasi-momentum $q$ to arrive at (2.73). In the IPW limit, the momentum distribution functions (2.70) degenerate to a delta comb

$$\mathscr{K}_n(s) \xrightarrow{g\to 1} \sum_{\ell=-\infty}^{\infty} \delta(s - \ell - \beta_p) K_n(\ell, s) \tag{2.74}$$

with support at discrete momentum values $q^\mu + \ell k^\mu$, where $\ell \in \mathbb{N}$. The coefficients $K_n(\ell, s)$ are related to generalized Bessel functions (see e.g. [Löt08, Löt09c]). The Volkov wave function in an infinite plane wave appears as an infinite sum over discrete levels

$$E_p(x) = \sum_{\ell=-\infty}^{\infty} e^{-i(q+\ell k)\cdot x} \mathcal{E}_p^{\text{IPW}}(\ell) \tag{2.75}$$

with momentum $q + \ell k$ which are called Zel'dovich levels [Zel67], see Figure 2.7. Furthermore, the level structure furnishes an easy interpretation of strong-field phenomena such as the appearance of harmonics or resonant singularities in second-order strong-field scattering processes (such as two-photon Compton scattering dealt within Chapter 4). Modifications of this level structure due to radiative corrections have been calculated in [Bec76].

There is a major difference between an IPW and a PPW: The sum over the Zel'dovich levels $\ell$ in Eq. (2.75) for an IPW is replaced by an integral in a PPW, i.e. in a pulsed field, the amount of energy absorbed from the laser field is not an integer multiple of the central laser frequency $\omega$, as for an IPW, but can take any value as does the numbers of photons $s$ exchanged with the laser field. Furthermore, the quasi-momentum $q^\mu$ which is present for infinite plane waves does not play any role for pulsed laser fields. The build-up of quasi-momentum is intrinsically related to the absorption of the Fourier-zero mode of the non-linear phase $f_p$ into a redefinition of momentum, as discussed in Section 2.1 for the equivalent in the classical theory.

The momentum space structure of the Volkov state in a PPW laser field is exhibited in Figure 2.8, where the modulus of the function $\mathscr{K}_+(s)$ is exhibited for different pulse shapes. In certain cases the structure of the functions $\mathscr{K}_n(s)$ resembles broadened Zel'dovich levels. Two mechanisms for the broadening of the levels appear: (1) short lasers have a bandwidth $\propto 1/\Delta\phi$, where $\Delta\phi$ is the pulse length parameter, due to Fourier's theorem and (2) a ponderomotive broadening happens, where a non-constant amplitude of the laser field leads to a broadening of the levels. The ponderomotive broadening is a combined non-linear
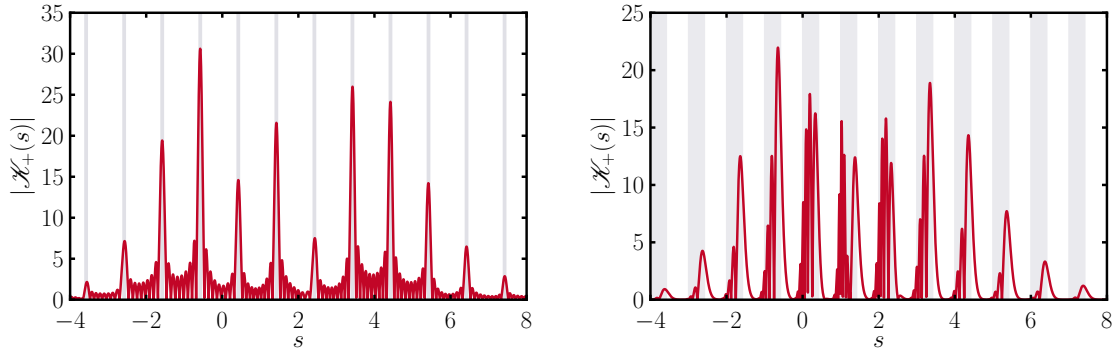
**Figure 2.8:** The momentum mode occupation number $\mathscr{K}_+(s)$ of a Volkov state in a PPW as a function of the photon number $s$ for a box-shaped pulse (left panel) and a Gaussian envelope (right panel). The structure of $\mathscr{K}_+(s)$ for a PPW can be interpreted as a broadening of Zel'dovich levels. The parameters are $a_0 = 1$, $m\gamma = 50$ GeV and $\theta = 2/\gamma$.
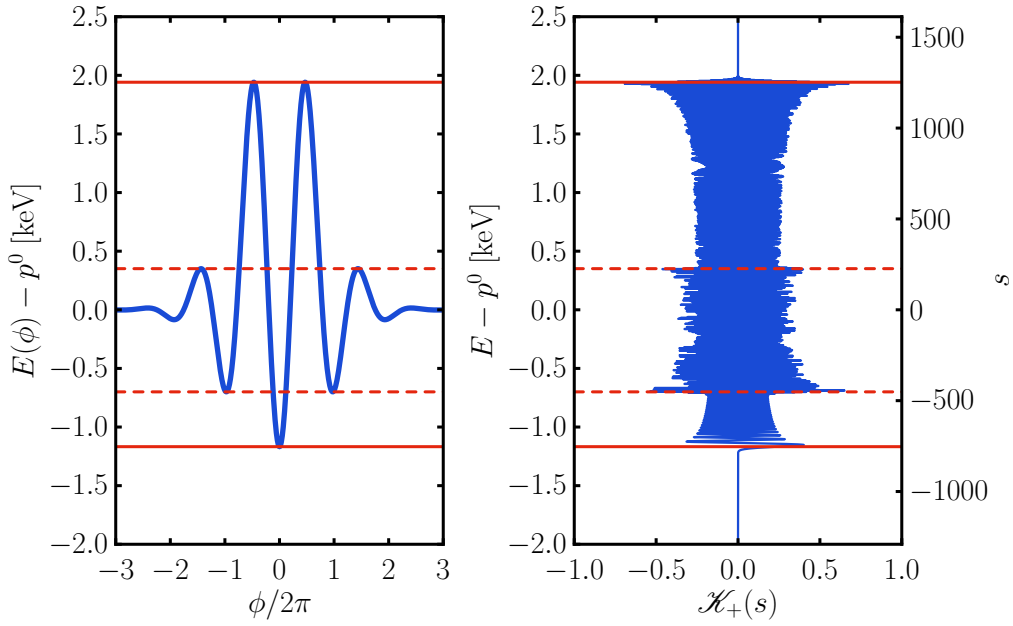


**Figure 2.9:** The energy along the classical trajectory of an electron in a short laser pulse as a function of the laser phase $\phi$ (left panel) is compared to the momentum mode occupation numbers $\mathscr{K}_+(s)$ of the Volkov state in the same pulse (right panel). The circularly polarized laser pulse has a Gaussian envelope with pulse length $\Delta\phi = 5$, $a_0 = 1$ and propagates along the negative $z$ axis. The asymptotic energy of the electron is $p^0 = 100\,m$ and the angle between the electrons initial momentum and the $z$ axis is $\theta = 1/\gamma$. The right panel corresponds to Figure 2.8 but with interchanged axes.

short-pulse effect. The width $\Delta s$ of a broadened Zel'dovich level due to the ponderomotive broadening effect (2) is $\beta_p$. Individual levels can be resolved as long as the combined effect of (1) and (2) is smaller than the level spacing, i.e. for $|1/\Delta\phi| + |\beta_p| < 1$. In most cases, however,

the parameter $\beta_p$ will be larger than unity such that the individual levels overlap, forming a continuous distribution with irregular peak structure. In Figure 2.8, the parameters are tuned to special values so that the individual broadened levels can be resolved. In the left panel of Figure 2.8, the pulse has a box-shaped envelope $g(\phi) = \sqcap(\phi)$ [see Eq. (A.34) in Appendix A.3] with constant amplitude and $\Delta\phi = 30$ such that there is no ponderomotive broadening in this case. The small side peaks are due to the non-smoothness of the pulse envelope. The width of the main peaks is $\Delta s \propto 1/\Delta\phi \approx 1/30$, indicated by grey shaded areas.[11]  In the right panel of Figure 2.8, a Gaussian envelope $g(\phi) = \exp\{-\phi^2/2\Delta\phi^2\}$ with the same pule length $\Delta\phi = 30$ was used. In addition to the broadening due to the frequency bandwidth in a pulse, the ponderomotive broadening is relevant here with parameters adjusted such that $\beta_p = 0.42$ and the total width of the levels is $\Delta s \simeq 0.45$. The broadened Zel'dovich levels are indicated as grey shaded areas in both panels of Figure 2.8.

The momentum mode occupation numbers $\mathscr{K}_n(s)$ of a Volkov state describing the electron propagation in a laser pulse have a close relation to the properties of the classical trajectory of an electron in the same laser pulse. It is known that the lowest and highest possible values of the energy $E$ along the classical trajectory determine the lowest and highest possible values of $s$ beyond which the functions $\mathscr{K}_n(s)$ drop to zero exponentially fast [Löt08, Löt09c]. The relation between photon number $s$ and energy $E$ is given by $E = p^0 + s\omega$, where $p^0 = m\gamma$ denotes the asymptotic energy, i.e. the initial value for $E(\phi)$ outside of the laser pulse, $p^0 = E(-\infty)$. The energy along a classical trajectory is exhibited in the left panel of Figure 2.9 and compared to the Volkov state occupation numbers $\mathscr{K}_+(s)$ in the right panel. The minimum and maximum energy along the trajectory are indicated by red solid lines. It is found that in a smooth laser pulse, also the local minima and maxima of the energy $E(\phi)$ that appear during the course of the pulse lead to pronounced structures in the Volkov state occupation numbers, e.g. in $\mathscr{K}_+(s)$. These local extremal points are depicted by red dashed lines in Figure 2.9.

This result concludes the study of the Volkov wave functions, which will be used in the following chapters as initial and final state wave functions to calculate $S$ matrix elements for non-linear one-photon and two-photon Compton scattering in intense and short laser pulses.

## 2.9   The laser-dressed Green's function

Similar to the Lippmann-Schwinger equation (2.56) for the Volkov states, there exists a Dyson-Schwinger equation for the laser dressed electron propagator

$$\mathcal{G}(x, y|A) = G_0(x - y) + \int d^4z\, G_0(x - z)e\slashed{A}(z)\mathcal{G}(z, x|A) \,, \tag{2.76}$$

where $A_\mu$ is the plane wave laser background field and $G_0$ is the free electron propagator. The solution $\mathcal{G}(x, y|A)$, which includes the interaction with the laser field non-perturbatively to all orders, is called Dirac-Volkov propagator. Several different representations of $\mathcal{G}(x, y|A)$ propagator are known, see e.g. [Ebe66, Bro64, Kib75, Baĭ75, Baĭ76, Mit75, Rit85]. For the calculation of tree level amplitudes the representation [Rit85]

$$\mathcal{G}(x, x'|A) = \int \frac{d^4P}{(2\pi)^4} E_P(x)G_0(P)\bar{E}_P(x') \,. \tag{2.77}$$

with the Volkov matrix functions $E_p$ is most suitable and will be used throughout this thesis. The limit of a vanishing laser field, $A_\mu \to 0$, gives the correct free electron propagator in

---

[11]Note that in a box-shaped pulse the main peaks are located at positions corresponding to the quasi-momentum $q$.

coordinate representation as the Fourier transformation

$$G_0(x - x') = \int \frac{d^4P}{(2\pi)^4} G_0(P) e^{-iP \cdot (x-x')} \tag{2.78}$$

due to the weak-field limit of the Volkov matrix functions $E_p(x) \to e^{-ip \cdot x}$.

The properties of the propagator (2.77) are determined to a large extent by the plane-wave background field. Since the background field depends only on the light-front variable $\phi$, one singles out the corresponding light-front integrals when calculating the Fourier transform of (2.77) or $S$ matrix elements where one has to integrate over $d^4x$ at each vertex (see Chapter 4 for the application to two-photon Compton scattering). The Fourier transform of the propagator is defined by[12]

$$\mathcal{G}(p, p'|A) = \int \frac{d^4P}{(2\pi)^4} d^4x \, d^4x' \, e^{ip \cdot x} E_P(x) G_0(P) \bar{E}_P(x') e^{-ip' \cdot x'} \,. \tag{2.79}$$

Using the spectral representation of the Volkov matrices, which explicitly emphasizes the dependence on the light-front coordinate $\phi$,

$$E_p(x) = \int \frac{ds \, d\phi}{2\pi} e^{-i(p+sk) \cdot x + is\phi} \Omega_p(\phi) \,, \tag{2.80}$$

$$\Omega_p(\phi) = \left(1 + \frac{e}{2k \cdot p} \slashed{k} \slashed{A}(\phi)\right) e^{-if_p(\phi)} \,. \tag{2.81}$$

one arrives at the intermediate result[13]

$$\mathcal{G}(p, p'|A) = (2\pi)^2 \int ds \, ds' d\phi \, d\phi' \delta^4(p' - p - s'k) e^{is(\phi-\phi')} e^{-is'\phi'}$$
$$\times \Omega_p(\phi) G_0(p - sk) \bar{\Omega}_p(\phi') \tag{2.82}$$

$$= (2\pi)^2 \int ds \, ds' d\phi \, d\phi' \delta^4(p' - p - s'k) e^{is(\phi-\phi')} e^{-is'\phi'}$$
$$\times \frac{\Omega_p(\phi)[\slashed{p} - s\slashed{k} + m]\bar{\Omega}_p(\phi')}{(p - sk)^2 - m^2 + i0^+} \,, \tag{2.83}$$

where only light-front integrals remain and all trivial transverse integrations have been carried out. Thus, the plane-wave background singles out the light-front momentum integrals over the propagator momentum instead of the usual time component in the instant time formulation of field theory. The integral over $s'$ is trivial due to the $\delta$ distribution, but the integral over $s$ has to be taken carefully. Since $k$ is a light-like momentum with $k^2 = 0$, the propagator denominator is linear in $s$:

$$\frac{1}{(p - sk)^2 - m^2 + i0^+} = -\frac{1}{2k \cdot p} \frac{1}{s - s_0 - i0_s^+} = -\frac{1}{k^- p^+} \frac{1}{s - s_0 - i0_s^+} \tag{2.84}$$

with the definitions of the pole position $s_0 = (p^2 - m^2)/(2k \cdot p)$ and the infinitesimal $0_s^+ = \text{sign}(k \cdot p) 0^+$. The position of the single first-order propagator pole $s = s_0 + i0_s^+$ in the complex $s$ plane depends on the sign of $k \cdot p = p^+ k^-/2$.[14] The two possibilities correspond to the propagation of particles (for $p^+ > 0$) and antiparticles (for $p^+ < 0$), which are

---

[12]Note the sign convention for $p'$ and $p$ corresponding to incoming and outgoing momenta, respectively.

[13]It can be shown easily by a direct calculation that $\Omega_{p-sk}(\phi) = \Omega_p(\phi)$ since $\Omega_p$ depends only on the components $p^+$ and $\boldsymbol{p}^\perp$.

[14]Note that $k^- = 2\omega > 0$ is the only non-vanishing component of the light-like laser four-momentum $k$ with $k^2 = k^+ k^- - \boldsymbol{k}_\perp^2 = 0$.
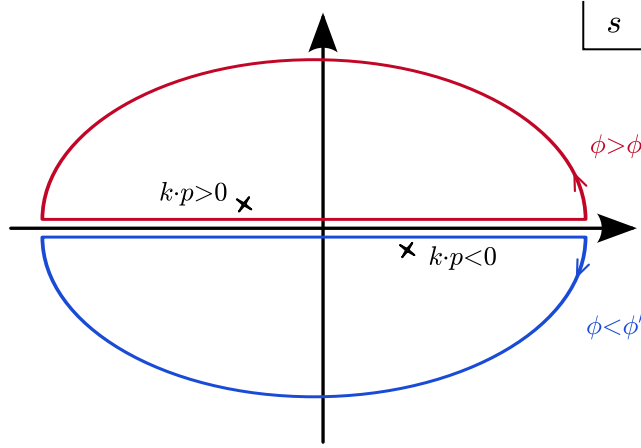
**Figure 2.10:** Contour integration over the pole structure of the Dirac Volkov propagator, introducing an ordering in the laser phase.

both described by the same propagator pole. This is different as compared to the usual *instant time* formalism where propagators possess two distinct poles which describe the propagation of particles and antiparticles on the positive and negative mass shells $p^0 = \pm\sqrt{\boldsymbol{p}^2 + m^2}$. Here, the two contributions from particles and antiparticles from the same propagator pole are separated by a divergence at $p^+ = 0$ in the prefactor of the $s$ integral [Hei07]. Taking into account also the $s$ dependence numerator of (2.83) one sees that, in contrast to the the instant time formulation, the integrand does not go to zero as $s \to \infty$. Before performing the pole integration one has to transform the integrand according to

$$\frac{\not{p} - s\not{k} + m}{s - s_0 - i0_s^+} = \frac{\not{p} - s_0\not{k} + m}{s - s_0 - i0_s^+} - \not{k} \,, \tag{2.85}$$

giving rise to the decomposition of the propagator $\mathcal{G} = \mathcal{G}_{\mathrm{T}} + \mathcal{G}_{\mathrm{Z}}$. The last term is the instantaneous zero-mode propagator

$$\mathcal{G}_{\mathrm{Z}}(p, p'|A) = (2\pi)^3 \frac{1}{2k \cdot p} \int ds'\delta^4(p' - p - s'k) \int d\phi e^{-is'\phi}\Omega_p(\phi)\not{k}\bar{\Omega}_p(\phi)\,. \tag{2.86}$$

The integration over $s$ in the first term of (2.85) is done by employing the residue theorem after closing the contour in the appropriate upper or lower half of the complex $s$ plane, depending on the sign of $\phi' - \phi$, such that the contribution from the arc at infinity vanishes (see Figure 2.10). The result reads

$$\int ds \frac{e^{is(\phi-\phi')}}{s - s_0 - i0_s^+} = 2\pi i\Big[\Theta(k \cdot p)\Theta(\phi - \phi') - \Theta(-k \cdot p)\Theta(\phi' - \phi)\Big]e^{i(s_0+i0_s^+)(\phi-\phi')}\,. \tag{2.87}$$

The contour integration introduced a light-front time ordering in the variables $\phi$ and $\phi'$, depending on the sign of $p^+$. Thus, modes with $p^+ < 0$ are propagated backwards in time. The time ordered part of the propagator reads

$$\mathcal{G}_{\mathrm{T}}(p, p'|A) = -(2\pi)^3 \frac{i}{2k \cdot p} \int ds'\delta^4(p' - p - s'k)$$
$$\times \int d\boldsymbol{\Phi} e^{-is'\phi'} e^{i(s_0+i0_s^+)(\phi-\phi')}\Omega_p(\phi)(\not{p} - s_0\not{k} + m)\bar{\Omega}_p(\phi') \tag{2.88}$$

with the integration measure $d\mathbf{\Phi} = d\phi d\phi'[\Theta(k \cdot p)\Theta(\phi - \phi') - \Theta(-k \cdot p)\Theta(\phi' - \phi)]$.

It is instructive to extract the free field limit of these expressions. In the limit $A_\mu \to 0$, one has $\Omega_p \to 1$, thus

$$G_{0,\mathrm{Z}}(p,p') = (2\pi)^4 \delta^4(p' - p) \frac{\slashed{k}}{2k \cdot p} \,, \tag{2.89}$$

$$G_{0,\mathrm{T}}(p,p') = (2\pi)^4 \delta^4(p' - p) \frac{\slashed{p} - s_0\slashed{k} + m}{p^2 - m^2 + i0^+} \,. \tag{2.90}$$

The combined result is

$$G_0(p,p') = (2\pi)^4 \delta(p - p') \frac{\slashed{p} + m}{p^2 - m^2 + i0^+} \,, \tag{2.91}$$

which is the correct free electron propagator.

To calculate the Dirac-Volkov propagator in an IPW laser field, $g \to 1$, in momentum space (2.79), one utilizes the periodicity of the oscillating parts of the non-linear phase exponential, which allows to write the Volkov matrix functions $E_p(x)$ as a discrete sum (2.75). Hence, with the quasi-momentum $Q = P + \beta_P k$,

$$\mathcal{G}^{\mathrm{IPW}}(p,p'|A) = \sum_{n,\ell=-\infty}^{\infty} \int d^4x d^4y \frac{d^4P}{(2\pi)^4} e^{i(p-Q-\ell k) \cdot x} e^{-i(p'-Q-nk) \cdot x'}$$
$$\times \mathcal{E}_P^{\mathrm{IPW}}(\ell) G_0(P) \bar{\mathcal{E}}_P^{\mathrm{IPW}}(n) \,. \tag{2.92}$$

The spacetime and momentum integrations provide the momentum conservation delta distribution and fix the propagator momentum $P = q - \ell k$. As result, the Dirac-Volkov propagator in an IPW laser field reads

$$\mathcal{G}(p,p'|A) = (2\pi)^4 \sum_{n,\ell=-\infty}^{\infty} \delta^4(p - p' - nk) \frac{\mathcal{E}_p^{\mathrm{IPW}}(\ell)(\slashed{p} - \ell\slashed{k} - \beta_p\slashed{k} + m)\bar{\mathcal{E}}_p^{\mathrm{IPW}}(n - \ell)}{(q - \ell k)^2 - m_\star^2 + i0^+}$$
$$\tag{2.93}$$

with $q = p + \beta_p k$. Note the equality $(p - \ell k - \beta_p k)^2 - m^2 = (p - \ell k + \beta_p k)^2 - m_\star^2$.

In an IPW laser field, the Dirac-Volkov propagator has an infinite series of poles in the complex $q^-$ plane below (above) the real axis for $p^+ > 0$ ($p^+ < 0$), with the pole positions given by $(q - \ell k)^2 - m_\star^2$, which yields the dispersion relations $q^- = (\boldsymbol{p}_\perp^2 + m_\star^2)/p^+ + \ell k^-$ for the various values of $\ell \in \mathbb{N}$. In contrast, in a PPW laser field there is always only a single pole at the free particle dispersion relation, $p^- = (\boldsymbol{p}_\perp^2 + m^2)/p^+$. The pole structure of the Fourier transformed propagator is strongly related to the Zel'dovich quasi-levels [Bec76]. The poles lead to the appearance of Oleinik resonance singularities in second-order strong-field processes. In the case of a finite PPW, instead of poles the Dirac-Volkov propagator has a resonance behaviour in the vicinity of the IPW poles.

# 3

# One-photon Compton scattering

T HE physical situation which is described here is the collision of a relativistic electron with a strong and short laser pulse. The electron $e$ with momentum $p$ interacts with the photons in the laser pulse and emits a single photon $\gamma$ with momentum $k'$ in the reaction

$$e(p) + \text{laser} \rightarrow e(p') + \text{laser} + \gamma(k')\,, \tag{3.1}$$

where in line with the assumption of a strong laser pulse described as a background field, the laser pulse is considered to be the same in the initial and final state. The strength of the laser pulse is characterized by the invariant laser strength parameter $a_0$. Strong laser fields imply that $a_0$ is of the order of unity or larger. In this regime, the interaction is inherently a multi-photon process, i.e. the electron interacts with many photons of the laser pulse simultaneously. The interaction of the electrons with the laser is treated exactly on the tree level and non-perturbatively by adopting the Furry picture and working with Volkov states which were discussed in Chapter 2. In the language of dressed electrons, the one-photon Compton process is the decay of a laser dressed electron state $e_V$ as

$$e_V(p) \rightarrow e_V(p') + \gamma(k')\,. \tag{3.2}$$

The Feynman diagram corresponding to this reaction is exhibited in Figure 3.1, where the Volkov electron states are depicted as double lines. In the literature, this process is also denoted as non-linear Compton scattering, high-intensity Compton scattering (HICS) or multi-photon Compton scattering. In this thesis, the notion one-photon Compton scattering will be the preferred wording to make the contrast to the two-photon Compton process, where two photons are emitted simultaneously. The two-photon Compton process is discussed in Chapter 4.

## 3.1   Introductory remarks

Present day high-intensity lasers are mostly short pulse lasers with pulse lengths of a few femtoseconds or tens of femtoseconds. For optical lasers with a wavelength of $\lambda = 800$ nm, i.e. a laser frequency of $\omega = 1.55$ eV, this corresponds to a dimensionless pulse length on the order of $\Delta\phi = 1 \ldots 50$. Presently, values of $a_0$ up to $a_0 = 100$ [Yan08] can be achieved in an experiment by a suitable focusing of the laser. With the prospect of the upcoming laser facilities, such as ELI, one can expect that the achievable peak value of $a_0$ will increase in the near future.
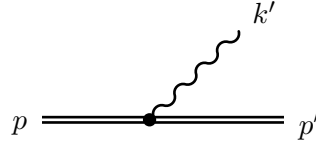
**Figure 3.1:** The Feynman diagram for non-linear one-photon Compton scattering. In strong-field QED, the one-photon Compton scattering appears as the decay of a laser dressed Volkov electron state (straight double lines) with momentum $p$ into another laser dressed electron with momentum $p'$ while emitting a photon (wavy line) with momentum $k'$. This process is of first order in perturbation theory (above the interaction with the background field).

The transition to the classical Thomson limit is obtained when the parameter $\varrho$, as defined in Eq. (1.11), which is the laser frequency measured in the rest frame of the electron in units of the electron mass $m$, is much smaller than unity. Hence, quantum effects scale with the parameter $\varrho$ in the case of $a_0 \ll 1$. In the opposite case of $a_0 \gg 1$, non-linear quantum effects have been shown to scale with the parameter [Rit85]

$$\chi_p = \frac{e}{m^3} \sqrt{(F_{\mu\nu}p^\nu)^2} \,. \tag{3.3}$$

Non-linear, strong-field quantum effects are supposed to become important as $\chi_p \sim 1$ approaches unity. These three parameters are related as $\chi_p = a_0 \varrho$ [Hei10b].

Thus, the non-linear quantum effects where $\chi_p \sim 1$ can be reached in various ways. Either a multi-GeV electron beam with $\varrho \sim 1$ is brought into collision with an optical high-intensity laser with $a_0 \sim 1$. This scenario was exploited in the SLAC E-144 experiment, where $\varrho = 0.82$, $a_0 = 0.45$ such that $\chi_p = 0.37$ [Bam99].[1] The FACET project [FAC] at SLAC envisages investigations with electron beams with energies of 20 GeV, where the non-linear quantum regime $\chi_p \sim 1$ could be achieved with a value of $a_0 \sim 4$. Nowadays, various lasers are available with $a_0 \gg 1$, such that the non-linear quantum regime $\chi_p \sim 1$ can be achieved already with much lower electron energies. For instance, with 1 GeV laser accelerated electrons [Lee06] it is possible to reach the non-linear quantum regime with a value of $a_0 \sim 100$ [Yan08]. However, not only the regime $\chi_p \sim 1$ is interesting, but also $\chi_p \ll 1$ and $a_0 \gtrsim 1$ provides interesting physics, considering the impact of short pulse effects on the non-linear Compton spectra. The operation of high-power lasers with high repetition rate allows for a paradigm shift in the strong-field experiments: It becomes possible to perform high-precision and high-statistics experiments with this new generation of lasers in combination with suitable electron sources, which could either be classical electron accelerators or laser accelerated electrons. Higher precision can be achieved by employing a weaker focusing such that the spatial volume where the intensity reaches the non-linear regime is very large. In such a set-up, the field invariants related to field gradients are much smaller and the validity of the assumption of null-fields, i.e. the vanishing of all field invariants will be a much better description for these experiments according to (1.9).

## 3.2   Calculation of the matrix element

The interaction of a laser dressed electron with photon modes different from the laser field are treated by perturbative $S$ matrix expansion. In particular for one-photon emission, the Born

---

[1]The values presented here differ by the values given in the reference by a factor of $\sqrt{2}$ which is related to the fact that in [Bam99] averaged values are employed while peak values are used in this thesis.

approximation of the matrix element is depicted in Figure 3.1. Within the Furry picture, this process describes the decay of a quasi-particle Volkov electron. The scattering nature of the process is highlighted when the quasi-particle states are expanded in powers of the background field and free electron states (see Appendix C.1). Using the Feynman rules of strong-field QED in the Furry picture from Section 2.3 (cf. also [Mit75]), the $S$ matrix element for this process is given by

$$S = \langle \boldsymbol{p}'r'; \boldsymbol{k}'\lambda'|\hat{S}[A]|\boldsymbol{p}r\rangle = -ie \int d^4x \, \bar{\Psi}_{p',r'}(x) e^{ik'\cdot x} \slashed{\epsilon}'^*_{(\lambda')} \Psi_{p,r}(x)\,, \tag{3.4}$$

where electron spin $(r, r')$ and photon polarization indices $(\lambda')$ are suppressed from now on. The integral expression on the right hand side can also be deduced from the matrix element $S = \langle \boldsymbol{p}'r'; \boldsymbol{k}', \lambda'|\hat{S}[A]|\boldsymbol{p}r\rangle$ via the reduction method presented in Appendix A.7. Since the Volkov states have a privileged dependence on the laser phase $\phi$ via the background field $A_\mu(\phi)$, the spatial integrations are conveniently performed in light-front coordinates with $d^4x = d\phi\, dx^- d^2\boldsymbol{x}^\perp/k^-$ yielding with the representation (2.42) of the Volkov wave functions

$$S = -ie \int d^4x \, \bar{u}_{p'} \bar{\Gamma}_{p'}(\phi) \slashed{\epsilon}'^* \Gamma_p(\phi) u_p \exp\{iS_p(\phi) - iS_{p'}(\phi) + ik'\cdot x\} \tag{3.5}$$

$$= -ie \frac{1}{k^-} \int d\phi\, d^2\boldsymbol{x}^\perp dx^- \, \bar{u}_{p'} \bar{\Gamma}_{p'}(\phi) \slashed{\epsilon}'^* \Gamma_p(\phi) u_p \exp\{i(k'+p'-p)\cdot x - if(\phi)\} \tag{3.6}$$

with the non-linear phase exponent $f = f_p - f_{p'}$ which reads

$$f(\phi) = \mathrm{Re}\left(\alpha_- \int\limits_0^\phi d\phi' g(\phi') e^{i(\phi'+\hat{\phi})}\right) + \beta \cos 2\xi \int\limits_0^\phi d\phi' g^2(\phi') \cos 2(\phi'+\hat{\phi})$$

$$+ \beta \int\limits_0^\phi d\phi' g^2(\phi')\,, \tag{3.7}$$

having defined the coefficients

$$\alpha_i = \alpha_{p,i} - \alpha_{p',i} = ma_0\left(\frac{\epsilon_i\cdot p}{k\cdot p} - \frac{\epsilon_i\cdot p'}{k\cdot p'}\right)\,, \qquad i \in \{1, 2, +, -\}\,, \tag{3.8}$$

$$\beta = \beta_p - \beta_{p'} = \frac{m^2 a_0^2}{4}\left(\frac{1}{k\cdot p} - \frac{1}{k\cdot p'}\right)\,. \tag{3.9}$$

In a situation, where ultrarelativistic electrons are scattered off a counterpropagating laser pulse, these parameters are of the order of $\alpha_i \sim a_0$ and $\beta \sim a_0^2$. The first line in (3.7) collects all oscillating parts of the non-linear phase exponent, which will be denoted as $\tilde{f}$ in the following, and the second line is denoted as ponderomotive part with the definition $\beta G_2 = \beta \int d\phi g^2(\phi)$ for later use. The ponderomotive part depends only on the time scale of the pulse envelope, which is given by the pulse length parameter $\Delta\phi$; it does neither depend on the polarization of the carrier wave $\xi$ nor on the carrier envelope phase $\hat{\phi}$, as does the oscillating part $\tilde{f}(\phi)$. For the precise definitions of $\xi$ and $\hat{\phi}$ see Appendix A.3. The first term in the first line of (3.7) can be evaluated as

$$\mathrm{Re}\left(\alpha_- \int\limits_0^\phi d\phi' g(\phi') e^{i(\phi'+\hat{\phi})}\right)$$

$$= \alpha_1 \cos\xi \int\limits_0^\phi d\phi' g(\phi') \cos(\phi'+\hat{\phi}) + \alpha_2 \sin\xi \int\limits_0^\phi d\phi' g(\phi') \sin(\phi'+\hat{\phi})\,. \tag{3.10}$$

Picking up the idea of the phase shift of the Volkov wave functions when going from $\phi = -\infty$ to $\phi = \infty$ from Chapter 2, one sees that the non-linear Compton matrix element accumulates a phase shift $\Delta f = f(\infty) - f(-\infty) = \Delta f_p - \Delta f_{p'}$, which is the difference of the phase shifts of the incoming and outgoing electron wave functions, where possible large contributions of $\Delta f_p$ and $\Delta f_{p'}$ may cancel. The same happens for the parameters $\alpha_i$ and $\beta$, where the possibly large contributions from the Volkov wave functions $\alpha_{i,p}, \ \alpha_{i,p'} \sim a_0 m / \omega_\star$ and $\beta_p, \ \beta_{p'} \sim a_0^2 m / \omega_\star$ cancel to yield the order of magnitude estimate $\alpha_i \sim a_0 s$ and $\beta \sim a_0^2 s$ (for the definition of $s$ see below). The dependence of the $S$ matrix in Eq. (3.6) on the spatial coordinates $x^1, x^2$ and $x^-$ is trivial and the corresponding integrations can be done immediately, yielding delta distributions which represent the conservation of the $\boldsymbol{p}^\perp$ and $p^+$ components of momentum via

$$
\begin{aligned}
\int dx^- d^2 \boldsymbol{x}^\perp & e^{i \frac{x^-}{2}(p'^+ + k'^+ - p^+)} e^{-i \boldsymbol{x}^\perp \cdot (\boldsymbol{p}'^\perp + \boldsymbol{k}'^\perp - \boldsymbol{p}^\perp)} \\
&= 2(2\pi)^3 \delta^2(\boldsymbol{p}^\perp - \boldsymbol{p}'^\perp - \boldsymbol{k}'^\perp) \delta(p^+ - p'^+ - k'^+) \\
&\equiv 2(2\pi)^3 \delta^3(\mathsf{p} - \mathsf{p}' - \mathsf{k}'),
\end{aligned}
\tag{3.11}
$$

where $\mathsf{p} \equiv (p^+, \boldsymbol{p})$ is an abbreviation for the three transverse momentum components with respect to the laser four-vector $k^\mu$. The remaining integration over the laser phase $\phi$ in

$$
\begin{aligned}
S = -ie(2\pi)^3 \delta^3(\mathsf{p} - \mathsf{p}' - \mathsf{k}') \frac{2}{k^-} \int d\phi \, \exp\{is\phi - if(\phi)\} \Big\{ \mathscr{T}_0 \\
+ g(\phi) \, e^{i(\phi+\hat\phi)} \mathscr{T}_- + g(\phi) \, e^{-i(\phi+\hat\phi)} \mathscr{T}_+ + g^2(\phi) \left[1 + \cos 2\xi \cos 2(\phi + \hat\phi)\right] \mathscr{T}_2 \Big\}
\end{aligned}
\tag{3.12}
$$

can not be done analytically in general due to the non-linearities in the exponent. To arrive at (3.12), the electron current factors $\mathscr{T}_n$ have been introduced:

$$
\mathscr{T}_0 = \bar{u}_{p'} \not{\epsilon}'^* u_p,
\tag{3.13}
$$

$$
\mathscr{T}_\pm = \bar{u}_{p'} \left( d_{p'} \not{\epsilon}_\pm \not{k} \not{\epsilon}'^* + d_p \not{\epsilon}'^* \not{k} \not{\epsilon}_\pm \right) u_p,
\tag{3.14}
$$

$$
\mathscr{T}_2 = 4(k \cdot \epsilon'^*) d_p d_{p'} \, \bar{u}_{p'} \not{k} u_p,
\tag{3.15}
$$

with $d_p = m a_0 / (4 \, k \cdot p)$ and $d_{p'} = m a_0 / (4 \, k \cdot p')$. Without the non-linear $\phi$ dependence in $f(\phi)$, Eq. (3.12) would contain the Fourier transforms of the pulse envelope $g$ and $g^2$ where the conjugate variable to the phase $\phi$ is $s$ defined by

$$
s \equiv \frac{k'^- + p'^- - p^-}{k^-} = \frac{k' \cdot p}{k \cdot p'}.
\tag{3.16}
$$

The last equality shows that $s$ is a Lorentz invariant quantity. It might be interpreted as a continuous number of absorbed photons from the laser pulse, as advocated e.g. in [Sei11b, Ild11a]. The reasoning is based on the fact that the energy-momentum conservation can be written compactly in the suggestive form

$$
p + sk = p' + k'.
\tag{3.17}
$$

Alongside this interpretation in terms of photons, $s$ is the value of exchanged momentum between the electron current and the background laser field $A^\mu$ in units of the central laser momentum $k$. Since the frequency $\omega'$ of the emitted photon has to be positive, also $s$ has to be positive. The condition $\omega' = 0$ would imply $s = 0$, i.e. the physical phase space is restricted to $s > 0$ or $\omega' > 0$. The relation between $\omega'$ and $s$ is

$$
\omega'(s) = \frac{s k \cdot p}{(p + sk) \cdot n'},
\tag{3.18}
$$

where $k' = \omega' n'$ with $n' = (1, \cos\varphi\sin\theta, \sin\varphi\sin\theta, \cos\theta)$. This means, either $s$ or $\omega'$ can be considered as independent variable, fixing the other one as $\omega' = \omega'(s)$ or $s = s(\omega')$. In either way the number of degrees of freedom of the final state phase space is three, often chosen to be the two angles $\theta$, $\varphi$ defining the direction of $n'$ and either $\omega'$ or $s$. In this thesis, $\omega'$ will be considered as the independent variable whenever possible since it is directly observable, while $s$ is not. With the additional definitions of the phase integrals

$$\begin{Bmatrix} \mathscr{A}_0(s) \\ \mathscr{A}_\pm(s) \\ \mathscr{A}_2(s) \end{Bmatrix} = \int\limits_{-\infty}^{\infty} d\phi \exp\{is\phi - if(\phi)\} \begin{Bmatrix} 1 \\ g(\phi)e^{\mp i(\phi+\hat\phi)} \\ g^2(\phi)\big[1 + \cos 2\xi \cos 2(\phi + \hat\phi)\big] \end{Bmatrix}, \tag{3.19}$$

the $S$ matrix element can be written as

$$S = -ie(2\pi)^3 \frac{2}{k^-}\delta^3(\mathsf{k}' + \mathsf{p}' - \mathsf{p})\mathscr{M}(s) \tag{3.20}$$

with the amplitude

$$\mathscr{M}(s) = \mathscr{T}_0\mathscr{A}_0(s) + \mathscr{T}_+\mathscr{A}_+(s) + \mathscr{T}_-\mathscr{A}_-(s) + \mathscr{T}_2\mathscr{A}_2(s). \tag{3.21}$$

What was accomplished by now is that the complete dependence on the laser pulse has been included into the phase integrals $\mathscr{A}_n(s)$ which have been separated from the electron current terms $\mathscr{T}_n$. The integrands of the phase integrals are scalar functions. All Dirac matrix structures have been extracted from the integrals. The evaluation of the phase integrals $\mathscr{A}_n(s)$ is the challenging part of the calculation of strong-field processes. While for IPW there do exist expansions of these integrals in terms of (generalized) Bessel functions (see Eq. (C.18) in Appendix C.2), the situation is not so clear for general PPW. In this thesis, several complementary methods are presented for the evaluation of these integrals, including a direct numerical integration (Section 3.4), expansions into harmonics similar to IPW (Section 3.9) picking up ideas of [Nar96b], completely analytic evaluations in terms of sums of special functions for certain pulse envelopes (Section 3.11), and an approximative evaluation for $a_0 \gg 1$ using a stationary phase approximation (Section 3.12).

The representation (3.20) furnishes a proper starting point for such analytical, approximative or numerical calculations. The integrals $\mathscr{A}_{+,-,2}(s)$ are numerically convergent due to the presence of the pulse envelope function in the pre-exponential. The integral $\mathscr{A}_0(s)$, however, is an infinite integral over a pure phase and diverges. Hence, it must be regularized. A possible method has been proposed in [Boc09], where one multiplies the integrand with a convergence factor $e^{-\varepsilon|\phi|}$, $\varepsilon > 0$, and performs an integration by parts. The result, corresponding to adiabatically switching on and off the external field, is

$$\mathscr{A}_0(s) = 2\pi\delta(s) + \frac{1}{s}\int\limits_{-\infty}^{\infty} d\phi\frac{df}{d\phi}\exp\{is\phi - if(\phi)\}. \tag{3.22}$$

The divergence has been extracted as a delta distribution yielding a divergence at $\omega' = 0$. As for the Volkov wave function, the contribution $\propto \delta(s)$ is related to the free motion outside the laser pulse. The condition $s = 0$ means interaction with zero laser photons, i.e. no energy exchange but is excluded from the physical phase space as discussed above. The second part of (3.22) containing the derivative of $f$ is convergent. It can be shown that the derivative $df/d\phi$ vanishes as $s \to 0$ such that $s^{-1}df/d\phi < \infty$ in that limit. A different, physically motivated procedure to find a regularized version of $\mathscr{A}_0(s)$ is to rely on gauge invariance, as proposed in [Ild11b]. Performing a gauge transformation $\epsilon'_\mu \to \epsilon'_\mu + \Lambda k'_\mu$ of the matrix element $\mathscr{M}(s)$ with an arbitrary gauge parameter $\Lambda$, one finds the matrix element $\mathscr{M}(s)$ to

be gauge invariant if and only if the different phase integrals $\mathscr{A}_n(s)$ fulfil the relation (the details of the calculation can be found in Appendix D.1)

$$s\mathscr{A}_0(s) = \frac{1}{2}\alpha_+\mathscr{A}_+(s) + \frac{1}{2}\alpha_-\mathscr{A}_-(s) + \beta\mathscr{A}_2(s)\,. \tag{3.23}$$

Upon evaluating the derivative $df/d\phi$ in the integral in (3.22), it can be shown that (3.22) is equivalent to (3.23) as the singular term does not appear there, since $s\delta(s) = 0$. Both results coincide on the physical phase space for $s > 0$. The regularized version (3.23) of $\mathscr{A}_0$ will be used in the subsequent numeric calculations. Using the Fourier representation of the Volkov states (2.69), one can find additional representations of the phase integrals $\mathscr{A}_n$ by

$$\begin{aligned}
\mathscr{A}_0 &= \mathscr{K}_0^* \star \mathscr{K}_0\,,\\
\mathscr{A}_\pm &= \mathscr{K}_0^* \star \mathscr{K}_\pm = \mathscr{K}_\mp^* \star \mathscr{K}_0\,,\\
\mathscr{A}_2 &= \mathscr{K}_\pm^* \star \mathscr{K}_\pm + \tfrac{1}{2}\cos 2\xi(\mathscr{K}_\mp^* \star \mathscr{K}_\pm)\,,
\end{aligned} \tag{3.24}$$

with $\mathscr{K}_n(s)$ from (2.70) and the convolution integral

$$\mathscr{K}_n^* \star \mathscr{K}_m \equiv \int \frac{d\ell}{2\pi}\mathscr{K}_n^*(\ell)\mathscr{K}_m(\ell + s)\,. \tag{3.25}$$

This representation of the phase integrals furnishes an interpretation of the Compton amplitude as the overlap of incoming and outgoing Volkov wave functions in momentum space, which can be considered as the generalization of the transitions between Zel'dovich quasi-levels [Zel67] to the case of pulsed laser fields.

It is instructive to consider the limit of weak laser fields, for which $a_0 \ll 1$. To obtain the weak-field limit of the $S$ matrix element one has to expand the amplitude $\mathscr{M}(s)$ into a series in powers of $a_0$, keeping only the leading terms of order $a_0$. Counting the powers of $a_0$ in the different terms of $\mathscr{M}$,

$$\mathscr{M} = \mathscr{A}_+(s)\left[\mathscr{T}_+ + \frac{\alpha_+}{2s}\mathscr{T}_0\right] + \mathscr{A}_-(s)\left[\mathscr{T}_- + \frac{\alpha_-}{2s}\mathscr{T}_0\right] + \mathscr{A}_2(s)\left[\mathscr{T}_2 + \frac{\beta}{s}\mathscr{T}_0\right]\,, \tag{3.26}$$

one recognizes that $s, \mathscr{T}_0 \propto a_0^0$, $\alpha_i, \mathscr{T}_\pm \propto a_0$ and $\beta, \mathscr{T}_2 \propto a_0^2$, thus, the terms $\propto \mathscr{A}_2(s)$ do not contribute in the weak-field limit. Furthermore, the expression in the brackets are of order $a_0^1$ such that in the lowest non-vanishing order the integrals $\mathscr{A}_\pm$ need to be expanded up to the order $a_0^0$, yielding

$$\mathscr{A}_\pm(s) \overset{a_0\to 0}{\to} e^{\mp i\hat{\phi}}\int\limits_{-\infty}^{\infty} d\phi\, g(\phi)e^{i(s\mp 1)\phi} \equiv e^{\mp i\hat{\phi}}\tilde{\mathscr{A}}(s\mp 1)\,, \tag{3.27}$$

the (shifted) Fourier transform of the pulse envelope. The weak-field approximation of the non-linear Compton amplitude reads

$$\mathscr{M}(s) = \tilde{\mathscr{A}}(s-1)\left[\mathscr{T}_+ + \frac{\alpha_+}{2s}\mathscr{T}_0\right]e^{-i\hat{\phi}}\,. \tag{3.28}$$

The term associated to $\tilde{\mathscr{A}}(s+1)$ is maximal for $s = -1$ and corresponds to the emission of one photon into the laser mode alongside the emission of the photon $k'$ without the absorption of photons from the laser. This term does not contribute to the $S$ matrix for weak laser fields.

A more systematic discussion of the weak-field limit is presented in Appendix C.1, where the Lippmann-Schwinger equation (2.56) is used to find the general expansion of the Volkov states in powers of $a_0$. Higher order terms are discussed, and it is shown there, that the weak-field limit of the non-linear one-photon Compton $S$ matrix coincides with the usual perturbative $S$ matrix for Compton scattering which is presented in many textbooks, e.g. [Itz80] under the notion of Klein-Nishina formula.

## 3.3   Emission probability, energy spectrum and cross section

In the standard formalism, scattering experiments are thought of as constant streams of particles interacting. When calculating emission probabilities, one has to square the $S$ matrix which contains a divergent factor corresponding to the square of the energy momentum conservation and which is interpreted as the volume of spacetime $VT$ as[2]

$$[(2\pi)^4\delta^4(P_i - P_f)]^2 = (2\pi)^8\delta^4(P_i - P_f)\delta^4(0) \to (2\pi)^4 VT\delta(P_i - P_f)\,. \tag{3.29}$$

On the purpose of rendering this quantity finite, usually the differential rate $d\dot{W} \propto |S|^2/T$, being the reaction probability per unit time, is considered.

    When considering finite laser pulses, the interaction is happening only within a finite (light-front) time interval. Thus, the (differential) reaction probability is a finite number and there is no need for the definition of a rate. On the formal level, the square of the $S$ matrix gives the expression

$$|S|^2 = (2\pi)^3 e^2\delta^3(\mathsf{p}' + \mathsf{k}' - \mathsf{p})\,(2\pi)^3\delta^3(0)\left(\frac{2}{k^-}\right)^2|\mathscr{M}(s)|^2\,, \tag{3.30}$$

with the light-front delta distribution $\delta^3(0)$. Thus, one defines the differential emission probability of photons per incoming electron and per laser pulse, also termed as photon yield, by

$$dW = \frac{1}{2p^+}|S|^2 d\Pi\,. \tag{3.31}$$

The Lorentz invariant phase space element of the final particle states is given by

$$d\Pi = \frac{d^3\mathsf{p}'}{(2\pi)^3 2p'^+}\frac{d^3\boldsymbol{k}'}{(2\pi)^3 2\omega'}\,. \tag{3.32}$$

For the electron with momentum $p'$ in the exit channel, the on-shell light-front phase space element has been used for convenience since it integrates the light-front delta distribution easily. In (3.31) the prefactor $1/2p^+$ has to be used instead of the canonical $1/2p^0$ [Itz80] to cancel all factors of volume from the final expression for the emission probability to obtain a Lorentz invariant expression for the emission probability since $(2\pi)^3\delta^3(0) = Vp^0/p^+$ [Rit85]. The factor $p^0/p^+$ varies between 1 for $\gamma = 1$ and $1/2$ for $\gamma \to \infty$. In [Mac09] it is argued that the factor $p^0/p^+$ is needed to compensate for an overestimation of the interaction time if the usual normalization is employed. This, however, is just a reformulation of the above statement of Lorentz invariance. The differential emission probability is given by

$$\frac{d^2W(r, r', \lambda')}{d\omega' d\Omega} = \frac{e^2\omega'}{64\pi^3 k\cdot pk\cdot p'}|\mathscr{M}(s; r, r', \lambda')|^2\,, \tag{3.33}$$

noting the electron spin and photon polarization indices explicitly now. Averaging over the spin of the incoming electron and summing over the spin of the outgoing electron and the polarization of the outgoing photon yields

$$\frac{d^2W}{d\omega' d\Omega} = \frac{1}{2}\sum_{r,r'=\uparrow,\downarrow}\sum_{\lambda'}\frac{d^2W(r, r', \lambda')}{d\omega' d\Omega}\,. \tag{3.34}$$

---

[2]Note that the spatial quantization volume $V$ is in general set to unity and noted explicitly only here.

Here, the emission probability is differential in the emitted photon energy $\omega'$. Going over to the dimensionless variable $s$ as defined in (3.16) and by noting that the differential transforms as

$$d\omega' = \frac{\omega'}{s}\frac{k \cdot p'}{k \cdot p}ds \,, \tag{3.35}$$

one may cast the emission probability into the form depending on $s$ explicitly

$$\frac{d^2W}{dsd\Omega} = \frac{e^2\omega'(s)}{64\pi^3(k \cdot p)^2 s}|\mathscr{M}(s)|^2 \,, \tag{3.36}$$

and similar for the spin and polarization averaged probability.

The differential energy spectrum $dI$, i.e. the emitted energy per solid angle and frequency interval, is related to the emission probability by

$$\frac{dI}{d\omega'd\Omega} = \omega'\frac{dW}{d\omega'd\Omega} = \frac{e^2\omega'^2}{64\pi^3 k \cdot p\, k \cdot p'}|\mathscr{M}(s)|^2 \,. \tag{3.37}$$

To arrive at an invariant cross section, one has to divide Eq. (3.34) by the normalized integrated flux of photons $N_\perp$ (cf. Appendix A.3 for the exact definition) in the laser pulse,

$$\frac{d^2\sigma}{d\omega'd\Omega} = \frac{1}{N_\perp}\frac{d^2W}{d\omega'd\Omega} \,. \tag{3.38}$$

The quantity $N_\perp$ can be related to an invariant effective phase interval $\Delta\phi_{\text{eff}}$, which is defined in (A.44), as

$$N_\perp = \frac{a_0^2 m^2}{2e^2}\Delta\phi_{\text{eff}} \,, \tag{3.39}$$

showing that $N_\perp$ has the correct physical dimension of an inverse area. In general, the effective phase interval $\Delta\phi_{\text{eff}}(g, g', \xi, \hat{\phi})$, depends on the envelope $g$, its derivative $g'$, the laser polarization $\xi$ and the carrier envelope phase $\hat{\phi}$. For long pulses with $\Delta\phi \gg 1$, a suitable and fairly accurate approximation is (See also the discussion in Appendix A.3 and Figure A.1 therein; for practical purposes $\Delta\phi \geq 5$ is sufficient.)

$$\Delta\phi_{\text{eff}} = \int\limits_{-\infty}^{\infty} d\phi g(\phi)^2 \,. \tag{3.40}$$

Thus, the carrier envelope phase and polarization dependence of $\Delta\phi_{\text{eff}}$ reveals itself only in the limit of very short pulses. If the effective pulse length can be approximated by (3.40), then $\Delta\phi_{\text{eff}} = \nu_2[g]\Delta\phi$, where $\nu_2[g]$ is a pulse shape dependent quantity. Explicit values for $\nu_2[g]$ for various pulse shapes used in this thesis are summarized in Table A.1 in Appendix A.3. The definition of the cross section (3.38) corresponds to a normalization on the same amount of energy in the laser pulse per unit transverse area. Using this definition, the total cross section is independent of both the pulse shape function $g$ and the pulse length $\Delta\phi$ supposed the condition $\Delta\phi \gg 1$ is fulfilled.[3] This has been checked numerically for $a_0 \ll 1$ by a comparison of

$$\frac{d\sigma}{d\Omega} = \int d\omega' \frac{d^2\sigma}{d\omega'd\Omega} \tag{3.41}$$

---

[3]A different definition of the cross section without this property has been employed in [Boc09].
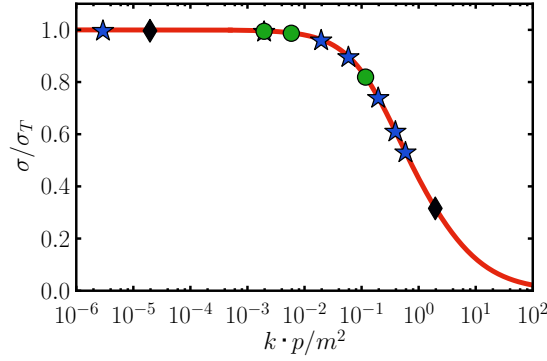
**Figure 3.2:** The total cross section for Compton scattering normalized to the Thomson cross section $\sigma_T$. Red curve: Klein-Nishina cross section. Symbols: numerically calculated cross section in a pulsed laser field with $a_0 = 0.001$ (blue stars: $\Delta\phi = 20$ for a hyperbolic secant pulse; green circles: $\Delta\phi = 30$ for a Gaussian pulse; black diamonds: $\Delta\phi = 100$ for a Gaussian pulse).

with the differential Klein-Nishina cross section [Ber80], or

$$\sigma = \int d\Omega \frac{d\sigma}{d\Omega} \tag{3.42}$$

with the total Klein-Nishina cross section. In particular, in the low energy limit the total Thomson cross section $\sigma_T = 665.25$ mb is obtained accurately, as exhibited in Figure 3.2 for different pulse shapes and pulse lengths.

## 3.4 Systematic numerical study of non-linear short pulse effects

After these formal developments, the focus will now turn to physics issues. As mentioned in the introductory remarks of this chapter, the experimental situation to be addressed is the collision of an ultrarelativistic electron with a counterpropagating laser pulse. (By a suitable Lorentz transformation this special kinematic situation of head-on collisions can be achieved.) The electron is characterized by the four-momentum $p^\mu$ with the energy $p^0 = m\gamma$ and the relativistic Lorentz factor $\gamma$. Alternatively, the electron energy can be formulated in terms of the rapidity $\zeta$ with $\gamma = \cosh\zeta$. Ultrarelativistic electrons have $\gamma, \zeta \gg 1$. To determine the photon emission probability explicitly, one has to evaluate the phase integrals $\mathscr{A}_n(s)$ defined in Eq. (3.19). One particular strategy involves a direct numerical integration of the $\mathscr{A}_n(s)$, where an adaptive Simpson integration method is used. Explicit representations of the Dirac spinors $u_p$ and $\bar{u}_{p'}$ [for details see Eqs. (A.75) and (A.76) in Appendix A.5] as well as of all four-vectors are implemented numerically for the Dirac current factors $\mathscr{T}_n$. The polarization vectors for the outgoing photon are taken as $\epsilon'^\mu_{(1)} = (0, \cos\theta\cos\varphi, \cos\theta\sin\varphi, -\sin\theta)$ and $\epsilon'^\mu_{(2)} = (0, -\sin\varphi, \cos\varphi, 0)$. The momentum four-vector of the outgoing photon is $k' = \omega' n'$ with the frequency $\omega'$ and $n'^\mu = (1, \boldsymbol{n}')$ with the unit vector $\boldsymbol{n}' = (\sin\theta\cos\varphi, \sin\theta\sin\varphi, \cos\theta)$. Thus, the transversality condition $k' \cdot \epsilon'_{(1,2)} = 0$ is implemented explicitly. The laser four-vector is $k^\mu = \omega n$ with $n^\mu = (1, 0, 0, -1)$.

### Frequency spectra

In Figure 3.3, the differential emission probability, averaged/summed over the electron spin and the outgoing photon polarization, is exhibited for laser amplitudes $a_0 = 1$ and $a_0 = 2$

and pulse duration $\Delta\phi = 20$ and $\Delta\phi = 50$ for a circularly polarized laser pulse with $\xi = \pi/4$ and carrier envelope phase $\hat{\phi} = 0$ as blue curves. The pulse envelope is taken as a hyperbolic secant, $g(\phi) = \cosh^{-1}\phi/\Delta\phi$. The pulse lengths correspond to $T_{\text{eff}} = 17$ fs ($T_{\text{eff}} = 42$ fs) for $\Delta\phi = 20$ ($\Delta\phi = 50$) and a laser frequency of $\omega = 1.55$ eV. The electron collides head-on with the laser pulse, and the emitted photon is considered to be emitted on-axis, i.e. in the backscattering direction $\theta = 0$. The primary electron energy is 40 MeV, which can be achieved with the superconducting electron linear accelerator ELBE at the HZDR [ELB]. Thus, the situation considered here corresponds to a set-up experimentally accessible at the HZDR using electrons from ELBE in combination with one of the high intensity lasers (DRACO [Deb09], PEnELOPE [PEN]).

In addition to the emission probability in a pulsed laser field, which is depicted in Figure 3.3 as blue curves, the full vertical red lines denote the intensity dependent non-linear Compton edges for the case of an IPW laser field,

$$\omega_1'(a_0) \approx \frac{\omega_1'(0)}{1 + \frac{a_0^2}{2}} \tag{3.43}$$

[cf. Eqs. (C.25] and (C.28)), while vertical grey dotted lines represent the respective linear Compton edges in the weak field limit of an IPW at $\omega' = \omega_1'(0) = 38$ keV for the given parameters. The linear weak-field Compton edge $\omega_1'(0)$ equals the Doppler up-shifted laser frequency, where the up-shift factor for the backscattering head-on geometry is exactly $e^{2\zeta} \simeq 25000$ for the kinematics considered here. The factor of $1 + a_0^2/2$ in the denominator of (3.43) is the intensity-dependent red-shift of the Compton edge.
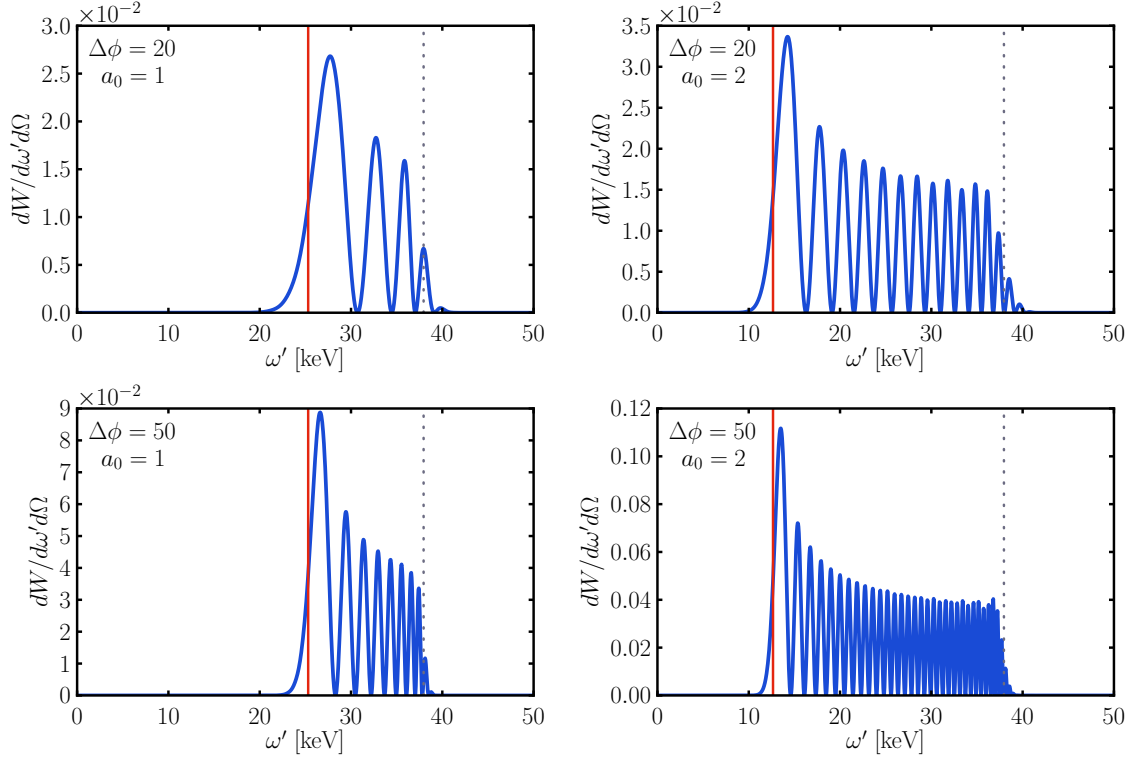
The emission probability in the pulsed laser field covers the whole range between the two Compton edges. In this interval, the emission probability is not constant or has a single peak, but instead one observes a number of $N_{\text{S-P}}$ sub-peaks within the first harmonic signal. The origin of these sub-peaks is the non-linear $\Delta\phi$-dependent modulation of the phase exponentials in the integrands of the quantities $\mathscr{A}_n(s)$, see (3.19). Radiation generated at different times during the course of the pulse, and therefore at different effective laser intensities $a_0^2 g^2(\phi)$, interferes thus generating the pattern of sub-peaks seen in Figure 3.3. The appearance of these sub-peaks is a non-linear short pulse effect. A combination of the finite bandwidth in a laser pulse due to the Fourier transform of the pulse envelope $g$ and the intensity modulation $a_0^2 g^2(\phi)$ leads to the emergence of the sub-peaks. The sub-peaks do disappear in strong infinite plane waves.

It has been known for a while that temporal modulations strongly affect the emission probabilities of non-linear Thomson scattering, with the main effect being the additional oscillatory substructures [Har96b, Kra04, Gao04]. Only very recently, a proper quantum mechanical description of this effect for non-linear Compton scattering has been given [Boc09, Sei11b]. The number $N_{\text{S-P}}$ of subsidiary peaks within the first harmonic scales linearly with the pulse duration $\Delta\phi$ and the intensity $a_0^2$ according to the empirical formula, valid for the hyperbolic secant pulse [Hei10b],

$$N_{\text{S-P}} = 0.16\, a_0^2\, \Delta\phi\,. \tag{3.44}$$

The same scaling of the number of sub-peaks $N_{\text{S-P}} \propto a_0^2 \Delta\phi$ was obtained in [Har10] for the low-energy limit of non-linear Thomson scattering. Reversing the arguments leading to (3.44) suggests the interesting possibility to actually determine the intensity of a laser pulse by counting the number of sub-peaks within the first harmonic if the pulse duration is known.

Further below, in Section 3.10, a general formula for the number of sub-peaks will be derived using a stationary phase analysis. The number of points where destructive interferences can occur, i.e. the number of sub-peaks, is determined as $N_{\text{S-P}} \propto |\Delta f|$, i.e. it is proportional

**Figure 3.3:** The one-photon emission probability $dW/d\omega'd\Omega$ as a function of the frequency $\omega'$ of the emitted photons at constant emission angles $\theta = \varphi = 0$ for $a_0 = 1$ (left panels) and $a_0 = 2$ (right panels). Upper (lower) panels correspond to a laser pulse duration of $\Delta\phi = 20$ ($\Delta\phi = 50$). The full vertical red lines denote the non-linear Compton edges for the ideal case of an IPW laser field, while dotted grey lines represent the respective linear Compton edges.

to the ponderomotive phase shift which is accumulated during the scattering [Har10]. In [Ghb12], a method was proposed to counteract the bandwidth increase and the emergence of the sub-peaks due to the non-linear interaction in a short pulse with finite bandwidth, using special chirped laser pulses.

In a real experiment, the contrast of these sub-peaks will be reduced by a variety of mechanisms. These include effects such as (*i*) the transverse ponderomotive force in focused beams, (*ii*) the influence of transverse intensity profiles as well as (*iii*) contributions due to the phase space distribution of the electron beam, in particular its energy spread $\Delta\gamma/\gamma$ and transverse beam emittance $\varepsilon$. These effects are discussed in some detail in Appendix F. It is shown there that a verification of the individual sub-peaks with a 100 TW or a PW class laser system in conjugation with a high quality electron source, such as ELBE or REGAE [REG, Har12], is within experimental reach.

The emitted radiation is characterized as a function of the frequency $\omega'$ and scattering angle $\theta$ in Figure 3.4. The electron parameters are the same as for Figure 3.3, and the laser has $a_0 = 1$ and $\Delta\phi = 20$. In the left panel of Figure 3.4, the emission probability is exhibited for linear laser polarization, characterized by $\xi = 0$, i.e. the laser polarization vector points along the positive $x$ axis. The decadic logarithm of the one-photon emission probability is shown in the plane of polarization, $\varphi = 0$ (right part of the panel, for positive values of $\theta$), and in the plane perpendicular to the polarization, $\varphi = \pi/2$ (left part of the panel, for negative values of $\theta$). Since the electron is relativistic, most of the radiation is emitted within
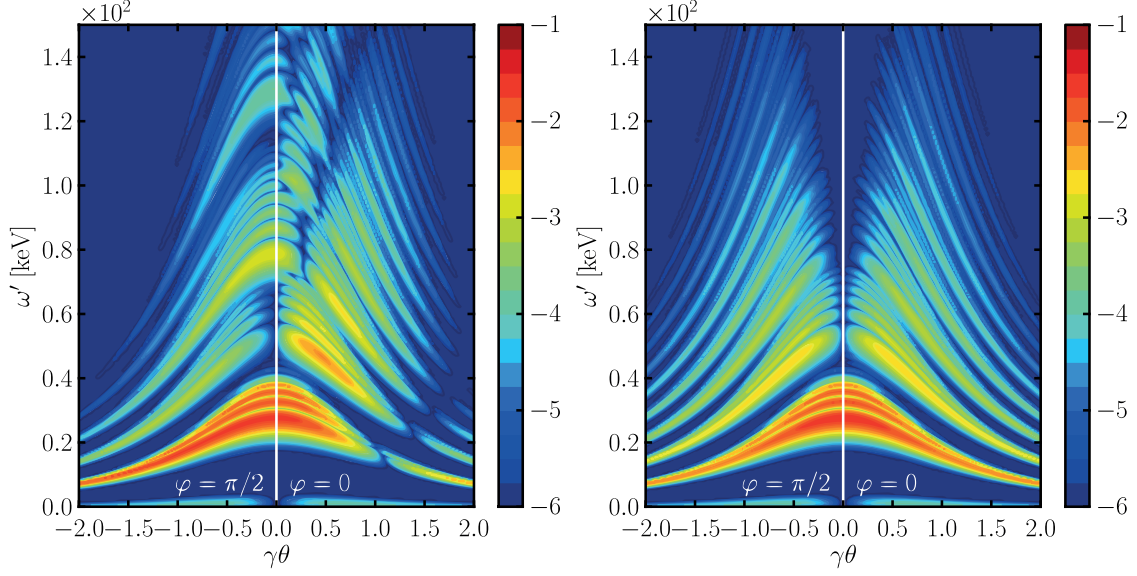
**Figure 3.4:** Survey of the emission probability for linear and circular polarization in the $\omega' - \theta$ plane, for $\varphi = 0$ and $\varphi = \pi/2$. The left panel is for linear laser polarization while the right panel is for circular polarization.

a cone around the forward direction of the electron, $\theta = 0$, with an opening angle $\gamma\theta \sim 1$. The Doppler up-shift factor strongly depends on the scattering angle $\theta$ as $\omega' = \frac{1+v}{1-v\cos\theta}\omega$, where $v = \tanh\zeta \approx 1$ is the electron velocity. Thus, the frequency of the emitted radiation strongly depends on the scattering angle with a maximum at $\theta = 0$. For linear polarization, the emission probability also depends on the azimuthal angle; for $\varphi = 0$ and $\varphi = \pi/2$ the emission probability behaves differently.

The case of circular polarization is depicted in the right panel of Figure 3.4. One clearly sees the so called dead-cone: For $\theta = 0$ there is no emission above the linear Compton edge $\omega_1'(0) = 38$ keV. The emission probability depends only marginally on the azimuthal angle $\varphi$ (this is different for ultra-short pulses).

The cases considered so far were for relatively long laser pulses, $\Delta\phi = 20$ and $50$, i.e. $\Delta\phi \gg 1$, such that the bandwidth of the laser pulse $\propto 1/\Delta\phi$ is much smaller than unity, i.e. the separation of neighbouring Zel'dovich levels of the initial and final Volkov states. The dominant origin for the width of the Zel'dovich levels is the accumulated ponderomotive phase shift $\Delta f$, which, in the limit of IPW, would provide the quasi-momentum. Therefore, this regime is denoted as ponderomotive regime. On the contrary, for ultra-short laser pulses, $\Delta\phi \sim 1$, such that the bandwidth is of the order of adjacent Zel'dovich levels, or even larger, the relation $1/\Delta\phi > 1$ holds. This regime is denoted as bandwidth dominated regime.

The discussion is continued with a systematic survey of the $a_0$ dependence of the emission spectra in both of these regimes, starting with the ponderomotive regime. To this end, the one-photon emission probabilities (divided by $a_0^2$) as a function of the scaled frequency $\omega'/e^{2\zeta}\omega$ for constant scattering angle $\theta$ are depicted in Figure 3.5. In each of the four panels of that figure, the dependence of the emission probability on the value of $a_0$ is exhibited as a series of curves for a certain value of the scattering angle $\theta$, depicting the transition from the linear regime for $a_0 = 0.01$ (yellow) to the non-linear regime with $a_0 = 1$ (black). At low intensity, there is a single peak, corresponding to the Fourier transform of the pulse envelope [cf. Eq. (3.28)]. Upon increasing the value of $a_0$, the height of the peak decreases (note
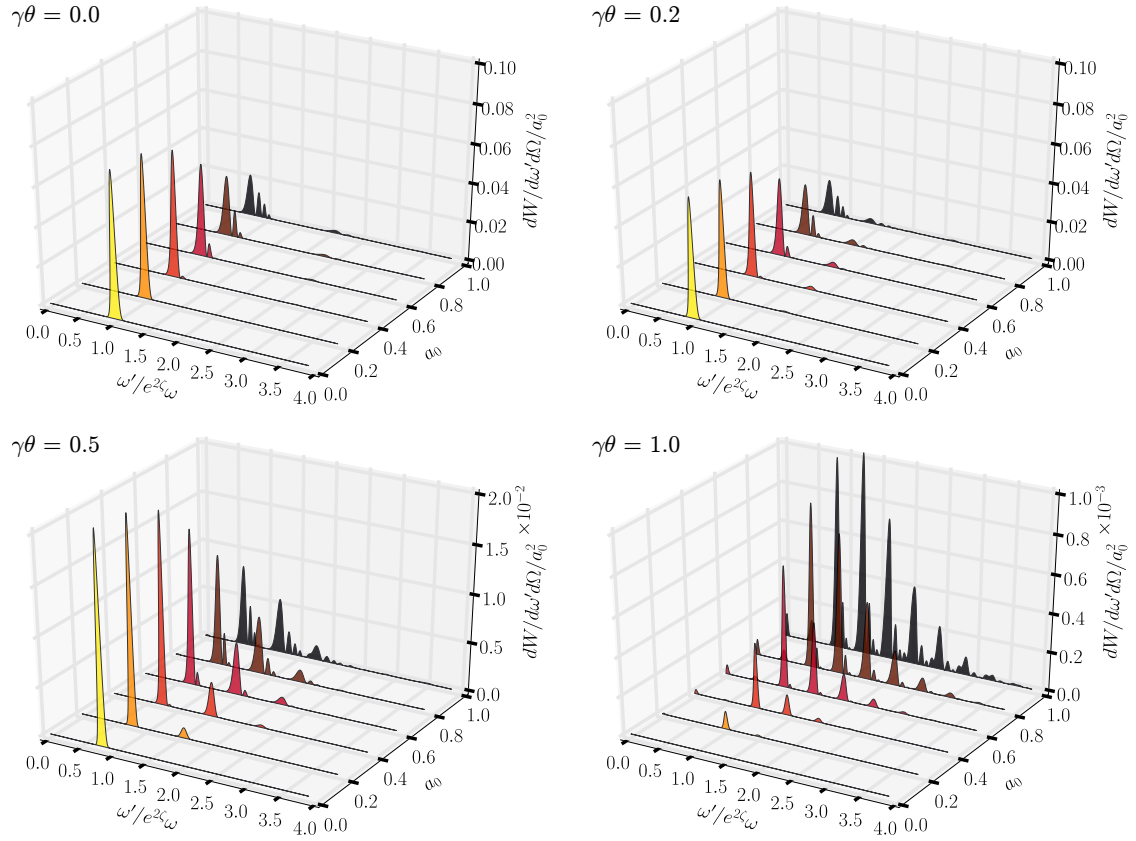
**Figure 3.5:** Survey of the frequency spectrum for non-linear Compton scattering, i.e. the emission probability as a function of the scaled frequency $\omega'/e^{2\zeta}\omega$, scaled by $a_0^2$, for various values of $a_0 = 0.01, 0.2, 0.4, 0.6, 0.8, 1.0$. In the different panels, the frequency spectrum is shown for the scattering angles $\gamma\theta = 0.0$ (top left), 0.2 (top right), 0.5 (bottom left) and 1.0 (bottom right). The pulse has Gaussian shape with $\Delta\phi = 20$.

that the emission probability has been divided by a factor of $a_0^2$ for illustration purposes), broadens and the spectral strength is distributed over an increasing number of sub-peaks. Furthermore, additional peaks at higher frequencies appear. These are higher harmonics. In the ponderomotive regime, the notion of harmonics is meaningful since the non-linear Compton amplitude can be expanded into a series of partial amplitudes which are denoted as harmonics (see discussion in Section 3.9).

The differential emission probability for an ultra-short Gaussian shaped laser pulse with $\Delta\phi = 2$ is exhibited in Figure 3.6 for various values of $a_0$ and linear laser polarization. The electron beam has $\gamma = 10^4$ and the radiation is observed in the plane of polarization ($\varphi = 0$) for scattering angles $\gamma\theta = 0.5$ (left panel ) and $\gamma\theta = 1.0$ (right panel). The curve for $a_0 = 1$ (yellow) shows no indications of sub-peaks as they were observed for longer pulses. Instead, the broad peaks are merged due to the large bandwidth in an ultra-short pulse. Upon increasing the laser strength even further the general characteristic shape of the peaks does not change as was observed in the ponderomotive regime, although their number increases. In particular, one does not observe the emergence of sub-peaks.

In Figure 3.7, the dependence of the emission probability on the carrier envelope phase $\hat{\phi}$ is exhibited for a linearly polarized laser pulse with $\Delta\phi = 2$, where the carrier envelope
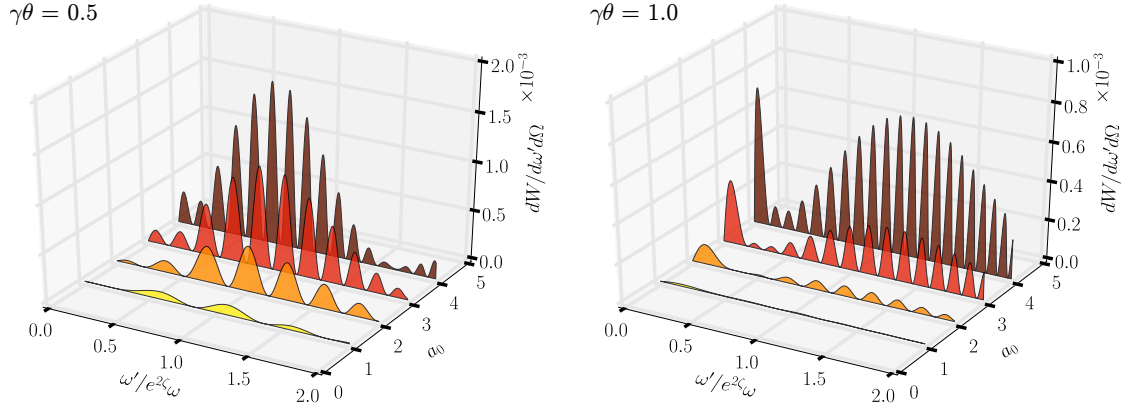
**Figure 3.6:** Differential emission probabilities in an ultra-short laser pulse with $\Delta\phi = 2$ and a Gaussian envelope. The left panel is for $\gamma\theta = 0.5$ and the right panel is for $\gamma\theta = 1.0$
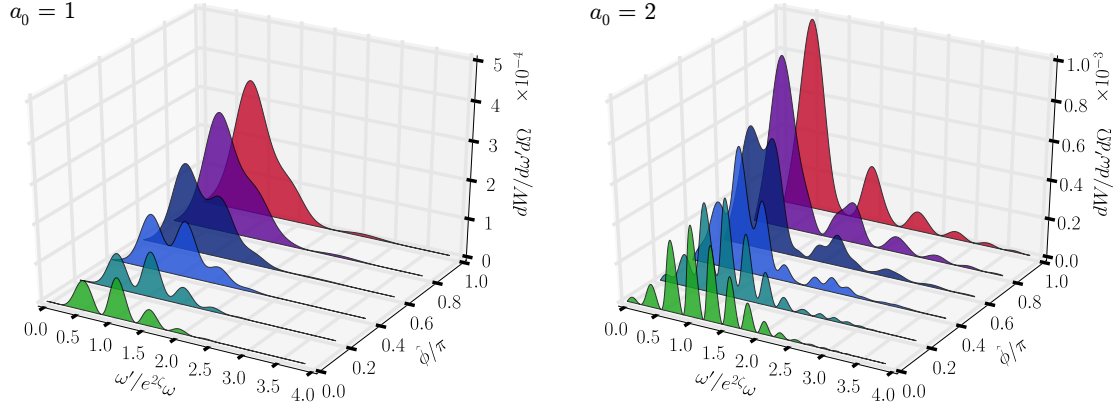


**Figure 3.7:** Dependence of the photon emission probability on the carrier envelope phase $\hat{\phi}$ for an ultra-short strong laser pulse with $\Delta\phi = 2$ for $a_0 = 1$ (left panel) and $a_0 = 2$ (right panel).

phase is varied in the range $\hat{\phi} = 0 \ldots \pi$. The laser strength is $a_0 = 1$ in the left panel and $a_0 = 2$ in the right panel (all other parameters correspond to the left panel of Figure 3.6). The frequency spectrum in Figure 3.7 shows a strong dependence on the carrier envelope phase. In the two panels the emission spectrum for $\hat{\phi} = 0$ consists of a series of small peaks which merge upon increasing $\hat{\phi}$ and for $\hat{\phi} = \pi$ one observes only a single peak for $a_0 = 1$ and a few very broad peaks for $a_0 = 2$.

For longer pulses, the dependence of the spectrum on the carrier envelope phase vanishes. For instance, in [Boc09] it was argued that the value of $\hat{\phi}$ becomes irrelevant for $\Delta\phi > 20$. Also for weak short laser pulses, e.g. for $\Delta\phi = 2$ and $a_0 = 0.1$, the value of the carrier envelope phase has a weak influence on the spectrum.

The transition from the bandwidth dominated regime for ultra-short pulses to the ponderomotively dominated regime for longer pulse lengths is exhibited in Figure 3.8, where the emission probability divided by the pulse length $\Delta\phi$ is shown as a function of scaled frequency $\omega'/e^{2\zeta}\omega$ for $\gamma = 100$, $\theta = 0.005$, $\varphi = 0$, linear laser polarization and $a_0 = 1$ for various values of the pulse length parameter $\Delta\phi$ in a sequence of curves. In the left panel, the
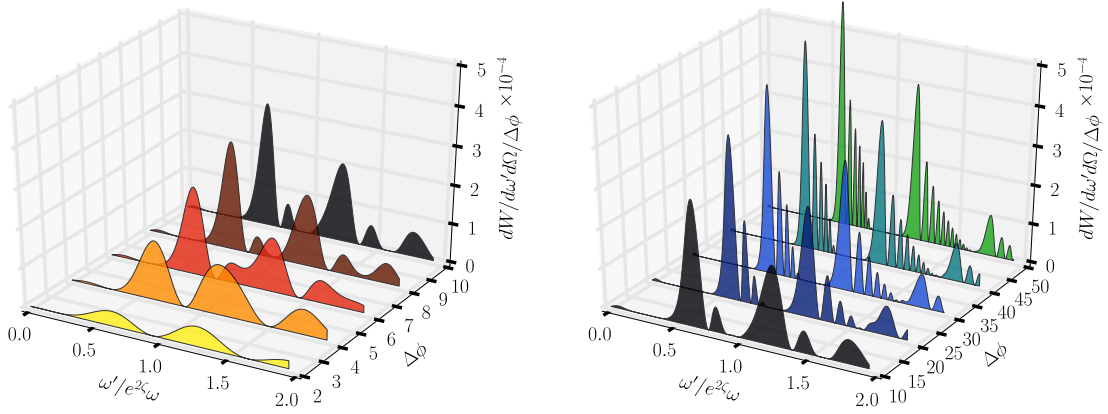
**Figure 3.8:** Evolution from bandwidth dominated regime (for small values of $\Delta\phi$) to the ponderomotive regime (for large values of $\Delta\phi$) by increasing the pulse length from $\Delta\phi = 2$ (yellow curve in the left panel) up to $\Delta\phi = 50$ (green curve in the right panel), keeping fixed all other parameters.

shorter pulse lengths are shown, for $\Delta\phi = 2 \dots 10$, while the right panel is for longer pulse lengths $\Delta\phi = 10 \dots 50$. The sub-peaks become clearly visible for a pulse length of the order of $\Delta\phi = 10$ which can be considered as the transition between the bandwidth-dominated regime and the ponderomotive regime in this case.

### Azimuthal distributions

Now, the azimuthal spectra are discussed, starting with linear polarization. While for long pulses and IPW each harmonic has a characteristic multi-pole pattern, this behaviour changes for ultra-short pulses and the emission can become unidirectional. In Figure 3.9, the dependence of the azimuthal spectra is exhibited for linear laser polarization for various values of $a_0$ and the carrier envelope phase $\hat{\phi}$. In the panels, the quantity

$$\frac{dI}{d\varphi} = \int d\omega' \int d\theta \sin\theta \frac{dI}{d\omega' d\Omega} \,, \tag{3.45}$$

is displayed, where the integration over the polar angle is done over a cone within an opening angle $\theta = 3/\gamma$ around the $z$ axis, which is the direction of the incoming electron. The energy integration has the lower boundary of 1 keV.[4]

The differential azimuthal energy spectrum $dI/d\varphi$ is exhibited in Figure 3.9 for a squared cosine pulse [cf. Eq. (A.35) Appendix A.3] with a pulse length of $\Delta\phi = \pi$, i.e. a laser pulse with one cycle of the carrier wave. At low laser intensity $a_0 = 0.1$ (upper left panel), the emission has a strong dipole pattern with the preferred emission in the plane transverse to the polarization of the laser (which is the $x$ axis). Upon increasing the laser strength up to $a_0 = 1$ (upper centre panel) $a_0 = 2$ (upper right panel) and $a_0 = 3$ (lower left panel), the shape develops towards an unidirectional emission. For large values of $a_0$, there is a strong dependence of the azimuthal emission probability on the carrier envelope phase $\hat{\phi}$. While for $\hat{\phi} = 0$ the emission probability has the strong unidirectional characteristics, this changes

---

[4]Here, the integrated energy spectrum $dI$ is used, instead of the integrated probability $dW$, for experimental reasons. One problem which arises in the experimental detection of Compton scattered photons are pile-ups in calorimeters, where two photons with energies $\omega_1$ are detected calorimetrically as a single photon with energy $2\omega_1$. This means of course that the detected photon number is 1 instead of 2. However, the detected energy is the same in both cases. The drawback of the energy spectrum is that it is not a Lorentz invariant quantity.
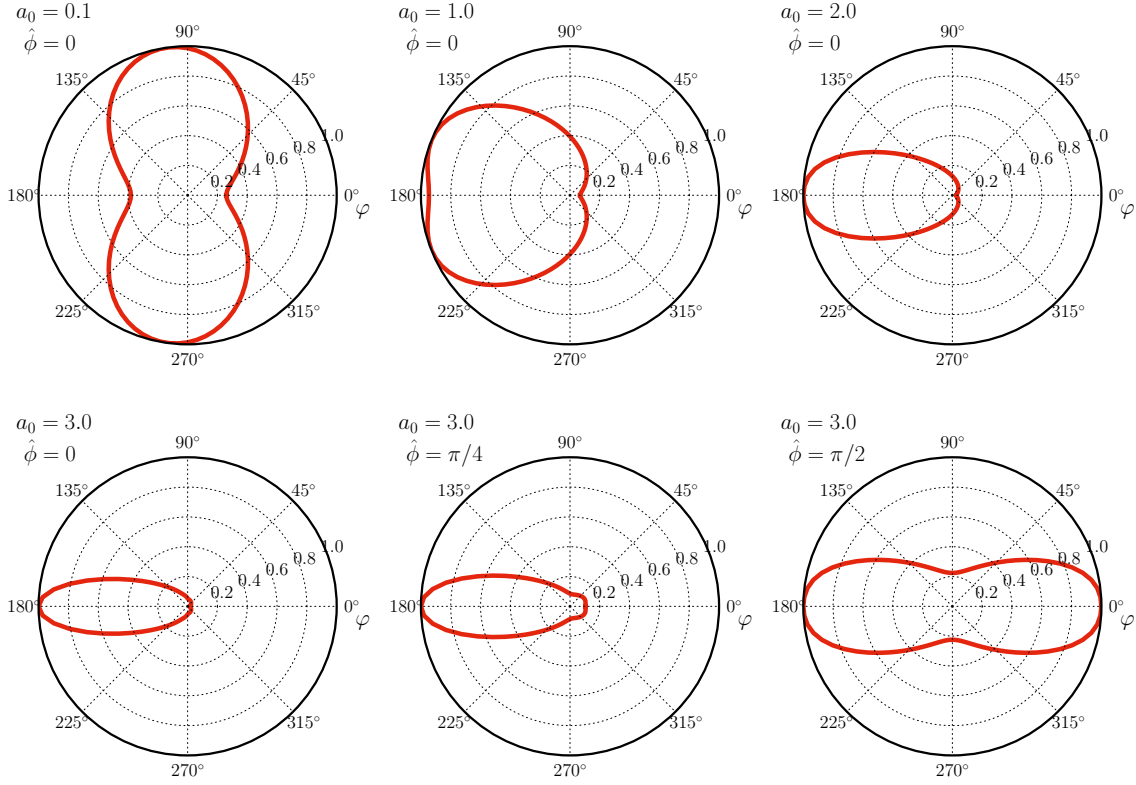
**Figure 3.9:** Azimuthal non-linear Compton spectra $dI/d\varphi$ for a squared cosine pulse envelope with $\Delta\phi = \pi$, i.e. a single-cycle pulse and linear laser polarization with $\xi = 0$. The upper three panels are for $\hat\phi = 0$ with increasing values of $a_0$ from left to right as denoted beneath each panel. The lower three panels depict the dependence of the azimuthal spectra on the value of the carrier envelope phase $\hat\phi$ for $a_0 = 3$. The distributions are normalized to unity.

upon increasing $\hat\phi$ up to $\hat\phi = \pi/2$. In the case of $\hat\phi = \pi/2$, the emission spectrum has a dipole type pattern in the direction of the polarization vector of the laser. Upon increasing $\hat\phi$ further up to $\hat\phi = \pi$, one would find a unidirectional emission with the maximum at $\varphi = 0$. This dependence on the carrier envelope phase $\hat\phi$ for $a_0 > 1$ is the basis for an experimental access to the carrier envelope phase proposed in [Mac10]. In that paper, and also in [Mac11, Kra12], the dependence of the spectrum on the carrier envelope phase was not discussed on the basis of the azimuthal spectra, but on asymmetries on the polar-angle spectra for $\varphi = 0$ and $\varphi = \pi$. This discussion is adequate for linear polarization, but obscures the view on the relevant quantities for general polarization. For instance, for circular polarization, the azimuthal symmetry which is always present for infinitely long laser pulses and only marginally broken for long laser pulses with $\Delta\phi \gg 1$, is completely lost in ultra-short pulses with $\Delta\phi \sim 1$. In the rightmost panel of Figure 3.10 the azimuthal spectrum $dI/d\varphi$ is exhibited for a circularly polarized single cycle laser pulse with $\xi = \pi/4$ and for $a_0 = 3$, showing the strong asymmetry. This is due to the fact that the vector potential has no azimuthal symmetry for an ultra-short pulse, since a distinguished direction is defined by the maximum of the laser pulse, i.e. for which the non-linearities are maximized. (For a single cycle laser pulse the vector potential vanishes in the opposite direction.) The azimuthal symmetry is replaced by another remarkable symmetry, namely a symmetry in the composite variable $\varphi - \hat\phi$, that
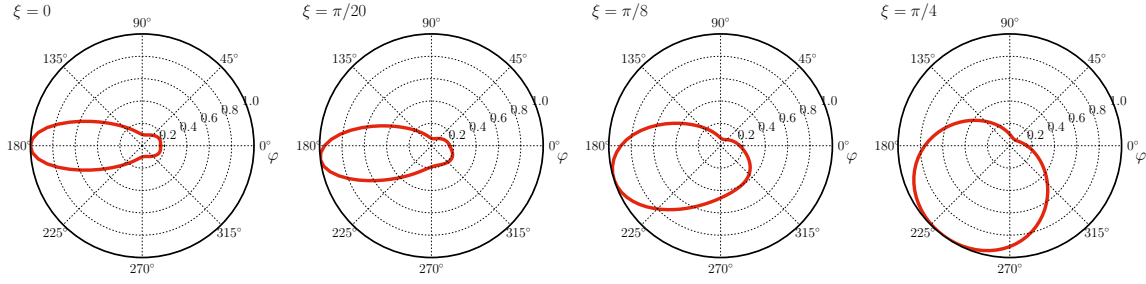
**Figure 3.10:** Polarization dependence of the azimuthal emission spectrum. The leftmost panel depicts linear polarization, while the rightmost panels is for circular polarization. In the two central panels, elliptically polarized laser pulses with different values of the ellipticity have been used.

means the distinguished direction depends on the value of the carrier envelope phase. It can be shown by an analytical calculation that the amplitude $\mathscr{M}(s)$ depends on $\varphi$ and $\hat{\phi}$ only in the combination $\varphi - \hat{\phi}$. For circular polarization one has $\cos 2\xi = 0$, such that the non-linear phase $f(\phi)$ depends on $\hat{\phi}$ only via the term proportional to $\alpha_-$, which reads

$$\text{Re}\left(\alpha_- \int d\phi g(\phi) e^{i(\phi+\hat{\phi})}\right) = \alpha_0 \text{Re}\left(\int d\phi g(\phi) e^{i(\phi-(\varphi-\hat{\phi}))}\right), \tag{3.46}$$

where

$$\alpha_- = \frac{ma_0}{\sqrt{2}} \frac{k'_x - ik'_y}{k \cdot p} = \frac{ma_0 \omega' \sin\theta}{\sqrt{2}\, k \cdot p'} e^{-i\varphi} \equiv \alpha_0 e^{-i\varphi}. \tag{3.47}$$

A further dependence on the carrier envelope phase $\hat{\phi}$ can be found in the two phase integrals $\mathscr{A}_\pm$. This dependence can also be cast into a form $\varphi - \hat{\phi}$ when calculating the emission spectrum $dI$.

The azimuthal emission spectra for a single cycle laser pulse as above for different laser polarization are exhibited for $a_0 = 3$ and $\hat{\phi} = 0.3\pi$ in Figure 3.10 for linear laser polarization ($\xi = 0$, left panel), elliptic polarization ($\xi = \pi/20$ and $\xi = \pi/8$, central two panels), and circular polarization ($\xi = \pi/4$, right panel). Indeed, the azimuthal emission spectra show a characteristic dependence on the polarization of the laser pulse, which gradually develops from the narrow unidirectional emission in the axis of polarization for linear polarization (left panel) to the directional emission into the preferential direction $\pi + \hat{\phi} \equiv 234°$ for circular polarization (right panel).

This concludes the study of the azimuthal spectra. It was shown that the energy integrated azimuthal spectra show a strong dependence on the laser polarization and the value of the carrier envelope phase for ultra-short laser pulses. The asymmetry for circular polarization is explained by the preferred direction where the vector potential reaches its maximum value. A remarkable symmetry in the composite variable $\varphi - \hat{\phi}$ for ultra-short circularly polarized laser pulses replaces the general azimuthal symmetry of infinitely long circularly polarized plane waves.

## 3.5   The classical radiation spectrum

In the limit of low energy, the derived expressions for the photon emission probability, energy spectrum and cross section need to coincide with appropriate classical expression for Thomson

scattering. These classical expressions are derived here in a concise way. The differential energy spectrum, emitted by an accelerated charged particle into the solid angle $d\Omega$ and the frequency interval $d\omega'$, corresponding to the quantum result (3.37),[5] is given by the covariant expression [Hei10b, Mit98]

$$\frac{d^2 I}{d\omega' d\Omega} = -\frac{\omega'^2}{16\pi^3} j(k')^* \cdot j(k') \,, \tag{3.48}$$

where

$$j^\mu(k') = e \int d\tau \, u^\mu(\tau) e^{ik' \cdot x(\tau)} \tag{3.49}$$

is the Fourier transform of the electron current

$$j^\mu(x) = e \int dx^\mu \delta^4(x - x(\tau)) = e \int d\tau \, u^\mu(\tau) \delta^4(x - x(\tau)) \,. \tag{3.50}$$

Here, $x^\mu(\tau)$ and $u^\mu(\tau)$ are the classical orbits in a given background field as solutions of the Lorentz force equation (2.1). A classical photon emission probability $\frac{d^2 W}{d\omega' d\Omega}$, which might serve as classical analogue to (3.34) (other names for that quantity are photon spectral density or photon yield), is derived from (3.48) by dividing out the energy of one photon:

$$\frac{d^2 W}{d\omega' d\Omega} = \frac{1}{\omega'} \frac{dI}{d\omega' d\Omega} = -\frac{\omega'}{16\pi^3} j(k') \cdot j^*(k') \,. \tag{3.51}$$

Employing the continuity equation $k' \cdot j(k') = 0$, one may eliminate $j^0 = \boldsymbol{n}' \cdot \boldsymbol{j}$ such that (3.51) turns into the more familiar but not manifestly covariant expression [Jac83]

$$\frac{d^2 W}{d\omega' d\Omega} = \frac{\omega'}{16\pi^3} |\boldsymbol{n}' \times \boldsymbol{j}(k')|^2 \,. \tag{3.52}$$

Using the orbits in the plane wave laser field Eqs. (2.7) and (2.8) together with the definition of the vector potential (A.24) one can evaluate the exponential in (3.49) yielding

$$k' \cdot x(\phi) = k' \cdot x_0 + z_0 \phi - z_1 \cos\xi \int d\phi g \cos\phi - z_2 \sin\xi \int d\phi g \sin\phi$$
$$- z_3 \int d\phi g^2 (1 + \cos 2\xi \cos 2\phi) \,, \tag{3.53}$$

where irrelevant constant phases, such as $k' \cdot x_0$, will be dropped in the following. The definitions of the quantities $z_i$ read

$$z_0 = \frac{k' \cdot u_0}{k \cdot u_0} \,, \tag{3.54}$$

$$z_{1,2} = \frac{a_0}{k \cdot u_0} \left( k' \cdot \epsilon_{1,2} - \frac{k' \cdot k}{k \cdot u_0} (\epsilon_{1,2} \cdot u_0) \right) \,, \tag{3.55}$$

$$z_3 = -\frac{a_0^2}{4} \frac{k' \cdot k}{(k \cdot u_0)^2} \,. \tag{3.56}$$

The part of the integral (3.49) which is proportional to $u_0^\mu$ is divergent, just as the phase integral $\mathscr{A}_0(s)$. A suitable integration by parts (after having introduced a convergence factor $e^{-\varepsilon|\phi|}$) to handle the surface terms yields the result

$$\int d\phi e^{ik' \cdot x} = \lim_{\varepsilon \to 0} \int d\phi \, e^{iz_0\phi + i\mathcal{P}(\phi) - \varepsilon|\phi|} = -\frac{1}{z_0} \int d\phi \frac{d\mathcal{P}}{d\phi} e^{ik' \cdot x} \tag{3.57}$$

---

[5]A label for the distinction of classical and quantum probability is left away here and noted where necessary.

with

$$\frac{d\mathcal{P}}{d\phi} = -\frac{k' \cdot a}{\kappa} + \frac{k' \cdot k}{\kappa^2}(a \cdot u_0) - \frac{k' \cdot k}{2\kappa^2}(a \cdot a) \,, \tag{3.58}$$

where $a_\mu(\phi) = eA_\mu(\phi)/m$ and $\kappa = k \cdot u_0$. Employing (3.58) in (3.49) one finds the result for the regularized current as

$$j^\mu(k') = \frac{e}{\kappa} \int d\phi \left\{ \eta^{\mu\nu}a_\nu(\phi) + \frac{a \cdot a}{2\kappa}\eta^\mu \right\} e^{ik' \cdot x} \tag{3.59}$$

with

$$\eta^{\mu\nu} = \frac{u_0^\mu k'^\nu}{k' \cdot u_0} - g^{\mu\nu} + \frac{k^\mu u_0^\nu}{\kappa} - \frac{u_0^\mu u_0^\nu}{\kappa}\frac{k' \cdot k}{k' \cdot u_0} \,, \tag{3.60}$$

$$\eta^\mu = \frac{k' \cdot k}{k' \cdot u_0}u_0^\mu - k^\mu \,, \tag{3.61}$$

fulfilling the transversality relations $k'_\mu\eta^\mu = k'_\mu\eta^{\mu\nu} = 0$ which ensures current conservation $k' \cdot j = 0$.

## 3.6   Comparison of Compton and Thomson scattering

The Thomson limit of Compton scattering is achieved in situations where the electron recoil, i.e. the momentum transfer due to the emission of a photon, is negligible. That statement can be formalized by defining the centre-of-mass energy squared (the Mandelstam variable[6]) $\mathfrak{s} = (p + sk)^2 = (p' + k')^2$ as the total incoming momentum, and the recoil parameter by

$$y \equiv \frac{\mathfrak{s} - m^2}{m^2} = 2s\frac{k \cdot p}{m^2} = 2s\varrho \,, \tag{3.62}$$

where one can state that the classical or Thomson limit is achieved for $y \to 0$ as the recoil free limit of Compton scattering. This means that even if the recoil parameter in the weak-field case $\varrho = k \cdot p/m^2$ may be small, one can be far away from the Thomson limit since $s$ can be large in strong laser fields with $a_0 \gg 1$. Another way of expressing this fact is the statement that in strong laser fields the parameter $\chi_p = a_0\varrho$ determines the relevance of non-linear quantum effects. The Mandelstam variable $\mathfrak{s}$ can be expressed as $\mathfrak{s} = m^2 + 2sk \cdot p = m^2(1+y)$, where the Thomson limit means neglecting the second, $s$ dependent contribution to the centre-of-mass energy. The parameter $y$ is a function of $\omega'$ since $s$ depends on $\omega'$,

$$y = 2s\frac{p \cdot k}{m^2} = \frac{2}{m^2}\frac{(p \cdot k')(p \cdot k)}{(p \cdot k - k' \cdot k)} \,, \tag{3.63}$$

which diverges at the point where $p \cdot k = k' \cdot k$, defining the frequency

$$\omega'_\infty = \frac{k \cdot p}{n' \cdot k} < \infty \,, \tag{3.64}$$

where the momentum transfer would be infinite.

Considering the kinematics now, it is noted that the frequency of back-scattered photons in Thomson scattering is obtained from the corresponding quantum expression (3.18) by neglecting the recoil $sk$ with respect to $p$ in the denominator, i.e.

$$\omega'_{\text{Th}}(s) = s\frac{k \cdot p}{p \cdot n'} \,, \qquad\qquad \omega'(s) = s\frac{k \cdot p}{(p + sk) \cdot n'} \tag{3.65}$$

---

[6]To avoid confusion, the Mandelstam variable will denoted as $\mathfrak{s}$ to distinguish it from the momentum transfer between the electron and the laser field $s$.

where the result for Compton scattering is given on the right.[7]  In the limit of infinite monochromatic waves one obtains the frequencies [cf. Eqs. (C.24) and (C.47)]

$$\omega'_{\ell,\mathrm{Th}} = \ell \frac{k \cdot q}{q \cdot n'} , \qquad\qquad\qquad \omega'_\ell = \ell \frac{k \cdot q}{(q + \ell k) \cdot n'} . \qquad (3.66)$$

Taking the limit $s \to \infty$ (or alternatively $\ell \to \infty$) in the above expressions one obtains

$$\lim_{\ell \to \infty} \omega'_\ell = \lim_{s \to \infty} \omega'(s) = \omega'_\infty < \infty , \qquad (3.67)$$

whereas

$$\lim_{\ell \to \infty} \omega'_{\ell,\mathrm{Th}} = \lim_{s \to \infty} \omega'_{\mathrm{Th}}(s) = \infty . \qquad (3.68)$$

Thus, $\omega'_\infty$ is the maximum available frequency of the outgoing photon in non-linear Compton scattering. The physical phase space for non-linear Compton scattering is restricted by $0 < \omega' < \omega'_\infty$ in contrast to the phase space in Thomson scattering where $0 < \omega' < \infty$, i.e. arbitrary high frequencies can be emitted in the classical theory. However, for the emission of high-frequency photons, that is for large values of $s$, where the electron interaction with many laser photons, one surely leaves the regions of applicability of the classical theory as the recoil parameter $y$ grows proportional to $s$. The bottom line is that in high-intensity laser fields with $a_0 \gg 1$, the photon emission has to be described within the quantum theory to account properly for the electron recoil, even if $\varrho$ is small, since many low energy laser photons can interact simultaneously with the electron such that the total recoil can have a non-negligible strength.

For the discussion of the Thomson limit, $y \to 0$, in the following it will be helpful to define the variable

$$\chi \equiv \frac{k \cdot p'}{k \cdot p} = 1 - \frac{k' \cdot k}{p \cdot k} = 1 - \frac{\omega'}{\omega'_\infty} , \qquad (3.69)$$

with $0 \leq \chi \leq 1$, where in the low-energy limit the relation $1 - \chi \ll 1$ holds. The function $\chi$ is related to the momentum transfer from the incoming electron to the outgoing electron via $p'^+ = \chi p^+$. Thus, $\chi$ is the fraction of momentum $p^+$ transferred from the incoming electron to the outgoing electron $p'^+$. Furthermore, the fraction of momentum transferred to the photon is $k'^+ = (1 - \chi)p^+$ thus, $1 - \chi$ is another measure of the electron recoil. One notes that $\chi$ is a monotonically decreasing function of $\omega'$. The point $\chi(\omega') = \chi(\omega'_\infty) = 0$ corresponds to $p'^+ = 0$ and $k'^+ = p^+$, i.e. the total amount of momentum is transferred from the incoming electron to the emitted photon. Further increasing $\omega' > \omega'_\infty$ would render both $\chi$ and $p'^+$ negative. If $p'^+ < 0$, then, due to the free particle dispersion relation,

$$p'^- = \frac{\boldsymbol{p}'^2_\perp + m^2}{p'^+} \qquad (3.70)$$

meaning that also $p'^- < 0$ and $p'^-$ diverges as $p'^+$ approaches zero. This, however, would lead to a negative energy $p'^0$ for the outgoing electron due to $p'^0 = (p'^+ + p'^-)/2 < 0$, which is forbidden, of course.

For the backscattering head-on geometry one obtains $\omega'_\infty = m/2$ for electrons initially at rest and $\omega'_\infty = me^\zeta/2 \approx p^0$ for ultrarelativistic particles, i.e. the maximum available frequency of the outgoing photon equals the energy of the incoming electron. The momentum

---

[7]Here, the classical expressions for Thomson scattering are denoted by the label "Th" to distinguish them form the corresponding quantum expressions.
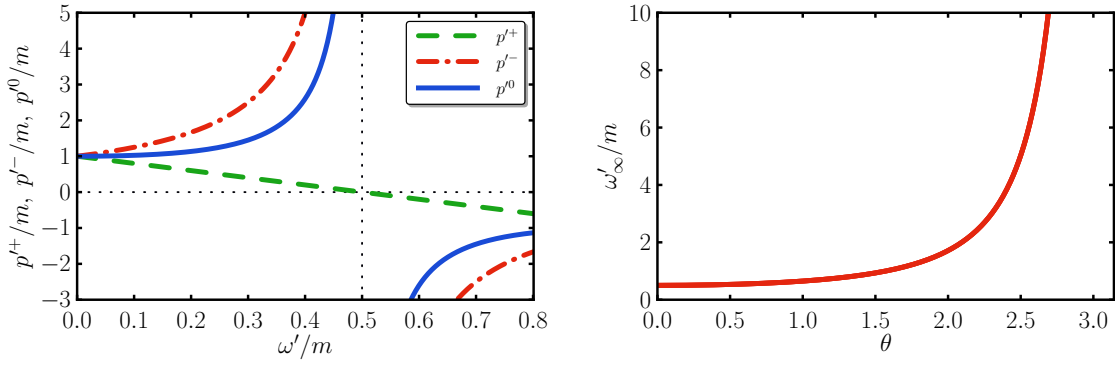
**Figure 3.11:** Left panel: Different components of the momentum $p'$ of the outgoing electron as a function of frequency $\omega'$ for the backscattering geometry ($\theta = 0$) in the rest frame of the incoming electron. Shown are $p'^-$ (red, dash-dotted), $p'^+$ (green, dashed) and $p'^0$ (blue, solid). The physical phase space has its support at $\chi > 0$, i.e. for $0 < \omega'/m < 0.5 = \omega'_\infty/m$ in this case. Right panel: Cut-off frequency $\omega'_\infty$ as a function of the scattering angle $\theta$, where $\theta = 0$ denotes the backscattering direction.

components $p'^+$, $p'^-$ and $p'^0$ are depicted in the left panel of Figure 3.11 as a function of $\omega'$ in the initial electron rest frame. The right panel of Figure 3.11 shows the dependence of $\omega'_\infty$ on the scattering angle $\theta$. It takes its minimum at the backscattering direction $\theta = 0$ and goes to infinity in the limit $\theta \to \pi$, i.e. for forward scattering. However, $\omega'_\infty(\theta) \simeq \omega'_\infty(\theta = 0)$ for all angles inside of the radiation cone with opening angle $\theta \sim 1/\gamma$ for ultrarelativistic electrons.

The consequences for scattering experiments are tremendous: The maximum achievable photon energy is determined by the energy of the incoming electron alone in the recoil dominated regime $y \gg 1$. This leads to a kinematic pile-up of the emission spectrum below $\omega'_\infty$ and a sharp cut-off of the emitted radiation at $\omega'_\infty$. This fact can be used to produce highly monochromatic $\gamma$-ray beams in a suitable Compton backscattering set-up [Har08].

To relate the Compton amplitude with the classical Thomson counterpart it is instructive to consider the low energy limit of the phase exponential $s\phi - f$ in the phase integrals $\mathscr{A}_n(s)$. The leading term in a low-energy expansion is therefore equivalent to taking the lowest order contribution in an expansion in $(1 - \chi)$. One can show that $s = \frac{k' \cdot p}{k \cdot p'} = z_0 + \mathcal{O}(1 - \chi)$. Similarly, one finds $\beta \to z_3$. Furthermore,

$$\alpha_{1,2} = \frac{ma_0 p \cdot \epsilon_{1,2}}{k \cdot p} - \frac{ma_0 p' \cdot \epsilon_{1,2}}{k \cdot p'}$$

$$\simeq \frac{ma_0}{k \cdot p} \left[ p \cdot \epsilon_{1,2} - (p \cdot \epsilon_{1,2} - k' \cdot \epsilon_{1,2}) \left( 1 - \frac{k' \cdot k}{k \cdot p} \right) \right] \to z_{1,2}, \quad (3.71)$$

which shows that

$$s\phi - f(\phi) \to k' \cdot x(\phi), \quad (3.72)$$

which agrees with the corresponding expression (3.53) obtained in a calculation for Thomson scattering (cf. [Hei10b, Sei11b]) up to terms of order $\mathcal{O}(1 - \chi)$ in the limit $y \to 0$.

## 3.7 Scaling properties of the photon emission probability

A series of plots showing the transition from Thomson to Compton scattering is exhibited in Figure 3.12 for ultrarelativistic electrons colliding head-on with a strong laser pulse. The

deviations between Thomson and Compton scattering are: (*i*) a non-linear red-shift in frequency, i.e. an overall compression of the peaks in frequency space related to the kinematic pile-up, i.e. emergence of the maximal frequency $\omega'_\infty$ in Compton scattering and (*ii*) a slight modification of the amplitude. It is obvious that the red-shift is much more pronounced at higher frequencies. For the chosen parameters ($a_0 = 1.0$ and $\omega = 1.55$ eV) the differences become significant for $\gamma \geq 10^4$, i.e. for $\varrho \geq 0.06$.

Based on these observations one finds that the classical [Thomson scattering, Eq. (3.51)] and quantum [Compton scattering, Eq. (3.34)] emission probabilities for arbitrary pulse shapes are related by the scaling law

$$\frac{d^2W}{d\omega'd\Omega}(\omega', \theta, \varphi) = \eta \frac{d^2W_{\mathrm{Th}}}{d\omega'd\Omega}(\omega'/\chi, \theta, \varphi) \tag{3.73}$$

with the two scaling factors $\eta$ and $\chi$. The frequency scaling factor $\chi$ is the purely kinematical factor introduced in Eq. (3.69). The overall rescaling factor $\eta$ can be found as

$$\eta \equiv \frac{1}{\omega'^2}\frac{d\sigma}{d\Omega} \bigg/ \frac{1}{\omega'^2_{\mathrm{Th}}}\frac{d\sigma_{\mathrm{Th}}}{d\Omega} \, , \tag{3.74}$$

where the differential cross sections for Compton scattering $d\sigma/d\Omega$ and Thomson scattering $d\sigma_{\mathrm{Th}}/d\Omega$ are the monochromatic IPW cross sections presented in Eqs. (C.43) and (C.54), respectively. For circular polarization, one has

$$\eta = \frac{\mathfrak{J}_\ell}{\mathfrak{K}_\ell} = 1 + \frac{x^2}{1+x}\frac{\mathfrak{L}_\ell}{2\mathfrak{L}_\ell - \frac{8}{a_0^2}J_\ell^2(z)} \, , \tag{3.75}$$

where $x = (1-\chi)/\chi$, $y_\star \equiv y/(1+a_0^2/2)$ and

$$z = 2\ell\frac{\sqrt{a_0^2/2}}{\sqrt{1+a_0^2/2}}\sqrt{\frac{x}{y_\star}\left(1 - \frac{x}{y_\star}\right)}. \tag{3.76}$$

The definitions of $\mathfrak{J}_\ell$, $\mathfrak{K}_\ell$ and $\mathfrak{L}_\ell$ are given in Eqs. (C.52) and (C.53), with $\ell = s - \beta$. In the limit $a_0 \to 0$ one gets

$$\lim_{a_0 \to 0} \eta = 1 + \frac{x^2}{1+x}\frac{1}{2 - 4\frac{x}{y_\star}(1 - \frac{x}{y_\star})} \tag{3.77}$$

which is a good approximation for $a_0 \lesssim 1$. For linear laser polarization, a similar relation for $\eta$ can be derived using the appropriate IPW cross section (e.g. using the results of [Iva04]).

Further differences between the classical and quantum emission probabilities arise in phase space regions where different harmonics overlap. There, the sub-peaks in the quantum calculation show completely different patterns in comparison to a classical calculation (see [Sei11b] for details). The generation of the sub-peaks is described as an interference effect [Hei10b]. Thus, when the harmonics overlap, for a fixed value of $\omega'$ the contributions of different harmonics and their interference is very sensitive to subtle changes in the phase of the integrals $\mathscr{A}_n(s)$, depending on whether the recoil of the electron is considered in the quantum case or it is neglected in the classical picture. This of course is a regime where the scaling (3.73) cannot be applied. The difference in the spectral distributions looks qualitatively similar to the results of [Har96a], where the influence of classical radiation reaction force on the spectrum was studied. The radiation reaction force also provides an electron recoil in the classical calculation, slightly changing the phases and leading to a modified spectrum. Although the numerical values of the recoil differ quantitatively between the Compton recoil and the radiation reaction force [Har05], the qualitative effect of the radiation spectra is the same.
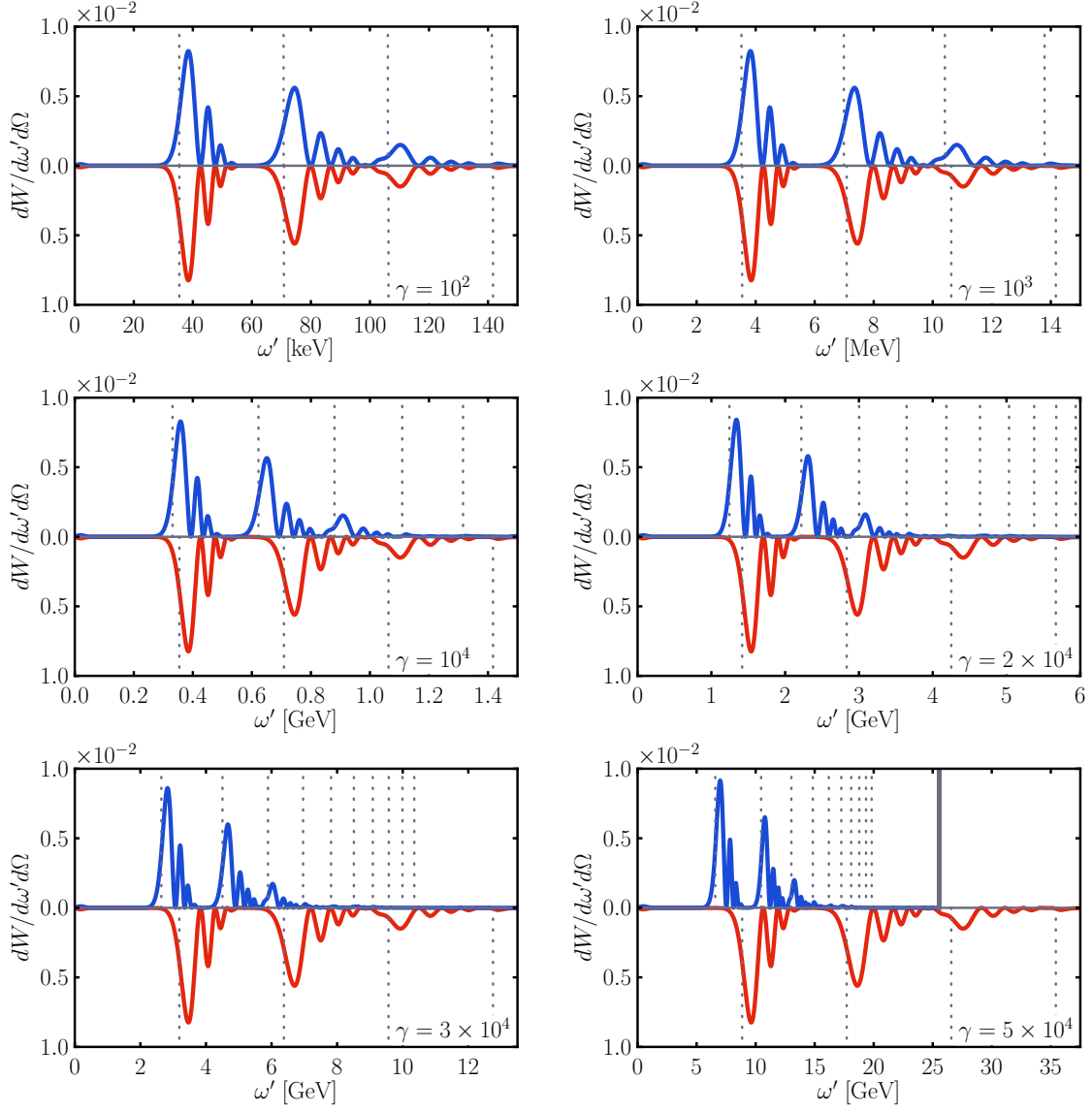
**Figure 3.12:** The photon spectrum as a function of the frequency $\omega'$ for $\gamma = 10^2$, $10^3$, $10^4$, $2 \times 10^4$, $3 \times 10^4$ and $5 \times 10^4$ from top left to bottom right for $\theta = 1/2\gamma$ and $\varphi = 0$ for a Gaussian pulse shape. The upper (lower) blue (red) curves are for a quantum (classical) calculation of Compton (Thomson) scattering. The vertical grey lines mark the positions of the classical ($\omega'_{\ell,\mathrm{Th}}$) and quantum ($\omega'_\ell$) harmonics in an IPW according to Eq. (3.66). The other parameters are $a_0 = 1.0$, $\omega = 1.55$ eV, $\Delta\phi = 20$ and $\xi = 0$, i.e. linear laser polarization. The thick grey vertical line in the bottom right panel depicts the cut-off frequency $\omega'_\infty = \gamma m = 25.5$ GeV for that case.

## 3.8   The slowly varying envelope approximation

One strategy for the evaluation of the photon emission probability (3.34) is based on a direct numerical integration of the phase integrals $\mathscr{A}_n(s)$ in (3.19), as employed above in Section 3.4. One particular complication is the fact that the integrand of $\mathscr{A}_n(s)$ includes integrals in the non-linear phase $f(\phi)$ itself, which are either complicated special functions or which are even unknown analytically for certain pulse envelopes. The numerical calculations can be simplified upon utilizing the slowly varying envelope approximation (SVEA) of the phase of the $\mathscr{A}_n(s)$ functions. Furthermore, this approximation is the starting point for some exact analytic calculations of the scattering amplitude $\mathscr{M}(s)$, which is presented below in Section 3.11. It provides a possibility to derive approximate expressions for the photon emission probability for $a_0 \gg 1$, where a direct numerical integration is hard to do. This approximation scheme is suitable for long pulses with $\Delta\phi \gg 1$, i.e. for many oscillations of the carrier wave under the envelope. To derive the approximation, an integration by parts is performed in the integrals in (3.7) yielding

$$\int d\phi\, g(\phi) e^{i\phi} = -i g(\phi) e^{i\phi} + i \int d\phi \frac{dg}{d\phi} e^{i\phi} \,,$$

$$\int d\phi\, g(\phi) \sin(\phi + \hat{\phi}) = -g(\phi) \cos(\phi + \hat{\phi}) + \int d\phi \frac{dg}{d\phi} \cos(\phi + \hat{\phi}) \,,$$

$$\int d\phi\, g(\phi) \cos(\phi + \hat{\phi}) = g(\phi) \sin(\phi + \hat{\phi}) - \int d\phi \frac{dg}{d\phi} \sin(\phi + \hat{\phi}) \,,$$

$$\int d\phi\, g^2(\phi) \cos 2(\phi + \hat{\phi}) = \frac{1}{2} g^2(\phi) \sin 2(\phi + \hat{\phi}) - \int d\phi\, g(\phi) \frac{dg}{d\phi} \sin 2(\phi + \hat{\phi}) \,. \tag{3.78}$$

The SVEA basically means neglecting the second terms containing integral and the derivative of the pulse shape $dg/d\phi$ because it is $\mathcal{O}(1/\Delta\phi)$ smaller than the first term. This means that the SVEA result for the non-linear phase reads

$$f_{\text{SVEA}}(\phi) = \tilde{f}_{\text{SVEA}}(\phi) + \beta G_2(\phi) \,, \tag{3.79}$$

while the oscillating part is

$$\tilde{f}_{\text{SVEA}}(\phi) = -\text{Re}\left( i\alpha_- g(\phi) e^{i(\phi + \hat{\phi})} \right) + \frac{\beta}{2} g^2(\phi) \sin 2(\phi + \hat{\phi}) \tag{3.80}$$

$$= \alpha_1 \cos\xi\, g(\phi) \sin(\phi + \hat{\phi}) - \alpha_2 \sin\xi\, g(\phi) \cos(\phi + \hat{\phi}) + \frac{\beta}{2} g^2(\phi) \sin 2(\phi + \hat{\phi}) \,, \tag{3.81}$$

and $G_2(\phi) = \int d\phi\, g^2(\phi)$. This is a generalizing the approximation scheme of [Nar96b] to arbitrary laser polarization; it was also employed in e.g. [Sei11b, Tit12].

Even for rather short pulses, such as for $\Delta\phi = 5$ meaning that the pulse length is 15 fs for a laser wavelength $\lambda = 800$ nm, the SVEA is quite a good approximation. For instance, the SVEA of the cosine integral in Eq. (3.78) is depicted in the left panel of Figure 3.13 in comparison to the full integral verifying only a minor deviation for $\Delta\phi = 5$. A similar comparison is given in the right panel of Figure 3.13 for the phase integral $\mathscr{A}_+(s)$ for $a_0 = 3$. For even shorter pulse lengths the validity of SVEA is reduced. As an empirical fact one can say that 5 oscillations in the pulse is the lower limit for the applicability of the SVEA, which coincides quite well with the statement of [Tit12] that the SVEA is a good approximation for $\Delta\phi > 2\pi$ for a hyperbolic secant pulse. Analysing the asymptotics of the non-linear phase $f$ for $\phi \to \pm\infty$ one sees that the oscillating part $\tilde{f}_{\text{SVEA}}$ is proportional to the envelope function $g$ in the SVEA and, thus, it vanishes in the limit $\phi \to \pm\infty$. In the SVEA, the only source
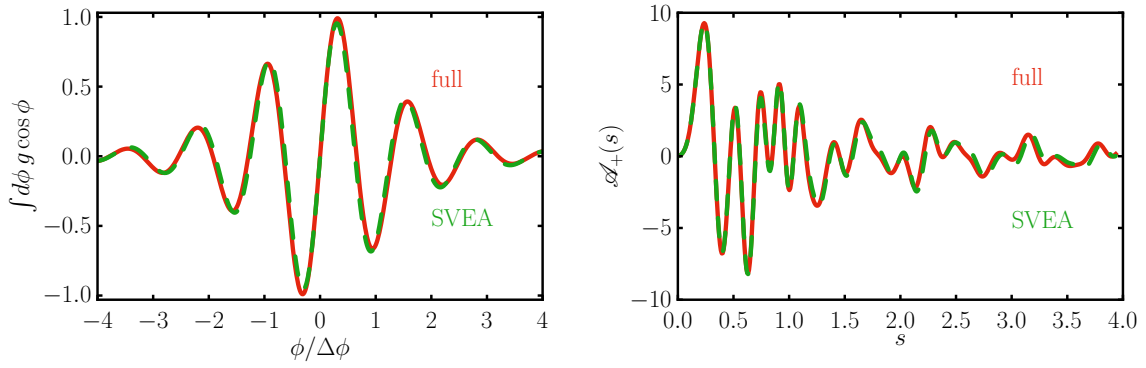
**Figure 3.13:** Left panel: Comparison of the integral $\int d\phi g \cos\phi$ (red solid curve) and the corresponding SVEA (green dashed curve), i.e. only the first term on the right hand side of Eq. (3.78) for a pulse length of $\Delta\phi = 5$ and for $\hat{\phi} = 0$. Right panel: The result for the real part of the phase integral $\mathscr{A}_+(s)$ using the full non-linear phase $f$ [red solid curve, cf. Eq (3.7)], compared to the SVEA of $\mathscr{A}_+(s)$ (green dashed curve), where $f_{\mathrm{SVEA}}$ is substituted for $f$ in (3.19) for $\Delta\phi = 5$ and $a_0 = 3$.

of a phase shift $\Delta f$ is the ponderomotive part $\beta G_2$ of $f$, thus, within the SVEA, one finds $\Delta f = \beta(G_2(\infty) - G_2(-\infty))$.

Now the focus is turned back to the full oscillating part $\tilde{f}$ of the non-linear phase exponent to expose the physical differences between the SVEA and the full result

$$\tilde{f}(\phi) = \int d\phi \Big[\alpha_1 \cos\xi g \cos(\phi + \hat{\phi}) + \alpha_2 \sin\xi g \sin(\phi + \hat{\phi}) + \beta \cos 2\xi g^2 \cos 2(\phi + \hat{\phi})\Big],$$

(3.82)

which contains integrals of the form

$$I_n = \int d\phi \Big[g(\phi)e^{i\phi}\Big]^n, \qquad n \in \{1, 2\}.$$

(3.83)

With these definitions, the oscillating parts of the non-linear phase read

$$\tilde{f}_1 = \mathrm{Re}\left(\alpha_- e^{i\hat{\phi}} I_1(\phi)\right),$$

(3.84)

$$\tilde{f}_2 = \beta \cos 2\xi \, \mathrm{Re}\left(e^{2i\hat{\phi}} I_2(\phi)\right),$$

(3.85)

where $\tilde{f} = \tilde{f}_1 + \tilde{f}_2$. The integrals $I_n$ can be evaluated for certain pulse envelopes, as listed in Appendix A.4. For instance, for a hyperbolic secant pulse, the results for $I_n$ read with $x = e^{\phi/\Delta\phi}$

$$\tilde{f}_1 = \Delta\phi \mathrm{Re}\left\{\frac{1}{a}\alpha_- e^{i\hat{\phi}} x^{2a} \, {}_2F_1(1, a; a+1; -x^2)\right\},$$

(3.86)

$$\tilde{f}_2 = \beta\Delta\phi \cos 2\xi \, \mathrm{Re}\left\{\frac{1}{a}e^{2i\hat{\phi}} x^{4a} \, {}_2F_1(2, 2a; 2a+1; -x^2)\right\}$$

(3.87)

with $a = (i\Delta\phi + 1)/2$ and the hypergeometric function ${}_2F_1$ [WFS]. For short pulses, $\Delta\phi \ll 1$, $a \to 1/2$ becomes real, and the hypergeometric function take the limiting values [Rys57]

$$ {}_2F_1(1, a; a+1; -x^2) \to {}_2F_1\left(1, \frac{1}{2}; \frac{3}{2}; -x^2\right) = \frac{1}{x}\arctan x,$$

(3.88)

$$ {}_2F_1(2, 2a; 2a+1; -x^2) \to {}_2F_1(2, 1; 2; -x^2) = \frac{1}{1+x^2},$$

(3.89)
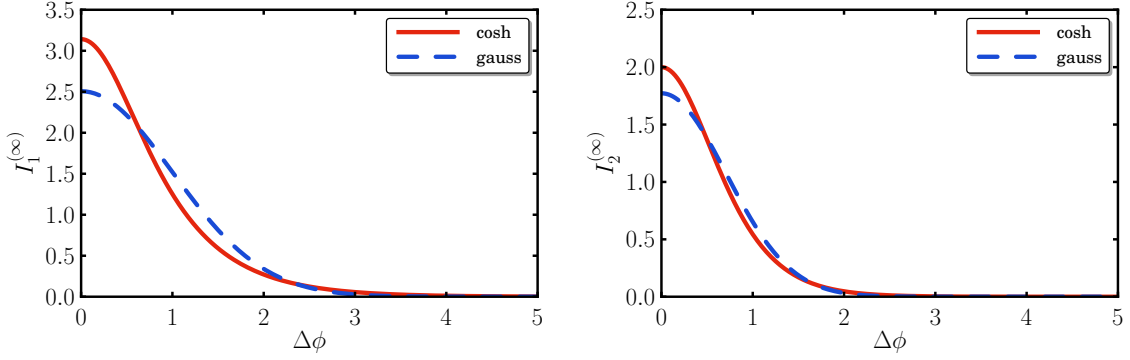
**Figure 3.14:** The phase shift functions $I_1^{(\infty)}$ (left panel) and $I_2^{(\infty)}$ (right panel) as a function of pulse length $\Delta\phi$ for the hyperbolic secant (red solid curves) and the Gaussian (blue dashed curves) pulse.

such that

$$\tilde{f}_1 = 2\Delta\phi \mathrm{Re}\left(\alpha_- e^{i\hat{\phi}}\right) \arctan\left(\exp\frac{\phi}{\Delta\phi}\right) , \tag{3.90}$$

$$\tilde{f}_2 = \Delta\phi\beta \cos 2\xi \, \cos 2\hat{\phi} \, \tanh\frac{\phi}{\Delta\phi} . \tag{3.91}$$

The complete phase reads for short pulses with $\Delta\phi \ll 1$

$$f(\phi) = \Delta\phi \mathrm{Re}\left(\alpha_- e^{i\hat{\phi}}\right) \arctan\left(\exp\frac{\phi}{\Delta\phi}\right)$$
$$+ \Delta\phi\beta(\cos^2\xi \, \cos^2\hat{\phi} + \sin^2\xi \sin^2\hat{\phi}) \tanh\frac{\phi}{\Delta\phi} , \tag{3.92}$$

recovering the result of [Mac11] for a single-cycle laser pulse with linear polarization, $\xi = 0$, and carrier envelope phase $\hat{\phi} = 0$.

In the opposite limit of long pulses, $\Delta\phi \gg 1$, the quantity $a$ becomes purely imaginary, $a \to i\Delta\phi/2$. The slowly varying envelope approximation can be obtained from Eqs. (3.86) and (3.87) by approximating [Rys57]

$$_2F_1(n, na; na + 1; -x^2) \to \, _2F_1(n, na; na; -x^2) = \frac{1}{(x^2 + 1)^n} , \tag{3.93}$$

which coincides with (3.81) for the hyperbolic secant envelope $g(\phi) = \cosh^{-1}\phi/\Delta\phi$. This explicitly shows how the general result Eqs. (3.86) and (3.87) for the hyperbolic secant pulse contains both the slowly varying envelope approximation for $\Delta\phi \gg 1$ and the single-cycle laser pulse approximation for $\Delta\phi \ll 1$ as limiting cases.

One of the main differences between the slowly varying envelope approximation and the full result is the build-up of an additional phase shift $\Delta\tilde{f}$ due to the oscillating part of the non-linear phase when going from the remote past, $\phi = -\infty$, to remote future, $\phi = +\infty$, in addition to the ponderomotive phase shift $\Delta f = \beta(G_2(\infty) - G_2(-\infty))$. In the SVEA, this phase shift is equal to zero, $\Delta\tilde{f}_{\mathrm{SVEA}} = 0$, as discussed above. In the exact expressions for the phase, however, the additional phase shift is non-zero and depends on the carrier envelope phase and polarization of the laser pulse via

$$\Delta\tilde{f} = \mathrm{Re}\left(\alpha_- e^{i\hat{\phi}}\right) \Delta\phi \, I_1^{(\infty)}(\Delta\phi) + \beta \cos 2\xi \, \cos 2\hat{\phi} \, \Delta\phi \, I_2^{(\infty)}(\Delta\phi) , \tag{3.94}$$

where the functions $I_n^{(\infty)}(\Delta\phi)$ are related to the asymptotics of the integrals $I_n$ (see Appendix A.4 for details). Thus, the total phase shift becomes now $\Delta f = \Delta f_{\text{SVEA}} + \Delta\tilde{f}$, where the first term is the ponderomotive phase shift originating from $\beta G_2$, which is also present in the SVEA, with $\Delta f_{\text{SVEA}} \propto \beta\Delta\phi$. The functions $I_1^{(\infty)}(\Delta\phi)$ and $I_2^{(\infty)}(\Delta\phi)$, depending only on the pulse length $\Delta\phi$ and the pulse shape, are depicted in Figure 3.14 for the hyperbolic secant (red solid curves) and Gaussian (blue dashed curves) pulse envelope. The additional phase is relevant for $\Delta\phi < 5$ only. For longer pulsed the phase shifts drop to zero exponentially fast. This explains why the slowly varying envelope is much better than expected, even down to $\Delta\phi = 5$, although it appears as an expansion in inverse powers of $\Delta\phi$.

In order to calculate higher order corrections in inverse powers of $\Delta\phi$ to the SVEA result one would have to perform further integrations by parts of the integrals on the right hand side of (3.78), e.g.

$$\int d\phi\, g e^{i\phi} = -ige^{i\phi} + g'e^{i\phi} + ig''e^{i\phi} - g'''e^{i\phi} + \dots. \tag{3.95}$$

Each term in a finite order approximation of that series contains a factor of $g$ or a derivative of $g$, which all vanish in the limit $\phi \to \pm\infty$. Thus, at any finite order approximation of the oscillating phase $\tilde{f}$, the phase shift $\Delta\tilde{f}$ will be identically zero. Thus, it is meaningless to calculate corrections to the SVEA to extend the range of applicability to pulses shorter than $\Delta\phi = 5$. The important effect of the phase shift cannot be obtained in this way.

## 3.9 Expansion into harmonics for pulsed plane waves

For the remainder of this chapter, the focus will be on laser pulses which fulfil the condition for the applicability of the SVEA. Then, in analogy with the harmonics in an IPW, as presented in Appendix C, one can also define harmonics for PPW given the condition $\Delta\phi \gg 1$ [Nar96b]. Since this is an approximation for long pulses, the carrier envelope phase $\hat{\phi}$ has only a marginal influence on the emission spectra and is, therefore, set to zero. Within the SVEA of pulsed laser fields, the oscillating part of the phase exponential[8] $\tilde{f}(\phi)$, as given in (3.81) is not periodic. However, non-periodic functions can be expanded into a (generalized) Fourier series over the floating interval $[\phi - \pi, \phi + \pi]$ according to [Nar96b]

$$e^{-i\tilde{f}(\phi)} = \sum_{\ell=-\infty}^{\infty} B_\ell(\phi) e^{-i\ell\phi}, \qquad \ell \in \mathbb{N} \tag{3.96}$$

with the non-constant, phase dependent Fourier coefficient functions

$$B_\ell(\phi) = \frac{1}{2\pi} \int_{\phi-\pi}^{\phi+\pi} d\phi'\, e^{i\ell\phi' - i\tilde{f}(\phi')} . \tag{3.97}$$

The form of the expansion coefficients $B_\ell(\phi)$ can be transferred from the corresponding Fourier expansion coefficients $B_\ell^{\text{IPW}}$ in monochromatic IPW (C.18) with the replacements $\bar{\alpha} \to \bar{\alpha}g(\phi)$ and $\beta \to \beta g^2(\phi)$, thus,

$$B_\ell^{\text{IPW}} \to B_\ell(\phi) = J_\ell(\bar{\alpha}g(\phi), \beta g^2(\phi)\cos 2\xi/2; \phi_0) , \tag{3.98}$$

where $\bar{\alpha} = |\alpha_-|$ and $\phi_0 = \arg\alpha_-$ such that $\alpha_- = \bar{\alpha}e^{i\phi_0}$, just as for IPW. In the limit of circular and linear laser polarizations, one may employ the corresponding expressions (C.19)

---

[8]The subscript SVEA will be omitted in the following. All quantities are assumed to be taken in the slowly varying envelope approximation.

and (C.20) for $B_\ell$, respectively. Plugging the Fourier series (3.96) into the expression for the phase integrals (3.19) one obtains the expansion of the latter ones as

$$
\begin{Bmatrix} \mathscr{A}_0(s) \\ \mathscr{A}_\pm(s) \\ \mathscr{A}_2(s) \end{Bmatrix} = \sum_\ell \int d\phi \begin{Bmatrix} B_\ell(\phi) \\ g(\phi)B_{\ell\mp1}(\phi) \\ g^2(\phi)\Big[B_\ell(\phi) + \frac{\cos 2\xi}{2}(B_{\ell+2}(\phi) + B_{\ell-2}(\phi))\Big] \end{Bmatrix}
$$
$$
\times \exp\{i(s-\ell)\phi - i\beta G_2(\phi)\}. \quad (3.99)
$$

This equation represents the general expression for the expansion of the phase integrals $\mathscr{A}_n(s)$ into a series of harmonics for arbitrary polarization of the laser pulse. Using this expansion, the non-linear Compton matrix element $\mathscr{M}(s)$ turns into a sum over partial amplitudes

$$
\mathscr{M}(s) = \sum_\ell \mathscr{M}_\ell(s). \tag{3.100}
$$

From here on, the case of circular laser polarization is considered with $B_\ell(\phi) = J_\ell(\bar{\alpha}g(\phi))e^{-i\ell\phi_0}$, such that the partial amplitudes can be written as

$$
\mathscr{M}_\ell(s) = e^{-i\ell\phi_0}\Big[\mathscr{T}_0 c_0^\ell(s-\ell) + \mathscr{T}_2 c_2^\ell(s-\ell) + e^{i\phi_0}\mathscr{T}_+ c_+^\ell(s-\ell)
$$
$$
+ e^{-i\phi_0}\mathscr{T}_- c_-^\ell(s-\ell)\Big] \quad (3.101)
$$

with the Dirac currents $\mathscr{T}_n$ from Eqs. (3.13) – (3.15) and purely real coefficients

$$
\begin{Bmatrix} c_0^\ell(s-\ell) \\ c_\pm^\ell(s-\ell) \\ c_2^\ell(s-\ell) \end{Bmatrix} = \int\limits_{-\infty}^{\infty} d\phi \begin{Bmatrix} J_\ell\big(\bar{\alpha}g(\phi)\big) \\ g(\phi)J_{\ell\mp1}\big(\bar{\alpha}g(\phi)\big) \\ g^2(\phi)J_\ell\big(\bar{\alpha}g(\phi)\big) \end{Bmatrix} \exp\{i(s-\ell)\phi - i\beta G_2(\phi)\}. \tag{3.102}
$$

In the expansion (3.100), the integer $\ell$ is interpreted as the net number of absorbed laser photons from the background field as for infinite monochromatic waves, thus labelling the harmonics. The seeming contradiction of continuous $s$ and integer $\ell$ can be resolved easily: In the energy momentum conservation (3.17) the photon four-momentum $k$ is calculated with the central frequency $\omega$. However, the pulsed laser field has a finite energy bandwidth $\Delta\omega/\omega \propto 1/\Delta\phi$. Therefore, it appears as if there would be a continuous photon number. Also the emitted photon spectrum is a continuous spectrum. It is impossible for PPW to formulate the energy-momentum conservation as $p + \ell k = p' + k'$ with integer $\ell$ which would imply that the harmonics have support on a delta comb. The energy-momentum conservation has to be stated as $p + sk = p' + k'$ and each of the harmonics $\ell$ has a broad support. In other words, for each harmonic $\ell$, there exists a range of values $s$ where the partial amplitude $\mathscr{M}_\ell(s)$ is substantially different from zero. The precise location of the support of the harmonics $\ell$ can be calculated using the following stationary phase analysis.

## 3.10   Stationary phase analysis

The integrals that determine the value of the coefficients $c_n^\ell(s-\ell)$ are of the form

$$
\int\limits_{-\infty}^{\infty} dx F(x)e^{iNG(x)} \tag{3.103}
$$

with an oscillating phase exponential; $N$ denotes the magnitude of the phase exponent. The stationary phase approximation, where the value of the integral is determined by the points of stationary phase, i.e. $dG/dx = 0$, is appropriate for $N \gg 1$. Thus, the values of the integrals (3.102) for the coefficients $c_n^\ell(s - \ell)$ are determined by the points where the exponential phase becomes stationary, i.e. where [Nar96b]

$$\frac{d}{d\phi}\left((s - \ell)\phi - \beta G_2(\phi)\right) \overset{!}{=} 0\,, \tag{3.104}$$

if the coefficients in the exponent $s$ and $\beta$ become large, in particular for $a_0 \gg 1$. The stationary phase points $\phi_\star$ are solutions of the equation

$$g(\phi_\star) = \sqrt{\frac{s - \ell}{\beta}}\,, \tag{3.105}$$

which are always found as pairs $\pm\phi_\star$ with $\phi_\star > 0$. The support of a certain harmonic $\ell$ is determined by the condition that there exist stationary phase points on the real axis, i.e. Eq. (3.105) possesses real solutions for $\phi_\star$. Explicit solutions for the stationary phase points for various pulse shapes are listed in Table 3.1.

The conditions for the existence of real stationary phase points are that in (3.105) the argument of the square root has to be positive and the value of the square root has to be larger than zero and smaller than unity since $0 \leq g(\phi) \leq 1$. Thus, for a given harmonic $\ell$, the allowed range of $s$ is bounded as (note that $\beta < 0$)

$$\beta + \ell \leq s \leq \ell\,, \tag{3.106}$$

independent of the explicit shape of the pulse (except for the box-shaped pulse where this method cannot be applied). Outside this region the stationary phase has an imaginary part leading to an exponential suppression of the coefficient functions $c_n^\ell(s - \ell)$. These regions where the harmonics have support are exhibited in Figure 3.15. In the left panel, where $s$ and $\beta$ are considered as independent variables, the support of the harmonics with $\ell = 1, 2, \ldots$ are indicated as differently coloured shaded areas. However, the variables $\beta$ can be expressed as a function of $s$ and the scattering $\theta$ as

$$\beta = -\frac{a_0^2 s}{4}\frac{1 - v}{1 - v\cos\theta}(1 + \cos\theta)\,, \tag{3.107}$$

for head-on collisions with $-\boldsymbol{p} \parallel \boldsymbol{k}$, where $v = \tanh\zeta = \sqrt{\gamma^2 - 1}/\gamma$ denotes the velocity of the initial electron. Since $s$ itself can be expressed as a function of $\omega'$ and $\theta$, the harmonic supports can be easily translated to the $\omega' - \theta$ phase space. This is exhibited in the right panel of Figure 3.15 as shaded areas for $\ell = 1 \ldots 8$ in colour and for $\ell \geq 9$ in grey. These areas are bounded by the IPW harmonics for the scattered frequency $\omega_\ell'(\theta; a_0)$ (cf. C.25), where the lower boundary of the PPW harmonic coincides with the IPW harmonic $\omega_\ell'(\theta; a_0)$ and the upper boundary of the PPW harmonic coincides with the IPW harmonic in a weak field $\omega_\ell'(\theta; 0)$. The individual harmonics start to overlap if the lower edge of the $\ell + 1$st harmonic coincides with the upper edge of the $\ell$th harmonic, i.e.

$$\omega_\ell'(\theta; a_0 \to 0) \geq \omega_{\ell+1}'(\theta; a_0). \tag{3.108}$$

This happens always for sufficiently large values of $a_0$ and $\ell$, see e.g. the right panel of Figure 3.15. The parameters in Figure 3.15 are $a_0 = 1$ and $\gamma = 100$. The black dashed, dotted and dash-dotted lines depict the same cuts in phase space in the left and right panels
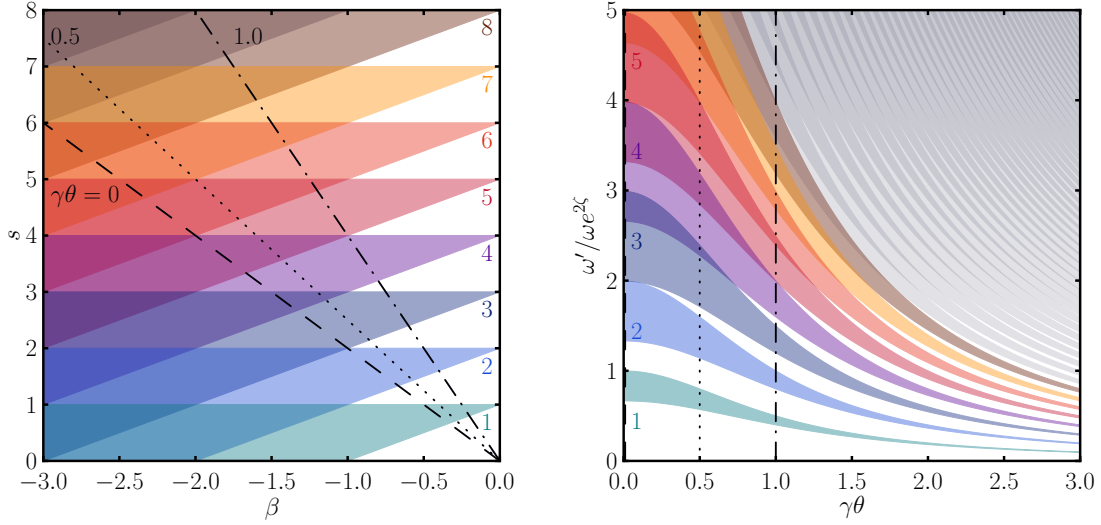
**Figure 3.15:** The support of the individual harmonics for different values of $\ell$ in a PPW in the $s - \beta$ plane (left panel) and in the $\omega' - \theta$ plane (right panel). The coloured labels in both panels are the values of $\ell$ corresponding to that particular harmonic. The dashed, dotted and dash-dotted lines in both panels depict the same cuts in phase space for constant values of $\gamma\theta = 0.0$, 0.5 and 1.0, respectively.

for constant values of $\gamma\theta = 0.0$, 0.5 and 1.0, respectively. This practically shows how the information of the left panel, where $s$ and $\beta$ are considered as independent variables, can be translated to the real physical phase space of $\omega'$ and $\theta$. The width of the harmonics as described here is a reformulation of the fact that in a (continuous) pulse (excluding the box-shaped pulse explicitly) the intensity changes continuously from zero up to the maximum value related to $a_0$. Simply speaking, during all the time the electron emits radiation with different intensity-dependent red-shifts which leads to the broadening of the harmonics. This is the ponderomotive broadening effect. The appearance of sub-peaks can be explained as an interference effect. This issue will be dealt with below.

As a result of energy-momentum conservation, one only has to consider harmonics with $\ell > 0$ in (3.100) since only these non-negative harmonics correspond to a net absorption of laser photons with a support for $s > 0$. As discussed above in Section 3.2, the statement $s > 0$ is equivalent to the statement that the frequency of the emitted photon must obey $\omega' > 0$. Thus, the sum in (3.100) effectively starts at $\ell = 1$. Beyond the stationary phase approximation, the harmonic supports will be larger than the predicted value in the stationary phase approximation (SPA) due to bandwidth effects, with the details depending on the shape of the pulse envelope. In general, stating that the bandwidth is $\propto 1/\Delta\phi$ one can say that the bandwidth-broadened harmonics are given by the interval

$$\beta + \ell - \Delta\phi^{-1} \leq s \leq \ell + \Delta\phi^{-1}. \tag{3.109}$$

As a result of this, the term with $\ell = 0$ can also contribute to the emission spectrum at low frequencies in the vicinity of $\omega' = 0$. Depending on the dominant broadening mechanism, one distinguishes the ponderomotive broadening regime and the bandwidth dominated regime. For long pulses $\Delta\phi \gg 1$ and thus $\Delta\phi^{-1} \ll 1$. Thus, for long pulses, one is in the ponderomotive regime.

**Table 3.1:** A collection of the derivatives of various envelope functions $g$ and various other important relations for the stationary phase analysis.

| | hyperbolic secant | Gaussian | squared cosine |
|---|---|---|---|
| $g(\phi)$ | $\frac{1}{\cosh\frac{\phi}{\Delta\phi}}$ | $\exp\left\{-\frac{\phi^2}{2\Delta\phi^2}\right\}$ | $\cos^2\frac{\pi\phi}{2\Delta\phi}\sqcap(\phi)$ |
| $g'(\phi)$ | $-\frac{1}{\Delta\phi}g\sqrt{1-g^2}$ | $-\frac{\phi}{\Delta\phi^2}g$ | $-\frac{\pi}{\Delta\phi}\sqrt{g-g^2}$ |
| $g''(\phi)$ | $\frac{g}{\Delta\phi^2}(1-2g^2)$ | $(\frac{\phi^2}{\Delta\phi^4}-\frac{1}{\Delta\phi^2})g$ | $\frac{\pi^2}{2\Delta\phi^2}(1-2g^2)$ |
| $g''(0)$ | $-\frac{1}{\Delta\phi^2}$ | $-\frac{1}{\Delta\phi^2}$ | $-\frac{\pi^2}{2\Delta\phi^2}$ |
| $\phi_\star$ | $\Delta\phi\,\mathrm{Arcosh}\sqrt{\frac{\beta}{s-\ell}}$ | $\Delta\phi\sqrt{\ln\frac{\beta}{s-\ell}}$ | $\frac{2\Delta\phi}{\pi}\arccos\left(\frac{s-\ell}{\beta}\right)^{\frac{1}{4}}$ |
| $g'(\phi_\star)$ | $-\frac{1}{\Delta\phi}\sqrt{1-\frac{s-\ell}{\beta}}\sqrt{\frac{s-\ell}{\beta}}$ | $-\frac{1}{\Delta\phi}\sqrt{-\frac{s-\ell}{\beta}\ln\frac{s-\ell}{\beta}}$ | $-\frac{\pi}{\Delta\phi}\sqrt{\sqrt{\frac{s-\ell}{\beta}}-\frac{s-\ell}{\beta}}$ |

The SPA of the integral (3.103) reads

$$\int_{-\infty}^{\infty} dx\, F(x)e^{iNG(x)} \xrightarrow{\text{SPA}} \sum_{x_\star} F(x_\star)\sqrt{\frac{2\pi}{iNG''(x_\star)}}\,e^{iNG(x_\star)}\,, \tag{3.110}$$

where the sum goes over all stationary points $x_\star$ on the real axis and $G''(x_\star) \equiv d^2G/dx^2|_{x=x_\star}$. Thus, the SPA of the coefficients (3.102) at a given value of $s$ is given by the sum of the contributions from the two symmetric stationary points

$$
\begin{aligned}
c_n^\ell(s-\ell) &= J_{L_n}\big(\bar{\alpha}g(\phi_\star)\big)g^{|n|}(\phi_\star)\sqrt{\frac{2\pi}{|\beta G_2''(\phi_\star)|}}\\
&\qquad\times \exp\left\{i(s-\ell)\phi_\star - i\beta G_2(\phi_\star) - i\frac{\pi}{4}\right\}\\
&\quad + J_{L_n}\big(\bar{\alpha}g(-\phi_\star)\big)g^{|n|}(-\phi_\star)\sqrt{\frac{2\pi}{|\beta G_2''(-\phi_\star)|}}\\
&\qquad\times \exp\left\{-i(s-\ell)\phi_\star - i\beta G_2(-\phi_\star) + i\frac{\pi}{4}\right\}\\
&= J_{L_n}\big(\bar{\alpha}g(\phi_\star)\big)g^{|n|}(\phi_\star)\sqrt{\frac{4\pi}{|\beta g(\phi_\star)g'(\phi_\star)|}}\cos\left\{(s-\ell)\phi_\star - \beta G_2(\phi_\star) - \frac{\pi}{4}\right\}
\end{aligned}
\tag{3.111}
$$

with the index

$$L_n = \begin{cases} \ell, & n = 0,2\,,\\ \ell\mp 1, & n = \pm\,, \end{cases} \tag{3.112}$$

using the definition that $|n| = 1$ for $n = \pm$, and $G_2''(\phi_\star) = 2g(\phi_\star)g'(\phi_\star)$. The explicit values for the stationary phase points as well as for the derivatives $g'$ are listed in Table 3.1. The oscillations of the coefficient functions $c_n^\ell$, i.e. the appearance of sub-peaks in the harmonics, stem from the cosine term in (3.111). This allows to estimate the number of sub-peaks $N_{\text{S-P}}$ in a given harmonic $\ell$ since the number of zeros $K$ in the harmonic equals the number of sub-peaks as $N_{\text{S-P}} = K$. The functions $c_n^\ell$ are zero whenever the contributions from the two

symmetric stationary points interfere destructively; they coincide with the zeros of the cosine term in (3.111), i.e. whenever the stationary phase points fulfil the additional equation

$$
\beta \left[ \phi_\star^k g^2(\phi_\star^k) - \int\limits_0^{\phi_\star^k} d\phi\, g^2(\phi) \right] - \left( \frac{1}{4} - k \right) \pi = 0 \tag{3.113}
$$

defining a series $(s_k)$ of zeros of the coefficient functions, $c_n^\ell(s_k - \ell) = 0$. The total number of zeros $K$ is the number of different integer values $k$ that can fulfil Eq. (3.113), i.e. $K = k_{\max} - k_{\min}$, which is determined by the range of values that the term in the square brackets in (3.113) can take. On noting that the function in the square brackets in (3.113) is a monotonically decreasing function of its argument $\phi_\star^k$, it suffices to consider the asymptotic values at $\phi_\star^k \to \pm\infty$. The first term in the square brackets goes to zero when approaching infinity due to the presence of the pulse envelope $g$. The range of values is therefore $\beta \int_{-\infty}^{\infty} d\phi\, g^2(\phi)$ which one easily recognizes as the ponderomotive phase shift $\Delta f$. To obtain the exact number of sub-peaks $N_{\text{S}-\text{P}}$ one has to include an additional factor of $1/2$ to correct for the double counting of the symmetric stationary phase points $\pm\phi_\star$. Since the ponderomotive phase shift is a function of $s$, with $s \sim \ell$ for the $\ell$th harmonic, one multiplies $\Delta f$ by a factor $\ell/s$ to obtain a number that characterizes a given harmonic $\ell$. The final result for the number of sub-peaks in the $\ell$th harmonic is given by

$$
N_{\text{S}-\text{P}} = \frac{|\Delta f|}{2\pi} \frac{\ell}{s} = \frac{\nu_2[g]|\beta\Delta\phi|}{2\pi} \frac{\ell}{s} = \ell\nu_2[g] \frac{a_0^2 \Delta\phi}{8\pi} \frac{1-v}{1-v\cos\theta}(1+\cos\theta) . \tag{3.114}
$$

The last line in (3.114) employs the representation (3.107) for $\beta$ and is valid for head-on collisions with $-\boldsymbol{p} \parallel \boldsymbol{k}$. The factor $\nu_2[g]$ is a characteristic number of order unity for each pulse shape $g$. Explicit values for the relevant pulse shapes are given in Table A.1 in Appendix A.3. This result is the proof for the empirical fact that the number of sub-peaks in a given harmonic scale as $N_{\text{S}-\text{P}} = P a_0^2 \Delta\phi$, as stated above in Section 3.4. There, in Eq. (3.44), the factor of proportionality $P$ was determined as $P = 0.16$ for backscattering of the first harmonic in a hyperbolic secant pulse ($\theta = 0$, $\ell = 1$) by counting the number of sub-peaks for various sets of numerical parameters. Here, using (3.114), the exact number for that situation is calculated as $P = 1/2\pi \simeq 0.159$. This result is a generalization of the findings of [Har10] within the classical theory of Thomson scattering for hyperbolic cosine pulse shapes in the backscattering direction to the quantum theory of Compton scattering for arbitrary pulse shapes and arbitrary scattering angles.

## 3.11   Analytical result for the partial amplitudes $\mathscr{M}_\ell(s)$

To understand the physical content and the pulse shape dependence of the partial matrix elements (3.101) beyond the general analysis of the preceding section using general stationary phase arguments one needs to study the pulse shape and pulse length dependence of the coefficients $c_n^\ell(s - \ell)$, defined in (3.102). However, the pulse envelope $g(\phi)$ inconveniently appears as argument of the Bessel functions there. Using the multiple argument formula for Bessel functions [WFS] the pulse envelope $g$ can be removed from the argument of the Bessel functions $J_\ell$ via a series expansion

$$
J_\ell(\bar{\alpha}g) = g^\ell(\phi) \sum_{k=0}^{\infty} (1 - g^2(\phi))^k \frac{J_{\ell+k}(\bar{\alpha})}{k!} \left( \frac{\bar{\alpha}}{2} \right)^k , \quad \ell \in \mathbb{N} \tag{3.115}
$$

which is a power series in $1 - g^2(\phi)$. The expansion coefficients contain Bessel functions of higher order $\geq \ell$ times powers of $\bar{\alpha}$, leading to a sequence of approximations by truncating
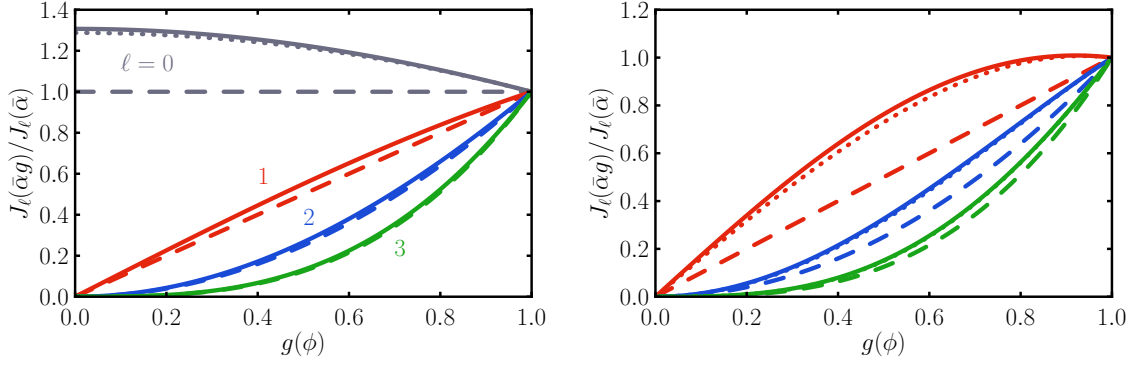
**Figure 3.16:** The functions $J_\ell(\bar{\alpha}g)$ scaled by $J_\ell(\bar{\alpha})$ as a function of $g$ for $\bar{\alpha} = 1$ (left panel) and $\bar{\alpha} = 2$ (right panel). The solid curves depict the full functions $J_\ell(\bar{\alpha}g)$ for $\ell = 0$ (grey), 1 (red), 2 (blue) and 3 (green). The dashed and dotted curves display the zeroth-order and first-order approximation, i.e. terms up to $k = 0$ and $k = 1$ are considered in Eq. (3.115), respectively.

the series at a finite order in $k$. The lowest order contribution, $k = 0$, explicitly reads $J_\ell(\bar{\alpha}g) \simeq g^\ell J_\ell(\bar{\alpha})$. For not too large values of $\bar{\alpha}$, i.e. for $\bar{\alpha}$ smaller than the first stationary point of the Bessel function where $dJ_\ell/d\bar{\alpha} = 0$, this lowest order term is sufficient (excluding $\ell = 0$). The behaviour of $J_\ell(\bar{\alpha}g)$ as a function of $g$ is exhibited in Figure 3.16 for $\bar{\alpha} = 1$ ($\bar{\alpha} = 2$) in the left (right) panel. The different curves are for $\ell = 0$ (grey), 1 (red), 2 (blue) and 3 (green). Full curves depict the full function $J_\ell(\bar{\alpha}g)$, while the dashed curves are for the zeroth-order ($k = 0$) approximation $J_\ell(\bar{\alpha}g) \simeq g^\ell J_\ell(\bar{\alpha})$ and the dotted curves are for the first-order approximation

$$J_\ell(\bar{\alpha}g) \simeq g^\ell J_\ell(\bar{\alpha}) + g^\ell(1 - g^2)J_{\ell+1}(\bar{\alpha})\frac{\bar{\alpha}}{2} \,. \tag{3.116}$$

For low lying harmonics, i.e. for small $\ell$, the expansion shows the worst convergence. One reason for this is that the first stationary point of the Bessel functions increases with the order of the Bessel function. Thus, for larger values of $\ell$, the series in $k$ in Eq. (3.115) might be truncated at a lower order. In Figure 3.16, the convergence for $\ell = 3$ is seen to be much better than for lower values of $\ell$; the zeroth-order approximation is sufficiently accurate even for $\bar{\alpha} = 2$, where the first-order is required for $\ell = 1$. In particular, for the $\ell = 0$ term, the zeroth-order approximation, i.e. the term with $k = 0$, is inaccurate since in the lowest-order approximation $J_0(\bar{\alpha})$ is a constant while $J_0(\bar{\alpha}g(\phi))$ is not (see grey curves in the left panel of Figure 3.16). For large values of $\ell$, $g(\phi)^\ell$ typically is much narrower than $g(\phi)$ itself [compare the orange curves in the two panels of Figure 3.17 for $\ell = 1$ (left) and 3 (right)]. Thus, higher harmonics are more sensitive to the high-intensity regions at the centre of the pulse, leading to a stronger accumulation of spectral strength in the vicinity of the non-linear IPW resonance at $s = \ell + \beta$. The higher-order correction $(1 - g^2)^k$ vanish at the centre of the pulse, they are sensitive to the low-intensity regions in the pulse, thus, leading to an increased emission in the vicinity of the linear IPW resonance at $s = \ell$. For larger values of $\ell$, the higher-order corrections in $k$ are suppressed due to smaller overlap of $g^\ell$ with $(1 - g^2)^k$, as one can observe by a comparison of the brown or black curves (for $k = 2$ or $k = 5$, respectively) in the two panels of Figure 3.17. In the right panel (for $\ell = 3$), the overlap is much smaller than in the left panel (for $\ell = 1$). The rapidly decreasing overlap between $g^\ell$ and $(1 - g^2)^k$ explains why for larger the value of $\ell$, fewer terms of the sum over $k$ have to be considered.

Employing the argument expansion series (3.115) for the Bessel functions in the definition
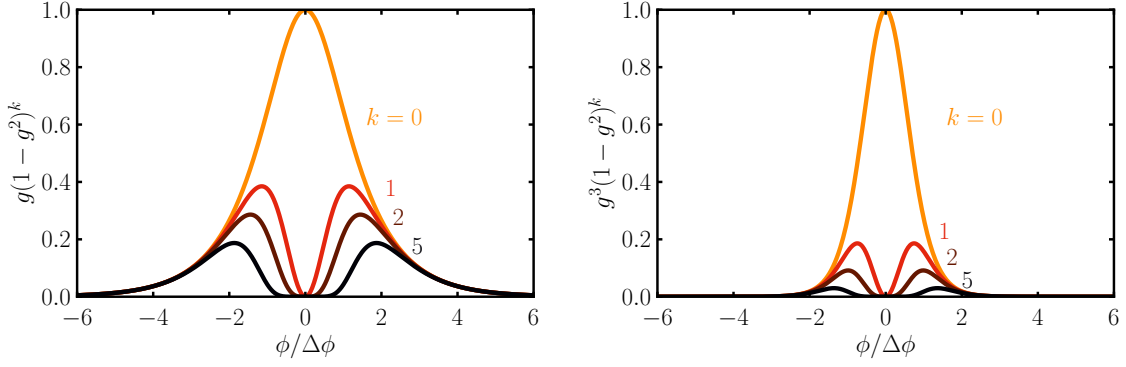
**Figure 3.17:** Contributions to the series in (3.115) as a function of the scaled phase $\phi/\Delta\phi$. The curves are for the leading term $k = 0$ (orange) as well as $k = 1$ (red), 2 (brown) and 5 (black). The left panel is for the first harmonic $\ell = 1$ and the right panel is for the third harmonic $\ell = 3$. Higher order terms in $k$ are sensitive to the edges of the pulse. For higher values of $\ell$ the higher-order terms in $k$ are suppressed due to smaller overlap of $g^\ell$ with $(1 - g^2)^k$.

of the coefficients $c_n^\ell$, the corresponding series representations for the latter ones read

$$
\begin{Bmatrix} c_0^\ell(s) \\ c_\pm^\ell(s) \\ c_2^\ell(s) \end{Bmatrix} = \sum_{k=0}^\infty \frac{1}{k!} \left( \frac{\bar{\alpha}}{2} \right)^k \begin{Bmatrix} J_{\ell+k}(\bar{\alpha}) \, \mathcal{B}_\ell^{(k)}(s, \beta) \\ J_{\ell+k\mp1}(\bar{\alpha}) \, \mathcal{B}_{\ell+1\mp1}^{(k)}(s, \beta) \\ J_{\ell+k}(\bar{\alpha}) \, \mathcal{B}_{\ell+2}^{(k)}(s, \beta) \end{Bmatrix} , \tag{3.117}
$$

where the ponderomotive integrals $\mathcal{B}_n^{(k)}(s, \beta)$ are defined by

$$
\mathcal{B}_n^{(k)}(s, \beta) = \int_{-\infty}^\infty d\phi \, g^n(\phi) \Big( 1 - g^2(\phi) \Big)^k e^{is\phi - i\beta G_2} . \tag{3.118}
$$

In the monochromatic IPW limit, $g \to 1$, these integrals collapse to $\mathcal{B}_n^{(k)}(s, \beta) \to \delta_{k0}\delta(s - \beta)$. For functions $\mathcal{B}_n^{(k)}$ with $k > 0$, recurrence relations can be found using $(1 - g^2)^k = (1 - g^2)^{k-1} - g^2(1 - g^2)^{k-1}$, yielding

$$
\mathcal{B}_n^{(k)}(s, \beta) = \mathcal{B}_n^{(k-1)}(s, \beta) - \mathcal{B}_{n+2}^{(k-1)}(s, \beta) . \tag{3.119}
$$

Subsequent applications of (3.119) furnishes a binomial-like sum rule, relating arbitrary terms with $k > 0$ to terms with $k = 0$ as

$$
\mathcal{B}_n^{(k)}(s, \beta) = \sum_{\nu=0}^k (-1)^\nu \binom{k}{\nu} \mathcal{B}_{n+2\nu}^{(0)}(s, \beta) . \tag{3.120}
$$

Thus, one has to calculate the coefficients with $k = 0$ only. The ponderomotive integrals $\mathcal{B}_n^{(k)}$ are well defined for $n > 0$ but in $\mathcal{B}_0^{(k)}$, in particular in $\mathcal{B}_0^{(0)}(s, \beta)$, the pre-exponential pulse shape function $g$ making the integral convergent is missing, therefore, this integral diverges. The origin of the divergence of $\mathscr{A}_0(s)$ has been localized formally in the expansion into harmonics as part of the contribution to the $\ell = 0$ harmonic. This coincides with the observation above that the divergence of $\mathscr{A}_0(s)$ is $\propto \delta(s)$. In particular, for the divergent expression $\mathcal{B}_0^{(0)}(s, \beta)$ one can regularize the integral by performing an integration by parts in

the spirit of [Boc09], yielding

$$\mathcal{B}_0^{(0)}(s,\beta) = \frac{\beta}{s}\mathcal{B}_2^{(0)}(s,\beta)\,. \tag{3.121}$$

For the divergent terms $\mathcal{B}_0^{(k)}(s,\beta)$ with $k \geq 1$, one may use the recursion relation (3.119) to reduce the order of $k$. The ponderomotive integrals (3.118), have the following analytical properties

$$\mathcal{B}_n^{(k)}(s,\beta)^* = \mathcal{B}_n^{(k)}(s,\beta)\,, \qquad\qquad \text{reality}\,, \tag{3.122}$$

$$\mathcal{B}_n^{(k)}(-s,-\beta) = \mathcal{B}_n^{(k)}(s,\beta)\,, \qquad\qquad \text{reflection symmetry}\,. \tag{3.123}$$

Furthermore, after a rescaling of the integration variable $\phi \to \phi/\Delta\phi$, the pulse length $\Delta\phi$ appears only as a global pre-factor and in combination $s\Delta\phi$ or $\beta\Delta\phi$, such that

$$\mathsf{B}_n^{(k)}(s\beta) \equiv \frac{1}{\Delta\phi}\mathcal{B}_n^{(k)}\left(\tfrac{s}{\Delta\phi},\tfrac{\beta}{\Delta\phi}\right) \tag{3.124}$$

is independent of the pulse length $\Delta\phi$. This provides a scale-invariant master-spectrum for all pulse lengths. The scale invariance is provided by the SVEA due to the fact that the oscillating part of the non-linear phase exponential is proportional to powers of the envelope function $g$, and the phase $\tilde{f}(\phi)$ has the same value at $\phi = \pm\infty$, thus, $\Delta\tilde{f} = 0$ as discussed above. The scale invariance is the reason why non-linear effects are expected also for weak laser fields, i.e. for values $a_0 \ll 1$, if the pulse length is sufficiently large [Har10]. The appearance of sub-peaks as non-linear effect is sensitive to the the parameter $a_0^2\Delta\phi$ as discussed in the previous Section 3.10 using stationary phase arguments. Here, the same result is obtained with the argument of the scale-invariant master spectrum. The scale invariance is broken for ultra-short laser pulses, i.e. for pulse lengths $\Delta\phi = \mathcal{O}(1)$, where the SVEA becomes inapplicable. Some examples for the master spectra are exhibited in Figure 3.18 for $g = \cosh^{-1}\phi/\Delta\phi$. The functions $\mathsf{B}_1^{(0)}$ (top left), $\mathsf{B}_3^{(0)}$ (top right), $\mathsf{B}_1^{(2)}$ (bottom left) and $\mathsf{B}_3^{(2)}$ (bottom right) are shown in the $s-\beta$ plane, considering $s$ and $\beta$ as independent variables. One clearly sees that the master spectra are non-zero in the region between the two lines $s = 0$ and $s = \beta$, where they are oscillating functions. Outside of this region, the functions $\mathsf{B}_n^{(k)}$ rapidly drop to zero. This support confirms the findings of the stationary phase analysis in Section 3.10. Another feature of the numeric results in Figure 3.18 is that the terms with $k = 2$ have the tendency to have larger values in the vicinity of the line $s = 0$, i.e. beneath the linear IPW resonance, which confirms the above assertion that the correction with higher values of $k$ are sensitive to the low-intensity regions of the pulse. Furthermore, for $\mathsf{B}_3^{(0)}$ (top right panel in Figure 3.18) one finds the anticipated accumulation of spectral strength in the vicinity of the non-linear IPW resonance at the line $s = \beta$.

The final formula for the $\ell$th partial amplitude, using the expansion (3.117) in (3.101), reads

$$\begin{aligned}
\mathcal{M}_\ell(s) = e^{-i\ell\phi_0}\sum_{k=0}^{\infty}\frac{1}{k!}\left(\frac{\bar{\alpha}}{2}\right)^k \Big\{ &\mathcal{T}_0\,J_{\ell+k}(\bar{\alpha})\,\mathcal{B}_\ell^{(k)}(s-\ell,\beta) \\
&+\ \mathcal{T}_2\,J_{\ell+k}(\bar{\alpha})\,\mathcal{B}_{\ell+2}^{(k)}(s-\ell,\beta) \\
&+\ \mathcal{T}_+\,J_{\ell+k-1}(\bar{\alpha})\,\mathcal{B}_\ell^{(k)}(s-\ell,\beta)\,e^{i\phi_0} \\
&+\ \mathcal{T}_-\,J_{\ell+k+1}(\bar{\alpha})\,\mathcal{B}_{\ell+2}^{(k)}(s-\ell,\beta)\,e^{-i\phi_0} \Big\}\,.
\end{aligned} \tag{3.125}$$

Employing also the recursion relation for the ponderomotive integrals $\mathcal{B}_n^{(k)}$, Eq. (3.119), one arrives at an expression for the partial matrix element where all $\mathcal{B}_n^{(k)}$ are replaced by
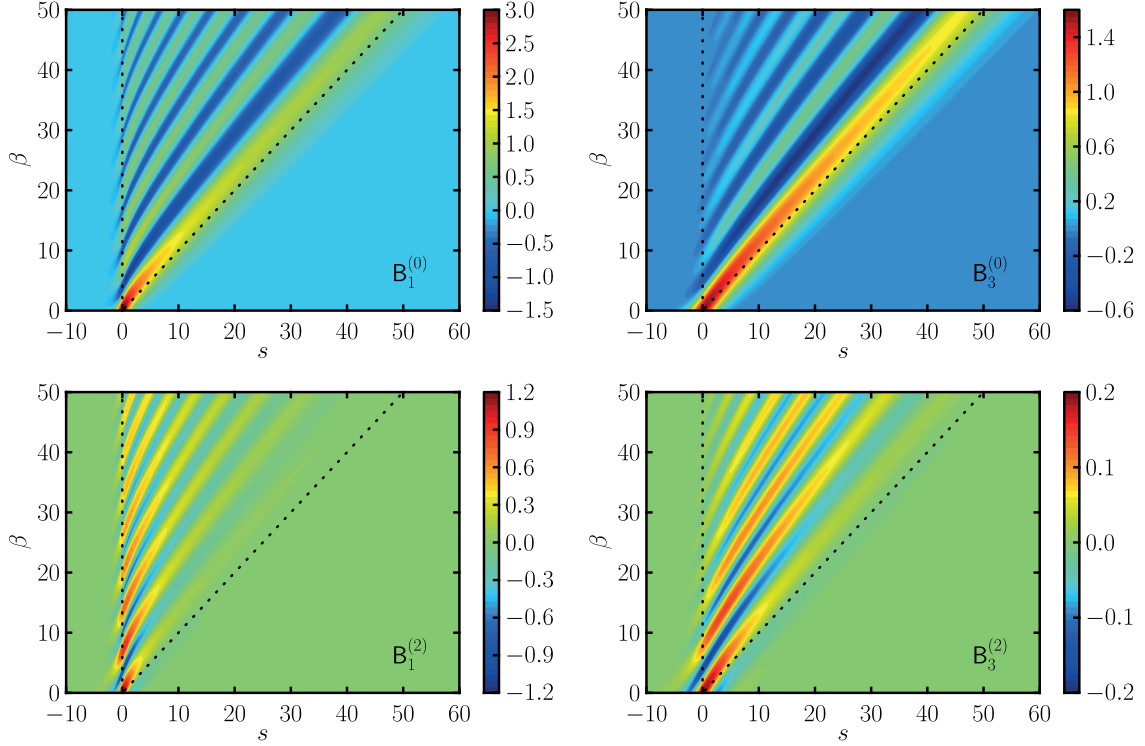
**Figure 3.18:** Contourplot of the ponderomotive master spectra $\mathsf{B}_n^{(k)}(s,\beta)$ as a function of $s$ and $\beta$ for various values of $(n,k) = (1,0)$ in top left panel panel, $(3,0)$ in the top right panel, $(1,2)$ in bottom left panel and $(3,2)$ in the bottom right panel.

$\mathcal{B}_n^{(0)} \equiv \mathcal{B}_n,$

$$\mathcal{M}_\ell(s) = e^{-i\ell\phi_0} \sum_{k=0}^{\infty} \sum_{\nu=0}^{k} \frac{(-1)^\nu}{k!} \left(\frac{\bar{\alpha}}{2}\right)^k \binom{k}{\nu}$$
$$\times \left\{ \mathcal{B}_{\ell+2\nu}(s-\ell,\beta) \Big[ \mathscr{T}_0 \, J_{\ell+k}(\bar{\alpha}) + \mathscr{T}_+ \, J_{\ell+k-1}(\bar{\alpha}) \, e^{i\phi_0} \Big] \right.$$
$$\left. + \mathcal{B}_{\ell+2\nu+2}(s-\ell,\beta) \Big[ \mathscr{T}_2 \, J_{\ell+k}(\bar{\alpha}) + \mathscr{T}_- \, J_{\ell+k+1}(\bar{\alpha}) \, e^{-i\phi_0} \Big] \right\} . \qquad (3.126)$$

In the case of not too strong fields ($\bar{\alpha} \lesssim 1$), the lowest-order approximation of the sum over $k$

$$\mathcal{M}_\ell(s) = e^{-i\ell\phi_0} \left\{ \mathcal{B}_\ell(s-\ell,\beta) \Big[ \mathscr{T}_0 \, J_\ell(\bar{\alpha}) + \mathscr{T}_+ \, J_{\ell-1}(\bar{\alpha}) \, e^{i\phi_0} \Big] \right.$$
$$\left. + \mathcal{B}_{\ell+2}(s-\ell,\beta) \Big[ \mathscr{T}_2 \, J_\ell(\bar{\alpha}) + \mathscr{T}_- \, J_{\ell+1}(\bar{\alpha}) \, e^{-i\phi_0} \Big] \right\} \qquad (3.127)$$

is sufficient.

If the pulse envelope $g$ is specified as a hyperbolic secant pulse, $g = \cosh^{-1} \phi/\Delta\phi$, it is possible to derive a completely analytical result for the partial amplitudes $\mathcal{M}_\ell$. In this case, the ponderomotive integrals $\mathcal{B}_n(s,\beta)$ possess a representation with special functions. It was discovered that the phase integrals (3.19) can have solutions as degenerate confluent hypergeometric functions [Har96b, Har02] or equivalently as Laguerre polynomials [Har10] for circular laser polarization and a hyperbolic secant envelope in the special case of backscattering, $\theta = 0$, for the fundamental harmonic, i.e. $\bar{\alpha} = 0$ and $\ell = 1$. For that special case it can

be shown that the SVEA is exact. In the general case of arbitrary scattering angle and for arbitrary harmonics, a generalization of the results of [Har02, Har10] can be derived. After three subsequent changes of variables in (3.118), $x = \exp \phi/\Delta\phi$, $z = (x^2 - 1)/(x^2 + 1)$ and $t = (1 + z)/2$, one arrives at

$$\mathcal{B}_n(s, \beta) = 2^{n-1} \Delta\phi \, e^{-i\Delta\phi\beta} \int\limits_0^1 dt \, t^{(n-2+i\Delta\phi s)/2} (1 - t)^{(n-2-i\Delta\phi s)/2} e^{2i\Delta\phi\beta t} \, . \tag{3.128}$$

The integral can be recognized as being related to the generalized Laguerre functions [WFS]

$$\mathcal{L}^\lambda_\mu(z) = -\frac{\sin \pi\mu}{\pi} \int\limits_0^1 dt \, e^{zt} \, t^{-\mu-1} (1 - t)^{\mu+\lambda} \tag{3.129}$$

with the constraints $\mathrm{Re}\,(\mu+\lambda) > -1$ and $\mathrm{Re}\,\mu < 0$. Identifying $z = 2i\Delta\phi\beta$, $\mu = -(n+i\Delta\phi s)/2$ and $\lambda = n - 1$ one obtains

$$\mathcal{B}_n(s, \beta) = \frac{2^{n-1}\Delta\phi\pi}{\sin \frac{\pi}{2}(n + i\Delta\phi s)} e^{-i\Delta\phi\beta} \mathcal{L}^{n-1}_{-(n+i\Delta\phi s)/2}(2i\Delta\phi\beta). \tag{3.130}$$

The previously considered case [Har10] mentioned above would correspond to $n = 1$ in this notation. The constraints $\mathrm{Re}\,(\mu + \lambda) = n/2 - 1 > -1$ and $\mathrm{Re}\,\mu = -n/2 < 0$ require $n > 0$. So again, the missing pre-exponential for $n = 0$ manifests itself in ill-defined mathematical relations that need to be handled with special care, e.g. by a regularization as in (3.121).

The completely analytical result for the partial amplitudes for hyperbolic secant pulse is given by

$$\mathcal{M}_\ell(s) = \pi\Delta\phi \frac{e^{-i\ell\phi_0 - i\Delta\phi\beta}}{\sin \frac{\pi}{2}(\ell + i(s - \ell)\Delta\phi)} \sum_{k,\nu} \frac{\bar{\alpha}^k}{k!} 2^{\ell-k+2\nu-1} \binom{k}{\nu}$$
$$\times \left\{ \mathcal{L}^a_b(2i\beta\Delta\phi) \left[ \mathscr{T}_0 \, J_\ell(\bar{\alpha}) + \mathscr{T}_+ \, J_{\ell-1}(\bar{\alpha}) \, e^{i\phi_0} \right] \right.$$
$$\left. -4\mathcal{L}^{a+2}_{b-1}(2i\beta\Delta\phi) \left[ \mathscr{T}_2 \, J_\ell(\bar{\alpha}) + \mathscr{T}_- \, J_{\ell+1}(\bar{\alpha}) \, e^{-i\phi_0} \right] \right\} , \tag{3.131}$$

with $a = \ell + 2\nu - 1$ and $b = -(\ell + 2\nu + i(s - \ell)\Delta\phi)/2$. This concludes the analytical study of the non-linear Compton scattering matrix element. All space-time integrations in $S$ matrix have been performed analytically under the condition $\Delta\phi \gg 1$ and for the hyperbolic secant pulse $g = \cosh^{-1} \phi/\Delta\phi$, yielding a series of generalized Laguerre functions, for which many mathematical properties are known.

The arguments of the Laguerre functions depend only on the values of $s$, $\beta$ and the pulse length, while the dependence on the variable $\bar{\alpha}$ is solely in the Bessel functions. This result could be used for further systematic studies of the non-linear Compton matrix element and may provide approximative results for specific values of these parameters.

## 3.12   Averaged spectra at ultra-high intensity

The emission probability $dW/d\omega' d\Omega$ can be determined by either a numerical integration of the phase integrals $\mathscr{A}_n(s)$ or by certain analytical manipulations as demonstrated in the preceding sections. For ultra-strong laser pulses with $a_0 \gg 1$, another method for calculating the emission probability is presented here, utilizing certain approximations on top of the stationary phase analysis presented in Section 3.10. In this section, all calculations are performed in the special

reference frame where the electron is initially at rest, i.e. $p^\mu = (m, 0, 0, 0)$, meaning that $\gamma = 1$ and the rapidity $\zeta = 0$. In this frame one has $\beta = -a_0^2 s / 4(1 + \cos\theta)$. Using the expansion of the matrix element $\mathscr{M}$ into partial amplitudes as in (3.100),

$$\mathscr{M}(s) = \sum_\ell \mathscr{M}_\ell(s), \qquad (3.132)$$

the square of $\mathscr{M}$ in the expression for the emission probability (3.34) is a coherent sum over all harmonics, which is actually a double sum

$$|\mathscr{M}(s)|^2 = \sum_{\ell,\ell'} \mathscr{M}_\ell^*(s) \mathscr{M}_{\ell'}(s) = \sum_\ell |\mathscr{M}_\ell(s)|^2 + \sum_{\ell' \neq \ell} \mathscr{M}_\ell^*(s) \mathscr{M}_{\ell'}(s), \qquad (3.133)$$

where the incoherent diagonal contributions are separated from the off-diagonal elements which lead to interferences between different harmonics whenever they are overlapping. The overlapping of harmonics can happen only for pulsed fields because of the broad support of each harmonic, and it is inevitable for large values of $a_0$ in pulsed laser fields; it does not appear for monochromatic laser fields where the support is a delta comb.

One may define the partial differential photon emission probability for a single harmonic by

$$\frac{dW_\ell}{d\omega' d\Omega} = \frac{1}{2} \sum_{\text{spin,pol}} \frac{e^2 \omega'}{64\pi^3 k \cdot p \, k \cdot p'} |\mathscr{M}_\ell|^2, \qquad (3.134)$$

such that

$$\frac{dW}{d\Omega d\omega'} = \sum_\ell \frac{dW_\ell}{d\omega d\Omega} + \text{interferences}. \qquad (3.135)$$

The partial differential emission probabilities $dW_\ell / d\omega' d\Omega$ are exhibited in Figure 3.19 for the first three harmonics $\ell = 1, 2$ and 3 in the special reference frame as a function of scaled frequency $\omega'/\omega$ and scattering angle $\theta$. The spectra are shown for $a_0 = 2$ and a pulse length of $\Delta\phi = 20$ for a hyperbolic secant pulse shape $g = \cosh^{-1} \phi / \Delta\phi$. Each of the harmonics consists of many sub-peak lines. In general, the interferences between different harmonics are important for differential observables, in particular, for energy resolved spectra, for not too high values of $a_0 \sim 1$. There, the substructures of the harmonics, which can be seen in Figure 3.19, yield interesting spectral information on the non-linear Compton scattering in short laser pulses [Sei11b, Mac11]. However, for high laser strength, $a_0 \gg 1$, the differential photon emission probability (3.134) is a rapidly oscillating function of the photon energy $\omega'$. The number of peaks per harmonic, given in Eq. (3.114), grows $\propto a_0^2$. That means, when measuring the energy spectrum with a spectrometer with finite energy resolution, one actually obtains an averaged spectrum. Denoting this average by $\langle \ldots \rangle$, one finds that

$$\left\langle \frac{dW}{d\Omega d\omega'} \right\rangle = \sum_\ell \left\langle \frac{dW_\ell}{d\Omega d\omega'} \right\rangle \qquad (3.136)$$

which means that the interference terms in (3.135) average to zero [Nar96b]. Similarly, the total emission probability $W$, integrated over the complete phase space, is determined by the diagonal elements alone as

$$W = \sum_\ell W_\ell, \qquad (3.137)$$
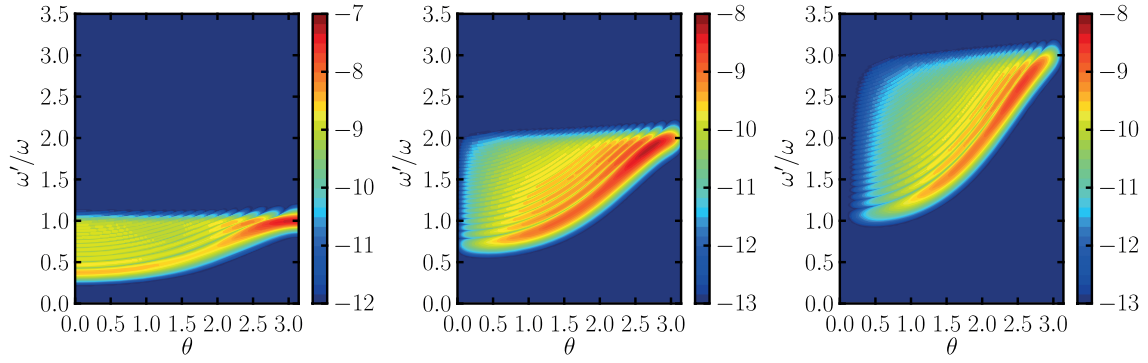
**Figure 3.19:** The differential emission probability for the first three harmonics $\ell = 1, 2$ and 3 (from left to right panels) in the special reference frame where $p^\mu = (m, 0, 0, 0)$ as a function of the scaled frequency $\omega'/\omega$ and scattering angle $\theta$. The colour code denotes the decadic logarithm of $dW_\ell/d\omega'd\Omega$ in units of inverse eV. The laser has an intensity parameter of $a_0 = 2$ and a pulse length parameter of $\Delta\phi = 20$.

i.e. the off-diagonal elements give no contribution to the total emission probability in the case of $a_0 \gg 1$. For large values of $a_0$, a direct numerical integration of the integrals (3.102) to calculate the coefficients $c_n^\ell(s - \ell)$ becomes hard since the integrands are rapidly oscillating functions of the laser phase $\phi$. However, for rapidly oscillating phase integrals, the stationary phase approximation for the coefficients (3.111) yields accurate results. The SPA result can be simplified further by observing that the many sub-peaks of the coefficient functions $c_n^\ell(s - \ell)$ to be averaged over stem from the cosine term in (3.111), which is a common factor in all contributions to the partial matrix element $\mathscr{M}_\ell$. Thus, the oscillations of the partial amplitudes are determined by

$$\mathscr{M}_\ell \sim \cos\left\{(s - \ell)\phi_\star - \beta G_2(\phi_\star) - \frac{\pi}{4}\right\} . \tag{3.138}$$

When squaring the matrix element to calculate the partial differential photon emission probability $dW_\ell$, one obtains

$$\langle|\mathscr{M}_\ell|^2\rangle \sim \left\langle\cos^2\left\{(s - \ell)\phi_\star - \beta G_2(\phi_\star) - \frac{\pi}{4}\right\}\right\rangle = \frac{1}{2} . \tag{3.139}$$

Since the interferences between different partial amplitudes with $\ell \neq \ell'$ cancel on average, one may translate the average back to the $c_n^\ell$ and replace the cosine in (3.111) by $1/\sqrt{2}$, defining the averaged functions by

$$\langle c_n^\ell(s - \ell)\rangle = J_{L_n}\big(\bar\alpha g(\phi_\star)\big)g^{|n|}(\phi_\star)\sqrt{\frac{2\pi}{|\beta g(\phi_\star)g'(\phi_\star)|}} . \tag{3.140}$$

However, even for large values of $a_0$ there are regions in phase space where the stationary phase method is inapplicable:

1. In the vicinity of the non-linear IPW resonance at $s - \ell = \beta$, the stationary points are located at the centre of the pulse and very close to each other. There, the first derivative $g'(\phi_\star)$ is almost zero and, therefore, the stationary phase approximation tends to diverge. The exponent has to be expanded up to the third-order derivative of

the phase around the point of zero convexity (where the second derivative of the phase in (3.102) vanishes), yielding [Nar96b]

$$c_n^\ell(s - \ell) = 2\pi J_L(\alpha) \left( \frac{1}{|\beta g''(0)|} \right)^{\frac{1}{3}} \mathrm{Ai}(-y) , \tag{3.141}$$

where

$$\mathrm{Ai}(y) = \frac{1}{2\pi} \int\limits_{-\infty}^{\infty} dt \exp \left\{ iyt + i\frac{t^3}{3} \right\} \tag{3.142}$$
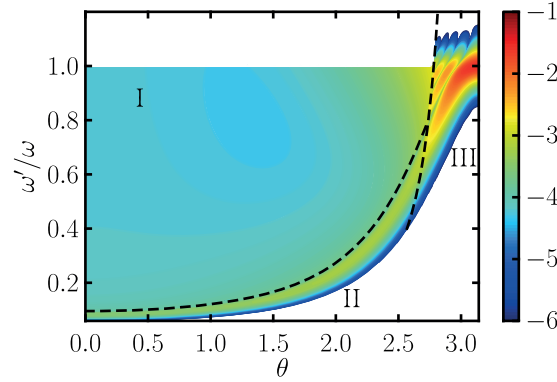
is the Airy function [WFS] with the argument

$$y = \frac{s - \ell - \beta}{|\beta g''(0)|^{\frac{1}{3}}} . \tag{3.143}$$

2. The stationary phase approximation is appropriate for large $|\beta| \gg 1$. However, in the vicinity of the forward scattering direction $\theta \approx \pi$, one finds that $|\beta|$ behaves as $|\beta| = a_0^2 \frac{\omega'}{\omega} \frac{\vartheta^2}{2}$, with $\vartheta = \pi - \theta \ll 2$, thus, the stationary phase method can be applied for angles $\vartheta^2 \gg a_0^{-2} \frac{\omega}{\omega'}$ only where $|\beta|$ is sufficiently large [Mac11].

Fortunately, these evaluation techniques complement one another, such that they may be combined together by suitable matching conditions to allow for an accurate calculation of the non-linear Compton scattering spectra. In doing so, the phase space is divided into three disjoint regions (I, II, III) where the three different evaluation schemes for the averaged coefficients $\langle c^\ell \rangle$ are applied. In Figure 3.20, these three regions are exhibited together with two transition lines which are determined by the two parameters $M_{1,2}$ (the subscripts 1 and 2 refer to conditions 1. and 2. above). The choice of these parameters can be motivated as follows: The parameter $M_1$ determines the transition line between the stationary phase approximation and the zero convexity approximation. The matching line is defined by $y = M_1 = const$ which should be in the range $1.4 < M_1 < 2.3381$ because for smaller values of $M_1$ the two stationary phase points would be too close to each other [Nar96b] and for larger values the two approximations start to differ too much. The stationary phase approximation is used for $y \geq M_1$ (region I in Figure 3.20), and the zero convexity approximation is employed for $y < M_1$ (region II in Figure 3.20). The parameter $M_2$ determines the transition between the direct numerical evaluation and the stationary phase/zero convexity approximation. The direct numerical integrations of $c_n^\ell$ have to be used whenever $|\Delta\phi\beta|$ becomes too small, thus, for $|\Delta\phi\beta| < M_2 = const$ (region II in Figure 3.20). The stationary phase and zero convexity approximations are hence used for $|\Delta\phi\beta| \geq M_2$. The numerical result for the emission probability was found to be rather insensitive to the specific value of $M_2$ in the range $10 < M_2 < 50$.

The formula for the phase space averaged partial emission probability reads

$$\left\langle \frac{d^2 W_\ell}{d\omega' d\Omega} \right\rangle = \frac{e^2 \omega'}{64\pi^3 k \cdot p\, k \cdot p'} \Bigg\{ (4p \cdot p' - 8m^2)\langle c_0^\ell(s - \ell)\rangle^2 - 2m^2 a_0^2 \langle c_0^\ell(s - \ell)\rangle \langle c_2^\ell(s - \ell)\rangle$$

$$+ \frac{m^2 a_0^2}{2} \left( \frac{k \cdot p}{k \cdot p'} + \frac{k \cdot p'}{k \cdot p} \right) \left[ \langle c_+^\ell(s - \ell)\rangle^2 + \langle c_-^\ell(s - \ell)\rangle^2 \right]$$

$$- 2\alpha k \cdot k' \langle c_0^\ell(s - \ell)\rangle \left[ \langle c_+^\ell(s - \ell)\rangle + \langle c_-^\ell(s - \ell)\rangle \right] \Bigg\} \tag{3.144}$$

**Figure 3.20:** Differential photon yield $dW_1/d\omega' d\Omega$ as a function of scaled frequency $\omega'/\omega$ and scattering angle $\theta$ for $a_0 = 5$, $\Delta\phi = 25$, and a hyperbolic secant pulse envelope in the special reference frame. In the different areas of phase space (I, II and II, which are delineated by dashed curves), different methods of evaluation for the coefficients $\langle c_n^\ell \rangle$ are employed. Parameters are $M_1 = 2.33$ and $M_2 = 10$. (Compare with Figure 3.19.)

with the averaged coefficients

$$
\langle c_n^\ell (s - \ell) \rangle =
\begin{cases}
J_{L_n}\left(\bar{\alpha}\sqrt{\frac{s-\ell}{\beta}}\right)\sqrt{\frac{s-\ell}{\beta}}^{|n|}\sqrt{\frac{2\pi}{\left|\beta\sqrt{\frac{s-\ell}{\beta}}g'(\phi_\star)\right|}} & y \geq M_1 \text{ and } |\beta\Delta\phi| \geq M_2\,, \\[2ex]
2\pi J_{L_n}(\bar{\alpha})\dfrac{1}{|\beta g''(0)|^{\frac{1}{3}}}\mathrm{Ai}(-y) & y < M_1 \text{ and } |\beta\Delta\phi| \geq M_2\,, \\[2ex]
c_n^\ell(s - \ell) & |\beta\Delta\phi| < M_2
\end{cases}
\tag{3.145}
$$

with $y$ from (3.143) and $L_n$ is defined in Eq. (3.112). The explicit values of $g'(\phi_\star)$ and $g''(0)$ can be taken from Table 3.1 for various pulse envelopes $g$. This method of approximation of the partial amplitudes $\mathscr{M}_\ell$ is not restricted to the non-linear Compton scattering process. It can be easily transferred to other strong-field processes such as stimulated pair production [Hei10a, Tit12, Nou12] or one-photon annihilation of $e^+e^-$ pairs [Ild11b] which are cross channel processes of non-linear Compton scattering.

For the numerical evaluation, the laser will be considered to have a frequency (in the laboratory system) of $\omega = 1.55$ eV colliding head-on with an electron beam with energy of 40 MeV, representing the conditions at ELBE at the HZDR described above in Section 3.4. The partial emission probability $W_\ell$ for the first and second harmonics in a hyperbolic secant pulse of duration $\Delta\phi = 20$ are presented in the left panel of Figure 3.21, where the emission probability in the pulsed field is represented by the symbols. The emission probability in a PPW is compared to an appropriate equivalent probability for an IPW. This equivalent emission probability from an infinite plane wave is obtained by multiplying the photon emission rate $\dot{W}_\ell$ in an IPW with the effective interaction time $T_{\mathrm{eff}} = \Delta\phi_{\mathrm{eff}}/\omega$ which is related to the invariant phase interval $\Delta\phi_{\mathrm{eff}}$ (see discussion in Appendix A.3 for details of the definition of $\Delta\phi_{\mathrm{eff}}$), thus, $W_\ell^{\mathrm{IPW}} = T_{\mathrm{eff}}\dot{W}_\ell$. This corresponds to a normalization to the same energy contained in the laser pulse. Within this approach, both the pulsed and monochromatic photon yields coincide for low $a_0 \ll 1$. That means that in the linear interaction regime pulsed and infinite plane waves give the same result for the emission probability. The dependence on the pulse shape drops out. For large values of $a_0 \gg 1$, the
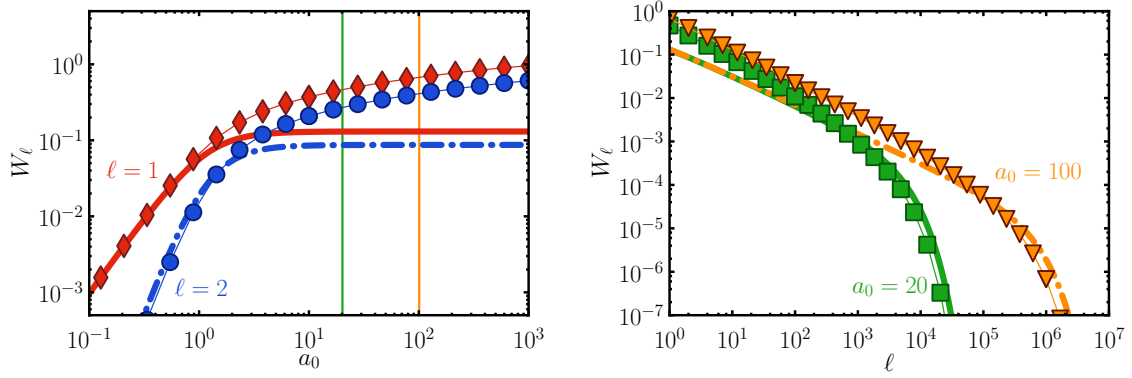
**Figure 3.21:** Partial photon yields $W_\ell$ in a hyperbolic secant pulse with $\Delta\phi = 20$ (symbols and interpolating thin curves) compared to the appropriately scaled yield in an IPW (thick solid and dash-dotted curves). The matching parameters are $M_1 = 2.33$ and $M_2 = 20$. Left panel: Behaviour of the first two harmonics $W_1$ (red diamonds and solid curve) and $W_2$ (blue circles and dash-dotted curve) as a function of $a_0$. Right panel: Partial emission probabilities $W_\ell$ for different laser strength $a_0 = 20$ (green squares and solid curve) and $a_0 = 100$ (orange triangles and dash-dotted curve). The two vertical lines in the left panel refer to the values of $a_0$ which are exhibited in the right panel.

emission probability in a pulsed laser field is enhanced by almost a factor of ten as compared to the emission probability in an IPW. The differences between pulsed and monochromatic yields at large values of $a_0$ are due to non-linear finite-size effects. The two vertical green and orange lines at $a_0 = 20$ and $a_0 = 100$, respectively, refer to the right panel of Figure 3.21, where the partial emission probability $W_\ell$ is shown for fixed values of $a_0 = 20$ (green solid curves and squares) and $a_0 = 100$ (orange dash-dotted curves and triangles) as a function of the harmonic number $\ell$ including harmonics up to $\ell = 10^7$. The symbols represent the calculation in a PPW; the thick curves are for the appropriate IPW emission probabilities. The cut-off harmonic in a monochromatic laser field can be estimated from the behaviour of the Bessel functions at large values of both the index and the argument as $\ell_{\max} \sim a_0^3$ [Wat22]. While for low harmonics the photon yield $W_\ell$ is larger in pulsed fields, the ordering of the two curves changes for high harmonics. There the emission probability in a PPW is smaller than the corresponding probability of an IPW.

Comparing the total photon yields $W = \sum_\ell W_\ell$, summed over all harmonics up to $\ell = 10^7$ in Figure 3.22, it is found that the total emission probability in a pulsed field (red diamonds) exceeds the IPW result by a factor of two for $a_0 = 100$. For the result in an IPW, the first harmonic, $\ell = 1$, is shown as black dashed curve, as well as the sum over the first 140 harmonics (solid green curve), showing the slow convergence of the sum over $\ell$. Additionally, an asymptotic approximation is depicted, which is equivalent to a constant crossed field approximation (blue solid curve, see e.g. [Rit85, Tit11]). Additionally, the dotted curve is a rough estimate for the asymptotic probability $W = \alpha a_0 \Delta\phi_{\mathrm{eff}}$ [DP10], with the effective phase interval $\Delta\phi_{\mathrm{eff}}$ defined in (A.44) and the fine structure constant $\alpha$.

## 3.13   Summary of Chapter 3

In this chapter, the process of non-linear one-photon Compton scattering in short strong laser pulses was considered in the framework of strong-field QED using Volkov states within the Furry picture where the laser pulse is modelled by a temporally shaped plane wave. An
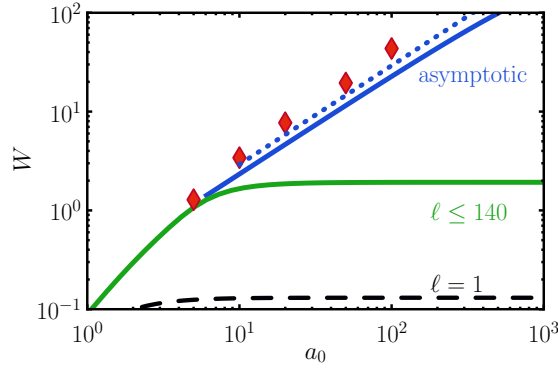
**Figure 3.22:** The total one-photon emission probability $W$ as a function of laser strength $a_0$. The results for pulsed laser fields are shown as symbols (red diamonds) being a factor of two above the asymptotic monochromatic result (solid blue curve) based on the constant crossed field approximation (cf. e.g. [Tit11]). The solid green curve shows the sum of the first 140 harmonics in a monochromatic wave (cf. [Tit11]). The blue dotted curve is a rough approximation to the asymptotic IPW result (see the text). The black dashed curve is the contribution from the first harmonic, $\ell = 1$, for an IPW.

expression for the $S$ matrix element was presented for the general case, i.e. for arbitrary scattering geometry, laser strength, pulse length, pulse shape, laser polarization and carrier envelope phase. The dependence of the $S$ matrix and the photon emission probability on the laser pulse is contained in three independent phase integrals $\mathscr{A}_\pm(s)$ and $\mathscr{A}_2(s)$. Several methods for calculating these phase integrals have been presented. A direct numerical integration of the corresponding expression allowed for a survey of the general features of the frequency spectra and the azimuthal spectra of non-linear Compton scattering in short laser pulses. Two different regimes, the ponderomotive regime and the bandwidth dominated regime, were identified for $\Delta\phi \gg 1$ and $\Delta\phi \sim 1$, respectively. It was shown that $\Delta\phi \sim 5$ can be considered as much larger than unity in this context.

In the ponderomotive regime, the frequency spectra acquire an interesting sub-peak structure in strong laser pulses. The origin of these sub-peaks is an interference effect of radiation produced at different times during the course of the pulse. This was verified using a stationary phase analysis. The number of these sub-peaks has been calculated; it is related to the value of the ponderomotive phase shift, $\Delta f \propto a_0^2 \Delta\phi$, which is the same term that leads to the emergence of the quasi-momentum in the limit of infinite plane waves. The ponderomotive regime has been studied further by deriving a completely analytical representation of the non-linear Compton amplitude in terms of generalized Laguerre functions.

For ultra-short laser pulses, $\Delta\phi \sim 1$, the emission spectra strongly depend on the value of the carrier envelope phase $\hat{\phi}$ for $a_0 > 1$, leading to observable effects in the frequency spectra and even more pronounced signatures in the azimuthal distributions. In the case of linear laser polarization, the emission is either unidirectional or dipole-like in the direction of the laser polarization, depending on the value of the carrier envelope phase. For circular polarization, the symmetry in the azimuthal angle $\varphi$ known from IPW is completely lost for $a_0 > 1$. A preferred direction is given by the direction where the laser vector potential reaches its maximum value. The azimuthal symmetry is replaced by a new symmetry in the composite variable $\varphi - \hat{\phi}$.

The low-energy limit of non-linear Thomson scattering was studied in comparison to non-linear Compton scattering. In the quantum theory of non-linear Compton scattering,

there exists a cut-off frequency $\omega'_\infty < \infty$, which restricts the possible physical phase space, while in the classical theory of Thomson scattering $\omega'_\infty \to \infty$. A scaling law for the Thomson and Compton emission probabilities was derived, based on the different physical phase spaces, i.e. the kinematic pile up below $\omega'_\infty$ for non-linear Compton scattering is mimicked by a suitable rescaling of the frequency variable. The scaling law allows to account for the quantum recoil in classical calculations by rescaling emission probabilities.

For ultra-strong laser pulses, $a_0 \gg 1$, an approximative calculation scheme for the emission probability was presented, where an averaging over the sub-peaks in phase space is included. Significantly modified partial and total photon yields in pulsed laser fields are found upon comparing to the case of IPW laser fields. The partial yield for the first harmonic can be up to a factor of ten larger than the corresponding IPW result for large values of $a_0$. The summed total photon yield is by a factor of two larger than the IPW result which is typically approximated by a constant crossed field at large values of $a_0$. This shows that the constant crossed field approximation gives the correct order of magnitude, but underestimates the total emission probability for pulsed laser fields.

The fact that the total emission probability in ultra-strong pulses with $a_0 \gg 1$ can exceed unity, $W^{(1)} \gtrsim 1$, is a hint that multi-photon emission channels need to be taken into account in that regime [DP10]. This will be elaborated further in the next chapter, where the process of two-photon emission in strong laser pulses is considered.

Effects due to the spatial focusing of the laser pulse, i.e. the extension to realistic spatial pulse distributions deserves further investigations. (The discussion in the present chapter is limited due to the fact that not even the single-particle wave functions in the field of a focused laser pulse are known, as generalizations of Volkov states.) Nonetheless, these are important issues in view of an experimental verification of the non-linear short pulse effects described in this chapter. In particular, the robustness of the sub-peaks with respect to realistic experimental conditions would be of great interest. The subjects of spatial focusing of the laser pulse as well as finite electron distributions are considered in Appendix F within the classical theory of Thomson scattering.

# 4

# Two-photon Compton scattering

Two-photon emission in an ultra-strong laser pulse, i.e. the simultaneous emission of two photons with momenta $k_{1,2}$ off an electron with momentum $p$ in a collision with an ultra-strong laser pulse is given by the reaction

$$e(p) + \text{laser} \to e(p') + \text{laser} + \gamma(k_1) + \gamma(k_2) \,. \tag{4.1}$$

This is the strong-field analogue of double Compton scattering [Man52], which is a pure quantum process, becoming manifest in the vanishing of the process in the low energy limit $(k \cdot p)/m^2 \to 0$. The strong-field process, described by the one-step reaction (4.1) can also happen due to the two-step process

$$e(p) + \text{laser} \to e(P) + \text{laser} + \gamma(k_1) \,, \tag{4.2}$$
$$e(P) + \text{laser} \to e(p') + \text{laser} + \gamma(k_2) \,, \tag{4.3}$$

where the intermediate electron with momentum $P$ becomes a real particle on the mass shell $P^2 = m^2$, which is enabled by the presence of the background laser field and is not possible for the weak-field process.

## 4.1   Introductory remarks

Two-photon Compton scattering in a strong-laser field, i.e. the reaction (4.1), is described by the $S$ matrix element $S = \langle \boldsymbol{p}'r'; \boldsymbol{k}_1\lambda_1; \boldsymbol{k}_2\lambda_2 | \hat{S}[A] | \boldsymbol{p}r \rangle$, with one electron with momentum $p$ and spin $r$ in the initial state $|\boldsymbol{p}r\rangle$, and with one electron with momentum $p'$ and spin $r'$ as well as two photons with momenta $k_{1,2}$ and polarizations $\lambda_{1,2}$ in the final state $\langle \boldsymbol{p}'r'; \boldsymbol{k}_1\lambda_1; \boldsymbol{k}_2\lambda_2|$. The reduction of the $S$ matrix element into the two Feynman diagrams of Figure 4.1 is outlined in Appendix A.7. This is a second-order process, meaning that the scattering operator $\hat{S}[A]$ has to be expanded up to the second order in the Dyson series. Thus, the Dirac-Volkov propagator appears in the Feynman diagrams. Two-photon Compton scattering in strong-field QED has been considered previously in constant crossed fields in relation to the two-loop electron mass operator [Mor75] and in infinite monochromatic plane-wave fields [Löt09b, Löt09a]. Also two-photon synchrotron emission in a strong constant magnetic field [Sok76] had been calculated. In this chapter, the two-photon Compton scattering is presented for pulsed plane-wave fields. There are significant modification of the two-photon Compton process in short laser pulses as compared to the case of infinite plane-wave fields
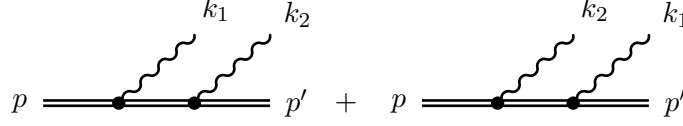
**Figure 4.1:** Feynman diagrams for the two-photon Compton process, i.e. the coherent emission of two photons (wavy lines). The double lines represent laser dressed Volkov in and out states and the Dirac Volkov propagator between the two vertices, respectively.

considered previously [Löt09b]. One of the most drastic modifications is the fact that there are no singularities in the resonant on-shell part of the scattering matrix element for PPW, as shown below.

Recently, the (incoherent) multi-photon emission in a strong laser field has been considered as quantum radiation reaction [DP10]. The discussion of radiation damping as multi-photon emission in the quantum picture (for the weak-field process) can also be found in [Hei41, Wil41, Bet46, Bla47]. The two-photon process considered here is the lowest order multi-photon emission process, going beyond the approximation of incoherent photon emission.

In this chapter, the laser field is considered to be linearly polarized with polarization parameter $\xi = 0$, i.e. the general expression for the laser vector potential (A.24) goes over to

$$A_\mu(\phi) = A_0 g(\phi)\epsilon_\mu \cos(\phi + \hat{\phi}), \tag{4.4}$$

where the single laser polarization vector is denoted as $\epsilon_\mu = (0, 1, 0, 0)$.

The present chapter is organized as follows: The derivation of the $S$ matrix element and a formula for the emission probability are presented, which allows for a later numerical investigation of the latter one. The weak-field limit $a_0 \ll 1$ is discussed, showing that the general strong-field matrix element coincides with the well known perturbative matrix element in the leading order expansion in $a_0$. The relation of the one-step and two-step processes described above are discussed. They are related to on-shell and off-shell contributions to the two-photon emission process. For the on-shell part of the $S$ matrix a factorization into products of one-photon emission $S$ matrices is shown explicitly. This is an expression of the optical theorem on the tree level [Ild11a]. The relevance of Oleinik resonances is discussed and the reappearance of the Oleinik singularities in the limit of infinite plane waves mentioned. Numerical results for the differential two-photon emission probability are analysed, highlighting the differences between infinite plane waves and pulsed laser fields. The two-photon to one-photon ratio is calculated and a value of $\mathcal{R} = 10^{-2}$ is obtained for $a_0 = 1$, which is two orders of magnitude larger than the result for weak fields. Some analytical results are obtained for a box-shaped pulse profile, where the dependence of the different parts of the emission probability on the pulse length become apparent.

## 4.2   Two-photon matrix element and emission probability

The reduction of the $S$ matrix element $S = \langle \boldsymbol{p}'r'; \boldsymbol{k}_1\lambda_1; \boldsymbol{k}_2\lambda_2|\hat{S}[A]|\boldsymbol{p}r\rangle$, as presented in Appendix A.7 leads to the two Feynman diagrams in Figure 4.1. They correspond to the two contributions to the $S$ matrix

$$S = -ie^2 \int d^4x\, d^4y\, \bar{\Psi}_{p'}(y)\not{\epsilon}_2^* e^{ik_2 \cdot y}\mathcal{G}(y, x|A)\not{\epsilon}_1^* e^{ik_1 \cdot x}\Psi_p(x) \ + \ (1 \leftrightarrow 2), \tag{4.5}$$

where $(1 \leftrightarrow 2)$ means the exchange of photons "*1*" and "*2*" in the second term accounting for the symmetrization of the two-photon wave function. In the above equations, $\Psi_p$ and $\bar{\Psi}_{p'}$ denote the Volkov wave functions for the electron in the initial and final states with momenta $p$ and $p'$, respectively; $\mathcal{G}(y, x|A)$ denotes the laser dressed Dirac-Volkov electron propagator [Rit85], see also Section 2.9. The momenta of the two emitted photons are denoted by $k_{1,2}$, while $\epsilon_{1,2}$ stand for the corresponding polarization vectors with $k_{1,2} \cdot \epsilon_{1,2} = 0$. Both, the Volkov wave function $\Psi_p(x)$ and the Dirac-Volkov propagator $\mathcal{G}(x, y|A)$, depend on the Volkov matrix functions $E_p(x)$, for which it is most suitable to employ the spectral decomposition

$$E_p(x) = \int \frac{ds d\phi}{2\pi} e^{-i(p+sk) \cdot x} e^{is\phi} \Omega_p(\phi) \,, \tag{4.6}$$

with

$$\Omega_p(\phi) = \left(1 + \frac{e}{(2k \cdot p)} \slashed{k} \slashed{A}(\phi)\right) e^{-if_p(\phi)} \tag{4.7}$$

and the non-linear phase

$$f_p(\phi) = \alpha_p \int\limits_0^\phi d\phi' a(\phi') + 2\beta_p \int\limits_0^\phi d\phi' a^2(\phi') \tag{4.8}$$

with coefficients $\alpha_p = m a_0 (p \cdot \epsilon)/(p \cdot k)$, $\beta_p = m^2 a_0^2/(4p \cdot k)$ and introducing the abbreviation $a(\phi) = g(\phi) \cos(\phi + \hat{\phi})$. Using the representation (2.77) for the Dirac-Volkov propagator, the $S$ matrix element (4.5) can be written as

$$S = -ie^2 \int d^4x d^4y \frac{d^4P}{(2\pi)^4} \bar{u}_{p'} \bar{E}_{p'}(y) \slashed{\epsilon}_2^* E_P(y) G_0(P) \bar{E}_P(x) \slashed{\epsilon}_1^* E_p(x) u_p \; + \; (1 \leftrightarrow 2) \,, \tag{4.9}$$

with the free electron propagator in momentum space $G_0(P) = (\slashed{P} - m + i0^+)^{-1}$. Using the spectral decomposition for the Volkov matrix functions in the $S$ matrix, one obtains

$$\begin{aligned}
S = -\frac{ie^2}{(2\pi)^8} \int & d^4x d^4y d^4P \, [ds][d\phi] e^{i(s_1\phi_1 - s_1'\phi_1' + s_2\phi_2 - s_2'\phi_2')} \\
& \times e^{i(p' + s_2' - P - s_2 k + k_2) \cdot y} \, e^{-i(p + s_1 k - P - s_1'k - k_1) \cdot x} \\
& \times \bar{u}_{p'} \bar{\Omega}_{p'}(\phi_2') \slashed{\epsilon}_2^* \Omega_P(\phi_2) G_0(P) \bar{\Omega}_P(\phi_1') \slashed{\epsilon}_1^* \Omega_p(\phi_1) u_p \; + \; (1 \leftrightarrow 2) \,,
\end{aligned} \tag{4.10}$$

where $[ds]$ is an abbreviation for the integration over all variables $ds_j$ and $ds_j'$; the same holds for $[d\phi]$. The integrations over $d^4x$ and $d^4y$ yield momentum conserving delta distributions

$$\begin{aligned}
S = -ie^2 \int & d^4P \, [ds][d\phi] e^{i(s_1\phi_1 - s_1'\phi_1' + s_2\phi_2 - s_2'\phi_2')} \\
& \times \delta^4(p' + k_2 - P + (s_2' - s_2)k) \, \delta^4(p - k_1 - P + (s_1 - s_1')k) \\
& \times \bar{u}_{p'} \bar{\Omega}_{p'}(\phi_2') \slashed{\epsilon}_2^* \Omega_P(\phi_2) G_0(P) \bar{\Omega}_P(\phi_1') \slashed{\epsilon}_1^* \Omega_p(\phi_1) u_p \; + \; (1 \leftrightarrow 2) \,.
\end{aligned} \tag{4.11}$$

Shifting the variables $s_{1,2} \to s_{1,2} + s_{1,2}'$ and integrating over $d^4P$ fixes the propagator momentum as $P = p - k_1 + s_1 k$. With the suitable definition of $P_1 = p - k_1$ one finds for the $S$ matrix the expression

$$\begin{aligned}
S = -ie^2 \int & [ds][d\phi] e^{i(s_1\phi_1 + s_2\phi_2)} e^{i(s_1'(\phi_1 - \phi_1') + s_2'(\phi_2 - \phi_2'))} \delta^4(p - k_1 - k_2 - p' + (s_1 + s_2)k) \\
& \times \bar{u}_{p'} \bar{\Omega}_{p'}(\phi_2') \slashed{\epsilon}_2^* \Omega_{P_1}(\phi_2) G_0(P_1 + s_1 k) \bar{\Omega}_{P_1}(\phi_1') \slashed{\epsilon}_1^* \Omega_p(\phi_1) u_p \; + \; (1 \leftrightarrow 2) \,,
\end{aligned} \tag{4.12}$$
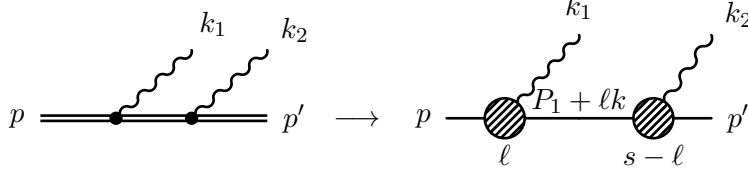
**Figure 4.2:** Feynman diagrams for the two-photon Compton process in a representation
using dressed vertices.

upon noting that the matrices $\Omega_p$ do depend only on the three momentum components which
are transverse to $k$, namely $p^1$, $p^2$ and $p^+$, with $k^1 = k^2 = k^+ = 0$, such that $\Omega_{P_1+sk} = \Omega_{P_1}$. The successive integrations over the primed variables $s'_{1,2}$ yield delta distributions
$\propto \delta(\phi'_{1,2} - \phi_{1,2})$ and the following integrations over $\phi'_{1,2}$ fix the values of $\phi'_{1,2} = \phi_{1,2}$, yielding

$$S = -ie^2(2\pi)^2 \int [ds][d\phi] e^{i(s_1\phi_1 + s_2\phi_2)} \delta^4(p - k_1 - k_2 - p' + (s_1 + s_2)k)$$

$$\times \bar{u}_{p'} \bar{\Omega}_{p'}(\phi_2) \not{\epsilon}_2^* \Omega_{P_1}(\phi_2) G_0(P_1 + s_1 k) \bar{\Omega}_{P_1}(\phi_1) \not{\epsilon}_1^* \Omega_p(\phi_1) u_p \; + \; (1 \leftrightarrow 2) . \quad (4.13)$$

Defining the dressed vertex functions

$$\eth_{P,p}^{\epsilon_1}(\phi) = \bar{\Omega}_P(\phi) \not{\epsilon}_1^* \Omega_p(\phi) = \bar{\Gamma}_P(\phi) \not{\epsilon}_1^* \Gamma_p(\phi) e^{if_P(\phi) - if_p(\phi)} \quad (4.14)$$

and with a last shift of variables $s_2 \to s = s_1 + s_2$ and denoting $\ell = s_1$, the intermediate
result for the $S$ matrix is given as

$$S = -ie^2(2\pi)^2 \int ds\, \delta^4(p + sk - k_1 - k_2 - p') \int d\phi_1 d\phi_2 d\ell$$

$$\times \bar{u}_{p'} \left( e^{i(s-\ell)\phi_2} \eth_{p',P_1}^{\epsilon_2}(\phi_2) \right) G_0(P_1 + \ell k) \left( e^{i\ell\phi_1} \eth_{P_1,p}^{\epsilon_1}(\phi_1) \right) u_p \; + \; (1 \leftrightarrow 2) . \quad (4.15)$$

This result for the $S$ matrix strongly resembles an alternative formulation of strong-field QED
where laser dressed vertices are employed instead of laser dressed propagators and initial- and
final-state wave functions [Mit75]. The physical meaning of Eq. (4.15) is interpreted easily
when it is read from right to left, see also Figure 4.2. The initial electron with momentum $p$
approaches the first vertex, where the electron interacts with the laser field and absorbs a
number of $\ell$ laser photons (with total momentum $\ell k$) while the first photon with momentum
$k_1$ is emitted. The amplitude for this partial process is described by the dressed vertex factor
$e^{i\ell\phi_1} \eth_{P_1,p}^{\epsilon_1}(\phi_1)$. After the interaction, the electron, which has a momentum $P_1 + \ell k$, freely
propagates to the second vertex. There, $s - \ell$ laser photons are absorbed from the background
field while the second photon with momentum $k_2$ is emitted. The total number of absorbed
laser photons is $s$ and is fixed by the energy momentum conservation upon performing the
integral over $ds$ as

$$s = \frac{p'^- + k_1^- + k_2^- - p^-}{k^-} = \frac{p' \cdot (k_1 + k_2) + k_1 \cdot k_2}{k \cdot p} . \quad (4.16)$$

The value of the photon exchange at the first vertex $\ell$ is not fixed. One has to coherently
add all allowed possibilities, which is implemented by the integral over $d\ell$. One could say
that the integral over $\ell$ in (4.15) accumulates all possible paths the system may take during
the interaction. The integral over $d\ell$ can be evaluated analytically by employing the contour
integration technique, similar to the discussion of the laser dressed propagator in Section 2.9

making possible a numerical evaluation of the two-photon $S$ matrix in (4.15). The free electron propagator is rewritten as

$$G_0(P_1 + \ell k) = \frac{\not{P}_1 + \ell \not{k} + m}{(P_1 + \ell k)^2 - m^2 + i0^+} = \frac{1}{2P_1 \cdot k} \frac{\not{P}_1 + \ell \not{k} + m}{\ell - \ell_1 + i0'^+} \tag{4.17}$$

to expose the single pole at $\ell = \ell_1 - i0'^+$ with

$$\ell_1 \equiv \frac{m^2 - P_1^2}{2k \cdot P_1} = \frac{p \cdot k_1}{k \cdot P_1} \tag{4.18}$$

and $0'^+ \equiv \mathrm{sign}(P_1^+)0^+$. The quantity $\ell_1$ controls the amount of momentum $\ell_1 k$ transferred to the electron such that the propagator momentum is on its mass shell, i.e. $(P_1 + \ell_1 k)^2 = m^2$. The sign of $P_1^+$ determines the location of the propagator pole to be below or above the real axis in the complex $\ell$ plane. For the process of two-photon Compton scattering discussed here, the momentum conservation for the plus component of the momentum reads $P_1^+ = p^+ - k_1^+ = p'^+ + k_2^+$. Since both $k_2^+ > 0$ and $p'^+ > 0$ are positive, as they belong to asymptotically free on-shell particles, also $P_1^+ > 0$. Thus, the propagator pole in (4.17) always lies below the real axis due to momentum conservation.

Since the integrand of the pole integration $d\ell$ does not vanish in the limit $\ell \to \pm\infty$, one has to transform the integrand according to

$$\frac{\ell}{\ell - \ell_1 + i0'^+} \to 1 + \frac{\ell_1}{\ell - \ell_1 + i0'^+} \tag{4.19}$$

such that the non-trivial part goes to zero as $\ell \to \infty$. With these preparations, the pole integration can be performed, yielding (with $\phi \equiv \phi_2$ and $\phi' \equiv \phi_1$)

$$\int_{-\infty}^{\infty} d\ell \frac{(\not{P}_1 + \ell \not{k} + m)e^{-i\ell(\phi-\phi')}}{\ell - \ell_1 + i0'^+}$$

$$= \not{k} \int_{-\infty}^{\infty} d\ell e^{-i\ell(\phi-\phi')} + (\not{P}_1 + \ell_1 \not{k} + m) \int_{-\infty}^{\infty} \frac{e^{-i\ell(\phi-\phi')}}{\ell - \ell_1 + i0'^+} \tag{4.20}$$

$$= 2\pi\delta(\phi - \phi')\not{k} - 2\pi i \Theta(\phi - \phi')e^{-i(\ell_1 - i0'^+)(\phi-\phi')}(\not{P}_1 + \ell_1 \not{k} + m). \tag{4.21}$$

The result of the pole-integration in (4.21) resembles the typical structure of a fermion propagator in light-front form [Kog70]. The last term in the last line of (4.21) introduces a time ordering (in the laser phase), meaning that the emission at the second vertex has to happen at a later (light-front) time than the emission at the first vertex by means of the step function $\Theta(\phi - \phi')$. Additionally, (4.21) includes a part $\propto \delta(\phi - \phi')$ where both photons are emitted simultaneously, which is related to the instantaneous zero-mode propagator. This contribution is specific to the fermion propagator and does not appear in the analysis of the trident process [Ild11a] with the photon propagator. Negative values of $P_1^+$ would shift the pole to the upper half plane corresponding to the opposite time ordering $\Theta(\phi' - \phi)$, as encountered in the analysis of the Fourier transformed Dirac-Volkov propagator in Section 2.9. As discussed there, this opposite time ordering corresponds to the propagation of anti-particles in the intermediate states. Thus, propagating anti-particles do not give any contribution to the two-photon Compton process due to the conservation of $P^+$ [Kog70]. The final result for the $S$ matrix of two-photon Compton scattering in a strong laser pulse is noted as

$$S = -ie^2(2\pi)^3 \frac{2}{k^-} \delta^3(\mathsf{p} - \mathsf{k}_1 - \mathsf{k}_2 - \mathsf{p}') \mathscr{M} \tag{4.22}$$

**Table 4.1:** The Dirac current coefficients $V_n$ and $U_{nl}$ of the two-photon Compton amplitude, using the abbreviations $X_p = \slashed{k}\slashed{\epsilon}\, m a_0/(2\, k \cdot p)$, $\bar{X}_p = \gamma^0 X_p^\dagger \gamma^0$ and $G_1 = \slashed{P}_1 + \ell_1 \slashed{k} + m$.

| | |
|---|---|
| $V_0$ | $\slashed{\epsilon}_2^* \slashed{k} \slashed{\epsilon}_1^*$ |
| $V_1$ | $(\bar{X}_{p'} \slashed{\epsilon}_2^* \slashed{k} \slashed{\epsilon}_1^* + \slashed{\epsilon}_2^* \slashed{k} \slashed{\epsilon}_1^* X_p)$ |
| $V_2$ | $\bar{X}_{p'} \slashed{\epsilon}_2^* \slashed{k} \slashed{\epsilon}_1^* X_p$ |
| $U_{00}$ | $\slashed{\epsilon}_2^* G_1 \slashed{\epsilon}_1^*$ |
| $U_{01}$ | $\slashed{\epsilon}_2^* G_1 (\bar{X}_{P_1} \slashed{\epsilon}_1^* + \slashed{\epsilon}_1^* X_p)$ |
| $U_{10}$ | $(\bar{X}_{p'} \slashed{\epsilon}_2^* + \slashed{\epsilon}_2^* X_{P_1}) G_1 \slashed{\epsilon}_1^*$ |
| $U_{11}$ | $(\bar{X}_{p'} \slashed{\epsilon}_2^* + \slashed{\epsilon}_2^* X_{P_1}) G_1 (\bar{X}_{P_1} \slashed{\epsilon}_1^* + \slashed{\epsilon}_1^* X_p)$ |
| $U_{02}$ | $\slashed{\epsilon}_2^* G_1 \bar{X}_{P_1} \slashed{\epsilon}_1^* X_p$ |
| $U_{20}$ | $\bar{X}_{p'} \slashed{\epsilon}_2^* X_{P_1} G_1 \slashed{\epsilon}_1^*$ |
| $U_{12}$ | $(\bar{X}_{p'} \slashed{\epsilon}_2^* + \slashed{\epsilon}_2^* X_{P_1}) G_1 \bar{X}_{P_1} \slashed{\epsilon}_1^* X_p$ |
| $U_{21}$ | $\bar{X}_{p'} \slashed{\epsilon}_2^* X_{P_1} G_1 (\bar{X}_{P_1} \slashed{\epsilon}_1^* + \slashed{\epsilon}_1^* X_p)$ |
| $U_{22}$ | $\bar{X}_{p'} \slashed{\epsilon}_2^* X_{P_1} G_1 \bar{X}_{P_1} \slashed{\epsilon}_1^* X_p$ |

with the amplitude

$$\mathcal{M} = \frac{1}{2k \cdot P_1} \left\{ \sum_{n=0}^{2} \mathscr{V}_n \mathscr{C}_n(s) - i \sum_{n,l=0}^{2} \mathscr{U}_{nl} \mathscr{B}_{nl}(s, \ell_1) \right\} \;+\; (1 \leftrightarrow 2) \tag{4.23}$$

and the phase integrals

$$\mathscr{C}_n(s) = \int d\phi \, a^n(\phi) \exp\{is\phi - i f_p(\phi) + i f_{p'}(\phi)\}, \tag{4.24}$$

$$\begin{aligned}
\mathscr{B}_{nl}(s, \ell_1) = \int d\phi \, d\phi' \, \Theta(\phi - \phi') a^n(\phi) \exp\{i(s - \ell_1)\phi - i f_{P_1}(\phi) + i f_{p'}(\phi)\} \\
\times \, a^l(\phi') \exp\{i\ell_1 \phi' - i f_p(\phi') + i f_{P_1}(\phi')\}
\end{aligned} \tag{4.25}$$

with $a(\phi) = g(\phi) \cos(\phi + \hat{\phi})$. The Dirac current coefficients read $\mathscr{V}_n = \bar{u}_{p'} V_n u_p$ and $\mathscr{U}_{nl} = \bar{u}_{p'} U_{nl} u_p$, where $V_n$ and $U_{nl}$ are summarized in Table 4.1. The phase integrals $\mathscr{C}_0$, $\mathscr{B}_{0l}$ and $\mathscr{B}_{n0}$ are numerically non-convergent due to the missing pre-exponential factors $g(\phi)$ and $g(\phi')$, respectively. However, these integrals can be defined as a superposition of convergent phase integrals by applying a gauge transformation $\epsilon_i^\mu \to \epsilon_i^\mu + \Lambda_i k_i^\mu$ [Ild11a], yielding, e.g.

$$(s - \ell_1)\mathscr{B}_{0l}(s, \ell_1) = i\mathscr{C}_l(s) + (\alpha_{P_1} - \alpha_{p'})\mathscr{B}_{1l}(s, \ell_1) + 2(\beta_{P_1} - \beta_{p'})\mathscr{B}_{2l}(s, \ell_1). \tag{4.26}$$

Thus, gauge invariance reduces the number of independent phase integrals from twelve to six well-behaved ones per channel. The calculations that lead to the relation (4.26) can be found in Appendix D together with further relations for the other divergent phase integrals. The argumentation that leads to relations like (4.26) is that the two-photon Compton amplitude $\mathcal{M}$ is invariant under the gauge transformations mentioned above if and only if the phase integrals fulfil the relations which are summarized in Eqs. (D.19) – (D.21), which is a possibility to define $\mathscr{C}_0$, $\mathscr{B}_{0l}$ and $\mathscr{B}_{n0}$ in a unique way based on basic principles of the theory.

Eliminating all of the divergent phase integrals, one arrives at the alternative expression for the two-photon amplitude

$$\mathcal{M} = \frac{1}{2k \cdot P_1} \left\{ \sum_{n=1}^{2} \widetilde{\mathscr{V}}_n \mathscr{C}_n(s) - i \sum_{n,l=1}^{2} \widetilde{\mathscr{U}}_{nl} \mathscr{B}_{nl}(s, \ell_1) \right\} \;+\; (1 \leftrightarrow 2) \tag{4.27}$$

with the modified Dirac current structures

$$\widetilde{\mathscr{V}}_1 = \mathscr{V}_1 + \mathscr{V}_0 \frac{\alpha_p - \alpha_{p'}}{s} - \frac{\mathscr{U}_{10}}{\ell_1} + \frac{\mathscr{U}_{01}}{s - \ell_1} + \mathscr{U}_{00} \left[ \frac{\alpha_p - \alpha_{p'}}{s(s - \ell_1)} - \frac{\alpha_{P_1} - \alpha_{p'}}{\ell_1(s - \ell_1)} \right], \tag{4.28}$$

$$\widetilde{\mathscr{V}}_2 = \mathscr{V}_2 + \mathscr{V}_0 \frac{2(\beta_p - \beta_{p'})}{s} - \frac{\mathscr{U}_{20}}{\ell_1} + \frac{\mathscr{U}_{02}}{s - \ell_1} + 2\mathscr{U}_{00} \left[ \frac{\beta_p - \beta_{p'}}{s(s - \ell_1)} - \frac{\beta_{P_1} - \beta_{p'}}{\ell_1(s - \ell_1)} \right], \tag{4.29}$$

$$\widetilde{\mathscr{U}}_{11} = \mathscr{U}_{11} + \mathscr{U}_{10} \frac{\alpha_p - \alpha_{P_1}}{\ell_1} + \mathscr{U}_{01} \frac{\alpha_{P_1} - \alpha_{p'}}{s - \ell_1} + \mathscr{U}_{00} \frac{\alpha_p - \alpha_{P_1}}{\ell_1} \frac{\alpha_{P_1} - \alpha_{p'}}{s - \ell_1}, \tag{4.30}$$

$$\widetilde{\mathscr{U}}_{12} = \mathscr{U}_{12} + \mathscr{U}_{10} \frac{2(\beta_p - \beta_{P_1})}{\ell_1} + \mathscr{U}_{02} \frac{\alpha_{P_1} - \alpha_{p'}}{s - \ell_1} + \mathscr{U}_{00} \frac{2(\beta_p - \beta_{P_1})}{\ell_1} \frac{\alpha_{P_1} - \alpha_{p'}}{s - \ell_1}, \tag{4.31}$$

$$\widetilde{\mathscr{U}}_{21} = \mathscr{U}_{21} + \mathscr{U}_{20} \frac{\alpha_p - \alpha_{P_1}}{\ell_1} + \mathscr{U}_{01} \frac{2(\beta_{P_1} - \beta_{p'})}{s - \ell_1} + \mathscr{U}_{00} \frac{\alpha_p - \alpha_{P_1}}{\ell_1} \frac{2(\beta_{P_1} - \beta_{p'})}{s - \ell_1}, \tag{4.32}$$

$$\widetilde{\mathscr{U}}_{22} = \mathscr{U}_{22} + \mathscr{U}_{20} \frac{2(\beta_p - \beta_{P_1})}{\ell_1} + \mathscr{U}_{02} \frac{2(\beta_{P_1} - \beta_{p'})}{s - \ell_1} + \mathscr{U}_{00} \frac{2(\beta_p - \beta_{P_1})}{\ell_1} \frac{2(\beta_{P_1} - \beta_{p'})}{s - \ell_1}. \tag{4.33}$$

The differential two-photon emission probability can be obtained in the usual way by squaring the $S$ matrix and multiplying with the phase space of the final state particles as $dW = \frac{1}{2p^+} |S|^2 d\Pi$ with the three-particle phase space element

$$d\Pi = \frac{d^3\mathsf{p}'}{(2\pi)^3 2p'^+} \frac{d^3\mathbf{k}_1}{(2\pi)^3 2\omega_1} \frac{d^3\mathbf{k}_2}{(2\pi)^3 2\omega_2}, \tag{4.34}$$

where the phase space element of the outgoing electron $p'$ is employed in light-front form for an easy integration of the delta distribution in $|S|^2$. The six-fold differential probability of two-photon emission per incident laser pulse finally reads

$$\frac{d^6W}{d\omega_1 d\Omega_1 d\omega_2 d\Omega_2} = \frac{\alpha^2 \omega_1 \omega_2}{64\pi^4 (k \cdot p)(k \cdot p')} |\mathscr{M}|^2 \tag{4.35}$$

with the fine structure constant $\alpha = e^2/4\pi$. This quantity of course depends on all the spin and polarization variables of the participating particles $(r, r', \lambda_1, \lambda_2)$, which are not noted explicitly. If one is not interested in the spin and polarization dependence, one should average the above expression over $r$ and sum over all final state polarizations and spin states $r', \lambda_1, \lambda_2$ as

$$\frac{d^6W}{d\omega_1 d\Omega_1 d\omega_2 d\Omega_2} = \frac{1}{2} \sum_{r, r', \lambda_1, \lambda_2} \frac{d^6W(r, r', \lambda_1, \lambda_2)}{d\omega_1 d\Omega_1 d\omega_2 d\Omega_2}. \tag{4.36}$$
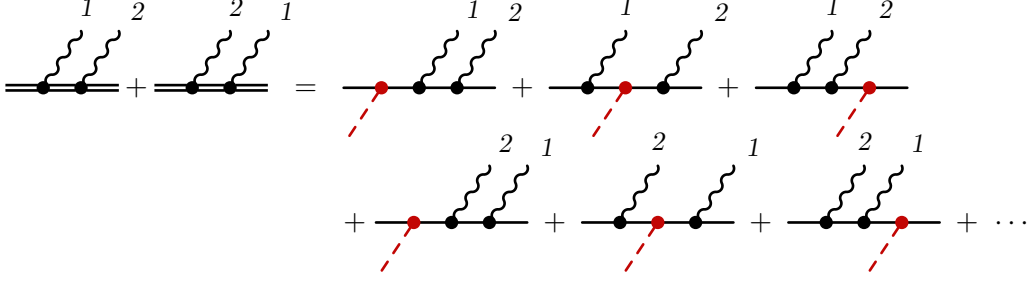
## 4.3   Weak-field expansion of the two-photon matrix element

For weak laser fields, characterized by $a_0 \ll 1$, the strong-field two-photon Compton amplitude (4.23) goes over to the perturbative result, known from [Man52, Jau76]. To extract the perturbative matrix element from the general expression (4.23), only terms up to the order of $a_0$ have to be taken into account. The Dirac current coefficients $\mathscr{T}_n$ and $\mathscr{U}_{nl}$ (see Table 4.1) behave as $\mathscr{V}_n \sim a_0^n$ and $\mathscr{U}_{nl} \sim a_0^{n+l}$, which reduces the number of relevant terms in (4.23)

$$\mathscr{M} = \frac{1}{2P_1 \cdot k} \left\{ \mathscr{V}_0 \mathscr{C}_0 + \mathscr{V}_1 \mathscr{C}_1 - i(\mathscr{U}_{00}\mathscr{B}_{00} + \mathscr{U}_{01}\mathscr{B}_{01} + \mathscr{U}_{10}\mathscr{B}_{10}) \right\} + (1 \leftrightarrow 2). \tag{4.37}$$

One uses the various gauge invariance relations (D.19) – (D.21) to regularize the ill-defined phase integrals with index zero. For instance, the transformed $\mathscr{B}_{10}$ is

$$\mathscr{B}_{10}(s, \ell_1) = -\frac{i}{\ell_1} \mathscr{C}_1(s) + \frac{\alpha_p - \alpha_{P_1}}{\ell_1} \mathscr{B}_{11}(s, \ell_1) + 2\frac{\beta_p - \beta_{P_1}}{\ell_1} \mathscr{B}_{12}(s, \ell_1), \tag{4.38}$$

**Figure 4.3:** Expansion of the non-perturbative two-photon Compton matrix element in powers of the interaction with the laser pulse up to the leading order in $a_0$, showing the non-vanishing contributions only.

where the first term is $\mathcal{O}(a_0^0)$, the second term is $\mathcal{O}(a_0^1)$ and the third term even is $\mathcal{O}(a_0^2)$. Any term but the first one may be safely neglected as they produce contributions in higher order than the leading order in $a_0$ when $\mathcal{B}_{10}$ is plugged into (4.37). Using this argumentation for all relevant terms one ends up with

$$\mathcal{M} = \frac{\mathscr{C}_1(s)}{2P_1 \cdot k} \left\{ \mathscr{V}_1 + \frac{(\alpha_p - \alpha_{p'})}{s} \mathscr{V}_0 + \frac{\alpha_p - \alpha_{p'}}{s(s - \ell_1)} \mathscr{U}_{00} - \frac{\alpha_{P_1} - \alpha_{p'}}{\ell_1(s - \ell_1)} \mathscr{U}_{00} + \frac{\mathscr{U}_{01}}{s - \ell_1} - \frac{\mathscr{U}_{10}}{\ell_1} \right\}$$
$$+ \ (1 \leftrightarrow 2). \quad (4.39)$$

Since the term in the brackets is of order $a_0^1$, the phase integral $\mathscr{C}_1(s)$ can be approximated in the leading order as

$$\mathscr{C}_1(s) \rightarrow \int d\phi\, e^{is\phi} g(\phi) \cos(\phi + \hat{\phi}) \equiv \tilde{\mathscr{C}}_1(s). \quad (4.40)$$

After some cumbersome manipulations, using the relations

$$\Delta(p + k) = \frac{1}{2p \cdot k}, \qquad\qquad \Delta(p' - k) = -\frac{1}{2p' \cdot k}, \quad\quad (4.41)$$

$$\Delta(p - k_1) = -\frac{1}{2\ell_1 P_1 \cdot k}, \qquad \Delta(p - k_1 + k) = \frac{1}{(1 - \ell_1)2P_1 \cdot k}, \quad (4.42)$$

$$\Delta(p - k_1 + k) = \frac{\ell_1}{\ell_1 - 1} \Delta(p - k_1), \quad\quad (4.43)$$

where $\Delta(p) = (p^2 - m^2 + i0^+)^{-1}$ is the scalar Feynman propagator, one finally ends up with the result

$$\mathcal{M} = ma_0 \tilde{\mathscr{C}}_1(s) \Big\{ \bar{u}_{p'} \not{\epsilon}_2^* G_0(p - k_1 + k) \not{\epsilon}_1^* G_0(p + k) \not{k} u_p$$
$$+ \bar{u}_{p'} \not{\epsilon}_2^* G_0(p - k_1 + k) \not{k} G_0(p - k_1) \not{\epsilon}_1^* u_p$$
$$+ \bar{u}_{p'} \not{k} G_0(p' - k) \not{\epsilon}_2^* G_0(p - k_1) \not{\epsilon}_1^* u_p \Big\} \ + \ (1 \leftrightarrow 2), \quad (4.44)$$

where the three contributions correspond to the three Feynman diagrams in the first line of Figure 4.3, where the first, second and third term correspond to the first, second and third Feynman diagram. The three diagrams in the second line of Figure 4.3 are obtained by interchanging photon "$1$" and "$2$". In the limit of a monochromatic IPW laser field, $g \rightarrow 1$, $\tilde{\mathscr{C}}_1(s) \rightarrow \pi[\delta(s - 1) + \delta(s + 1)]$, where the second term is excluded by energy momentum

conservation. Using this result in the amplitude (4.44), one obtains the $S$ matrix in the weak-field approximation

$$
\begin{aligned}
S = \frac{-ie^2 m a_0}{2} (2\pi)^4 \delta^4(p + k - k_1 - k_2 - p') \Big\{ &\bar{u}_{p'} \slashed{\epsilon}_2^* G_0(p - k_1 + k) \slashed{\epsilon}_1^* G_0(p + k) \slashed{\epsilon} u_p \\
&+ \bar{u}_{p'} \slashed{\epsilon}_2^* G_0(p - k_1 + k) \slashed{\epsilon} G_0(p - k_1) \slashed{\epsilon}_1^* u_p \\
&+ \bar{u}_{p'} \slashed{\epsilon} G_0(p' - k) \slashed{\epsilon}_2^* G_0(p - k_1) \slashed{\epsilon}_1^* u_p \Big\} \; + \; (1 \leftrightarrow 2)
\end{aligned}
\tag{4.45}
$$

which is, except for the different global normalization, equivalent to the textbook result for the $S$ matrix for perturbative double Compton effect [Jau76].

## 4.4   On-shell and off-shell contributions

It is known that in strong-field second-order processes the intermediate particles can come on their mass shell due to the presence of the background field [Ole67, Ole68, Löt09b, Hu10, Ild11a]. Thus, the $S$ matrix for two-photon Compton scattering contains contributions from virtual off-shell and real on-shell intermediate electrons. For IPW laser fields this fact leads to the emergence of Oleinik singularities, i.e. unphysical divergences of the $S$ matrix, which have to be regularized, e.g. by including an imaginary mass contribution to the propagator denominator, which is related to the imaginary part of the mass operator $\Sigma$ and to the total probability of one-photon Compton scattering via the optical theorem [Löt08, Löt09b]. This is an implementation of the radiative width of the Zel'dovich quasi-energy levels due to single-photon decay [Ole68, Bec76]. In [Ild11a] it was shown for the trident pair-production process that the matrix element is free of singularities in pulsed laser fields. Here, this method is applied to the two-photon Compton process, where the internal particle is a fermion instead of the photon in the trident process.

According to [Ild11a], the virtual off-shell contributions can be separated from the resonant on-shell contributions due to real intermediate electrons by applying the Sokhotsky-Weierstraß theorem, which is valid in the distributional sense,

$$
\frac{1}{\ell - \ell_1 + i0^+} = \mathcal{P} \frac{1}{\ell - \ell_1} - i\pi \delta(\ell - \ell_1) \,,
\tag{4.46}
$$

where $\mathcal{P}$ denotes the principal value part. Using this relation in the expression (4.21) for the pole integral, one finds the decomposition

$$
\int_{-\infty}^{\infty} d\ell \, \frac{e^{-i\ell(\phi - \phi')}}{\ell - \ell_1 + i0^+} = \mathcal{P} \int_{-\infty}^{\infty} \frac{e^{-i\ell(\phi - \phi')}}{\ell - \ell_1} - i\pi e^{-i\ell_1(\phi - \phi')} \,.
\tag{4.47}
$$

Using methods of complex analysis, the principal value of an integral can be calculated by taking the arithmetic average of evading the pole above (complex path $C_+$) and below ($C_-$) the real line [Sch12]

$$
\begin{aligned}
\mathcal{P} \int_{-\infty}^{\infty} d\ell \, \frac{e^{-i\ell(\phi - \phi')}}{\ell - \ell_1} &\equiv \frac{1}{2} \left( \int_{C_+} d\ell \, \frac{e^{-i\ell(\phi - \phi')}}{\ell - \ell_1} + \int_{C_-} d\ell \, \frac{e^{-i\ell(\phi - \phi')}}{\ell - \ell_1} \right) \\
&= -i\pi [\Theta(\phi - \phi') - \Theta(\phi' - \phi)] e^{-i\ell_1(\phi - \phi')} \,.
\end{aligned}
\tag{4.48}
$$

By means of the $\delta$ distribution in (4.46) it becomes clear that the imaginary part of (4.46) is precisely the contribution of intermediate on-shell particles since $\delta(\ell - \ell_1)$ singles out the

on-shell values of the propagator momentum $P_1 + \ell k \to P_1 + \ell_1 k$, where $(P_1 + \ell_1 k)^2 = m^2$. By recalling that principal value integration ($\mathcal{P}$) effectively means cutting out a small interval around the pole at $\ell = \ell_1$ it becomes clear that principal value part of $\mathcal{M}$ refers to the virtual (off-shell) process.

Thus, the two-photon amplitude $\mathcal{M}$ is decomposed into an off-shell part $\mathcal{M}_{\text{off}}$, related to the principal value, and an on-shell part $\mathcal{M}_{\text{on}}$ related to the pole contribution of the propagator where the propagator momentum is forced on its mass shell. The on-shell part refers to the two-step process, where the two photons are emitted independently [Ild11b]. This has also been denoted as Compton cascade in the literature [Löt09b].

From the technical point of view, this decomposition affects only the two-dimensional phase integrals $\mathcal{B}_{nl}$. The domain of integration in (4.25) is a triangle due to the appearance of the step function $\Theta(\phi - \phi')$, which is the only occasion where the integrations over $d\phi$ and $d\phi'$ are coupled. The above decomposition (4.47) into principal value and delta contribution divides the domain of integration of the $\mathcal{B}_{nl}$ according to

$$\Theta(\phi - \phi') = \frac{1}{2}\text{sign}(\phi - \phi') + \frac{1}{2} \tag{4.49}$$

such that

$$\mathcal{B}_{nl,\text{off}} = \frac{1}{2} \int d\phi \, d\phi' \, \text{sign}(\phi - \phi') a^n(\phi) a^l(\phi') e^{i(s-\ell_1)\phi - i f_{P_1}(\phi) + i f_{p'}(\phi)} e^{i\ell_1 \phi' - i f_P(\phi') + i f_{P_1}(\phi')} \, .$$

$$\mathcal{B}_{nl,\text{on}} = \frac{1}{2} \int d\phi \, d\phi' \, a^n(\phi) a^l(\phi') e^{i(s-\ell_1)\phi - i f_{P_1}(\phi) + i f_{p'}(\phi)} e^{i\ell_1 \phi' - i f_P(\phi') + i f_{P_1}(\phi')} \, . \tag{4.50}$$

For the on-shell part of $\mathcal{B}_{nl}$, the two integrations over $d\phi$ and $d\phi'$ decouple.[1] With these results the on- and off-shell parts of the two-photon amplitude can be given as

$$\mathcal{M}_{\text{off}} = \frac{1}{2k \cdot P_1} \left\{ \sum_{n=0}^{2} \mathcal{V}_n \mathcal{C}_n(s) + \sum_{n,l=0}^{2} \mathcal{U}_{nl} \mathcal{B}_{nl,\text{off}}(s,\ell_1) \right\} + (1 \leftrightarrow 2) \, , \tag{4.51}$$

$$\mathcal{M}_{\text{on}} = -\frac{1}{2k \cdot P_1} \sum_{n,l=0}^{2} \mathcal{U}_{nl} \mathcal{B}_{nl,\text{on}}(s,\ell_1) + (1 \leftrightarrow 2) \, . \tag{4.52}$$

One finds for the squared amplitude $|\mathcal{M}|^2 = |\mathcal{M}_{\text{off}}|^2 + |\mathcal{M}_{\text{on}}|^2$, i.e. there is no interference between the off- and on-shell parts, or between the one-step and two-step processes. It is therefore possible to define on-shell and off-shell emission probabilities according to

$$\frac{d^6 W_{\text{on,off}}}{d\omega_1 d\Omega_1 d\omega_2 d\Omega_2} = \frac{\alpha^2 \omega_1 \omega_2}{64\pi^4 (k \cdot p)(k \cdot p')} |\mathcal{M}_{\text{on,off}}|^2 \, ,$$

$$\frac{d^6 W}{d\omega_1 d\Omega_1 d\omega_2 d\Omega_2} = \frac{d^6 W_{\text{off}}}{d\omega_1 d\Omega_1 d\omega_2 d\Omega_2} + \frac{d^6 W_{\text{on}}}{d\omega_1 d\Omega_1 d\omega_2 d\Omega_2} \tag{4.53}$$

It can be shown that the on-shell part of the $S$ matrix factorizes into a product of two one-photon $S$ matrices for each of the two channels. To show the factorization of the on-shell part of the $S$ matrix, it is convenient to apply again the Sokhotsky-Weierstraß theorem, i.e. to force the propagator momentum on its mass shell in Eq. (4.15), where one has the replacement

$$G_0(P_1 + \ell k) \to -\frac{i\pi}{2k \cdot P_1} (\slashed{P}_1 + \ell \slashed{k} + m)\delta(\ell - \ell_1) \, . \tag{4.54}$$

---

[1] For $\hat{\phi} = 0$ it can be shown that $\mathcal{B}_{nl,\text{on}} = \text{Re}\,\mathcal{B}_{nl}$ and $\mathcal{B}_{nl,\text{off}} = \text{Im}\,\mathcal{B}_{nl}$ with the symmetric choice of the lower integration boundary of the non-linear phase integrals $f_p$ in Eq. (4.8).

**Figure 4.4:** Diagrammatic representation of the on-shell part of the two-photon Compton matrix element and the factorization into two one-photon $S$ matrix elements. The dashed vertical lines indicate the pole contribution of that propagator, i.e. the propagator is replaced by a delta distribution according to the Sokhotsky-Weierstraß theorem.

With this result the on-shell part $S_{\mathrm{on}}$ of the $S$ matrix reads

$$S_{\mathrm{on}} = -ie^2(2\pi)^2 \frac{-i\pi}{2k \cdot P_1} \frac{2}{k^-} \delta^3(\mathsf{p} - \mathsf{p}' - \mathsf{k}_1 - \mathsf{k}_2)$$

$$\times \int d\phi_1 d\phi_2 \bar{u}_{p'} e^{i(s-\ell_1)\phi_2} \mho^{\epsilon_2}_{p',P_1}(\phi_2)\, G_1\, e^{i\ell_1\phi_1} \mho^{\epsilon_1}_{P_1,p}(\phi_1) u_p \; + \; (1 \leftrightarrow 2)\,. \quad (4.55)$$

Employing the completeness relation for spinors $G_1 = \sum_{r''} u_{P_1+\ell_1 k, r''} \bar{u}_{P_1+\ell_1 k, r''}$ to the numerator of the propagator ($r''$ is the spin of the intermediate electron), one obtains

$$S_{\mathrm{on}} = \frac{1}{2} \sum_{r''=\uparrow,\downarrow} (-ie)^2 (2\pi)^3 \frac{1}{2P_1^+} \left(\frac{2}{k^-}\right)^2 \delta^3(\mathsf{p} - \mathsf{p}' - \mathsf{k}_2 - \mathsf{k}_1)$$

$$\times \int d\phi_2 \bar{u}_{p'} e^{i(s-\ell_1)\phi_2} \mho^{\epsilon_2}_{p',Q_1}(\phi_2) u_{Q_1,r''}$$

$$\times \int d\phi_1 \bar{u}_{Q_1,r''} e^{i\ell_1\phi_1} \mho^{\epsilon_1}_{Q_1,p}(\phi_1) u_p \; + \; (1 \leftrightarrow 2) \quad (4.56)$$

with $Q_1 = P_1 + \ell_1 k$ being the on-shell value of the propagator momentum with $Q_1^2 = m^2$. Using the identity

$$\delta^3(\mathsf{p} - \mathsf{p}' - \mathsf{k}_1 - \mathsf{k}_2) = \int d^3\mathsf{p}''\, \delta^3(\mathsf{p}'' - \mathsf{p}' - \mathsf{k}_2)\, \delta^3(\mathsf{p} - \mathsf{p}'' - \mathsf{k}_1)\,, \quad (4.57)$$

the on-shell part of $S$ factorizes on the amplitude level

$$S_{\mathrm{on}} = \frac{1}{2} \int \frac{d^2\mathsf{p}''}{(2\pi)^3 2p''^+} \sum_{r''=\uparrow,\downarrow} S^{(1)}_{\mathsf{p}''\to\mathsf{p}'\mathsf{k}_2}(s-\ell_1)\, S^{(1)}_{\mathsf{p}\to\mathsf{p}''\mathsf{k}_1}(\ell_1)$$

$$+ \frac{1}{2} \int \frac{d^2\mathsf{p}''}{(2\pi)^3 2p''^+} \sum_{r''=\uparrow,\downarrow} S^{(1)}_{\mathsf{p}''\to\mathsf{p}'\mathsf{k}_1}(s-\ell_2)\, S^{(1)}_{\mathsf{p}\to\mathsf{p}''\mathsf{k}_2}(\ell_2)\,, \quad (4.58)$$

where $S^{(1)}$ denotes the $S$ matrix for the one-photon Compton process given in Eq. (3.20). The product of the one-photon $S$ matrices has to be integrated over all intermediate states with the Lorentz invariant measure $d^3\mathsf{p}''/(2\pi)^2 2p''^+$ and summation over the intermediate spin $r''$. The factorization is realized on the amplitude level for each channel separately. A diagrammatic representation is exhibited in Figure 4.4. This result is a consequence of the optical theorem [Pes95]: The absorptive part of an amplitude is equal to to a sum over all possible real intermediate state particles, integrated with a Lorentz invariant integration measure. In numerical calculations of differential spectra, the interference between the two Feynman diagrams on the left hand side of Figure 4.4, i.e. between the direct channel and the exchange channel, can be of the same order of magnitude as the non-interference terms.

In the weak-field limit $a_0 \ll 1$, the off-shell part of the $S$ matrix is proportional to $a_0$ in lowest order, as discussed above in Section 4.3, corresponding to the absorption of one laser photon (see also Figure 4.3). Contrarily, the leading order contribution to the on-shell part is $\propto a_0^2$, since at least two laser photons are needed to satisfy the on-shell energy momentum conservation. For each one-photon Compton matrix element $S^{(1)}$ on the right hand side of the Eq. (4.58) one has to employ the weak-field expansion [see Eq. (3.28) and Appendix C.1], which is of order $a_0$.

## 4.5   Oleinik singularities and the IPW limit

In the limit of IPW laser fields, the on-shell part of the two-photon $S$ matrix, i.e. the Compton cascade or the two-step process, diverges. These divergences appear where the propagator momentum reaches its mass shell. This phenomenon is termed Oleinik resonance singularities [Ole67, Ole68]. In the above expression for the $S$ matrix in a PPW laser field, no such singularities are present. In particular all divergent phase integrals $\mathscr{C}_n$ and $\mathscr{B}_{nl}$ can be regularized by the requirement of gauge invariance.

Here, the IPW limit of the two-photon Compton matrix element is calculated to reveal the emergence of the Oleinik singularities for these laser fields. The calculation is similar to Section 2.9, where the IPW limit of the Dirac-Volkov propagator was discussed. A proper starting point is the expression (4.15) for the two-photon $S$ matrix. In the case of an IPW laser field, each of the vertex functions contains a part $\Phi_i$ that is periodic with the laser frequency [Flo83],

$$e^{i\ell\phi}\mho_{P_1,p}^{\epsilon_1}(\phi) = e^{i(\ell-\beta_p+\beta_{P_1})\phi}\Phi_1(\phi) \tag{4.59}$$

The periodicity of $\Phi_1$ allows for a Fourier series expansion of the latter, such that

$$\int d\phi\, e^{i\ell\phi}\mho_{P_1,p}^{\epsilon_1}(\phi) = \sum_{n=-\infty}^{\infty} 2\pi\delta(\ell-\beta_p+\beta_{P_1}-n)\Xi_{P_1,p}^{\epsilon_1}(n)\,, \tag{4.60}$$

with the Fourier coefficients $\Xi_{P_1,p}^{\epsilon_1}(n)$ which are complicated functions of generalized Bessel functions times products of several Dirac matrices. Their explicit form is of no relevance for the discussion here (for explicit representations of these expressions see e.g. [Löt09a]). Using a similar decomposition for the second vertex, the $S$ matrix reads

$$S = -ie^2(2\pi)^4 \sum_{n',n} \int ds\, d\ell\, \delta(s-\ell-\beta_{P_1}+\beta_{p'}-n')\delta(\ell-\beta_p+\beta_{P_1}-n)$$

$$\times\, \delta^4(p+sk-k_1-k_2-p')\frac{\bar{u}_{p'}\Xi_{p',P_1}^{\epsilon_2}(n')(\slashed{P}_1+\ell\slashed{k}+m)\Xi_{P_1,p}^{\epsilon_1}(n)u_p}{(P_1-\ell k)^2-m^2+i0^+}\; +\;(1\leftrightarrow 2)\,. \tag{4.61}$$

Performing the integrals over $d\ell$ and $ds$ one obtains

$$S = -ie^2(2\pi)^4 \sum_{n',n} \delta^4(q+n'k-k_1-k_2-q')$$

$$\times\, \frac{\bar{u}_{p'}\Xi_{p',P_1}^{\epsilon_2}(n'-n)(\slashed{P}_1+(n+\beta_p-\beta_{P_1})\slashed{k}+m)\Xi_{P_1,p}^{\epsilon_1}(n)u_p}{(q-k_1-nk)^2-m_\star^2+i0^+}\; +\;(1\leftrightarrow 2)\,, \tag{4.62}$$

where the quasi-momentum $q^\mu = p^\mu + \beta_p k^\mu$ and the effective mass $m_\star^2 = q^2$ have been introduced. Abbreviating the expression in the numerator as $J^{21}(n'-n,n)$, the $S$ matrix in

IPW laser fields reads [Löt09b, Löt09a]

$$S = -ie^2(2\pi)^4 \sum_{n'=1}^{\infty} \sum_{n=-\infty}^{\infty} \delta^4(q + n'k - k_1 - k_2 - q')$$

$$\times \left( \frac{J^{21}(n'-n,n)}{(q-k_1-nk)^2 - m_\star^2 + i0^+} + \frac{J^{12}(n'-n,n)}{(q-k_2-nk)^2 - m_\star^2 + i0^+} \right), \tag{4.63}$$

The $S$ matrix diverges if any of the two propagator denominators becomes zero. This defines the resonance conditions as

$$(q - k_{1,2} - nk)^2 - m_\star^2 = 0. \tag{4.64}$$

Solving for $\omega_{1,2}$, the resonance frequencies read [Löt09a]

$$\omega_{1,2}^{\text{res}}(n) = \frac{nk \cdot q}{(q + nk) \cdot n_{1,2}} = \frac{nk \cdot p}{[p + (n + \beta_p)k] \cdot n_{1,2}}, \tag{4.65}$$

where $n_{1,2} = (1, \cos\varphi_{1,2}\sin\theta_{1,2}, \sin\varphi_{1,2}\sin\theta_{1,2}, \cos\theta_{1,2})$ is the unit vector in the direction of $k_{1,2}$ (with $\theta_{1,2}$ and $\varphi_{1,2}$ denoting the usual polar and azimuthal angles of the emitted photons). The resonances for $\omega_1$ ($\omega_2$) emerge when the first (second) propagator denominator in (4.63) vanishes, which corresponds to first (second) Feynman diagram in Figure 4.1 and coincide with the one-photon Compton IPW harmonics (C.24). The difference between the IPW and PPW case is the following: For pulsed fields the propagator denominator can also vanish. However, these pole contributions are rendered finite due to the integration over $d\ell$, e.g. in Eq. (4.20). In contrast, for the case of IPW considered here, the integration is replaced by a sum due to the infinite extent of the laser field. Hence, in the case of IPW one has a sum over divergences. In calculations of physical processes within the IPW model for the laser fields these singularities have to be regularized, which has been done in the literature by including the imaginary part of the electron mass operator to the propagator denominator [Ole68, Bec76, Ros96, Sch07, Löt09a]. Since the imaginary part of the (one-loop) mass operator $\Sigma$ is related to the total emission one-photon emission probability, this replacement accounts for the finite lifetime of Volkov electrons, which spontaneously emit photons via the one-photon Compton effect [Hu11]. The appearance of Oleinik resonances is related to the existence of Zel'dovich levels of the Volkov wave functions and the Dirac-Volkov propagator in the case of IPW [Ole68]. For finite temporal laser pulses, the Zel'dovich levels are broadened, which leads to finite results for the on-shell contributions to two-photon Compton scattering and other second-order strong-field processes. The singularities are replaced by resonance structures as can be seen in the numerical results below.

The energy momentum conservation in (4.63) leads to an expression for $\omega_2$ as a function of $\omega_1$ and the scattering angles

$$\omega_2(\omega_1, n') = \frac{n'k \cdot q - (q + n'k) \cdot k_1}{[q + n'k - k_1] \cdot n_2} = \frac{n'k \cdot p - p \cdot k_1 - \left(n' + \frac{m^2 a_0^2}{4k \cdot p}\right) k \cdot k_1}{\left[p + \left(n' + \frac{m^2 a_0^2}{4k \cdot p}\right) k - k_1\right] \cdot n_2}. \tag{4.66}$$

While in a PPW the two frequencies $\omega_{1,2}$ are independent of each other, the above equation induces a correlation between $\omega_1$ and $\omega_2$, with the harmonic number $n' \in \mathbb{N}$.

## 4.6 Numerical results

For the numerical evaluations, the initial electrons are considered to have a Lorentz factor $\gamma = p^0/m = 10^4$, available, e.g. at the European XFEL electron beam [XFE], in head-on

collisions with a laser pulse with frequency $\omega = 1.55$ eV. The calculations have been performed for a pulse shape $g(\phi) = \cos^2(\frac{\pi\phi}{2\Delta\phi})$ for $-\Delta\phi \geq \phi \geq \Delta\phi$ and zero otherwise, such that $\Delta\phi$ is the dimensionless FWHM pulse length. (A similar kinematic situation with the same centre-of-mass energy could be achieved by colliding an XFEL X-ray pulse [XFE] with low energy electrons, e.g. $\gamma = 10$, provided by an optical laser acceleration set-up [Fau06].)

In Figures 4.5, 4.6 and 4.7, the numerical results for the differential two-photon emission probability are exhibited as a function of $\omega_1$ and $\omega_2$. In the case of an IPW there is the strict correlation $\omega_2(\omega_1, n')$, such that one can expect the most drastic differences between an IPW and a PPW to be evident in this phase space cut. Since the motion of the electron is relativistic, the radiation is produced in a cone around the spatial direction of $p$ with a typical opening angle of $1/\gamma$. The differential probability is shown at the scattering angles $\theta_{1,2} = 1/\gamma$ and $\varphi_1 = \pi/2$ and $\varphi_2 = 3\pi/2$, i.e. the two photons are emitted in a plane perpendicular to the polarization plane of the laser.

In Figure 4.5, the differential two-photon emission probability, is shown for a moderately strong laser pulse with $a_0 = 0.1$ and a pulse length of $\Delta\phi = 20$, which corresponds to 9 fs FWHM. The left panel (a) is the off-shell part of the emission probability with the contributions from virtual intermediate particles, Eq. (4.51). The dash-dotted lines in (a) depict the harmonic frequencies $\omega_2(\omega_1, n')$ for $n' = 1, 2, 3$, i.e. the energy correlation in an IPW. The first harmonic, $n' = 1$, approximatively fulfils $\omega_1 + \omega_2 \approx 295$ MeV. The off-shell emission probability in a pulsed laser field is aligned with these lines, it resembles a broadened IPW harmonic. In the centre panel (b) the on-shell probability, i.e. the contribution from real intermediate particles is exhibited which are particularly strong in the vicinity of the Oleinik resonances $\omega_{1,2}^{\text{res}}$, which are drawn in this plot as dotted lines. For the given parameters, the first Oleinik resonance, $n = 1$ is located at $\omega_{1,2}^{\text{res}} = 291$ MeV. In contrast to the IPW case where this contribution would be singular, one finds a finite resonance behaviour for PPW, with the strongest peak at $\omega_1 = \omega_2 = 291$ MeV. In the right panel (c) of Figure 4.5, the sum of these two contributions is shown. As stated above, there are no interference terms between the off-shell and on-shell contributions.

In Figure 4.6, differential two-photon probability is presented for a stronger laser field with $a_0 = 1$ and the same pulse length $\Delta\phi = 20$ as in Figure 4.5. The off-shell part exceeds the on-shell part for low frequencies $\omega_{1,2} < 200$ MeV where there are no resonances; the lowest Oleinik resonance is shifted to $\omega_{1,2}^{\text{res}} = 236$ MeV due to the intensity dependent red-shift. In general, the on- and off-shell contributions are aligned with the corresponding IPW harmonics as above, although the emission probability is distributed more in the $\omega_1 - \omega_2$ phase space. Furthermore, also the off-shell part develops resonance like structures at the positions where the Oleinik resonances coincide. One observes that the ponderomotive broadening sets in; the PPW harmonics consist of several sub-peaks. This behaviour is much more pronounced for a longer pulse, e.g. for $\Delta\phi = 50$ (corresponding to 21 fs FWHM), which is exhibited in Figure 4.7. For $a_0 = 1$, in Figures 4.6 and 4.7, the differential spectrum is dominated by the on-shell part in almost the whole $\omega_1 - \omega_2$ phase space for both $\omega_{1,2} > 200$ MeV, where it is roughly one order of magnitude larger than the off-shell part. This is a generic feature also for different scattering angles. The off-shell part exceeds to on-shell part for at least one of the $\omega_{1,2}$ below 200 MeV, where the maxima of the distribution are roughly aligned with the different harmonics $n'$ of the IPW energy correlation.

The Figures 4.5, 4.6 and 4.7 evidence the striking differences to the IPW case: The strict $\omega_2(\omega_1)$ correlation of (4.66) gets completely lost. Instead, resonance like structures with sub-peaks appear which are produced by the ponderomotive broadening mechanism, resembling the ones observed in the one-photon Compton process. Furthermore, the on-shell part leads to finite resonances in a PPW laser field instead of the singular result in the IPW case.
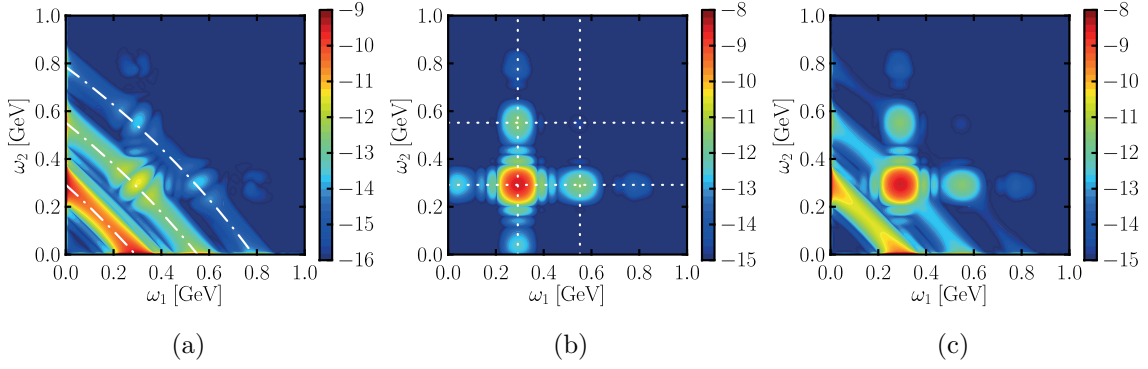
**Figure 4.5:** Contour plots of the differential two-photon emission probability as a function of $\omega_1$ and $\omega_2$ for $a_0 = 0.1$ and $\Delta\phi = 20$, showing the off-shell contribution (a), the on-shell contribution (b) and the sum of both (c). In (a) the IPW harmonics $\omega_2(\omega_1, n')$ are shown for $n' = 1, 2, 3$ as dash-dotted curves, while in (b) the dotted lines represent the Oleinik resonances $\omega_{1,2}^{\mathrm{res}}$, Eq. (4.65), for $n = 1, 2$. For parameters see the text.
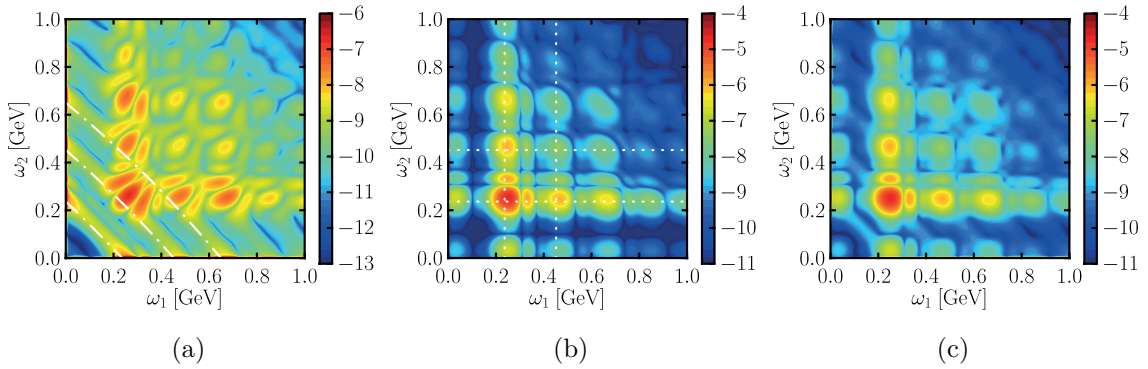


**Figure 4.6:** The same as in Figure 4.5 but for $\Delta\phi = 20$ and $a_0 = 1$.
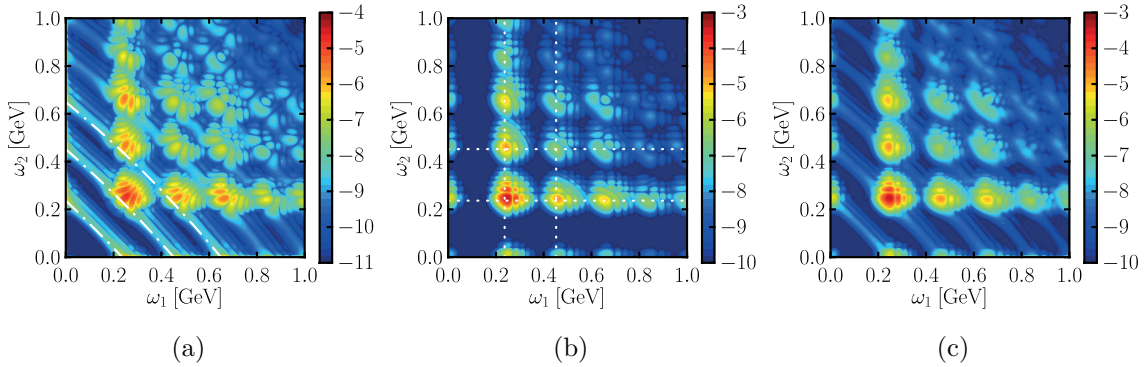


**Figure 4.7:** The same as in Figure 4.5 but for $\Delta\phi = 50$ and $a_0 = 1$.

## 4.7   The inclusive two-photon probability and comparison with one-photon emission

In Figure 4.8, the inclusive spectrum

$$\frac{d^3W}{d\omega_1 d\Omega_1} = \int d\omega_2 d\Omega_2 \left( \frac{d^6W}{d\omega_1 d\Omega_1 d\omega_2 d\Omega_2} \right) \tag{4.67}$$

is exhibited, arising from (4.35) by integrating over the phase space of photon "*2*" which allows for a comparison between one-photon and two-photon emission. For soft photons $\omega_2 \to 0$, the emission probability of two-photon emission becomes divergent. The cancellation of this infrared divergence by soft virtual photons due to loop corrections of one-photon scattering is ensured by the Bloch-Nordsieck theorem [Blo37] as in the perturbative case. The calculation of the infrared divergent parts and their cancellation is presented in Appendix E. It is shown there, that the laser dressed vertex $\mho^{\epsilon_2}_{P,p} \to \not{\epsilon}^*_2$ goes to the free (non-dressed) vertex if the frequency of the emitted photon goes to zero $\omega_2 \to 0$, such that the infrared divergence in the strong-field QED process has the same structure as in perturbative QED. The exact cancellations of the infrared divergence of weak-field perturbative double Compton scattering with the one-loop radiative corrections to one-photon Compton scattering have been shown in [Bro52]. For practical purposes, however, an infrared cut-off $\omega_2^{\min} = 100$ keV is included in the frequency integral in (4.67) to avoid the soft-photon divergence in the spirit of [Löt09b]. The value of the integral is rather insensitive to a variation of the cut-off in the range of $1 - 1000$ keV.

The inclusive spectrum accounts for the experimental observation of only one of the two photons. To compare with one-photon Compton backscattering, the backscattering direction $\theta_1 = \varphi_1 = 0$ is chosen. In the case of strong laser fields, e.g. for $a_0 = 1$ in Figure 4.8, the inclusive spectrum is found about two orders of magnitude below the one-photon spectrum for $\omega_1 > 200$ MeV. At photon energies $\omega_1 < 200$ MeV, the two-photon process exceeds the one-photon process (see Figure 4.8), opening, at least in principle, a window to access its observation without coincidence measurements.

Approximating the integrations over the solid angle of photon "*1*" as

$$\frac{dW}{d\omega_1} = \int d\Omega_1 \frac{dW}{d\omega_1 d\Omega_1} \approx \frac{2\pi}{\gamma^2} \left. \frac{dW}{d\omega_1 d\Omega_1} \right|_{\theta_1 = \varphi_1 = 0} \tag{4.68}$$

and integrating over $\omega_1$, one can estimate the total number of produced pairs as $1.1 \times 10^{-3}$ per pulse and electron as compared to $5 \times 10^{-2}$ coming from the one-photon Compton process. With an assumed laser repetition rate of 10 Hz one can expect 950 two-photon events as compared to 43000 single photon events in one day which should be sufficient for an experimental observation. The coincidence detection of rare two-photon events, where both photons are emitted within a small opening angle has been successfully demonstrated in the photon splitting process [Akh02]. The experimental sensitivity might be increased by a simultaneous detection of the scattered electrons (like in photon tagging). The electron beam should be a dilute beam tuned to one interaction per laser pulse.

In the weak-field regime the rate of the two-photon Compton process is suppressed by a factor of $\alpha\varrho^2$ relative to the one-photon Compton process for $\varrho = k \cdot p/m^2 \ll 1$ [Hei34], (see also Figure 1.5). For the momenta considered here, with $\varrho = 0.06$, the estimated suppression in the weak field regime is $3 \times 10^{-5}$. To discuss the relevance of the two-photon emission in strong laser fields, the two-photon to one-photon ratio is defined as

$$\mathcal{R} = \frac{dW^{(2)}}{d\Omega_1} \bigg/ \frac{dW^{(1)}}{d\Omega_1} , \tag{4.69}$$
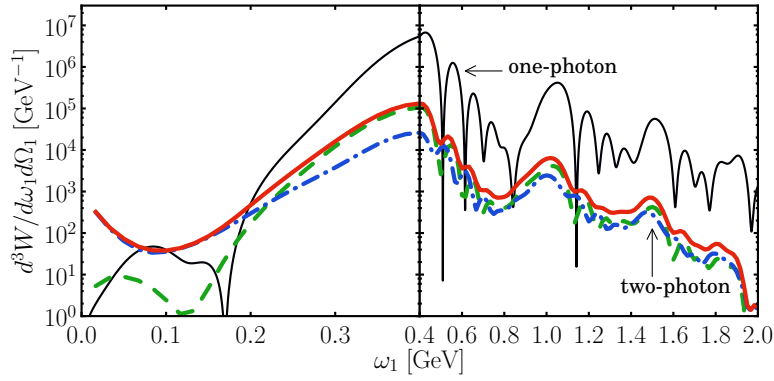
**Figure 4.8:** The inclusive two-photon spectrum (red solid curve; the green dashed curve and the blue dash-dotted curve depict the on-shell and off-shell contributions) in comparison to the one-photon Compton spectrum (thin black solid curve) as a function of the photon frequency $\omega_1$. The low-energy range below 400 MeV where the two-photon probability exceeds the one-photon probability is magnified.

taken in the direction $\varphi_1 = \theta_1 = 0$. For $\Delta\phi = 10$ (see Figure 4.9) a value of $\mathcal{R} = 10^{-2}$ is obtained at $a_0 = 1$ which is about two orders of magnitude larger than the perturbative estimate. For lower values of $a_0 < 0.1$ the suppression of the two-photon probability rapidly approaches a constant value of $\mathcal{R} = 10^{-4}$, as anticipated in [Hei34]. Considering the on-shell and off-shell contributions, [where $W^{(2)}_{\mathrm{on,off}}$ are employed in the definition of $\mathcal{R}$ in Eq. (4.69),] it is found that the ratio for the on-shell process $\mathcal{R}_{\mathrm{on}} = 0.01a_0^2$ for $a_0 < 1$. The off-shell ratio $\mathcal{R}_{\mathrm{off}}$ is independent of $a_0$ for $a_0 < 0.1$, with a value of $\mathcal{R}_{\mathrm{off}} = 10^{-4}$. Above $a_0 > 0.1$ the value of $\mathcal{R}_{\mathrm{off}}$ increases and reaches $\mathcal{R}_{\mathrm{off}} = 10^{-3}$ at $a_0 = 1$. These findings show that even at moderate intensities of $a_0 = 1$, the probability for two-photon emission is significantly enhanced as compared to the weak-field case. The ratio of $\mathcal{R} = 0.01$ means that for each 100 photons that are emitted via one-photon Compton process, there is one emitted pair due to the two-photon process. The tendencies in Figure 4.9 indicate that the two-photon process might be even more important for $a_0 \gg 1$. However, for larger values of $a_0$, starting at $a_0 \geq 3$, considerable numerical uncertainties on the order of 50% and larger were encountered, such that a definite answer on that issue cannot be given at the moment.

## 4.8   The pulse length dependence of the two-photon emission probability

The pulse length dependence of the cascade part and the coherent part of the emission probability are different. While the coherent part of the emission probability is proportional to $\Delta\phi$, the cascade part has a dependence $\propto \Delta\phi^2$, since it is the product of two one-photon events which are $\propto \Delta\phi$ each [Hu11]. In this section, the pulse length dependence of the different contributions (on-shell and off-shell contributions) to the two-photon emission probability is studied for a box-shaped pulse envelope $g(\phi) = \sqcap(\phi)$ with constant amplitude [see Eq. (A.34)], for which the pulse length dependence of the two-photon amplitude $\mathcal{M}$, Eq. (4.23), can be evaluated completely analytically. This is achieved by relating the phase integrals $\mathscr{C}_n(s)$ and $\mathscr{B}_{nl}(s, \ell_1)$ over the complete pulse to reduced phase integrals $C_n(s)$ and $B_{nl}(s, \ell_1)$, which are defined over the fundamental interval of periodicity of their integrands $\phi, \phi' \in [-\pi, \pi]$. The dependence on the pulse length then appears in the prefactors of these reduced phase integrals. It is convenient to use as pulse length parameter the number of full
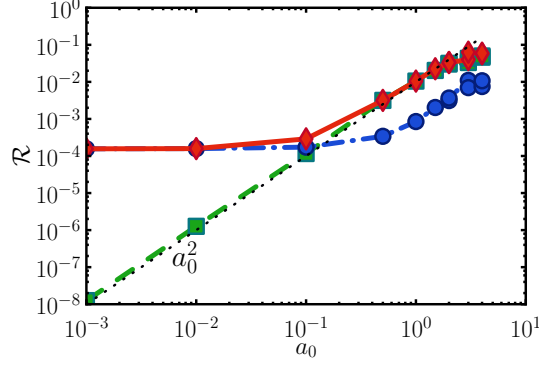
**Figure 4.9:** The dependence of the two-photon to the one-photon ratio $\mathcal{R}$ (red solid curve with diamonds) as a function of $a_0$ for $\Delta\phi = 10$. The green dashed curve with squares depicts the on-shell ratio $\mathcal{R}_{\text{on}}$ while the blue dash-dotted curve with circles is for the off-shell ratio $\mathcal{R}_{\text{off}}$. To guide the eye, the black dotted line depicts the slope of $a_0^2$.

oscillations $N = \Delta\phi/2\pi$, such that the domain of the $\phi$ and $\phi'$ integrations for the full phase integrals $\mathscr{C}_n(s)$ and $\mathscr{B}_{nl}(s, \ell_1)$ is the interval $[-N\pi, N\pi]$ for $n, l \in \{1, 2\}$. The phase integrals with index 0 have still an infinite integration range and are defined through Eqs. (D.19) – (D.21). By partitioning the interval $[-N\pi, N\pi]$ into $N$ subintervals $[-\pi, \pi]$ and shifting the integration variables, the one-dimensional integral is evaluated to be (setting $\hat{\phi} = 0$)

$$\mathscr{C}_n(s) = \int\limits_{-N\pi}^{N\pi} d\phi \cos^n\phi \, e^{i(s - \beta_p + \beta_{p'})\phi - i(\alpha_p - \alpha_{p'})\sin\phi - i(\frac{\beta_p}{2} - \frac{\beta_{p'}}{2})\sin 2\phi} \tag{4.70}$$

$$= \sum_{j=0}^{N-1} \int\limits_{-N\pi+2\pi j}^{-N\pi+2\pi(j+1)} d\phi \cos^n\phi \, e^{i(s - \beta_p + \beta_{p'})\phi - i(\alpha_p - \alpha_{p'})\sin\phi - i(\frac{\beta_p}{2} - \frac{\beta_{p'}}{2})\sin 2\phi} \tag{4.71}$$

$$= \sum_{j=0}^{N-1} e^{iz(2\pi j - (N-1)\pi)} C_n(s) \tag{4.72}$$

with $z = s - \beta_p + \beta_{p'}$. In the last line, the integration variable has been transformed $\phi \to \phi + (N-1)\pi - 2\pi j$ and the periodicity of the trigonometric functions has been utilized. The complete dependence on the summation variable $j$ has been taken out of the integral. The sum can be evaluated yielding

$$\sum_{j=0}^{N-1} e^{iz(2\pi j - (N-1)\pi)} = \frac{\sin\pi N z}{\sin\pi z} \, . \tag{4.73}$$
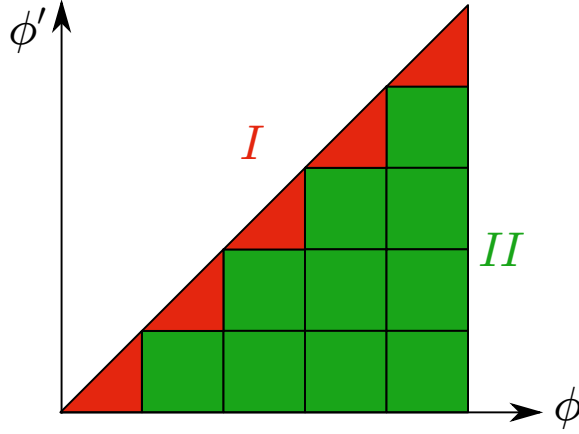
This prefactor defines the support of the spectrum as diffraction pattern, converging to a delta comb upon taking $N \to \infty$, eventually.
The integral over the fundamental interval $[-\pi, \pi]$,

$$C_n(s) = \int\limits_{-\pi}^{\pi} d\phi \, F_n(\phi; z, \alpha_p - \alpha_{p'}, \beta_p - \beta_{p'}) \, , \tag{4.74}$$

is the phase integral over a single oscillation of the laser, having defined the integral kernel

$$F_n(\phi; z, \alpha, \beta) = (-1)^{n(N-1)} \cos^n\phi \, e^{iz\phi - i(-1)^{N-1}\alpha\sin\phi - i\frac{\beta}{2}\sin 2\phi} \, . \tag{4.75}$$

**Figure 4.10:** Decomposition of the domain of integration of the two-dimensional phase integrals $\mathscr{B}_{nl}$, which is the large triangle, into fundamental domains $I$ (red, consisting of $N$ fundamental triangles) and $II$ (green, consisting of $N(N-1)/2$ fundamental squares). The pulse length here is $N = 5$.

The fundamental integral $C_n$, which is a purely real quantity, does still depend on the pulse length $N$ via the factors $(-1)^{N-1}$. However, it is relevant only whether $N$ is an even or odd an number, giving two different values of the integral in (4.74). Thus, when discussing the pulse length dependence or when taking the limit $N \to \infty$ one should stay within one of these two classes. This behaviour is related to the fact that for even values of $N$ one has an additional shift of $\pi$ to reach the fundamental interval $[-\pi, \pi]$.

The two-dimensional phase integrals $\mathscr{B}_{nl}$ are a bit more involved to analyse. The two-dimensional domain of integration in (4.25) is a triangle via the action of the Heaviside step functions. A decomposition into fundamental domains involves a distinction into a series of $N$ fundamental triangles (domain $I$) and $N(N-1)/2$ fundamental squares (domain $II$), thus, $\mathscr{B}_{nl} = \mathscr{B}_{nl}^I + \mathscr{B}_{nl}^{II}$, see Figure 4.10. Considering first the domain $I$ yields, using similar shifts of the integration variables as for the calculation of $\mathscr{C}_n$,

$$B_{nl}^I(s, \ell_1) = \frac{\sin \pi N z}{\sin \pi z} B_{nl}(s, \ell_1) \tag{4.76}$$

with the integral over the fundamental triangle

$$B_{nl}(s, \ell_1) = \int\limits_{-\pi}^{\pi} d\phi \int\limits_{-\pi}^{\phi} d\phi' \, F_n(\phi; x, \alpha_{P_1} - \alpha_{p'}, \beta_{P_1} - \beta_{p'}) F_l(\phi'; y, \alpha_p - \alpha_{P_1}, \beta_p - \beta_{P_1}) \tag{4.77}$$

which is a complex number. The integral over domain $II$ requires the evaluation of a double sum with the result

$$\mathscr{B}_{nl}^{II} = \frac{i}{2} \left\{ \frac{e^{i\pi x}}{\sin \pi x} \frac{\sin \pi N z}{\sin \pi z} - \frac{e^{i\pi N x}}{\sin \pi x} \frac{\sin \pi N y}{\sin \pi y} \right\} B_{nl}'(s, \ell_1), \tag{4.78}$$

$$B_{nl}'(s, \ell_1) = \int\limits_{-\pi}^{\pi} d\phi \, F_n(\phi; x, \alpha_{P_1} - \alpha_{p'}, \beta_{P_1} - \beta_{p'}) \int\limits_{-\pi}^{\pi} d\phi' \, F_l(\phi'; y, \alpha_p - \alpha_{P_1}, \beta_p - \beta_{P_1})$$

$$= 2\mathrm{Re}\, B_{nl}(s, \ell_1) \tag{4.79}$$

with $x = s - \ell_1 - \beta_{P_1} + \beta_{p'}$, $y = \ell_1 - \beta_p + \beta_{P_1}$ and $x + y = z$. The fundamental phase integrals are not independent as the value of $B'_{nl}$ equals twice the real part of $B_{nl}$. In total, the two-photon amplitude $\mathcal{M}$ is given by

$$\mathcal{M} = \frac{1}{2k \cdot P_1} \left( \frac{\sin \pi N z}{\sin \pi z} \sum_{n=1}^{2} \widetilde{\mathcal{V}}_n C_n(s) \right.$$

$$\left. -i \sum_{n,l=1}^{2} \widetilde{\mathcal{U}}_{nl} \left[ \frac{\sin \pi N z}{\sin \pi z} B_{nl} + i \left\{ \frac{e^{i\pi x}}{\sin \pi x} \frac{\sin \pi N z}{\sin \pi z} - \frac{e^{i\pi N x}}{\sin \pi x} \frac{\sin \pi N y}{\sin \pi y} \right\} \mathrm{Re}\, B_{nl} \right] \right)$$

$$+ \; (1 \leftrightarrow 2) \,.$$

The final result for the on- and off-shell parts of the two-photon amplitude reads

$$\mathcal{M}_{\mathrm{off}} = \frac{\mathcal{Z}_1}{2k \cdot P_1} \left( \sum_{n=1}^{2} \widetilde{\mathcal{V}}_n C_n(s) + \sum_{n,l=1}^{2} \widetilde{\mathcal{U}}_{nl} \, \mathrm{Im}\, B_{nl}(s, \ell_1) \right)$$

$$+ \frac{\mathcal{Z}_3}{2k \cdot P_1} \sum_{n,l=1}^{2} \widetilde{\mathcal{U}}_{nl} \, \mathrm{Re}\, B_{nl}(s, \ell_1) \; + \; (1 \leftrightarrow 2) \,, \tag{4.80}$$

$$\mathcal{M}_{\mathrm{on}} = - \frac{\mathcal{Z}_2}{2k \cdot P_1} \sum_{n,l=1}^{2} \widetilde{\mathcal{U}}_{nl} \, \mathrm{Re}\, B_{nl}(s, \ell_1) \; + \; (1 \leftrightarrow 2) \tag{4.81}$$

with the same decomposition into off-shell and on-shell parts as employed in (4.51) and (4.52). These expression for $\mathcal{M}_{\mathrm{on,off}}$ are employed in (4.53) to calculate the on- and off-shell emission probabilities in a box-shaped pulse envelope. All the dependence on the pulse length has been extracted from the phase integrals and is now located in the prefactors which resemble diffraction patterns, which are given by

$$\mathcal{Z}_1 = \frac{\sin \pi N z}{\sin \pi z} \,, \tag{4.82}$$

$$\mathcal{Z}_2 = \frac{\sin \pi N x}{\sin \pi x} \frac{\sin \pi N y}{\sin \pi y} \,, \tag{4.83}$$

$$\mathcal{Z}_3 = \frac{\sin \pi N z}{\sin \pi z} \frac{\cos \pi x}{\sin \pi x} - \frac{\sin \pi N y}{\sin \pi y} \frac{\cos \pi N x}{\sin \pi x} \,. \tag{4.84}$$

The numerical results for the emission probability in the box-shaped pulse are exhibited in Figure 4.11, calculated in the rest frame of the incoming electron, with initial Lorentz factor $\gamma = 10^4$ (i.e. the rapidity is $\zeta = 9.9$) as before and $a_0 = 1$. The scattering angles are taken as the non-symmetric values $\theta_1 = 0.1$, $\theta_2 = 0.5$, $\varphi_1 = \pi$ and $\varphi_2 = 0.1\pi$. The emission spectra are exhibited in Figure 4.11 as a function of the scaled energies $\omega_1/\omega_\star$ and $\omega_2/\omega_\star$, where $\omega_\star = \omega e^\zeta$ is the laser frequency boosted to the rest frame of the electron. For the case of a short pulse, consisting of $N = 2$ oscillations of the carrier wave in Figure 4.11 (a), the emission probability as a function of $\omega_1$ and $\omega_2$ shows no specific structures related to the diffraction patterns $\mathcal{Z}_i$, $i \in \{1, 2, 3\}$. The emission is distributed over the exhibited part of the phase space with certain structures that roughly resemble the ones in Figure 4.6. Upon increasing the pulse length to $N = 10$ (b), the picture drastically changes. The diffraction patterns condense to narrow peaks, which are located at the positions of the Oleinik resonance frequencies $\omega_{1,2}^{\mathrm{res}}$. This behaviour becomes even stronger if the pulse length is further increased to $N = 20$ (c). Furthermore, some of the diagonal lines in Figure 4.11 (b) and (c) can be related to the IPW harmonics $\omega_2(\omega_1, n')$.
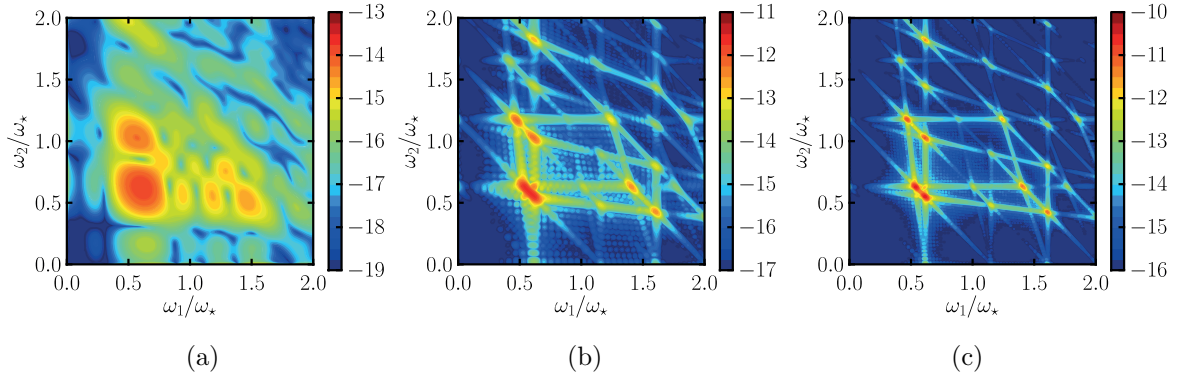
**Figure 4.11:** Two-photon emission probability in a box-shaped laser pulse with as a function of the scaled frequencies $\omega_{1,2}/\omega_\star$, where $\omega_\star$ denotes the laser frequency in the rest frame of the initial electron, for $N = 2$ (a), 10 (b) and 20 (c) oscillations of the carrier wave, respectively. For parameters see the text.

As mentioned above, the functions $\mathcal{Z}_i$, $i \in \{1, 2, 3\}$ are diffraction patterns, which are periodic when considered as functions of the independent variables $x$ and $y$ with the period one. These diffraction patterns condense to delta combs in the limit $N \to \infty$. In particular, from $\mathcal{Z}_1$, one obtains the condition $z = s - \beta_p + \beta_{p'} = n'$, where $n' \in \mathbb{N}$. With the definition of $s$ from (4.16), one precisely gets the IPW energy correlation $\omega_2(\omega_1, n')$, Eq. (4.66), when solving for $\omega_2$. This shows the transition from a pulsed laser field to an infinite laser field in the case of a box-shaped pulse. From the diffraction pattern $\mathcal{Z}_2$ and from the corresponding expression for the second Feynman diagram, one obtains in the limit $N \to \infty$ the Oleinik resonance frequencies $\omega_{1,2}^{\mathrm{res}}$, Eq. (4.65), due to $\ell_{1,2} - \beta_p + \beta_{P_{1,2}} = n$ with $n \in \mathbb{N}$. The diffraction pattern $\mathcal{Z}_3$ does not provide such an easy interpretation. It can be shown that $\mathcal{Z}_3$ vanishes at the Oleinik resonances, but strongly peaks in the vicinity of these resonances.

The complete dependence of the emission probability on the pulse length is contained in the diffraction patterns $\mathcal{Z}_i$ (except for the aforementioned distinction of even and odd values of $N$). Thus, to study the pulse length dependence of the different contributions to the two-photon emission probability, is is sufficient to consider the pulse length dependence of these diffraction patterns. It convenient to employ the periodicity of the diffraction pattern expressions $\mathcal{Z}_i$ and to calculate the integrals over the fundamental range of periodicity thereof, defining

$$I_{ij}(N) = \int\limits_0^1 dx \int\limits_0^1 dy\, \mathcal{Z}_i(x, y)\mathcal{Z}_j(x, y)\,, \tag{4.85}$$

as a measure for the pulse length dependence of the various contributions. As a result one finds the values

$$I_{11} = N\,, \tag{4.86}$$
$$I_{22} = N^2\,, \tag{4.87}$$
$$I_{33} = N(N - 1)\,, \tag{4.88}$$
$$I_{13} = 0\,. \tag{4.89}$$

The last value of $I_{13} = 0$ is particularly interesting, since it states that there is no interference between the two terms $\propto \mathcal{Z}_1$ and $\propto \mathcal{Z}_3$ when squaring the amplitude $\mathcal{M}_{\mathrm{off}}$. As expected

[Hu11], the value of $I_{11}$, which is related to the off-shell amplitude is proportional to the pulse length $N$. That means, in the limit $N \to \infty$, the two-photon emission *rate* $\dot{W} \propto W/N$, i.e. the emission probability divided by the interaction time $N$, stays finite. Furthermore, the value for the on-shell part $I_{22} = N^2$ signals the appearance of Oleinik singularities in the IPW limit, since the emission rate $\dot{W}$ is proportional to $N$ and therefore diverges in the limit $N \to \infty$. The result for $I_{33}$, which is part of the off-shell amplitude is not as easy to interpret, since it scales as $\propto N^2$, although it has been identified as part of the off-shell process. Thus, in pulsed laser fields, there is a resonant enhancement of the off-shell process. A more detailed study of the behaviour of this contribution in the limit $N \to \infty$ is required, going beyond this simple approximation. It turns out that the distinction between the two-step cascade and the true one-step two-photon emission is not as straightforward. Such ambiguities were also approached in calculations of the two-photon decay of excited atomic states [Lab09].

## 4.9   Summary of Chapter 4

In this chapter, the complete evaluation of the differential probability of two-photon emission by an electron in a short intense laser pulse was presented. The on-shell part of the matrix element factorizes into subsequent one-photon Compton processes and gives naturally a finite contribution to the differential probability due to the temporal pulse structure. It was shown how the Oleinik resonance singularities, which are associated with the infinite series of poles of the Dirac-Volkov propagator in the case of IPW laser fields, emerge from the general expression for the two-photon $S$ matrix upon taking the limit $g \to 1$. The weak-field limit of the $S$ matrix was calculated and it was shown that it coincides with the textbook results for the double Compton scattering.

The result allows for the first time for an unambiguous comparison of the probability of the two-photon process in relation to the one-photon process for realistic pulsed laser fields by calculating the inclusive two-photon probability. It was found that the inclusive two-photon probability exceeds the one-photon probability for the low-frequency part of the spectrum $< 200$ MeV. Above this frequency, the two-photon probability is found to be two orders of magnitude below the one-photon probability. The two-photon to one-photon ratio $\mathcal{R}$ was discussed as a function of $a_0$ and it was found that for $a_0 \ll 1$ the perturbative value of $\mathcal{R} = 10^{-4}$ is obtained. For larger values of $a_0 \sim 1$ the ratio increases and reaches values of $\mathcal{R} > 10^{-2}$, which means that at higher laser intensity the two-photon process becomes more relevant.

The experimental detection scheme for two-photon Compton scattering described above in Section 4.7 is complementary to the one used for the observation of the perturbative weak-field double Compton scattering in [Bra56, Sek88, San00] in the following sense: In the mentioned experiments the scattering of single incoherent photons on a solid-density target was observed via coincidence measurements. To achieve the non-linear interaction regime, $a_0 \sim 1$ one necessarily has a high density of laser photons. Therefore, the density of the scatterers (in this case the electrons) should be reduced and tuned to an appropriate level to allow for coincidence measurements.

The presented approach furthermore opens the avenue towards a detailed study of the two-photon polarization which is considered as a signature of the Unruh radiation in [Che99, Sch08]. Further studies are necessary to evaluate the relevance of the off-shell contributions in view of the quantum radiation reaction. The factorization of the on-shell part of the $S$ matrix and the resonant enhancement of the off-shell part need to be confronted with a complete incoherent model for two-photon emission [DP10] to estimate the relevance of the coherent part of the process.

# 5 Chapter 5
# Summary & Outlook

THE purpose of this thesis is to advance the understanding of strong-field QED processes in pulsed laser fields, with the focus on the one-photon and two-photon Compton scattering processes, i.e. photon emission processes in collisions of relativistic electrons with high-intensity ultra-short laser pulses. A realistic description of the finite pulse length in such experiments is made necessary by the present and upcoming generation of high-intensity lasers. In majority, these lasers achieve the high output-power via ultra-short pulse lengths on the order of femtoseconds.

Chapter 2 serves as introduction to the theory of strong-field QED. The study of coherent and semi-coherent photon states provided an equivalence between the semi-coherent states and the description of the laser field as classical background field, which allows to work in the Furry picture where the one-particle states are Volkov states, i.e. solutions of the Dirac equation in the presence of the plane wave background field. These Volkov states and also the Dirac-Volkov propagator are constructed with the help of Volkov matrix functions whose completeness and orthogonality are essential for employing Volkov solutions as basis for the Furry picture. Employing the analytic light-front structure of these matrices, which is partly derived in Appendix B, a new and very simple proof of these properties is given in Appendix B.3. The properties of Volkov states in pulsed laser fields are discussed, comparing with the case of infinite plane wave fields. The modification of the Zel'dovich levels, which appear in the latter case are highlighted. The sum over discrete values of momentum in the case of infinite plane waves turns into an integral over continuous values of momentum exchanged between the electron and the laser field. These differences lead to a modified pole structure of the laser dressed Dirac-Volkov propagator in pulsed laser fields. The infinite series of poles in the case of infinite plane waves does not appear for pulsed laser fields, where finite resonances occur instead. The light-front structure of strong-field QED in laser fields becomes apparent via the pole integration of the propagator, singling out a light-like coordinate and the resultant light-front time ordering. A correspondence between the classical orbits of charged particles in a pulsed laser field and the Volkov states in the same laser field is emphasized. Local minima and maxima of the energy along the classical trajectory leave imprints in the momentum space occupation numbers of the Volkov states at that particular energies.

In Chapter 3, the one-photon Compton emission process is described in detail in strong pulsed laser fields utilizing the framework of strong-field QED, where the Volkov wave functions are employed as initial and final states for the electrons.

The expression for the $S$ matrix in a strong pulsed laser field with finite temporal envelope involves integrals over the laser phase with complex non-linear exponentials as integrands. These functions determine the emission probabilities, i.e. the one-photon spectra and need to be evaluated, which has to be done numerically in general. However, for the special hyperbolic secant pulse envelope, a completely analytical expression for the non-linear Compton amplitude has been calculated in terms of generalized Laguerre functions.

Two different regimes of non-linear one-photon Compton scattering have been identified: (*i*) the ponderomotive regime, where the appearance of the spectrum is determined by the ponderomotive part of the non-linear phase exponents (i.e. the slowly varying part related to the ponderomotive potential) and (*ii*) the bandwidth dominated regime, were the form of the spectrum is dominated by the large bandwidth of the laser pulse.

In the ponderomotive regime, that is for pulse lengths $T \geq 10 \ldots 20$ fs, the frequency spectra acquire an interesting sub-peak structure in strong laser pulses, with the dimensionless laser strength $a_0 > 1$. The number of these sub-peaks is determined by the ponderomotive part of the non-linear exponential, which is proportional to $a_0^2 T$; it is an interplay between the laser bandwidth and the variation of the laser intensity that leads to the emergence of the sub-peaks.

The azimuthal distributions of radiation have been studied for ultra-short single-cycle laser pulses, for $T \sim 2 \ldots 5$ fs. In this regime, the emission spectra strongly depend on the value of the carrier envelope phase for $a_0 > 1$. In the case of linear laser polarization, the emission is either unidirectional or dipole-like in the direction of the laser polarization, depending on the value of the carrier envelope phase. For circular polarization, the symmetry in the azimuthal angle known from IPW is completely lost for $a_0 > 1$. The azimuthal symmetry is replaced by a new symmetry in a composite variable: the difference between the azimuthal angle and the carrier envelope phase.

The low-energy limit of non-linear Thomson scattering was studied in comparison to non-linear Compton scattering. In Compton scattering, a cut-off frequency exists due to the electron recoil. As a result, a scaling law was found which takes into account the different phase spaces of Thomson and Compton scattering. The scaling law allows to mimic the effect of the electron recoil in classical calculations.

For ultra-strong laser pulses, $a_0 \gg 1$, an approximative calculation scheme for the emission probability was presented. The photon yield in a pulsed field was found to be larger than in comparable infinite plane wave and constant crossed field models.

In Chapter 4, the two-photon Compton emission process in strong pulsed laser fields is discussed. The complete evaluation of the differential probability of two-photon emission by an electron in a short intense laser pulse was presented. In contrast to one-photon Compton scattering, this is a second-order strong field process which involves the intermediate propagation of an electron via the Dirac-Volkov propagator. This fact makes the analysis far more complicated. An integration over the propagator pole produces light-front time ordered contributions as well as instantaneous parts related to the light-front zero-mode propagator. Furthermore, the propagator momentum can be on its mass shell due to the presence of the background field, leading to a distinction of on-shell and off-shell parts related to real and virtual intermediate particles, respectively. The on-shell part of the matrix element factorizes into subsequent one-photon Compton processes and gives naturally a finite contribution to the differential probability due to the temporal pulse structure in contrast to infinite plane waves, where the on-shell part diverges due to Oleinik resonance singularities.

A numerical analysis of the differential two-photon emission probability showed striking differences between the case of a pulsed and and infinite laser field. As one can infer from the different behaviour of the propagator in these two cases, the emission probability has a resonance-like structure but no divergences. For the used parameters, the effect of

ponderomotive broadening and the emergence of sub-peaks was observed also for two-photon Compton scattering. The weak-field limit of the $S$ matrix was calculated and it was shown that it coincides with the textbook results for the double Compton scattering.

When comparing the inclusive two-photon probability to the one-photon Compton probability, a two-photon to one-photon ratio $\mathcal{R} = 10^{-2}$ was obtained for a moderately strong laser amplitude of $a_0 = 1$. This value of $\mathcal{R}$ is two orders of magnitude larger than the perturbative estimate due to [Man52]. The calculation of the inclusive two-photon probability involves the integration over the phase space of one of the two photons. In soft-photon region, i.e. when a low-energy photon, $\omega_1 \to 0$, is emitted, the two-photon emission probability is infrared divergent. The cancellation of this infrared singularity with contributions of virtual photons from the radiative corrections of one-photon Compton scattering is discussed (the details are presented in Appendix E). In the soft-photon limit the dressed vertex becomes the free vertex, such that the cancellation of the infrared divergent parts in strong-field QED proceeds as for perturbative QED.

Important issues concerning the experimental observability of the strong-field finite-size effects are discussed in Appendix F. There, the subject of realistic experimental conditions including finite electron distributions and the spatial focusing of the laser pulses are considered. There are promising results that some of the effects may be observable when loosely focusing the light of a (sub-)petawatt laser to achieve non-linear intensity with $a_0 \sim 1$ homogeneously (with low gradients) in a large spatial volume and probing the centre of that region with a high-quality electron source such as ELBE or REGAE.

## Outlook

An important problem to be tackled in future work would be to go beyond the plane-wave approximation in a quantum description of these strong-field processes, that is to find solutions of the Dirac equation in more general field configurations, in particular for focused laser pulses. This would be desirable in view of a more realistic description of experimental conditions of strong-field QED scattering processes that do not posses a classical limit. Such processes would include the cross channels of one-photon Compton scattering, but also the spin-dependence of one-photon Compton scattering as well as all second-order and higher-order strong-field QED processes.

For the process of two-photon Compton scattering, a study of the polarization properties of the two emitted photons, in particular with respect to their entanglement, would be interesting and could provide further experimental detection schemes of the two-photon process. Similar studies have been done for infinite plane wave fields or for weak laser fields [Sch08, Löt09b]. The polarization of the emitted photons could be measured using Compton polarimetry [Thi09] verifying their degree of entanglement. The claimed connection between two-photon Compton emission and Unruh radiation in [Che99] needs further investigations.

Azimuthal photon distributions and further frequency spectra could be calculated, extending the investigations of the two-photon emission probability to larger values of $a_0$. A refinement of the numerical integration methods are necessary to extend the study of the inclusive two-photon Compton probability to the regime $a_0 \gg 1$. Alternatively, an application of the approximative calculation method presented for one-photon Compton scattering could be fruitful. With this, an answer could be given to the question of the importance of two-photon emission in the limit $a_0 \gg 1$. A first study addressing differential spectra in this "full quantum regime" with $a_0 \gg 1$ and $\chi_p \sim 1$ was recently published [Mac12].

Concerning the relations between quantum multi-photon emission and the classical theory of radiation damping, further study is necessary to fully understand the importance of the
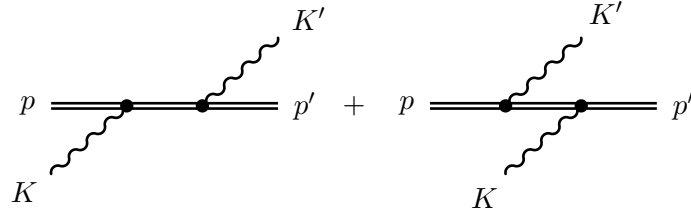
**Figure 5.1:** Feynman diagrams for laser assisted Compton scattering: An X-ray photon with momentum $K$ scatters off an electron (plasma) which is irradiated by a strong laser pulse. This process could be measured in a combination of a petawatt laser with the European XFEL at DESY.

coherent and incoherent parts of the amplitudes. The generalization of the two-photon emission process to general $N$-photon emission should be achievable with the methods presented in this thesis (recently, the three-photon Compton process was calculated in the perturbative weak-field regime in usual QED [Löt12]). However, the final particle phase spaces of these $N$-photon channels are high-dimensional. This means that a full numerical analysis of the $N$-photon phase space will be demanding.

Various other second-order strong-field processes in pulsed laser fields could be calculated with the methods presented in this thesis, such as laser assisted Compton scattering, laser assisted Bremsstrahlung, laser assisted Bethe-Heitler pair creation, etc. due to the similar structures of the strong-field matrix elements and the emerging integrals over the laser phase. The pole structure is similar in all of these processes with the possible difference being the contribution of propagating antiparticles, i.e. the opposite time ordering. Also for second-order strong field processes involving a photon propagator, such as the trident pair production or laser assisted electron-electron scattering, the structure of the $S$ matrix is not very different.

In a recent article by [Cro12], the experimental detection of non-inertial effects in quantum field theory was proposed in a combination of high-power lasers and radiation from an X-ray free electron laser. The experimental setting consists of a pre-formed electron plasma, which is irradiated by a strong laser pulse with an intensity of $10^{19}$ W/cm$^2$ in order to accelerate the plasma electrons. High-energy X-ray photons from an XFEL are to be scattered off the plasma electrons; the acceleration could be measured via an effective temperature of the plasma, modifying the backscattered spectra (a higher temperature means a broader spectrum). In the language of strong-field QED, this scattering process would correspond to laser assisted Compton scattering (also denoted as resonant Compton scattering in [Ole68]). It could be described well as a second-order strong-field QED process, namely as a cross channel of two-photon Compton emission as depicted in Figure 5.1, where an X-ray photon with momentum $K$ scatters off a laser dressed Volkov electron into a final state with momentum $K'$. The presence of the strong laser field would modify the dynamics of the charged particles and one would expect a number of subsidiary lines due to the absorption and emission of laser photons beneath the main Compton line. The frequency of the optical laser is much smaller than the frequency of the X-ray photon such that the different lines are very close together on the scale of keV, resembling a broadening of the main Compton peak. These investigations could be performed with the methods provided in this thesis for two-photon Compton scattering by relying on crossing invariance.

# A

# Notations, conventions and important relations

T HIS appendix serves as a collection of important relations used throughout this thesis concerning the employed units in Section A.1, light-front coordinates in Section A.2, important integrals in Section A.4 and the Dirac algebra in Section A.5. A detailed discussion of the laser vector potential $A_\mu(\phi)$ is given in Section A.3. The formulation of quantum field theory in the Furry picture is presented in Section A.6. The reduction of $S$ matrix elements using the perturbative expansion of the operator $\hat{S}[A]$ in the background field is outlined in Section A.7.

## A.1 Units, notations & conventions

Throughout this thesis, natural units are employed with

$$\hbar = c = 1 \,. \tag{A.1}$$

All physical units are measured in powers of electron volt (eV). The transition to lengths, times and other physical units is achieved with the conversion factors

$$
\begin{aligned}
1 \text{ µm} &= 5.0677309 \text{ eV}^{-1} \,, \\
1 \text{ fs} &= 1.5192675 \text{ eV}^{-1} \,, \\
1 \text{ J} &= 6.24150934326 \times 10^{18} \text{ eV} \,, \\
1 \text{ mb} &= 2.568189687 \times 10^{-18} \text{ eV}^{-2} \,, \\
1 \text{ W/cm}^2 &= 1.599662 \times 10^{-6} \text{ eV}^4 \,, \\
1 \text{ J/cm}^3 &= 4.795667 \times 10^{4} \text{ eV}^4 \,, \\
1 \text{ V/m} &= 6.516266 \times 10^{-7} \text{ eV}^2 \,, \\
1 \text{ T} &= 1.953527 \times 10^{2} \text{ eV}^2 \,,
\end{aligned}
\tag{A.2}
$$

which employ the CODATA recommended values for fundamental physical constants [Moh12]

$$
\begin{aligned}
\alpha^{-1} &= 137.035\,999\,074(44) \,, \\
m &= 0.510\,998\,928(11) \text{ MeV} \,, \\
\hbar c &= 197.326\,9718(44) \text{ MeV fm} \,, \\
c &= 299792458 \text{ m/s} = 0.299792458 \text{ µm/fs} \,, \\
\varepsilon_0 &= 8.854187817 \times 10^{-12} \text{ As/Vm} \,.
\end{aligned}
\tag{A.3}
$$

The contravariant components of Minkowski four-vectors are denoted by upper Greek indices

$$(x^\mu) = (x^0, x^1, x^2, x^3),$$

(A.4)

and the Minkowski metric $g_{\mu\nu}$ (in Cartesian coordinates) is

$$(g_{\mu\nu}) = \text{diag}\,(1, -1, -1, -1).$$

(A.5)

Covariant components of Minkowski four-vectors read

$$x_\mu = g_{\mu\nu} x^\nu,$$

(A.6)

where Einstein's summation convention is applied for indices that appear twice on the same side of an equation. Scalar products between four-vectors are written as

$$k \cdot x = g_{\mu\nu} k^\mu x^\nu = k_\mu x^\mu.$$

(A.7)

Scalar products of four-vectors with Dirac matrices (see AppendixA.5) are denoted using Feynman's slash

$$\slashed{k} \equiv \gamma^\mu k_\mu.$$

(A.8)

The spatial components of four-vectors are denoted by Latin indices $x_i$ and the vector is set in bold face $(\boldsymbol{x}_i) = (x_1, x_2, x_3)$. For scalar products between three-vectors the notation $\boldsymbol{x} \cdot \boldsymbol{k}$ is used. The electron charge $e$ is related to the fine structure constant via

$$\alpha = \frac{e^2}{4\pi}.$$

(A.9)

## A.2   Light-front coordinates

The light-front components of a four-vector with Cartesian coordinates $(x^\mu) = (x^0, x^1, x^2, x^3)$ are defined as

$$x^- = x^0 - x^3, \qquad x^+ = x^0 + x^3, \qquad \boldsymbol{x}^\perp = (x^1, x^2).$$

(A.10)

The inverse coordinate transformation is given by $x^0 = \frac{1}{2}(x^+ + x^-)$ and $x^3 = \frac{1}{2}(x^+ - x^-)$. Because the laser four-momentum $k$ is light-like, $k^2 = 0$, it can always be chosen to have only a single non-vanishing component in light-cone coordinates, which is $k^- = 2\omega$ through this thesis. This means that the coordinate system is aligned such that the laser pulse propagates along the negative $z$ axis. Thus, the vector $n^\mu = k^\mu/\omega$ defines the light-front via $n \cdot x = x^+ = const$. The metric tensor in light-front coordinates, using the arrangement of components $(x^\mu) = (x^+, x^-, \boldsymbol{x}^\perp)$, has non-diagonal components

$$(g_{\mu\nu}) = \begin{pmatrix} 0 & \frac{1}{2} & 0 & 0 \\ \frac{1}{2} & 0 & 0 & 0 \\ 0 & 0 & -1 & 0 \\ 0 & 0 & 0 & -1 \end{pmatrix}, \qquad (g^{\mu\nu}) = \begin{pmatrix} 0 & 2 & 0 & 0 \\ 2 & 0 & 0 & 0 \\ 0 & 0 & -1 & 0 \\ 0 & 0 & 0 & -1 \end{pmatrix}.$$

(A.11)

The covariant components of a four-vector are related to the contravariant components as

$$x_- = \frac{1}{2}x^+, \qquad x_+ = \frac{1}{2}x^-, \qquad \boldsymbol{x}_\perp = -\boldsymbol{x}^\perp,$$

and scalar products become

$$x \cdot y = x^+ y_+ + x^- y_- + \boldsymbol{x}^\perp \cdot \boldsymbol{y}_\perp = \frac{1}{2} x^+ y^- + \frac{1}{2} x^- y^+ - \boldsymbol{x}_\perp \cdot \boldsymbol{y}_\perp \,. \tag{A.12}$$

The determinant of the metric reads $\sqrt{-g} = \sqrt{-\det g_{\mu\nu}} = 1/2$, thus the Lorentz invariant integration measure is

$$\sqrt{-g}\, d^4 x = \frac{1}{2}\, dx^+ dx^- d^2 \boldsymbol{x}_\perp \,. \tag{A.13}$$

For a four-dimensional delta distribution one writes in light-front form

$$\delta^4(p) = \frac{1}{\sqrt{-g}} \delta(p^+)\delta(p^-)\delta(p^1)\delta(p^2) = 2\,\delta^3(\mathsf{p})\delta(p^-)\,. \tag{A.14}$$

The transverse light-like three vector (with respect to the laser four-vector) is declared as $\mathsf{p} \equiv (p^+, \boldsymbol{p}^\perp)$ and formatted using a sans-serif font. The corresponding integration measure is given as $d^3\mathsf{p} \equiv dp^+ dp^1 dp^2$. The free particle dispersion relation $(p^0)^2 = \boldsymbol{p}^2 + m^2$ for massive particles reads in light-front coordinates

$$p^- = \frac{\boldsymbol{p}_\perp^2 + m^2}{p^+}\,. \tag{A.15}$$

The Lorentz invariant on-shell phase space element is

$$\int \frac{d^4 p}{(2\pi)^4}(2\pi)\delta(p^2 - m^2) = \frac{d^3 \boldsymbol{p}}{(2\pi)^3 2p^0}\,, \qquad p^0 = \sqrt{\boldsymbol{p}^2 + m^2} \qquad \text{(Cartesian)}\,, \tag{A.16}$$

$$= \frac{d^3 \mathsf{p}}{(2\pi)^3 2p^+}\,, \qquad p^+ = \frac{\boldsymbol{p}_\perp^2 + m^2}{p^-} \qquad \text{(light-front)}\,. \tag{A.17}$$

Thus,

$$1 = \int \frac{d^3 \boldsymbol{p}}{(2\pi)^3 2p^0}(2\pi)^3 2p^0 \delta^3(\boldsymbol{p} - \boldsymbol{p}') = \int \frac{d^3 \mathsf{p}}{(2\pi)^3 2p^+}(2\pi)^3 2p^+ \delta^3(\mathsf{p} - \mathsf{p}') \tag{A.18}$$

with the Lorentz invariant on-shell delta distributions

$$(2\pi)^3 2p^0 \delta^3(\boldsymbol{p} - \boldsymbol{p}') = (2\pi)^3 2p^+ \delta^3(\mathsf{p} - \mathsf{p}')\,. \tag{A.19}$$

To verify this equation it is sufficient to show that

$$\begin{aligned}
\delta(p^+ - p'^+) &= \delta(p^3 - p'^3 + p^0 - p'^0) \\
&= \delta\left(p^3 - p'^3 + \sqrt{(p^3)^2 + \boldsymbol{p}_\perp^2 + m^2} - \sqrt{(p'^3)^2 + \boldsymbol{p}_\perp'^2 + m^2}\right) = \delta\left(f(p^3)\right) \\
&= \left|\frac{df}{dp^3}\right|^{-1}_{p'^3 = p^3} \delta(p^3 - p'^3) \\
&= \frac{p^0}{p^+}\delta(p^3 - p'^3)\,,
\end{aligned} \tag{A.20}$$

since $\delta^2(\boldsymbol{p}_\perp - \boldsymbol{p}'_\perp)$ is identical in light-front coordinates and in Cartesian coordinates and

$$\frac{df}{dp^3} = 1 + \frac{p^3}{\sqrt{(p^3)^2 + \boldsymbol{p}_\perp^2 + m^2}} = 1 + \frac{p^3}{p^0} = \frac{p^+}{p^0}\,. \tag{A.21}$$

## A.3    Description of the laser field

It has been stated [Mil06a] that the electric field produced by a laser has to fulfil the constraint

$$\int\limits_{-\infty}^{\infty} \boldsymbol{E}(t, \boldsymbol{x})dt = 0\,. \tag{A.22}$$

These fields are denoted as *nonunipolar* fields. Electric fields, where the value of the integral (A.22) is non-zero, represent fields with a non-vanishing dc component and are called *unipolar*; they can be produced from nonunipolar laser fields in non-linear optical media [Koz11]. The implications of such fields on the Volkov states and non-linear Compton scattering has been studied recently [Din12]. As a consequence of (A.22), the vector potential describing a laser pulse must fulfil [Kra12]

$$\lim_{t \to -\infty} \boldsymbol{A}(t, \boldsymbol{x}) = \lim_{t \to \infty} \boldsymbol{A}(t, \boldsymbol{x})\,, \tag{A.23}$$

since $\boldsymbol{E} = -\partial_t \boldsymbol{A}$ in a gauge where the scalar potential $\Phi$ vanishes, as used in this thesis. Equation (A.23) means that at any spatial point $\boldsymbol{x}$ the value of the vector potential has to be the same before the pulse arrived and after the pulse has passed. In this thesis, the laser vector potential is modelled by the plane wave

$$A^\mu(\phi) = A_0\, g(\phi) \operatorname{Re} \left[\epsilon_+^\mu \exp\left\{-i(\phi + \hat{\phi})\right\}\right] \tag{A.24}$$

with the phase $\phi = k \cdot x$, where $k$ is the wave four-vector with $k \cdot k = 0$, i.e. it is a light-like four-vector. The time-component of $k$ is the frequency $\omega = k^0$ of the carrier wave. The frequency spectrum of the pulse is of course given by the Fourier transform of the pulse envelope $g(\phi)$. In (A.24), $\hat{\phi}$ denotes the carrier envelope phase and $\epsilon_+^\mu$ is a transverse complex polarization vector defined below. The vector potential defined in (A.24) is a vacuum solution of the wave equation $\Box A^\mu(x) = 0$ and obeys the Lorenz gauge condition $\partial \cdot A(x) = 0$, which can also be stated as $k \cdot A = 0$, i.e. the vector potential is transverse to the propagation direction. In addition to the Lorenz gauge condition, the scalar potential $\Phi$ can always be chosen to be vanishing for plane-wave fields. The dimensionless laser strength parameter $a_0$ is defined as $a_0 \equiv eA_0/m$.

### Laser polarization

The four-vector $\epsilon_+^\mu$ is a complex polarization vector of the laser field which is defined by

$$\epsilon_\pm^\mu = \cos\xi \epsilon_1^\mu \pm i \sin\xi \epsilon_2^\mu \tag{A.25}$$

with $\epsilon_1^\mu = (0, 1, 0, 0)$ and $\epsilon_2^\mu = (0, 0, 1, 0)$ and the scalar products $\epsilon_i \cdot \epsilon_j = -\delta_{ij}$ for $i, j \in \{1, 2\}$, which is orthogonal to the propagation direction $k \cdot \epsilon_i = 0$, i.e. the laser field is a purely transverse electromagnetic plane-wave field of arbitrary spectral composition and polarization. With this definition, the real part of the vector potential can be given explicitly as

$$A^\mu = A_0 g(\phi) \left\{\epsilon_1^\mu \cos\xi \cos(\phi + \hat{\phi}) + \epsilon_2^\mu \sin\xi \sin(\phi + \hat{\phi})\right\}\,. \tag{A.26}$$

The scalar products between the complex polarization vectors read $\epsilon_+ \cdot \epsilon_- = -1$ and $\epsilon_+ \cdot \epsilon_+ = \epsilon_- \cdot \epsilon_- = -\cos 2\xi$. In (A.25), the parameter $\xi \in [-\pi/2, 3\pi/4)$ determines the polarization state of the laser. For $\xi = 0$ ($\xi = \pi/2$) the laser is linearly polarized in the $x$ ($y$) direction. For $\xi = \pm \pi/4$, the four-vector $\epsilon_+$ describes a circularly polarized wave with positive (negative) helicity for the upper (lower) sign [Jac83]. For other values of $\xi$, the laser is elliptically polarized

[Pan02b]. The ellipse's major and minor axes are the the $x$ and $y$ axes for $\xi \in (-\pi/4, \pi/4)$ and vice versa for $\xi \in (\pi/4, 3\pi/4)$. The scalar products between the different polarization vectors can be summarized as $\epsilon_i \cdot \epsilon_j = -C_{ij}$ with the symmetric matrix

$$
C_{ij} = \begin{pmatrix} 1 & 0 & \cos\xi & \cos\xi \\ 0 & 1 & i\sin\xi & -i\sin\xi \\ \cos\xi & i\sin\xi & \cos2\xi & 1 \\ \cos\xi & -i\sin\xi & 1 & \cos2\xi \end{pmatrix} \begin{matrix} 1 \\ 2 \\ + \\ - \end{matrix} \,,
$$

$$
\begin{matrix} \phantom{C_{ij}} & 1 & 2 & + & - \end{matrix}
$$

(A.27)

The Stokes parameters $s_\mu$ [Jac83] as a common measure for the polarization properties of a plane wave read for the vector potential (A.24) in the linear basis, defined using the complex vector potential $\mathfrak{A}^\mu = A_0 g(\phi) \epsilon_+^\mu e^{-i(\phi+\hat\phi)}$ with $A^\mu = \text{Re}\,\mathfrak{A}^\mu$

$$
s_0 = |\epsilon_1 \cdot \mathfrak{A}|^2 + |\epsilon_2 \cdot \mathfrak{A}|^2 = \frac{1}{2} A_0^2 g^2(\phi)\,,
$$

(A.28)

$$
s_1 = |\epsilon_1 \cdot \mathfrak{A}|^2 - |\epsilon_2 \cdot \mathfrak{A}|^2 = s_0 \cos 2\xi\,,
$$

(A.29)

$$
s_2 = 2\text{Re}\left[(\epsilon_1 \cdot \mathfrak{A})^*(\epsilon_2 \cdot \mathfrak{A})\right] = 0\,,
$$

(A.30)

$$
s_3 = 2\text{Im}\left[(\epsilon_1 \cdot \mathfrak{A})^*(\epsilon_2 \cdot \mathfrak{A})\right] = s_0 \sin 2\xi\,.
$$

(A.31)

The vector potential (A.25) is normalized in such a way that for $\Delta\phi \gg 1$ the mean energy density or the energy flux $\langle \boldsymbol{E}^2 \rangle \propto -A_\mu A^\mu = g^2(\phi) A_0^2/2$, where $\langle \ldots \rangle$ means averaging over the fast oscillations of the carrier wave, is independent of the polarization $\xi$.

### Laser pulse envelope

For the pulse envelope $g(\phi)$ one assumes that $g(0) = 1$, the symmetry $g(\phi) = g(-\phi)$ and the limit $\lim_{\phi\to\infty} g(\phi) = 0$. The length of the pulse envelope is characterized by the dimensionless pulse length parameter $\Delta\phi$. It determines also the spectral bandwidth of the laser pulse in Fourier space as being $\propto 1/\Delta\phi$. Some explicit examples for various pulse envelopes which are used through this thesis include the hyperbolic secant pulse

$$
g(\phi) = \frac{1}{\cosh\left(\dfrac{\phi}{\Delta\phi}\right)}\,,
$$

(A.32)

the Gaussian pulse

$$
g(\phi) = \exp\left\{-\frac{\phi^2}{2\Delta\phi^2}\right\}\,,
$$

(A.33)

the box-shaped pulse

$$
g(\phi) = \sqcap(\phi) = \Theta(\Delta\phi - \phi)\Theta(\Delta\phi + \phi)
$$

(A.34)

with the Heaviside step function $\Theta(x)$, and a squared cosine pulse

$$
g(\phi) = \cos^2\left(\frac{\pi\phi}{2\Delta\phi}\right)\sqcap(\phi)\,.
$$

(A.35)

A collection of properties of these pulse envelope functions is presented in Table A.1, where the characteristic moments for the pulse shapes

$$
\mu_n[g] = \int_{-\infty}^{\infty} dx\, x^n g(x)\,, \qquad\qquad \nu_n[g] = \frac{1}{\Delta\phi} \int_{-\infty}^{\infty} dx\, g^n(x)
$$

(A.36)

are exhibited.

**Table A.1:** A collection of the various pulse shape functions which are utilized throughout this thesis with some characteristic moments.

| $g$ | $\frac{1}{\cosh\frac{\phi}{\Delta\phi}}$ | $\exp\left\{-\frac{\phi^2}{2\Delta\phi^2}\right\}$ | $\cos^2\frac{\pi\phi}{2\Delta\phi}\sqcap(\phi)$ | $\sqcap(\phi)$ |
|---|---|---|---|---|
| $\mu_0[g]$ | $\pi\Delta\phi$ | $\sqrt{2\pi}\Delta\phi$ | $\Delta\phi$ | $2\Delta\phi$ |
| $\mu_2[g]/\mu_0[g]/\Delta\phi^2$ | $\frac{1}{4}\pi^2$ | $1$ | $\frac{\pi^2-6}{3\pi^2}\simeq 0.131$ | $\frac{1}{3}$ |
| $\mu_4[g]\mu_0[g]/\mu_2[g]^2$ | $5$ | $3$ | $\frac{9(120-20\pi^2+\pi^4)}{5(\pi^2-6)^2}\simeq 2.406$ | $\frac{9}{5}$ |
| $\nu_1[g]$ | $\pi$ | $\sqrt{2\pi}$ | $1$ | $2$ |
| $\nu_2[g]$ | $2$ | $\sqrt{\pi}$ | $\frac{3}{4}$ | $2$ |
| $\nu_3[g]$ | $\frac{\pi}{2}$ | $\sqrt{\frac{2}{3}\pi}$ | $\frac{5}{8}$ | $2$ |
| $\nu_4[g]$ | $\frac{4}{3}$ | $\sqrt{\frac{1}{2}\pi}$ | $\frac{35}{64}$ | $2$ |
| $\nu_5[g]$ | $\frac{3\pi}{8}$ | $\sqrt{\frac{2}{5}\pi}$ | $\frac{63}{128}$ | $2$ |
| $\nu_n[g]$ | $2^{n-1}\frac{\Gamma^2(n/2)}{\Gamma(n)}$ | $\sqrt{\frac{2}{n}\pi}$ | $\frac{2}{\sqrt{\pi}}\frac{\Gamma(n+1/2)}{\Gamma(n+1)}$ | $2$ |
| FWHM$[g]$ | $2\Delta\phi\,\mathrm{Arcosh}\,2$ | $2\Delta\phi\sqrt{2\ln 2}$ | $\Delta\phi$ | $2\Delta\phi$ |

### Laser field strength tensor

The field strength tensor of the laser field $F_{\mu\nu} = \partial_\mu A_\nu - \partial_\nu A_\mu$ reads

$$F^{\mu\nu} = \frac{ma_0}{e}\mathrm{Re}\left[f_+^{\mu\nu}(g'-ig)e^{-i\phi}\right] \tag{A.37}$$

$$= \frac{ma_0}{e}\left[f_1^{\mu\nu}\cos\xi\left(g\cos(\phi+\hat{\phi})\right)' + f_2^{\mu\nu}\sin\xi\left(g\sin(\phi+\hat{\phi})\right)'\right], \tag{A.38}$$

$$f_i^{\mu\nu} = k^\mu\epsilon_i^\nu - k^\nu\epsilon_i^\mu, \qquad i\in\{1,2,+,-\}, \tag{A.39}$$

with the prime denoting the derivative with respect to the phase $\phi = k\cdot x$. The basic tensors $f_{\mu\nu}^i$ fulfil the relations $k^\mu f_{\mu\nu}^i = 0$ and

$$\epsilon_i^\mu f_{\mu\nu}^j = C_{ij}k_\nu, \qquad\qquad f_{\mu\nu}^i f_j^{\nu\alpha} = C_{ij}k_\mu k^\alpha, \qquad \text{for } i\in\{1,2,+,-\}. \tag{A.40}$$

Thus, the vector potential (A.24) describes a null-field with $F_{\mu\nu}F^{\mu\nu} = 0$ and $F_{\mu\nu}{}^\star F^{\mu\nu} = 0$.
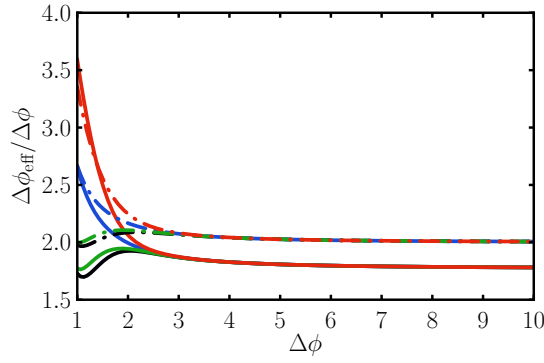
### Laser energy momentum tensor and normalization

The (symmetric) energy momentum tensor [Jac83] of the laser field

$$T^{\mu\nu} = F^\mu{}_\alpha F^{\alpha\nu} + \frac{1}{4}g^{\mu\nu}F^{\alpha\beta}F_{\alpha\beta}, \tag{A.41}$$

can be evaluated with (A.38) as

$$T^{\mu\nu} = \frac{m^2a_0^2}{2e^2}k^\mu k^\nu\Big[(g^2+g'^2)$$
$$-\cos 2\xi\left\{(g^2-g'^2)\cos 2(\phi+\hat{\phi}) + 2g'g\sin 2(\phi+\hat{\phi})\right\}\Big]. \tag{A.42}$$

**Figure A.1:** Relation between the pulse length parameter $\Delta\phi$ and the effective phase interval $\Delta\phi_{\text{eff}}$. For $\Delta\phi > 5$, the effective phase interval $\Delta\phi_{\text{eff}}$ is proportional to $\Delta\phi$, with the asymptotic value of $\Delta\phi_{\text{eff}}/\Delta\phi = \nu_2[g]$. Dash-dotted curves depict the hyperbolic secant pulse (A.32) while solid curves are for a Gaussian pulse (A.33). The different colours are for various values of laser polarization $\xi$ and carrier envelope phase $\hat{\phi}$.

With the energy density[1] $w = T^{00}$ one may write for the energy momentum tensor $T^{\mu\nu} = n^\mu n^\nu w$ with the propagation direction $n^\mu = k^\mu/\omega$, thus, the Poynting vector becomes $\boldsymbol{S} = w\,\boldsymbol{n}$. One may define a photon number density[2] $\varrho$ corresponding to the classical field distribution $A_\mu$ via the definition $\varrho \equiv w/\omega$, assuming that each photon carries an energy $\omega$. For $g = 1$ and averaging over $\phi$ one obtains the average energy density $\bar{w} = m^2 a_0^2 \omega^2/2e^2$ and the average photon number density $\bar{\varrho} = m^2 a_0^2 \omega/2e^2$.

One needs to define a proper flux factor for the definition of the cross section, given an emission probability. A proposed quantity with the correct physical dimension is the number of photons per transverse area

$$N_\perp = \frac{1}{\omega} \int_{-\infty}^{\infty} d\phi \varrho(\phi) = \bar{\varrho}\frac{\Delta\phi_{\text{eff}}}{\omega} \,, \tag{A.43}$$

defining an effective equivalent phase interval

$$\Delta\phi_{\text{eff}} \equiv \frac{1}{\bar{\varrho}} \int_{-\infty}^{\infty} d\phi \varrho(\phi)$$
$$= \int_{-\infty}^{\infty} d\phi \left[ (g^2 + g'^2) - \cos 2\xi \left\{ (g^2 - g'^2)\cos 2(\phi + \hat{\phi}) + 2g'g\sin 2(\phi + \hat{\phi}) \right\} \right] \,. \tag{A.44}$$

Figure A.1 shows the relations between the pulse length parameter $\Delta\phi$ and the effective phase interval $\Delta\phi_{\text{eff}}$. For long pulses with $\Delta\phi > 5$ the effective phase interval approaches the asymptotic value $\Delta\phi_{\text{eff}} = \nu_2[g]\Delta\phi$. (Explicit values for $\nu_2[g]$ are given in Table A.1.) For ultra-short pulses, $\Delta\phi \sim 1$, the value of the effective phase interval $\Delta\phi_{\text{eff}}$ strongly depends on the laser polarization $\xi$ and the carrier envelope phase $\hat{\phi}$.

---

[1]The physical dimension of the energy density is $[w] = 1\,\text{eV}^4 = 2.085 \times 10^{-5}\,\text{J/cm}^3$. For details on the conversion of units the reader is referred to AppendixA.1.

[2]With units $[\varrho] = 1\,\text{eV}^3 = 1.301 \times 10^{14}\,\text{cm}^{-3}$.

A dimensionfull effective pulse length (in units of time) is defined by $T_{\text{eff}} = \Delta\phi_{\text{eff}}/\omega$, with the help of which one can write for the photon number per pulse per transverse area $N_\perp = \bar{\varrho} T_{\text{eff}}$ and for the energy per pulse per transverse area $\mathcal{W}_\perp = \omega N_\perp = \bar{w} T_{\text{eff}}$

The quantity $N_\perp$ allows for an unambiguous definition of cross sections for arbitrary pulsed fields [see Eq. (3.38) for the definition of the cross section for one-photon Compton scattering]. Different pulse shapes are compared by their energy per transverse area.

The total energy per laser pulse $\mathcal{W} = \int d^3x\, w$ is, therefore, $\mathcal{W} = \mathcal{W}_\perp A_\perp$, where $A_\perp$ denotes the transverse size of the focus area. At the diffraction limit the laser spot radius is on the order of $\lambda$, such that the spot area is $A_\perp = \pi\lambda^2$, yielding, for a diffraction limited laser focus, the relation $\mathcal{W}_D = \frac{\pi^2 m^2}{2\alpha} a_0^2 T_{\text{eff}}$, or in common units $\mathcal{W}_D[\text{Joule}] = 1.9 \times 10^{-5}\, T_{\text{eff}}[\text{fs}]\, a_0^2$. Turning this around allows to estimate the achievable values of $a_0$ with optimal conditions as

$$a_0 \simeq 200\sqrt{\frac{\mathcal{W}_D[\text{Joule}]}{T_{\text{eff}}[\text{fs}]}} \simeq 200\sqrt{P[\text{PW}]}\,, \tag{A.45}$$

where $P[\text{PW}]$ denotes the laser power in petawatt.

## A.4   Important integrals

For the evaluation of the non-linear phase exponents $f(\phi)$ [cf. e.g. Eq. (3.7)] of $S$ matrix elements in strong-field QED in short laser pulses one has to know certain integrals of the pulse envelope. These are collected here. It is sufficient to know the oscillating phase integrals

$$I_n(\phi) = \int d\phi \Big[ g(\phi) e^{i\phi} \Big]^n \tag{A.46}$$

and the ponderomotive integral

$$G_2(\phi) = \int d\phi\, g^2(\phi) \tag{A.47}$$

for the different pulse envelopes $g$. Furthermore, the asymptotics of the quantities $I_n$ is defined as

$$I_n^{(\infty)} = \frac{1}{\Delta\phi} \left( \lim_{\phi\to\infty} I_n(\phi) - \lim_{\phi\to-\infty} I_n(\phi) \right). \tag{A.48}$$

### Hyperbolic secant pulse

For a hyperbolic secant pulse,

$$g(\phi) = \frac{1}{\cosh\frac{\phi}{\Delta\phi}} \tag{A.49}$$

the ponderomotive integral is

$$G_2(\phi) = \Delta\phi \tanh\frac{\phi}{\Delta\phi} \tag{A.50}$$

and the oscillating phase integrals are

$$I_1(\phi) = \int d\phi \frac{e^{i\phi}}{\cosh\frac{\phi}{\Delta\phi}} = \frac{\Delta\phi}{a} x^{2a}\, {}_2F_1(1, a; a+1; -x^2)\,, \tag{A.51}$$

$$I_2(\phi) = \int d\phi \frac{e^{2i\phi}}{\cosh^2\frac{\phi}{\Delta\phi}} = \frac{\Delta\phi}{a} x^{4a}\, {}_2F_1(2, 2a; 2a+1; -x^2) \tag{A.52}$$

with $x = e^{\phi/\Delta\phi}$, $a = (i\Delta\phi+1)/2$ and the hypergeometric function $_2F_1$ [WFS]. The asymptotics is given by

$$I_1^{(\infty)} = \text{Re}\left\{\psi\left(\tfrac{a+1}{2}\right) - \psi\left(\tfrac{a}{2}\right)\right\} = \frac{1}{a}\Gamma(1+a)\Gamma(1-a)\,, \tag{A.53}$$

$$I_2^{(\infty)} = 2\,\text{Re}\left\{1 + (1-2a)\left[\psi\left(\tfrac{2a+1}{2}\right) - \psi(a)\right]\right\} = \frac{1-2a}{a}\Gamma(1+2a)\Gamma(1-2a)\,, \tag{A.54}$$

where $\psi(z) = \frac{d}{dz}\log\Gamma(z)$ is the digamma function and $\Gamma(z)$ is the gamma function [WFS].

### Gaussian pulse

For the Gaussian envelope

$$g(\phi) = \exp\left\{-\frac{\phi^2}{2\Delta\phi^2}\right\} \tag{A.55}$$

the corresponding integrals read

$$G_2(\phi) = \frac{1}{2}\sqrt{\pi}\Delta\phi\,\text{erf}\,\frac{\phi}{\Delta\phi}\,, \tag{A.56}$$

$$I_1(\phi) = \int d\phi\, e^{i\phi} e^{-\frac{\phi^2}{2\Delta\phi^2}} = \sqrt{\frac{\pi}{2}}\Delta\phi\, e^{-\frac{\Delta\phi^2}{2}}\,\text{erf}\left(\frac{\phi - i\Delta\phi^2}{\sqrt{2}\Delta\phi}\right)\,, \tag{A.57}$$

$$I_2(\phi) = \int d\phi\, e^{2i\phi} e^{-\frac{\phi^2}{\Delta\phi^2}} = \sqrt{\frac{\pi}{4}}\Delta\phi\, e^{-\Delta\phi^2}\,\text{erf}\left(\frac{\phi}{\Delta\phi} - i\Delta\phi\right)\,, \tag{A.58}$$

where $\text{erf}\,(x)$ is the error function [WFS] and the asymptotics is

$$I_1^{(\infty)} = \sqrt{2\pi}e^{-\frac{\Delta\phi^2}{2}}\,, \tag{A.59}$$

$$I_2^{(\infty)} = \sqrt{\pi}e^{-\Delta\phi^2}\,. \tag{A.60}$$

### Squared cosine pulse

For the squared cosine pulse

$$g(\phi) = \cos^2\frac{\phi}{2N} \tag{A.61}$$

the phase integrals read

$$G_2(\phi) = \frac{3}{8}\phi + \frac{N}{2}\sin\frac{\phi}{N} + \frac{N}{16}\sin\frac{2\phi}{N}\,, \tag{A.62}$$

$$I_1(\phi) = \int d\phi\, e^{i\phi}\cos^2\frac{\phi}{2N} = \frac{e^{i\phi}}{2i(N^2-1)}\left(N^2 - 1 + N^2\cos\frac{\phi}{N} - iN\sin\frac{\phi}{N}\right)\,, \tag{A.63}$$

$$I_2(\phi) = \int d\phi\, e^{2i\phi}\cos^4\frac{\phi}{2N} = \frac{e^{2Ix}}{16i(4N^4-5N^2+1)}\left(12N^4 - 15N^2 + 3\right.$$
$$+ 16N^2(N^2-1)\cos\frac{\phi}{N} + N^2(4N^2-1)\cos\frac{2\phi}{N}$$
$$\left. -8iN(N^2-1)\sin\frac{\phi}{N} - iN(4N^2-1)\sin\frac{2\phi}{N}\right)\,, \tag{A.64}$$

with $N = \Delta\phi/\pi$ being the number of full oscillations. The asymptotics is

$$I_1^{(\infty)} = \frac{\sin\pi N}{N - N^3}\,, \tag{A.65}$$

$$I_2^{(\infty)} = \frac{3}{8N}\frac{\sin 2\pi N}{1 - 5N^2 + 4N^4}\,. \tag{A.66}$$

## A.5 Dirac algebra and spinors

The algebra of Dirac $\gamma$ matrices $\{\gamma^\mu, \gamma^\nu\} = 2g^{\mu\nu}$ is utilized in the standard representation, in particular for the numerical evaluation of the matrix elements

$$\gamma^0 = \begin{pmatrix} 1 & 0 & 0 & 0 \\ 0 & 1 & 0 & 0 \\ 0 & 0 & -1 & 0 \\ 0 & 0 & 0 & -1 \end{pmatrix}, \qquad \gamma^1 = \begin{pmatrix} 0 & 0 & 0 & 1 \\ 0 & 0 & 1 & 0 \\ 0 & -1 & 0 & 0 \\ -1 & 0 & 0 & 0 \end{pmatrix},$$

$$\gamma^2 = \begin{pmatrix} 0 & 0 & 0 & -i \\ 0 & 0 & i & 0 \\ 0 & i & 0 & 0 \\ -i & 0 & 0 & 0 \end{pmatrix}, \qquad \gamma^3 = \begin{pmatrix} 0 & 0 & 1 & 0 \\ 0 & 0 & 0 & -1 \\ -1 & 0 & 0 & 0 \\ 0 & 1 & 0 & 0 \end{pmatrix}. \tag{A.67}$$

With the additional definitions $\gamma^5 = i\gamma^0\gamma^1\gamma^2\gamma^3 = -\frac{i}{4!}\epsilon_{\alpha\beta\mu\nu}\gamma^\alpha\gamma^\beta\gamma^\mu\gamma^\nu$ and the antisymmetric tensors $\sigma^{\mu\nu} = \frac{i}{2}[\gamma^\mu, \gamma^\nu]$, the 16 matrices $\{1, \gamma^\mu, \sigma^{\mu\nu}, i\gamma^5\gamma^\mu, \gamma^5\}$ form a complete orthonormal set of basis elements for the Clifford algebra with the scalar product $(A, B) = \frac{1}{4}\mathrm{tr}\, AB$. The projections of an element $X$ of the Clifford algebra onto these basis elements are labelled according to their transformation properties under Lorentz transformations as scalar $\mathcal{S}$, vector $\mathcal{V}^\mu$, tensor $\mathcal{T}^{\mu\nu}$, axial vector $\mathcal{A}^\mu$ and pseudoscalar $\mathcal{P}$. They are defined as

$$\mathcal{S}[X] = (1, X) = \frac{1}{4}\mathrm{tr}\, X,$$

$$\mathcal{P}[X] = (\gamma^5, X) = \frac{1}{4}\mathrm{tr}\, \gamma^5 X,$$

$$\mathcal{V}^\mu[X] = (\gamma^\mu, X) = \frac{1}{4}\mathrm{tr}\, \gamma^\mu X,$$

$$\mathcal{A}^\mu[X] = (i\gamma^5\gamma^\mu, X) = \frac{1}{4}\mathrm{tr}\, i\gamma^5\gamma^\mu X,$$

$$\mathcal{T}^{\mu\nu}[X] = (\sigma^{\mu\nu}, X) = \frac{1}{4}\mathrm{tr}\, \sigma^{\mu\nu} X, \tag{A.68}$$

and one has

$$X = \mathcal{S} + \mathcal{P}\gamma^5 + \mathcal{V}_\mu\gamma^\mu + \mathcal{A}_\mu i\gamma^5\gamma^\mu + \frac{1}{2}\mathcal{T}_{\mu\nu}\sigma^{\mu\nu}. \tag{A.69}$$

The Dirac adjoint is defined as $\bar{X} = \gamma^0 X^\dagger \gamma^0$. The orthogonality of the basic spinors is represented as

$$\bar{u}_{p,r} u_{p,r'} = 2m\delta_{rr'}, \qquad\qquad \bar{u}_{p,r} v_{p,r'} = 0,$$

$$\bar{v}_{p,r} v_{p,r'} = -2m\delta_{rr'}, \qquad\qquad \bar{v}_{p,r} u_{p,r'} = 0, \tag{A.70}$$

where the Dirac adjoint spinor is defined as $\bar{u} = u^\dagger \gamma^0$. The completeness relations for spinors read

$$\sum_{r=\uparrow,\downarrow} u_{p,r}\bar{u}_{p,r} = \not{p} + m \equiv 2m\Lambda_+,$$

$$\sum_{r=\uparrow,\downarrow} v_{p,r}\bar{v}_{p,r} = \not{p} - m \equiv -2m\Lambda_-, \tag{A.71}$$

where $\Lambda_\pm$ is a projector on the subspace of solutions of the Dirac equation with positive (negative) energy. The basic spinors fulfil the algebraic equations

$$(\not{p} - m)u_p = 0,$$

$$(\not{p} + m)v_p = 0, \tag{A.72}$$

and the relations

$$\bar{u}_p \gamma^\mu u_p = 2p^\mu \,,$$
$$\bar{u}_p \gamma^\mu \gamma^\nu u_p = 2m g^{\mu\nu} \,,$$
$$\bar{u}_p \sigma^{\mu\nu} u_p = 0 \,. \tag{A.73}$$

As explicit representation for numerical evaluations, the following spinors are utilized

$$u_p = \frac{m + \not{p}}{\sqrt{m + p^0}} u_0 \,, \tag{A.74}$$

$$v_p = \frac{m - \not{p}}{\sqrt{m + p^0}} v_0 \,, \tag{A.75}$$

with

$$u_{0,\uparrow} = (1, 0, 0, 0)^T \,, \qquad\qquad u_{0,\downarrow} = (0, 1, 0, 0)^T \,,$$
$$v_{0,\uparrow} = (0, 0, 1, 0)^T \,, \qquad\qquad v_{0,\downarrow} = (0, 0, 0, 1)^T \,. \tag{A.76}$$

## A.6   Important relations from quantum field theory

### Normalization conventions

As example, consider a neutral scalar field with $\mathcal{L} = \frac{1}{2}(\partial_\mu \Phi)^2 - \frac{1}{2}m^2 \Phi^2$. The following five normalization constants can be chosen:

1.  The single particle wave function normalization: $\varphi_p(x) = N_W e^{-ipx}$.

2.  The normalization of the scalar product: $(\varphi_p, \varphi_q) = N_S^{-1} \int d\sigma^\mu \varphi_p^*(x) i \overleftrightarrow{\partial}_\mu \varphi_q(x)$.

3.  The orthogonality of single particle wave functions: $(\varphi_p, \varphi_q) = N_O \delta^3(\boldsymbol{p} - \boldsymbol{q})$.

4.  The eigenmode decomposition of the field operator: $\hat{\Phi}(x) = N_Z^{-1} \int d^3 p (\varphi_p \hat{a}_p + \varphi_p^* \hat{a}_p^\dagger)$.

5.  The commutators of annihilation and creation operators: $[\hat{a}_p, \hat{a}_q^\dagger] = N_A \delta^3(\boldsymbol{p} - \boldsymbol{q})$.

The five normalization factors $N_W$, $N_S$, $N_O$, $N_Z$, $N_A$ are constrained by the two relations $N_O = 2\omega_p (2\pi)^3 N_W^2 / N_S$ and $N_A = N_Z^2 / (N_O N_S)$. A survey of various normalization conventions used in text books on quantum field theory is given in Table A.2. In this thesis, the normalization convention of [Itz80] is employed, except for the normalization of the basic Dirac spinors for which $\bar{u}u = 2m$ is used (see also Section A.5), such that the above normalization factors are equal for bosons and fermions.

### Commutation relations

The electron ($\hat{c}_{\boldsymbol{p}r}$), positron ($\hat{d}_{\boldsymbol{p}r}$) and photon ($\hat{a}_{\boldsymbol{k}\lambda}$) annihilation and creation operators fulfil the commutation relations in the Furry picture

$$[\hat{a}_{\boldsymbol{k}\lambda}, \hat{a}_{\boldsymbol{k}'\lambda'}] = 0 \,, \quad [\hat{a}_{\boldsymbol{k}\lambda}^\dagger, \hat{a}_{\boldsymbol{k}'\lambda'}^\dagger] = 0 \,, \quad [\hat{a}_{\boldsymbol{k}\lambda}, \hat{a}_{\boldsymbol{k}'\lambda'}^\dagger] = -(2\pi)^3 2\omega_k \delta^3(\boldsymbol{k} - \boldsymbol{k}') g_{\lambda\lambda'} \,, \quad (A.77)$$

$$\{\hat{c}_{\boldsymbol{p}r}, \hat{c}_{\boldsymbol{p}'r'}\} = 0 \,, \quad \{\hat{c}_{\boldsymbol{p}r}^\dagger, \hat{c}_{\boldsymbol{p}'r'}^\dagger\} = 0 \,, \quad \{\hat{c}_{\boldsymbol{p}r}, \hat{c}_{\boldsymbol{p}'r'}^\dagger\} = (2\pi)^3 2\omega_p \delta^3(\boldsymbol{p} - \boldsymbol{p}') \delta_{rr'} \,. \quad (A.78)$$

$$\{\hat{d}_{\boldsymbol{p}r}, \hat{d}_{\boldsymbol{p}'r'}\} = 0 \,, \quad \{\hat{d}_{\boldsymbol{p}r}^\dagger, \hat{d}_{\boldsymbol{p}'r'}^\dagger\} = 0 \,, \quad \{\hat{d}_{\boldsymbol{p}r}, \hat{d}_{\boldsymbol{p}'r'}^\dagger\} = (2\pi)^3 2\omega_p \delta^3(\boldsymbol{p} - \boldsymbol{p}') \delta_{rr'} \quad (A.79)$$

with the on-shell energies $\omega_k = |\boldsymbol{k}|$ for photons and $\omega_p = p^0 = \sqrt{\boldsymbol{p}^2 + m^2}$ for electrons and positrons.

**Table A.2:** A survey of various normalization conventions in quantum field theory.

| | $N_W$ | $N_S$ | $N_O$ | $N_Z$ | $N_A$ |
|---|---|---|---|---|---|
| [Ber80] | $\frac{1}{\sqrt{2\omega}}$ | $(2\pi)^3$ | $1$ | $\sqrt{2\pi}^3$ | $1$ |
| [Itz80] | $1$ | $1$ | $2\omega(2\pi)^3$ | $2\omega(2\pi)^3$ | $2\omega(2\pi)^3$ |
| [Ryd94] | $\frac{1}{\sqrt{2\omega(2\pi)^3}}$ | $1$ | $1$ | $\sqrt{2\omega(2\pi)^3}$ | $2\omega(2\pi)^3$ |
| [Fra91, Kak93] | $\frac{1}{\sqrt{2\omega(2\pi)^3}}$ | $1$ | $1$ | $1$ | $1$ |

### Single particle states

Single particle Hilbert space states are defined and normalized in a Lorentz covariant manner as

$$\hat{a}^\dagger_{\boldsymbol{k}\lambda}|0\rangle_\gamma = |\boldsymbol{k}\lambda\rangle_\gamma \,, \qquad\qquad {}_\gamma\langle \boldsymbol{k}\lambda|\boldsymbol{k}'\lambda'\rangle_\gamma = -(2\pi)^3 2\omega_k \delta^3(\boldsymbol{k} - \boldsymbol{k}')g_{\lambda\lambda'} \,, \tag{A.80}$$

$$\hat{c}^\dagger_{\boldsymbol{p}r}|0\rangle_{e^-} = |\boldsymbol{p}r\rangle_{e^-} \,, \qquad\qquad {}_{e^-}\langle \boldsymbol{p}r|\boldsymbol{p}'r'\rangle_{e^-} = (2\pi)^3 2\omega_p \delta^3(\boldsymbol{p} - \boldsymbol{p}')\delta_{rr'} \,, \tag{A.81}$$

$$\hat{d}^\dagger_{\boldsymbol{p}r}|0\rangle_{e^+} = |\boldsymbol{p}r\rangle_{e^+} \,, \qquad\qquad {}_{e^+}\langle \boldsymbol{p}r|\boldsymbol{p}'r'\rangle_{e^+} = (2\pi)^3 2\omega_p \delta^3(\boldsymbol{p} - \boldsymbol{p}')\delta_{rr'} \,. \tag{A.82}$$

### Eigenmode expansion of the field operators

The eigenmode expansion of the field operators reads

$$\hat{\mathcal{A}}^\mu(x) = \sum_{\lambda=0}^3 \int \frac{d^3\boldsymbol{k}}{(2\pi)^3 2\omega_k} \left( \chi^\mu_{k,(\lambda)}(x)\hat{a}_{\boldsymbol{k}\lambda} + \chi^{\mu*}_{k,(\lambda)}(x)\hat{a}^\dagger_{\boldsymbol{k}\lambda} \right) \,, \tag{A.83}$$

$$\hat{\Psi}(x) = \sum_r \int \frac{d^3\boldsymbol{p}}{(2\pi)^3 2\omega_p} \left( \Psi^{(+)}_{p,r}(x)\hat{c}_{\boldsymbol{p}r} + \Psi^{(-)}_{p,r}(x)\hat{d}^\dagger_{\boldsymbol{p}r} \right) \,, \tag{A.84}$$

$$\hat{\bar{\Psi}}(x) = \sum_r \int \frac{d^3\boldsymbol{p}}{(2\pi)^3 2\omega_p} \left( \bar{\Psi}^{(+)}_{p,r}(x)\hat{c}^\dagger_{\boldsymbol{p}r} + \bar{\Psi}^{(-)}_{p,r}(x)\hat{d}_{\boldsymbol{p}r} \right) \,, \tag{A.85}$$

with the Gupta-Bleuler condition for physical photon states $\partial^\mu \hat{\mathcal{A}}^{(+)}_\mu |\Phi\rangle = 0$ where $\hat{\mathcal{A}}^{(+)}_\mu$ is the positive frequency part of $\hat{\mathcal{A}}_\mu$. The single-particle wave functions read

$$\chi^\mu_{k,(\lambda)}(x) = e^{-ik\cdot x}\epsilon^\mu_{(\lambda)} \,, \tag{A.86}$$

$$\Psi^{(+)}_{p,r}(x) = E_p(x)u_{p,r} = e^{-ip\cdot x}\Omega_p(x)u_{p,r} \,, \tag{A.87}$$

$$\Psi^{(-)}_{p,r}(x) = E_{-p}(x)v_{p,r} = e^{ip\cdot x}\Omega_{-p}(x)v_{p,r} \,, \tag{A.88}$$

where $\Psi^{(+)}_{p,r}(x)$ and $\Psi^{(-)}_{p,r}(x)$ are the positive and negative energy Volkov wave functions, respectively. The quantities $E_p(x)$ denotes the Volkov matrix functions defined in (2.42) with $E_p(x) = e^{-ip\cdot x}\Omega_p$ (see also Appendix B) and the Dirac adjoint spinors are defined as $\bar{\Psi} = \Psi^\dagger \gamma^0$. The scalar product in the space of the wave functions for Dirac fermions reads [Bag90]

$$(\Psi_1, \Psi_2) = \int_\sigma d\sigma_\mu \bar{\Psi}_1(x)\gamma^\mu \Psi_2(x) \tag{A.89}$$

with an arbitrary space-like or light-like hypersurface $\sigma$ in Minkowski space and the infinitesimal surface normal element $d\sigma_\mu$ thereon, and

$$(\Psi_{p,r}^{(+)}, \Psi_{p',r'}^{(+)}) = (2\pi)^3 \, 2p^0 \, \delta_{rr'} \delta^3(\boldsymbol{p} - \boldsymbol{p}') = (2\pi)^3 \, 2p^+ \, \delta_{rr'} \delta^3(\mathsf{p} - \mathsf{p}') \,, \tag{A.90}$$

$$(\Psi_{p,r}^{(-)}, \Psi_{p',r'}^{(+)}) = (\Psi_{p,r}^{(+)}, \Psi_{p',r'}^{(-)}) = 0 \,. \tag{A.91}$$

## A.7   The reduction of matrix elements

The perturbative expansion of the operator $\hat{S}[A]$ in the Furry picture [see Eq. (2.36)] utilizes the Dyson series [Wei95]

$$\hat{S}[A] = \mathsf{T} \exp\left\{-i \int d^4x \mathscr{H}_{\text{int}}(x)\right\} \tag{A.92}$$

$$= \sum_{n=0}^{\infty} \frac{(-i)^n}{n!} \int d^4x_1 \cdots d^4x_n \mathsf{T}\Big(\mathscr{H}_{\text{int}}(x_1) \cdots \mathscr{H}_{\text{int}}(x_n)\Big) \tag{A.93}$$

with the interaction Hamiltonian density

$$\mathscr{H}_{\text{int}}(x) \equiv e : \hat{\bar{\Psi}}(x)\gamma^\mu \hat{A}_\mu(x)\hat{\Psi}(x) : \,, \tag{A.94}$$

where $: \cdots :$ denotes the normal ordering of the enclosed operators. The reduction of an $S$ matrix element is shown for the example of one-photon Compton scattering with the initial state containing an electron with momentum $\boldsymbol{p}$ and spin $r$. The final state contains an electron characterized by $\boldsymbol{p}'$ and $r'$, and a photon with momentum $\boldsymbol{k}'$ in the polarization state $\lambda'$. This is a first-order process described by the first-order term in the Dyson series (A.93)

$$S^{(1)} = \langle \boldsymbol{p}'r'; \boldsymbol{k}'\lambda'|\hat{S}[A]|\boldsymbol{p}r\rangle = \langle \boldsymbol{p}'r'; \boldsymbol{k}'\lambda'| \left(-i \int d^4x \mathscr{H}_{\text{int}}(x)\right) |\boldsymbol{p}r\rangle \tag{A.95}$$

$$= -ie \int d^4x \langle 0|\hat{c}_{\boldsymbol{p}'r'}\hat{a}_{\boldsymbol{k}'\lambda'} : \hat{\bar{\Psi}}(x)\gamma^\mu \hat{A}_\mu(x)\hat{\Psi}(x) : \hat{c}_{\boldsymbol{p}r}^\dagger|0\rangle \tag{A.96}$$

Employing the Wick theorem [Ber80], the operator product in the above equation can be reduced to the completely contracted expression

$$\langle 0|\hat{c}_{\boldsymbol{p}'r'}\hat{a}_{\boldsymbol{k}'\lambda'} : \hat{\bar{\Psi}}(x)\gamma^\mu \hat{A}_\mu(x)\hat{\Psi}(x) : \hat{c}_{\boldsymbol{p}r}^\dagger|0\rangle = \underline{\hat{c}_{\boldsymbol{p}'r'}\hat{\bar{\Psi}}(x)}\,\gamma^\mu \underline{\hat{a}_{\boldsymbol{k}'\lambda'}\hat{A}_\mu(x)}\,\underline{\hat{\Psi}(x)\hat{c}_{\boldsymbol{p}r}^\dagger} \tag{A.97}$$

The contractions between the field operators and the creation and annihilation operators are defined as the vacuum expectation values of these operators and are given by the single-particle wave functions [Ber80]

$$\underline{\hat{c}_{\boldsymbol{p}'r'}\hat{\bar{\Psi}}(x)} = \langle 0|\hat{c}_{\boldsymbol{p}'r'}\hat{\bar{\Psi}}(x)|0\rangle = \bar{\Psi}_{p',r'}^{(+)}(x) \,, \tag{A.98}$$

$$\underline{\hat{\Psi}(x)\hat{c}_{\boldsymbol{p}r}^\dagger} = \langle 0|\hat{\Psi}(x)\hat{c}_{\boldsymbol{p}r}^\dagger|0\rangle = \Psi_{p,r}^{(+)}(x) \,, \tag{A.99}$$

$$\underline{\hat{a}_{\boldsymbol{k}'\lambda'}\hat{A}^\mu(x)} = \langle 0|\hat{a}_{\boldsymbol{k}'\lambda'}\hat{A}^\mu(x)|0\rangle = \chi_{k',(\lambda')}^{\mu*} \,, \tag{A.100}$$

with the Volkov wave functions $\Psi_{p,r}^{(+)}(x)$ and $\bar{\Psi}_{p',r'}^{(+)}(x)$. The final result for the $S$ matrix element for non-linear one-photon Compton scattering in strong-field QED reads

$$S^{(1)} = -ie \int d^4x \, \bar{\Psi}_{p',r'}^{(+)}(x) \, \slashed{\epsilon}_{(\lambda')}^* e^{ik' \cdot x} \, \Psi_{p,r}^{(+)}(x) \,. \tag{A.101}$$

For the second-order process of two-photon Compton scattering, where there are two photons with momenta $k_{1,2}$ and polarizations $\lambda_{1,2}$ in the exit channel, the Dyson series has to be taken up to the second-order term

$$S^{(2)} = \frac{(-i)^2}{2!} \langle \boldsymbol{p}'r'; \boldsymbol{k}_1\lambda_1; \boldsymbol{k}_2\lambda_2 | \mathsf{T} \int d^4x d^4y \,\mathscr{H}_{\mathrm{int}}(x)\mathscr{H}_{\mathrm{int}}(y) | \boldsymbol{p}r \rangle \,. \tag{A.102}$$

Upon applying the Wick theorem to the time ordered product, one encounters contractions between electron field operators and adjoint electron field operators giving rise to the Dirac-Volkov propagator [Rom69]

$$\underline{\hat{\Psi}(x)\hat{\bar{\Psi}}(y)} = \langle 0 | \mathsf{T}\hat{\Psi}(x)\hat{\bar{\Psi}}(y) | 0 \rangle = i\mathcal{G}(x,y|A) \,, \tag{A.103}$$

with

$$\langle 0 | \mathsf{T}\hat{\Psi}(x)\hat{\bar{\Psi}}(y) | 0 \rangle = -\langle 0 | \mathsf{T}\hat{\bar{\Psi}}(y)\hat{\Psi}(x) | 0 \rangle \,. \tag{A.104}$$

When calculating the contractions, there are 2! equivalent ways of contracting the fermion operators, where only the integration variables are interchanged [Ber80], yielding

$$\langle 0 | \mathsf{T}\hat{c}_{\boldsymbol{p}'r'}\hat{a}_{\boldsymbol{k}_1\lambda_1}\hat{a}_{\boldsymbol{k}_2\lambda_2} : \hat{\bar{\Psi}}(x)\gamma_\mu\hat{\mathcal{A}}^\mu(x)\hat{\Psi}(x) :: \hat{\bar{\Psi}}(y)\gamma_\nu\hat{\mathcal{A}}^\nu(y)\hat{\Psi}(y) : \hat{c}^\dagger_{\boldsymbol{p},r} | 0 \rangle \tag{A.105}$$

$$= 2! \,\underline{\hat{c}_{\boldsymbol{p}'r'}\hat{\bar{\Psi}}(x)} \left[ \underline{\hat{a}_{\boldsymbol{k}_1\lambda_1}\hat{\mathcal{A}}^\mu(x)}\gamma_\mu\underline{\hat{\bar{\Psi}}(x)\hat{\Psi}(y)}\gamma_\nu\underline{\hat{a}_{\boldsymbol{k}_2\lambda_2}\hat{\mathcal{A}}^\nu(y)} \right.$$
$$\left. + \,\underline{\hat{a}_{\boldsymbol{k}_2\lambda_2}\hat{\mathcal{A}}^\mu(x)}\gamma_\mu\underline{\hat{\bar{\Psi}}(x)\hat{\Psi}(y)}\gamma_\nu\underline{\hat{a}_{\boldsymbol{k}_1\lambda_1}\hat{\mathcal{A}}^\nu(y)} \right] \underline{\hat{\Psi}(y)\hat{c}_{\boldsymbol{p}r}} \tag{A.106}$$

$$= -2i \left[ \bar{\Psi}^{(+)}_{\boldsymbol{p}',r'}(x)\not{\epsilon}^*_1 e^{ik_1\cdot x}\mathcal{G}(x,y|A)\not{\epsilon}^*_2 e^{ik_2\cdot y}\Psi^{(+)}_{\boldsymbol{p},r}(y) \right.$$
$$\left. + \,\bar{\Psi}^{(+)}_{\boldsymbol{p}',r'}(x)\not{\epsilon}^*_2 e^{ik_2\cdot x}\mathcal{G}(x,y|A)\not{\epsilon}^*_1 e^{ik_1\cdot y}\Psi^{(+)}_{\boldsymbol{p},r}(y) \right] \,. \tag{A.107}$$

Plugging this result into (A.102), one immediately finds the expression (4.5) for the two-photon Compton $S$ matrix. This concludes these general considerations on quantum field theory in the Furry picture. It was shown how the $S$ matrix elements for one-photon and two-photon Compton scattering in the Chapters 3 and 4, respectively, can be derived from the perturbative Dyson series expansion of the scattering operator $\hat{S}[A]$ in the presence of a background field, employing the Wick theorem.

# B
## Strong-field QED in the path integral approach

ONSIDERING the Furry picture in the path integral formalism provides an elegant tool to obtain the corresponding Feynman rules and $n$-point functions [Vai92, Fra81]. The general idea is to find a unitary transformation $\Omega$, that transforms the Dirac operator with a background field $A_\mu$ into the free Dirac operator:

$$\Omega^{-1}(\not{p} - e\not{A} - m)\Omega = \not{p} - m \,. \tag{B.1}$$

The existence of such an unitary transformation is assumed here and verified a posteriori by an explicit calculation of $\Omega$ in Section B.2. The transition to the Furry picture is related to the stability of the vacuum state under the action of the background field [Fra81] and the unitarity of $\Omega$. In Section B.3, a new and simple proof of the orthogonality and completeness of the Volkov matrix functions $E_p$, which are related to $\Omega$, is presented.

## B.1 The path integral with background fields

The starting point is the generating functional in the presence of a background field $A_\mu$ which reads

$$Z[J_\mu, \bar{\eta}, \eta] = \int \mathcal{D}\mathcal{A}_\mu \mathcal{D}\bar{\Psi}\mathcal{D}\Psi \exp\left\{i \int d^4x \left[\mathcal{L} + J_\mu \mathcal{A}^\mu + \bar{\eta}\Psi + \bar{\Psi}\eta\right]\right\} \tag{B.2}$$

with the Lagrangian $\mathcal{L} = \mathcal{L}_\mathsf{f} + \mathcal{L}_\mathsf{g} + \mathcal{L}_\mathsf{int}$, and

$$\mathcal{L}_\mathsf{f} = \bar{\Psi}(i\not{\partial} - e\not{A} - m)\Psi \,, \tag{B.3}$$

$$\mathcal{L}_\mathsf{g} = -\frac{1}{4}\mathcal{F}_{\mu\nu}\mathcal{F}^{\mu\nu} - \frac{1}{2\xi_g}(\partial_\mu \mathcal{A}^\mu)^2 \,, \tag{B.4}$$

$$\mathcal{L}_\mathsf{int} = -e\bar{\Psi}\not{A}\Psi \,. \tag{B.5}$$

Adopting a perturbative picture for the interaction of the fermions with the quantized electromagnetic field $\mathcal{A}_\mu$, the generating functional may be rewritten as

$$Z[J_\mu, \bar{\eta}, \eta] = \exp\left\{i \int d^4x \mathcal{L}_\mathsf{int}\left(\frac{\delta}{i\delta J^\mu}, \frac{\delta}{i\delta\eta}, \frac{\delta}{i\delta\bar{\eta}}\right)\right\} Z_\mathsf{g}[J_\mu] Z_\mathsf{f}[\bar{\eta}, \eta] \,, \tag{B.6}$$

where the fields have been replaced by derivatives with respect to the appropriate sources according to

$$\mathcal{A}_\mu \to \frac{\delta}{i\delta J^\mu}, \qquad \bar{\Psi} \to \frac{\delta}{i\delta\eta}, \qquad \Psi \to \frac{\delta}{i\delta\bar{\eta}} \tag{B.7}$$

in the interaction Lagrangian which has been taken out of the functional integral. The remaining generating functional factorizes into a free gauge part $Z_\mathsf{g}$ and a fermion part $Z_\mathsf{f}$ containing the interaction with the background field $A_\mu$

$$Z_\mathsf{g}[J_\mu] = \int \mathcal{D}\mathcal{A}_\mu \exp\left\{i\int d^4x\left(\mathcal{L}_\mathsf{g} + J_\mu\mathcal{A}^\mu\right)\right\}, \tag{B.8}$$

$$Z_\mathsf{f}[\bar{\eta},\eta] = \int \mathcal{D}\bar{\Psi}\mathcal{D}\Psi \exp\left\{i\int d^4x\left(\mathcal{L}_\mathsf{f} + \bar{\eta}\Psi + \bar{\Psi}\eta\right)\right\}. \tag{B.9}$$

The transition to the Furry picture is done by a unitary transformation $\Omega$ of the fermion fields

$$\Psi = \Omega\chi, \qquad \bar{\Psi} = \bar{\chi}\Omega^{-1}, \tag{B.10}$$

such that $\mathcal{L}_\mathsf{f}$ looks like a free Lagrangian

$$\bar{\Psi}(\slashed{p} - e\slashed{A} - m)\Psi = \bar{\chi}(\slashed{p} - m)\chi, \tag{B.11}$$

in terms of the new fields $\chi$ and $\bar{\chi}$. The functional integration measure is invariant under the transformation (B.10) of the fields. The fermionic generating functional $Z_\mathsf{f}$ reads in terms of the new fields

$$Z_\mathsf{f}[\bar{\eta},\eta] = \int \mathcal{D}\bar{\chi}\mathcal{D}\chi \exp\left\{i\int d^4x\left[\bar{\chi}(i\slashed{\partial}_x - m)\chi + \bar{\chi}\Omega^{-1}\eta + \bar{\eta}\Omega\chi\right]\right\}. \tag{B.12}$$

Proceeding with the standard procedure to "complete the squares" in the exponent, or more precisely to shift the integration variables by a classical field $\chi \to \chi - \chi_{\mathrm{cl}}$ and $\bar{\chi} \to \bar{\chi} - \bar{\chi}_{\mathrm{cl}}$ [Kak93]

$$\chi_{\mathrm{cl}}(x) = \int d^4y\, G_0(x-y)\Omega^{-1}(y)\eta(y), \tag{B.13}$$

which is a solution of the classical field equation with the source $\Omega^{-1}\eta$,

$$(i\slashed{\partial}_x - m)\chi_{\mathrm{cl}}(x) = \Omega^{-1}(x)\eta(x), \tag{B.14}$$

and similarly for $\bar{\chi}_{\mathrm{cl}}$. The Green's function of the Dirac operator $(i\slashed{\partial}_x - m)G_0(x) = \delta(x)$ is employed above in (B.13). For the fermionic part of the generating functional one obtains the result

$$Z_\mathsf{f}[\bar{\eta},\eta] = Z_\mathsf{f}[0,0]\exp\left\{-i\int d^4x\, d^4y\, \bar{\eta}(x)\Omega(x)G_0(x-y)\Omega^{-1}(y)\eta(y)\right\}. \tag{B.15}$$

This allows the calculation of all $n$-point functions of the theory by calculating the functional derivatives with respect to the source terms. The corresponding $S$ matrix elements are calculated via LSZ reduction [Pes95]. For instance, the propagator, i.e. the electron 2-point function, in the presence of a background $A_\mu$ field has a representation as [Vai92]

$$\mathcal{G}(x,y|A) = \frac{1}{Z_\mathsf{f}[0,0]}\frac{\delta^2 Z_\mathsf{f}[\eta,\bar{\eta}]}{\delta\eta(y)\delta\bar{\eta}(x)}\bigg|_{\bar{\eta}=\eta=0} = \Omega(x)G_0(x-y)\Omega^{-1}(y). \tag{B.16}$$

## B.2   Construction of the unitary transformation $\Omega$

In this section, the unitary transformation $\Omega$ will be constructed explicitly. In [Vai92], the transformation $\Omega$ was calculated for a plane-wave background field $A_\mu$ in Fock-Schwinger gauge, where $(x - x')^\mu A_\mu(x) = 0$ with a rather lengthy expression for the background field vector potential $A_\mu$. Here, a different derivation will be presented in the covariant Lorenz gauge with $\partial \cdot A(x) = 0$ which is consistent with the form of gauge fixing in (2.34) and the form of the laser vector potential (A.24) used throughout this thesis. It will be shown that the transformation $\Omega(x)$ is related to the Volkov matrix function $E_p(x)$. The searched unitary transformation $\Omega$ is defined by

$$\slashed{p} - e\slashed{A} = \slashed{\pi} = \Omega \slashed{p} \Omega^{-1} \, . \tag{B.17}$$

It is convenient to construct $\Omega$ in two steps as a product $\Omega = UV$ with commutating factors $[U, V] = 0$, where $U$ refers to the spin-0 case and $V$ contains the spin-$\frac{1}{2}$ structure. First a new auxiliary momentum is defined

$$\bar{\pi}^\mu \equiv p^\mu - \frac{eA \cdot p}{k \cdot p} k^\mu + \frac{e^2 A^2}{2k \cdot p} k^\mu \tag{B.18}$$

with $\bar{\pi}^2 = \pi^2$ and $[\bar{\pi}^\mu, \bar{\pi}^\nu] = 0$. The momenta $\bar{\pi}^\mu$ and $\pi^\mu$ are related by $\pi^\mu = \Lambda^\mu{}_\nu \bar{\pi}^\nu$ with the local Lorentz transformation

$$\Lambda^\mu{}_\nu = g^\mu{}_\nu + \frac{e}{k \cdot p}(k^\mu A_\nu - k_\nu A^\mu) - \frac{e^2 A^2}{2(k \cdot p)^2} k^\mu k_\nu \, , \tag{B.19}$$

i.e. $\Lambda^\mu{}_\nu$ is an orthogonal transformation $\Lambda^\mu{}_\nu g_{\mu\sigma} \Lambda^\sigma{}_\kappa = g_{\nu\kappa}$. Even more, $\Lambda^\mu{}_\nu$ is an element of the local little group $E_2(\phi)$ (that is the Euclidean group in two dimensions) since $\Lambda^\mu{}_\nu k^\nu = k^\mu$ [Bro84, Wei95]. The transformation $U$ is obtained by solving

$$\bar{\pi}^\mu = U p^\mu U^{-1} \, . \tag{B.20}$$

The ansatz $U = \exp\{-i\Gamma(\phi)\}$ leads to a differential equation for the unknown function $\Gamma(\phi)$ via

$$\frac{d\Gamma}{d\phi} = \frac{ep \cdot A(\phi)}{k \cdot p} - \frac{e^2 A^2(\phi)}{k \cdot p} \, , \tag{B.21}$$

with the solution

$$\Gamma(\phi, \phi_0) = \frac{1}{2k \cdot p} \int_{\phi_0}^{\phi} d\phi' \left[ 2p \cdot A(\phi') - e^2 A^2(\phi') \right] \, , \tag{B.22}$$

which gives the solution for $U$. To calculate the transformation for the spin-$\frac{1}{2}$ case one notes that

$$\slashed{\pi} = VU\gamma^\mu p_\mu U^{-1} V^{-1} = V\gamma^\mu \bar{\pi}_\mu V^{-1} = \gamma^\mu \Lambda_{\mu\nu} \bar{\pi}^\nu \, . \tag{B.23}$$

The matrix $V$ has to fulfil the relation

$$\Lambda_\mu{}^\nu \gamma^\mu = V\gamma^\nu V^{-1} \, , \tag{B.24}$$

thus, $V$ is a spinor representation of the Lorentz transformation $\Lambda$. A convenient ansatz for this transformation is $V = \exp\{c\sigma_{\mu\nu}\Lambda^{\mu\nu}\}$ with an unknown constant $c$. Using this expression in (B.24) one obtains

$$V = \exp\left\{\frac{2iec}{k \cdot p}\slashed{k}\slashed{A}\right\}$$

(B.25)

To determine $c$, one has to evaluate the matrix on the right hand side of (B.24) with the Hadamard lemma

$$e^{tX}Ye^{-tX} = \sum_{n=0}^{\infty}\frac{t^n}{n!}Z_n\,,$$

(B.26)

$$Z_n = [X, Z_{n-1}]\,,\qquad Z_0 = Y\,.$$

(B.27)

Here, $t = \frac{2iec}{k \cdot p}$, $Y = \gamma^\nu$ and $X = \slashed{k}\slashed{A}$ are identified. The calculation yields

$$Z_1 = [\slashed{k}\slashed{A}, \gamma^\nu] = \slashed{k}\{\slashed{A}, \gamma^\nu\} - \{\slashed{k}, \gamma^\nu\}\slashed{A} = 2(A^\nu\slashed{k} - k^\nu\slashed{A})\,,$$

(B.28)

$$Z_2 = -4A^2 k^\nu \slashed{k}\,,$$

(B.29)

$$Z_n = 0 \qquad\text{for } n \geq 3\,,$$

(B.30)

thus,

$$V\gamma^\nu V^{-1} = \gamma^\mu\left[g_{\mu\ \nu} + \frac{4iec}{k \cdot p}\left(A^\nu k_\mu - k^\nu A_\mu\right) + \frac{8e^2c^2A^2}{(k \cdot p)^2}k_\mu k^\nu\right] = \gamma^\mu\Lambda_\mu^{\ \nu}\,.$$

(B.31)

A comparison of coefficients between (B.31) and (B.19) yields $c = -i/4$, thus, the transformation $V$ reads

$$V = \exp\left\{\frac{e}{2k \cdot p}\slashed{k}\slashed{A}(\phi)\right\} = 1 + \frac{e}{2k \cdot p}\slashed{k}\slashed{A}(\phi)$$

(B.32)

The final result for the transformation $\Omega$ is

$$\Omega_p(\phi) = \left[1 + \frac{e}{2k \cdot p}\slashed{k}\slashed{A}(\phi)\right]\exp\left\{-\frac{i}{2k \cdot p}\int^\phi d\phi'\left[2ep \cdot A(\phi') - e^2A^2(\phi')\right]\right\}\,,$$

(B.33)

which is indeed related to the Volkov matrix function as $E_p(x) = \Omega_p(\phi)e^{-ip \cdot x}$ differing only by a free plane wave phase factor.

## B.3    A proof of the completeness and orthogonality of the Volkov matrix functions

In this section, a new proof of the completeness and orthogonality of the Volkov $E_p$ matrix functions will be presented, using general properties of $E_p(x)$. Here, the momentum $p$ is taken to be off the mass shell, $p^2 \neq m^2$. The orthogonality (B.34) and completeness (B.35) relations for the Volkov matrices read

$$\int d^4x \bar{E}_p(x)E_q(x) = (2\pi)^4\delta^4(p - q)\,,$$

(B.34)

$$\int d^4p E_p(x)\bar{E}_p(y) = (2\pi)^4\delta^4(x - y)\,,$$

(B.35)

which are important relations for employing the Volkov states as initial and final states for the perturbation series. Several proofs of the above equations were given in the literature, but they are rather lengthy and employ certain additional properties for the background field [Rit85, Zak05, Löt08, Boc11a].

The given proof of the above relations makes use of the following general properties:

1. The Volkov matrix functions have a representation as $E_p(x) = \Omega_p(\phi)e^{-ip \cdot x}$ as shown in the preceding section.

2. The matrices $\Omega_p(\phi)$ are unitary with respect to the Dirac adjoint, i.e. $\bar{\Omega}_p(\phi) = \Omega_p^{-1}(\phi)$, such that $\bar{\Omega}_p(\phi)\Omega_p(\phi) = \Omega_p(\phi)\bar{\Omega}_p(\phi) = 1$.

3. The unitary matrices $\Omega_p(\phi)$ depend only on the phase $\phi$ of the background field, which is proportional to the light-front coordinate $x^+ = \phi/\omega$, where $\omega$ is frequency of the background wave field.

4. $\Omega_p(\phi)$ depends only on three components of momentum $p^+, \boldsymbol{p}_\perp$.

Thus, writing these dependencies explicitly as $\Omega_{p^+,\boldsymbol{p}_\perp}(x^+) \equiv \Omega_p(\phi)$ in the following, the proof becomes simple when using light-front coordinates for the integrations in (B.34) and (B.35), i.e. using $d^4x = dx^+dx^-d^2\boldsymbol{x}_\perp/2$ and $d^4p = dp^+dp^-d^2\boldsymbol{p}_\perp/2$, as well as the light-front delta distributions $\delta^3(\mathsf{p} - \mathsf{q}) = \delta(p^+ - q^+)\delta^2(\boldsymbol{p}_\perp - \boldsymbol{q}_\perp)$.

### Proof of orthogonality

$$
\begin{aligned}
\int d^4x \, \bar{E}_p(x) E_q(x) &= \int d^4x \, \bar{\Omega}_{p^+,\boldsymbol{p}_\perp}(x^+)\Omega_{q^+,\boldsymbol{q}_\perp}(x^+) \, e^{i(p-q)\cdot x} \\
&= \frac{1}{2} \int dx^+ dx^- d^2\boldsymbol{x}_\perp \, \bar{\Omega}_{p^+,\boldsymbol{p}_\perp}(x^+)\Omega_{q^+,\boldsymbol{q}_\perp}(x^+) \\
&\qquad\qquad\qquad \times e^{i\frac{x^+}{2}(p^- - q^-) + i\frac{x^-}{2}(p^+ - q^+) - (\boldsymbol{p}_\perp - \boldsymbol{q}_\perp)\cdot\boldsymbol{x}_\perp} \\
&= (2\pi)^3\delta^3(\mathsf{p} - \mathsf{q}) \int dx^+ \, \bar{\Omega}_{p^+,\boldsymbol{p}_\perp}(x^+)\Omega_{q^+,\boldsymbol{q}_\perp}(x^+) \, e^{i\frac{x^+}{2}(p^- - q^-)} \\
&= (2\pi)^3\delta^3(\mathsf{p} - \mathsf{q}) \int dx^+ \, \bar{\Omega}_{p^+,\boldsymbol{p}_\perp}(x^+)\Omega_{p^+,\boldsymbol{p}_\perp}(x^+) \, e^{i\frac{x^+}{2}(p^- - q^-)} \\
&= (2\pi)^3\delta^3(\mathsf{p} - \mathsf{q}) \int dx^+ e^{i\frac{x^+}{2}(p^- - q^-)} \\
&= (2\pi)^4\delta^4(p - q) \, .
\end{aligned}
\tag{B.36}
$$

### Proof of completeness

$$
\begin{aligned}
\int d^4p \, E_p(x)\bar{E}_p(y) &= \int d^4p \, \Omega_{p^+,\boldsymbol{p}_\perp}(x^+)\bar{\Omega}_{p^+,\boldsymbol{p}_\perp}(y^+) \, e^{-ip\cdot(x-y)} \\
&= (2\pi)\delta(x^+ - y^+) \int dp^+ d^2\boldsymbol{p}_\perp \, \Omega_{p^+,\boldsymbol{p}_\perp}(x^+)\bar{\Omega}_{p^+,\boldsymbol{p}_\perp}(y^+) \\
&\qquad\qquad\qquad \times e^{-i\frac{p^+}{2}(x^- - y^-) + i\boldsymbol{p}_\perp\cdot(\boldsymbol{x}_\perp - \boldsymbol{y}_\perp)} \\
&= (2\pi)\delta(x^+ - y^+) \int dp^+ d^2\boldsymbol{p}_\perp e^{-i\frac{p^+}{2}(x^- - y^-) + i\boldsymbol{x}_\perp\cdot\boldsymbol{p}_\perp} \\
&= (2\pi)^4\delta^4(x - y) \, .
\end{aligned}
\tag{B.37}
$$

This concludes the proof of the completeness and orthogonality of the Volkov matrix functions $E_p(x)$, where the light-front structure of the unitary matrices $\Omega(\phi)$ was employed.

# C

# The weak-field and IPW limits of one-photon Compton scattering

$\mathrm{T}$HE weak-field limit of the one-photon Compton matrix element was concisely discussed at the end of Section 3.2, where the starting point was the final result for the non-linear Compton $S$ matrix. Here, in Section C.1, a more detailed derivation is presented, based on an iterative solution of the Lippmann-Schwinger equation (2.56) for the Volkov state. In the following sections, the limit of infinite monochromatic plane waves is presented, providing important relations for the discussion in Chapter 3. The Appendix closes with a discussion of the numerical convergence in the limit of long pulses and the relation between long pulses and monochromatic infinite plane waves.

## C.1   Weak-field expansion of the non-linear Compton matrix element

A systematic expansion of the non-linear Compton matrix element can be achieved by employing the iterative solution of the Lippmann-Schwinger equations (2.56) for the Volkov state $\Psi_p$ and the adjoint Volkov state $\bar{\Psi}_p$. Using a symbolic notation (where the spacetime integrations are not noted explicitly), the expansion reads

$$\Psi_p = \psi_p + G_0 e\slashed{A}\psi_p + G_0 e\slashed{A}G_0 e\slashed{A}\psi_p + \dots, \tag{C.1}$$

$$\bar{\Psi}_{p'} = \bar{\psi}_{p'} + \bar{\psi}_{p'} e\slashed{A}G_0 + \bar{\psi}_{p'} e\slashed{A}G_0 e\slashed{A}G_0 + \dots, \tag{C.2}$$

where $\psi_p$ and $\bar{\psi}_{p'}$ denote the respective free Dirac wave functions, $G_0$ stands for the free Dirac propagator and $e\slashed{A}$ is the interaction with the laser field. Using these expansions, the non-linear Compton matrix element is decomposed as

$$
\begin{aligned}
S = \bar{\Psi}_{p'}\slashed{\epsilon}'\Psi_p = {}& \bar{\psi}_{p'}\slashed{\epsilon}'\psi_p \\
& + \bar{\psi}_{p'}\slashed{\epsilon}'G_0 e\slashed{A}\psi_p + \bar{\psi}_{p'} e\slashed{A}G_0\slashed{\epsilon}'\psi_p \\
& + \bar{\psi}_{p'}\slashed{\epsilon}'G_0 e\slashed{A}G_0 e\slashed{A}\psi_p + \bar{\psi}_{p'} e\slashed{A}G_0\slashed{\epsilon}'G_0 e\slashed{A}\psi_p + \bar{\psi}_{p'} e\slashed{A}G_0 e\slashed{A}G_0\slashed{\epsilon}'\psi_p \\
& + \mathcal{O}(a_0^3).
\end{aligned}
\tag{C.3}
$$

The diagrammatic representation of this expansion of the $S$ matrix element (3.4) in the interaction with the laser field, i.e. in powers of $a_0$, is given in Figure C.1. Each laser-electron vertex (red dot) corresponds to a factor $e\slashed{A}$ and is proportional to a factor of $a_0$.

The zeroth-order term [the first line in (C.3)] is exactly the free electron-photon vertex which is known to vanish due to momentum conservation. The laser vector potential describes

**Figure C.1:** Expansion of the non-perturbative non-linear Compton matrix element in the Furry picture (cf. Figure 3.1) in powers of the interaction with the laser background field. The black box denotes the two leading-order Feynman diagrams that lead to the Klein-Nishina formula, eventually.

both the absorption ($e^{-ik \cdot x}$) and emission ($e^{ik \cdot x}$) of laser photons. From the first order [the second line of (C.3)], only the diagrams with the absorption of a laser photon (in the black box) are non-vanishing. These give rise to the perturbative matrix element which eventually yields the Klein-Nishina cross section.

Before showing the equivalence of the expanded Volkov matrix elements with usual perturbation theory, some comments on the higher order terms seem necessary. From the 12 possible second order terms in the second and third line of Figure C.1 [each term in the third line of Eq. (C.3) corresponds to $2^2$ diagrams], only the three ones in the second line are non-vanishing, where both laser photons are absorbed. All the other ones are zero due to momentum conservation. From the third order, only the non-vanishing contributions are shown. The terms in the first pair of brackets in the last line of Figure C.1 provide the lowest order terms of the third harmonic. The terms in the second pair of brackets contain the absorption and re-emission of a laser photon, giving the same energy-momentum conservation as the first harmonic. Thus, these terms have to be considered as a correction to the first harmonic of order $a_0^3$. Consequently, one could identify further corrections of higher order in $a_0$ all contributing to the same harmonic.

Turning now to the evaluation of the lowest non-vanishing contribution of the $S$ matrix, which is linear in the background field, the Volkov wave functions in the matrix element in Eq. (3.4) have to be expanded up to terms linear in $A_\mu$. To make contact with standard perturbation theory, the background field is assumed to be monochromatic, i.e. $g = 1$ in this section. Reintroducing the integrations, the linearized Volkov wave functions read

$$\Psi_p(x) = \psi_p(x) + \int d^4y \, G_0(x-y) e A\!\!\!/ \psi_p(y) \,, \tag{C.4}$$

$$\bar{\Psi}_{p'}(x) = \bar{\psi}_p(x) + \int d^4y \, \bar{\psi}_p(y) e A\!\!\!/(y) G_0(x-y) \,, \tag{C.5}$$

yielding the $s$- and $u$-channel terms if the expansion is plugged into the matrix element (3.4),

namely $S = S_{(s)} + S_{(u)}$ with

$$S_{(s)} = -ie \int d^4x \, \bar{\psi}_{p'}(x) \not{\epsilon}'^* \int d^4y G_0(x-y) e\not{A}(y)\psi_p(y) e^{ik' \cdot x}, \tag{C.6}$$

$$S_{(u)} = -ie \int d^4x \int d^4y \, \bar{\psi}_{p'}(y) e\not{A}(y) G_0(x-y) \not{\epsilon}'^* \psi_p(x) e^{ik' \cdot x}. \tag{C.7}$$

As discussed above, only the parts of the laser field describing the absorption of laser photons ($\propto e^{-ik \cdot x}$) lead to an energy momentum conservation that can be satisfied. The $s$-channel contribution is

$$S_{(s)} = \frac{-iema_0}{2} \int d^4x d^4y e^{i(k'+p') \cdot x} \bar{u}_{p'} \not{\epsilon}'^* G_0(x-y) \not{\epsilon}_+ u_p e^{-i(p+k) \cdot y} \tag{C.8}$$

$$= \frac{-i(2\pi)^4 ema_0}{2} \delta^4(k'+p'-k-p) \bar{u}_{p'} \not{\epsilon}'^* G_0(p+k) \not{\epsilon}_+ u_p \tag{C.9}$$

with the Fourier transformed free electron propagator

$$\int d^4y e^{-i(p+k) \cdot y} G_0(x-y) = e^{-i(p+k) \cdot x} G_0(p+k). \tag{C.10}$$

For the $u$-channel one obtains

$$S_{(u)} = \frac{-iema_0}{2} \int d^4x d^4y e^{i(k'-p) \cdot x} \bar{u}_{p'} \not{\epsilon}_+ G_0(x-y) \not{\epsilon}'^* u_p e^{-i(p'-k) \cdot x} \tag{C.11}$$

$$= \frac{-i(2\pi)^4 ema_0}{2} \delta^4(k'+p'-k-p) \bar{u}_{p'} \not{\epsilon}_+ G_0(p'-k) \not{\epsilon}'^* u_p. \tag{C.12}$$

In total one finds

$$S = \frac{-ie(2\pi)^4 ma_0}{2} \delta^4(k+p-k'-p') \Big[ \bar{u}_{p'} \not{\epsilon}'^* G_0(p+k) \not{\epsilon}_+ u_p + \bar{u}_{p'} \not{\epsilon}_+ G_0(p'-k) \not{\epsilon}'^* u_p \Big], \tag{C.13}$$

which is, apart from the global normalization, exactly the matrix element for linear Compton scattering, leading eventually to the Klein-Nishina formula [Itz80]. Using for the prefactor the definition of $a_0 = eA_0/m$ one finds

$$\frac{-iema_0}{2} = -ie^2 \frac{A_0}{2} \rightarrow -ie^2 \tag{C.14}$$

upon choosing $A_0 = 2$. With the chosen normalization for the single-particle states $|\boldsymbol{k}\lambda\rangle$, the perturbative photon wave functions are normalized to $2\omega_k$ particles per unit volume [Itz80]. Comparing this with the normalization of the background field, for which the energy density is $\bar{w} = m^2 a_0^2 \omega^2/(2e^2) = \omega^2 A_0^2/2$, one notes that upon choosing $A_0 = 2$ both normalizations would coincide: $\bar{w} = \omega(2\omega)$, i.e. the energy density $\bar{w}$ is given by the energy of one photon $\omega$ times $2\omega$ photons per unit volume.

## C.2    The limit of infinite plane waves[1]

The first goal is to derive the $S$ matrix in the limit of infinite plane waves using the previous result for arbitrary laser pulse envelopes $g$. It is clear that only the phase integrals $\mathscr{A}_n$ (3.19) in $\mathscr{M}$ (3.21) need to be modified as the other terms do not depend on the pulse envelope $g$ at all.

The case of an infinite monochromatic plane wave laser field is obtained formally by taking the limit $g \to 1$. The numerical convergence of the phase integrals in the limit $\Delta\phi \to \infty$ is not so straightforward and discussed below in Section C.4 of this Appendix. In the case of an infinite plane wave, the carrier envelope phase $\hat{\phi}$ becomes insignificant. Therefore, it will be set to zero from the beginning in this Appendix.

The non-linear phase exponent in the phase integrals $\mathscr{A}_n$ in Eqs. (3.19) becomes in the monochromatic limit, where the integrals in (3.7) have been evaluated and a irrelevant constant phase has been dropped,

$$s\phi - f(\phi) = (s - \beta)\phi - \bar{\alpha}\sin(\phi + \phi_0) - \frac{\beta}{2}\cos 2\xi \sin 2\phi = (s - \beta)\phi - \tilde{f}(\phi) \qquad (C.15)$$

with the geometric mean $\bar{\alpha} = \sqrt{\alpha_+ \alpha_-} = |\alpha_\pm|$ [for the definition of $\alpha_\pm$ see Eq. (3.8)], such that $\alpha_+ = \bar{\alpha}e^{-i\phi_0}$ and $\alpha_- = \bar{\alpha}e^{i\phi_0}$ with the complex argument $\phi_0 = \arg(\alpha_-) = \arctan_2(-\alpha_2\sin\xi, \alpha_1\cos\xi)$. The oscillating part of the exponential in (C.15) can be expanded into a Fourier series over the interval of periodicity $[-\pi, \pi]$ according to

$$e^{-i\tilde{f}} = e^{-i\bar{\alpha}\sin(\phi+\phi_0) - i\frac{\beta}{2}\cos 2\xi \sin 2\phi} = \sum_{\ell=-\infty}^{\infty} B_\ell e^{-i\ell\phi}, \qquad (C.16)$$

with the Fourier coefficients

$$B_\ell = \frac{1}{2\pi}\int_{-\pi}^{+\pi} d\phi' e^{i\ell\phi' - i\tilde{f}(\phi')}, \qquad (C.17)$$

which is a generalization of the Jacobi-Anger expansion [Erd53]. The signs in the exponent of (C.16) are chosen such that terms with $\ell > 0$ can later be interpreted as absorption of laser photons. In the general case of arbitrary elliptical polarization, the coefficients are two-variable one-parameter Bessel functions [Kor06], defined as

$$B_\ell \equiv J_\ell(\bar{\alpha}, \beta\cos 2\xi /2; \phi_0) = \sum_{n=-\infty}^{\infty} J_{\ell-2n}(\bar{\alpha})J_n(\beta\cos 2\xi /2)e^{-i(\ell-2n)\phi_0}, \qquad (C.18)$$

where $J_\ell$ are ordinary Bessel functions of the first kind [Wat22]. A particularly simple and well known limit for the coefficients is obtained for circular polarization, where $\cos 2\xi = 0$ and

$$B_\ell(\text{circular}) = \sum_n J_{\ell-2n}(\bar{\alpha})J_n(0)e^{-i(\ell-2n)\phi_0} = J_\ell(\bar{\alpha})e^{-i\ell\phi_0}. \qquad (C.19)$$

The case of linear laser polarization has been extensively studied in [Löt09c, Leu11]. For example for $\xi = 0$ the coefficients read

$$B_\ell(\text{linear}) = \sum_{n=-\infty}^{\infty} J_{\ell-2n}(\alpha_1)J_n(\beta/2). \qquad (C.20)$$

---

[1]The presentation in this and the following section is partly based on the publication [Hei10b].

With these expansions, the $\phi$ integrals in (3.19) become

$$\int d\phi e^{i(s-\beta-\ell)\phi} = 2\pi\delta(s-\beta-\ell)\,, \tag{C.21}$$

yielding delta distributions $\delta(s-\ell-\beta)$. This means that for infinite plane waves the variable $s$ cannot be arbitrary anymore. Instead $s = s(\ell) = \ell + \beta$ with integer $\ell$ corresponding to the $\ell$th harmonic, i.e. the absorption of $\ell$ photons from the background field. The extra term $\beta = \beta_p - \beta_{p'}$ is absorbed into the definition of the quasi-momenta. Multiplying the argument of the delta distribution with $k^-$ and writing the expression explicitly one has

$$k^-(s-\beta-\ell) = (p'^- + \beta_{p'}k^-) - (p^- + \beta_p k^-) + k'^- - \ell k^- \equiv q'^- - q^- + k'^- - \ell k^- \tag{C.22}$$

where the terms in brackets are the minus components of the electron quasi-momenta $q = p + \beta_p k$ and $q' = p' + \beta_{p'}k$, respectively. Note that only $p^-$, the conjugate momentum to the laser phase $\phi$, is modified by an intensity dependent contribution, i.e. the light-front transverse components of momentum and quasi-momentum are equal $q^+ = p^+$, $\boldsymbol{q}_\perp = \boldsymbol{p}_\perp$, abbreviated as $\mathsf{q} = \mathsf{p}$. The energy-momentum conservation can now be written in the form

$$q + \ell k = q' + k'\,, \qquad \ell \in \mathbb{N}\,. \tag{C.23}$$

As a consequence, the frequency of the scattered photons becomes in an IPW

$$\omega'_\ell = \omega'(s(\ell)) = \frac{\ell k \cdot q}{(q + \ell k) \cdot n'} \tag{C.24}$$

with again $\ell \in \mathbb{N}$, giving rise to the notion of discrete harmonics with a strict correlation $\omega'_\ell(\theta)$ for each $\ell$. Writing the scalar products explicitly for the important case of a head-on collision of the electron with the laser beam, $-\boldsymbol{p} \parallel \boldsymbol{n}$, one arrives at

$$\omega'_\ell(\theta) = \frac{\ell\omega e^{2\zeta}}{\frac{1-v\cos\theta}{1-v} + \left[\ell\frac{\omega}{m}e^\zeta + \frac{a_0^2}{4}\right](1+\cos\theta)} \tag{C.25}$$

with the electron rapidity $\zeta = \operatorname{arccosh}\gamma$ and velocity $v = \tanh\zeta$. Defining the total momentum $P = q + \ell k$, the formula for the frequency of the scattered photon (C.25) can be reformulated as

$$\omega'_\ell = \frac{\ell\omega}{1 + \kappa_\ell(a_0)\,e^{-\zeta}\,(1+\cos\theta)} \tag{C.26}$$

with

$$\kappa_\ell(a_0) \equiv \ell\omega/m - \sinh\zeta + \frac{1}{4}a_0^2\,e^{-\zeta} \equiv -\boldsymbol{P}\cdot\boldsymbol{n}\frac{1}{m} \tag{C.27}$$

being the projection of the total momentum onto the optical axis, $\boldsymbol{n} = \boldsymbol{k}/\omega$, measured in units of $m$. The vanishing of the latter, $\boldsymbol{n}\cdot\boldsymbol{P} = -m\kappa_\ell = 0$, defines an intensity and $\ell$ dependent centre-of-mass frame in which the scattered frequencies are precisely the harmonic multiples, $\omega'_\ell = \ell\omega$ [Har09]. For $\kappa_\ell < 0$ one is in the inverse Compton regime where the electrons transfer energy to the emitted photons, $\omega'_\ell > \ell\omega$, thus causing an overall blue-shift, and the emission is into directions $\theta < 90°$, i.e. most of the radiation is backscattered. (This is of course the physical basis for Compton generated X-rays.) For $\kappa_\ell = 0$, the direction of emission is very sensitive to the details of the longitudinal electron dynamics. It has been supposed to use this parameter regime for precise tests of radiation reaction [DP09]. In the inverse Compton

regime, the maximum scattered frequency, i.e. the Compton edge, occurs upon backscattering ($\theta = 0$) and is given by

$$\omega'_{\ell,\max} = \frac{\ell\omega e^{2\zeta}}{1 + 2\ell\frac{\omega}{m}e^{\zeta} + a_0^2/2} \simeq \frac{4\ell\gamma^2\omega}{1 + a_0^2/2} \equiv 4\ell\gamma_\star^2\omega \,. \tag{C.28}$$

The approximation above holds for small electron energies $\gamma$ and large intensities, more precisely when

$$4\gamma\ell\frac{\omega}{m} \ll 1 \ll a_0^2 \,, \tag{C.29}$$

which is very well satisfied for the parameters envisaged at the HZDR ($\gamma = 100$, $\omega = 1.55$ eV, $a_0 = 10$) but was not so for the SLAC E-144 experiment ($\gamma = 10^5$, $\omega = 2.35$ eV, $a_0 = 1$). As $\gamma_\star^2 = \gamma^2/(1 + a_0^2/2) < \gamma^2$ the linear ($\ell = 1$) Compton edge is red-shifted, $\omega'_{\ell,\max} < 4\gamma^2\omega$, by a factor of $1/(1 + a_0^2/2)$ in a strong laser pulse. Hence, if one is primarily interested in up-shifting the laser frequency (e.g. for X-ray generation), the intensity $a_0$ should certainly not exceed unity.

Having discussed the kinematics of the process now, the focus is turned back to the calculation of the $S$ matrix. The phase integrals (3.19) read in the limit of infinite plane waves

$$\mathscr{A}_0(s) \to 2\pi \sum_{\ell=-\infty}^{\infty} \delta(s - \ell - \beta)B_\ell \,,$$

$$\mathscr{A}_\pm(s) \to 2\pi \sum_{\ell=-\infty}^{\infty} \delta(s - \ell - \beta)B_{\ell\mp1} \,,$$

$$\mathscr{A}_2(s) \to 2\pi \sum_{\ell=-\infty}^{\infty} \delta(s - \ell - \beta)\Big[B_\ell + \frac{\cos 2\xi}{2}(B_{\ell+2} + B_{\ell-2})\Big] \,, \tag{C.30}$$

where they have support on a delta comb. Using these results in the (3.20), the general expression for the scattering matrix in a monochromatic plane wave field reads

$$S = (2\pi)^4 \sum_\ell \delta^4(k' + q' - \ell k - q)M^{(\ell)} \,, \tag{C.31}$$

$$M^{(\ell)} = \big[\mathscr{T}_0 + \mathscr{T}_2\big]B_\ell + \mathscr{T}_+B_{\ell-1} + \mathscr{T}_-B_{\ell+1} + \frac{\mathscr{T}_2}{2}\cos 2\xi\big[B_{\ell-2} + B_{\ell+2}\big] \,. \tag{C.32}$$

The gauge invariance of the matrix elements $M^{(\ell)}$ is ensured automatically by recursion relations of the generalized Bessel functions (cf. also Appendix D). For a circularly polarized laser, the partial amplitudes $M^{(\ell)}$ acquire the particularly simple form

$$M^{(\ell)} = e^{-i\ell\phi_0}\big[(\mathscr{T}_0 + \mathscr{T}_2)J_\ell(\bar{\alpha}) + \mathscr{T}_+e^{i\phi_0}J_{\ell-1}(\bar{\alpha}) + \mathscr{T}_-e^{-i\phi_0}J_{\ell+1}(\bar{\alpha})\big] \,, \tag{C.33}$$

which coincides with textbook results (e.g. [Ber80]).

The $S$ matrix element (C.31) with the partial amplitudes (C.33) for circular polarization is readily translated into an emission rate [Ber80]. The differential rate per incoming electron for emitting a single photon of frequency $\omega'$ in an infinite monochromatic laser wave with frequency $\omega$ per incident electron is given by [Nar65]

$$\frac{d\dot{W}}{dx} = \sum_{\ell=1}^{\infty} \frac{d\dot{W}_\ell}{dx} \,, \qquad\qquad \frac{d\dot{W}_\ell}{dx} = \frac{e^2m^2}{16\pi}\frac{1}{q^0}\frac{a_0^2}{2}\frac{\mathfrak{J}_\ell(z_\ell(x))}{(1+x)^2} \,, \tag{C.34}$$

where the spin and polarization summations have been performed. The non-trivial part of the rate is encoded in the function $\mathfrak{J}_\ell$, which reads for circular laser polarization

$$\mathfrak{J}_\ell(z_\ell) \equiv -\frac{8}{a_0^2} J_\ell^2(z_\ell) + \left(2 + \frac{x^2}{1+x}\right) \left[J_{\ell-1}^2(z_\ell) + J_{\ell+1}^2(z_\ell) - 2J_\ell^2(z_\ell)\right]. \tag{C.35}$$

The $J_\ell$ are Bessel functions of the first kind depending on the invariant argument

$$z_\ell(x) \equiv 2\ell \, \frac{\sqrt{a_0^2/2}}{\sqrt{1 + \frac{a_0^2}{2}}} \sqrt{\frac{x}{y_\ell^\star}\left(1 - \frac{x}{y_\ell^\star}\right)} \tag{C.36}$$

which is composed of two further invariants, namely

$$x \equiv \frac{k \cdot k'}{k \cdot p'}, \qquad y_\ell^\star \equiv \ell y_1^\star \equiv \frac{2\ell \, k \cdot p}{m_\star^2}, \quad (0 \le x \le y_\ell^\star). \tag{C.37}$$

Note that $z_\ell = 0$ when $x$ acquires its minimum or maximum value. For linear laser polarization the function $\mathfrak{J}_\ell$ involves generalized two-parameter Bessel functions [cf. Eq. (C.20)]. The corresponding expressions can be found e.g. in [Iva04]. The rate (C.34) is readily transformed into a cross section upon dividing by the flux factor [Iva04],

$$j \equiv \frac{k \cdot q}{\omega q^0} \, \bar{\varrho}_\omega, \tag{C.38}$$

with the photon density $\bar{\varrho}_\omega$, which is related to the laser intensity as

$$a_0^2 = 2\frac{e^2 \bar{\varrho}_\omega}{m^2 \omega}. \tag{C.39}$$

One thus ends up with the differential cross section

$$\frac{d\sigma_\ell}{dx} = \pi r_e^2 \, \frac{m^2}{k \cdot p} \frac{\mathfrak{J}_\ell(z)}{(1+x)^2}, \tag{C.40}$$

which indeed has the correct dimensions of an area. With $r_e = \alpha/m \simeq 2.8$ fm as the classical electron radius, one gets $\pi r_e^2 = 25$ fm$^2 = 250$ mb. Expanding $\mathfrak{J}_\ell(z)$ for small $a_0$ one recovers again the Klein-Nishina cross section [Nar65, Ber80].[2]

For what follows, the rates and cross sections will be needed in the laboratory frame where a head-on collision between laser and electron beam is assumed. The frequency of the scattered photon is then given by (C.26), and the invariants (C.37) become

$$x = \frac{\frac{\omega'}{m}(1 + \cos\theta)}{e^\zeta - \frac{\omega'}{m}(1 + \cos\theta)}, \tag{C.41}$$

$$y_1^\star = \frac{2e^\zeta}{1 + \frac{a_0^2}{2}} \frac{\omega}{m}. \tag{C.42}$$

This yields the following differential cross sections

$$\frac{d\sigma_\ell}{d\omega'} = \frac{r_e^2 \pi}{\boldsymbol{n} \cdot \boldsymbol{P}} \frac{m^2}{k \cdot p} \mathfrak{J}_\ell(z_\ell), \qquad\qquad \frac{d\sigma_\ell}{d\Omega} = \frac{r_e^2}{2\ell} \left(\frac{\omega'}{\omega e^\zeta}\right)^2 \mathfrak{J}_\ell(z_\ell). \tag{C.43}$$

---

[2]Note that in [Ber80] Gaussian units are used rather than Heaviside-Lorentz which amounts to a reshuffling of factors of $4\pi$.
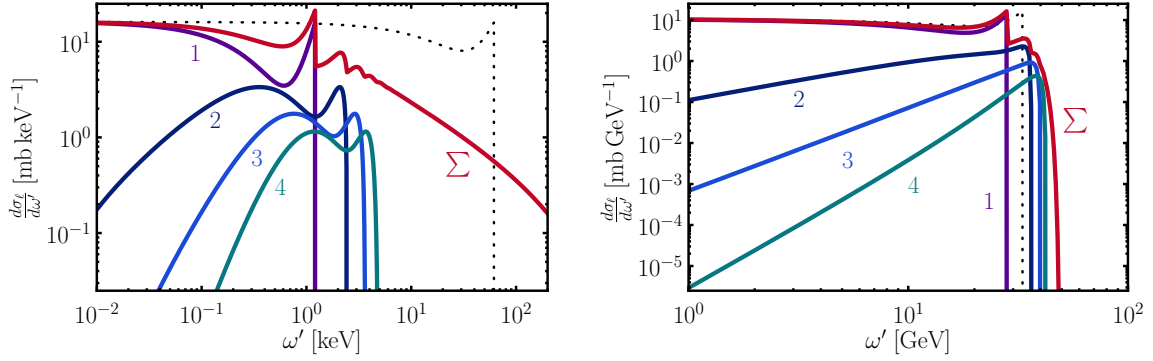
**Figure C.2:** Partial differential cross sections for the first few harmonics $\ell = 1, 2, 3$ and $4$ in non-linear Compton back-scattering (head-on collision) of monochromatic waves (solid curves) as a function of the photon frequency $\omega'$. In the summed cross section labelled by $\Sigma$, terms up to $n = 1000$ are included. For comparison, the Klein-Nishina cross section [Ber80] is shown as dotted curve. Left panel: HZDR like parameters $a_0 = 10$, $\gamma = 100$, $\omega = 1.55$ eV. Right panel: SLAC like parameters $a_0 = 1$, $\gamma = 10^5$, $\omega = 2.35$ eV.

The individual harmonic cross sections (C.43) are plotted in Figure C.2. One clearly sees that the contribution of each harmonic has its own frequency range given by $\ell\omega \leq \omega'_\ell \leq \omega'_{\ell,\mathrm{max}}$, cf. (C.28), with the individual supports overlapping to some extent. The contributions of higher harmonics, $\ell > 1$, become more and more suppressed in amplitude. These features are sufficient to guarantee the convergence of the cross section summed over all harmonics [Har09],

$$d\sigma \equiv \sum_{\ell=1}^{\infty} d\sigma_\ell \,. \tag{C.44}$$

The result of the summation (up to $n = 1000$) is shown in Figure C.2 as red solid curve labelled by $\Sigma$. Two main features can be seen to arise, in particular in the left panel of Figure C.2. First, as discussed above, the linear Compton 'edge' is red-shifted by a factor of $1 + a_0^2/2$ from about $4\gamma^2\omega \simeq 60$ keV down to 1 keV. This is a rather drastic effect and it should be straightforward to verify experimentally. Second, higher harmonics show up as additional peaks in the summed cross section with the peak heights decreasing rapidly with $\ell$. From the properties of the Bessel functions $J_\ell(z)$ for large argument and large index one can assert that the Bessel functions with $\ell > a_0^3$ are exponentially suppressed. Thus, harmonics with $\ell > a_0^3$ will contribute only marginally to the spectrum and the sum in (C.44) can be truncated at values of the order of $\ell = a_0^3$.

## C.3   The classical low energy limit: Non-linear Thomson scattering

In this section, the results for non-linear Compton scattering from the previous section are compared with the results for non-linear Thomson scattering considered, for instance, in [Sar70, Esa93]. As stated in [Nik64b, Nar65] and further analysed in [Har09, Hei10b] the Thomson limit is obtained when the invariant $y^\star_\ell$ defined in (C.37) becomes small. In what follows, explicit relations between the general Compton expressions and their classical (Thomson) limit are to be found. To this end the quantum corrections are separated off from the purely classical results. A proper starting point is the momentum projection (C.27) which

may be rewritten as

$$\kappa_\ell = \kappa_0 + \frac{1}{2} y_\ell^\star \left( 1 + \frac{a_0^2}{2} \right) e^{-\zeta} , \tag{C.45}$$

where $\kappa_0$ is obtained by setting $\ell = 0$. Replacing $\kappa_\ell \to \kappa_0$ in the scattered frequency (C.26) for head-on collisions straightforwardly yields the (non-linear) Thomson limit

$$\omega'_{\ell,\mathrm{Th}} = \frac{\ell\omega}{1 + \kappa_0 e^{-\zeta}(1 + \cos\theta)} \equiv \ell\omega'_{1,\mathrm{Th}} . \tag{C.46}$$

This suggests that the general formula for arbitrary collision geometry is obtained by setting $\ell = 0$ in the denominator of (C.24) which yields

$$\omega'_{\ell,\mathrm{Th}} = \frac{\ell\omega \, n \cdot u}{n' \cdot u + \dfrac{a_0^2}{4n \cdot u} \, n \cdot n'} \tag{C.47}$$

meaning that the frequencies $\omega'_{\ell,\mathrm{Th}}$ are indeed integer multiples of a fundamental frequency $\omega'_{1,\mathrm{Th}}$, with $p^\mu = mu^\mu$, $k'^\mu = \omega'n'^\mu$ and $k^\mu = \omega n^\mu$. At this point it is instructive to compare with the low-intensity ("linear") limit (or proper Thomson limit), where $\ell = 1$, $a_0 \to 0$ and (C.47) condenses to

$$\omega' = \frac{k \cdot u}{n' \cdot u} \, \omega . \tag{C.48}$$

This is the Doppler shift in disguise upon noting that for a head-on collision and backscattering $n \cdot u = \gamma(1 + v) = e^\zeta$ and $n' \cdot u = \gamma(1 - v) = e^{-\zeta}$. Expressing the invariant $x$ from (C.37) in terms of the scattering angle $\theta$ it becomes explicitly $\ell$-dependent [Har09], $x \equiv x_\ell = \ell x_1$, with

$$x_1 = \frac{\frac{\omega}{m} e^{-\zeta}(1 + \cos\theta)}{1 + \kappa_0 e^{-\zeta}(1 + \cos\theta)} . \tag{C.49}$$

Comparing with (C.46) one finds the relation

$$\omega'_\ell = \frac{\omega'_{\ell,\mathrm{Th}}}{1 + x_\ell} . \tag{C.50}$$

As $x_\ell$ is bounded by $y_\ell^\star$ the Thomson limit implies $x_\ell \to 0$ so that Compton and Thomson expressions should generically differ by terms of order $x_\ell$ as in (C.50). Moving on to the emission rates, again, all terms depending on $x_\ell$ are to be isolated. Following [Har09, Hei10b] the ratio $r = x_1/y_1^\star$ is defined with $0 \le r \le 1$, and $z_\ell$ from (C.36) is rewritten as

$$z_\ell = \ell z_1 = \sqrt{2}\ell \frac{a_0}{\sqrt{1 + \frac{a_0^2}{2}}} \sqrt{r(1 - r)} , \quad (0 \le z_1 < 1) . \tag{C.51}$$

It is important to take the Thomson limits, $x_1 \to 0$ and $y_1^\star \to 0$, in such a way that the ratio $r$ stays fixed as a result of which $z_\ell$ remains unchanged. One may therefore decompose the spectral function (C.35) into a classical (Thomson) part and an $x_\ell$ dependent correction,

$$\mathfrak{J}_\ell(z_\ell) = \mathfrak{K}_\ell(z_\ell) + \frac{x_\ell^2}{1 + x_\ell} \mathfrak{L}_\ell(z_\ell) , \tag{C.52}$$

where (suppressing the overall argument $z_\ell$)

$$\mathfrak{L}_\ell \equiv J_{\ell-1}^2 + J_{\ell+1}^2 - 2J_\ell^2 , \quad \text{and} \quad \mathfrak{K}_\ell \equiv -8J_\ell^2/a_0^2 + 2\mathfrak{L}_\ell. \tag{C.53}$$
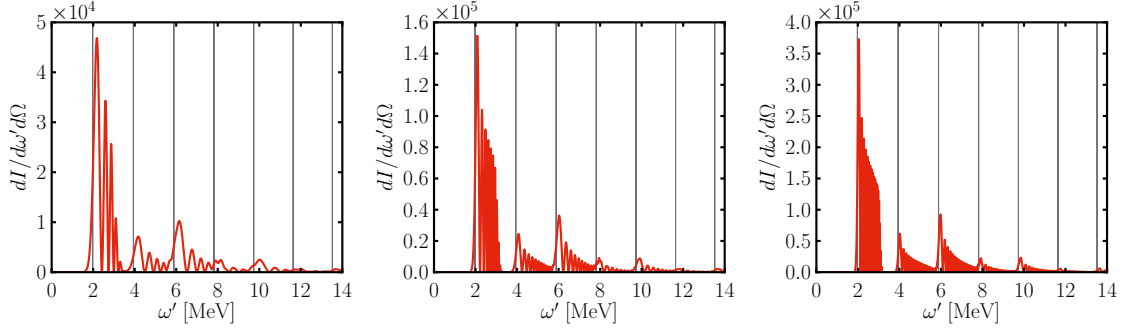
**Figure C.3:** Differential intensity as a function of $\omega'$ in non-linear Compton scattering for a Gaussian pulse envelope with $\Delta\phi = 20$ (left), 50 (centre) and 100 (right) for linear polarization and $a_0 = 1.5$. Further parameters are $\gamma = 1000$, $\theta = 1/\gamma$ and $\varphi = \pi/2$.

This yields the Thomson limit of the cross section (C.43),

$$\left(\frac{d\sigma_\ell}{d\Omega}\right)_{\text{Th}} = \frac{r_e^2}{2\ell}\left(\frac{\omega'}{\omega e^\zeta}\right)^2 \mathfrak{K}_\ell(z_\ell), \tag{C.54}$$

where only the classical part, $\mathfrak{K}_\ell$, of $\mathfrak{J}_\ell$ contributes. Factoring $\mathfrak{K}_\ell$ out from (C.43) the Compton to Thomson ratio may calculated explicitly,

$$\frac{d\sigma_\ell}{d\Omega}\Big/\left(\frac{d\sigma_\ell}{d\Omega}\right)_{\text{Th}} = \frac{1}{(1+x_\ell)^2} + \frac{x_\ell^2}{2(1+x_\ell)^3}\left(1 + \frac{8}{a_0^2}\frac{J_\ell^2}{\mathfrak{K}_\ell}\right) = 1 + O(x_\ell). \tag{C.55}$$

Again, Compton and Thomson results differ by terms of order $x_\ell$.

## C.4 The relation between long pulses and monochromatic infinite plane waves

In this section, the contact is made between long but finite laser pulses and the limit of infinite plane waves as discussed above. As an example, increasing the pulse length parameter $\Delta\phi$ (cf. Appendix A.3) from 20 to 50 to 100 does not lead to an accumulation of spectral weight at the non-linear Compton frequencies $\omega_\ell'(\theta)$ as could be expected naively, see Figure C.3. The number of sub-peaks increases but the average shape of the harmonic bunch is more or less the same for $\Delta\phi = 20$, 50 and 100 with the same spectral width. In fact, to obtain the limit of infinite plane waves in the sense of the preceding sections, it is not efficient to take simply the limit $\Delta\phi \to \infty$.

Taking the naive limit $\Delta\phi \to \infty$, i.e. keeping the shape of the pulse envelope unchanged, would correspond to switching on the laser infinitely slowly, i.e. an infinitely slow increase of the output power of the laser. This, however, will certainly not be a good description of a real laser. Realistically, the laser will reach its full amplitude within a few cycles of the carrier wave and then persist on that level. Thus, the single parameter model for laser pulses has limitations for very long pulse duration $\Delta\phi \to \infty$. For long laser pulses it is necessary to introduce a more detailed model for the laser pulse with more than one parameter, where one of the parameters describes the switching on and off of the pulse and a second parameter describes the length that the laser stays on its maximum, described by a flat-top pulse. The total pulse length now consists of the rise "time" $\Delta\phi_r$ and the
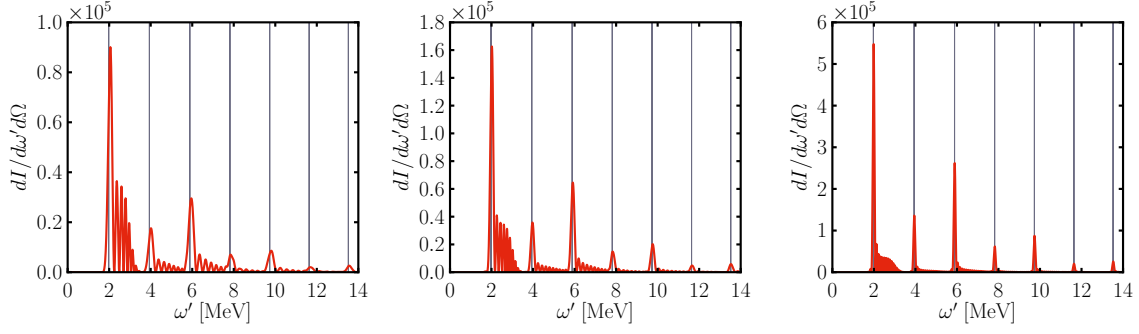
**Figure C.4:** Same as Figure C.3, but for a pulse with a central flat-top section as described in Eq. (C.56). The pulse length parameters are $\Delta\phi_f = 10$ (left), 20 (centre) and 50 (right). The edges of the pulse are sections of the Gaussian envelope with $\Delta\phi_r = 20$.

flat-top "time" $\Delta\phi_f$. The flat-top part of the pulse is parametrized as a box-shaped pulse $g_{\text{flat}}(\phi) = \Theta(\phi + \Delta\phi_f)\Theta(\Delta\phi_f - \phi) = \sqcap_{\Delta\phi_f}(\phi)$, with the Heaviside step function $\Theta(\phi)$. The rising and trailing edges of the pulse use the shifted single parameter pulses. Thus, the complete pulse is parametrized as

$$g(\phi; \Delta\phi_r, \Delta\phi_f) = g(\phi - \Delta\phi_f)\Theta(\phi - \Delta\phi_f) + \sqcap_{\Delta\phi_f}(\phi) + g(\phi + \Delta\phi_f)\Theta(-\phi - \Delta\phi_f).$$
$$(C.56)$$

The spectrum converges rather fast to sharp peaks centred at the non-linear Compton frequencies $\omega'_\ell(\theta)$ upon increasing $\Delta\phi_f$ from 10 to 20 and 50, as recognized in the three panels of Figure C.4, while keeping $\Delta\phi_r = 20$ constant.

# D

## Appendix D

# Gauge invariance of the matrix elements

Here, the gauge invariance of the matrix elements $\mathscr{M}$ for one- and two-photon Compton scattering is studied. A quantum gauge transformation is carried out by the transformation $\epsilon_i \to \epsilon_i + \Lambda_i k_i$, where $\epsilon_i$ is the polarization vector of any external photon line, $k_i$ is the corresponding four-momentum and $\Lambda_i$ is an arbitrary $c$-number. Writing the matrix element, involving $n$ external photons from the quantized radiation field, as

$$\mathscr{M} = \mathscr{M}_{\mu_1 \mu_2 \cdots \mu_n} \epsilon_1^{\mu_1} \epsilon_2^{\mu_2} \cdots , \tag{D.1}$$

one can reformulate the gauge invariance of the matrix element as

$$0 = \mathscr{M}_{\mu_1 \mu_2 \cdots} k_1^{\mu_1} \epsilon_2^{\mu_2} \cdots = \mathscr{M}_{\mu_1 \mu_2 \cdots} \epsilon_1^{\mu_1} k_2^{\mu_2} \cdots = \cdots . \tag{D.2}$$

These relations allow for a gauge invariant definition of non-convergent phase integrals, which appear in the calculation of the strong-field one-photon and two-photon $S$ matrix elements. One can also turn the argumentation around and use some prescription [Boc09, Sei11b] to make these integrals convergent and then check whether this procedure leads to a gauge invariant result. In either way, the gauge invariance of the matrix element is a strong constraint providing a sensitive test for the matrix elements since subtle cancellations occur.

There is another gauge transformation related to the external laser field via the transformation

$$\epsilon_+ \to \epsilon_+ + \Lambda k , \tag{D.3}$$

where $\epsilon_+$ denotes the polarization vector of the background laser field. Replacing $\epsilon_+$ by $k$, the transformed Volkov matrix functions $E_p(x)$ read

$$E_p(x; \epsilon_+ \to k) = \exp\{-ip \cdot x - ima_0 \mathrm{Re} \int d\phi g(\phi) e^{i(\phi + \hat{\phi})}\} , \tag{D.4}$$

where the non-linear phase function $f_p$ becomes independent of $p$. Thus, differences such as $f_p - f_{p'} = 0$, which always appear in the matrix elements, vanish. All matrix elements are invariant under the transformation (D.3) [Löt08].

## D.1   One-photon Compton scattering

The photon polarization vector of the outgoing photon $\epsilon'$ appears only in the Dirac coefficients $\mathscr{T}_n$. In the transformed Dirac coefficients, abbreviating $\mathscr{T}_n(\epsilon' \to k') \equiv \mathscr{T}_n^{\triangleright}$, one has to massively utilize ($i$) momentum conservation $k' = sk + p - p'$, ($ii$) the fact that the spinors $u_p$ are eigenvectors of $\not{p}$ with eigenvalue $m$, $\not{p}u_p = mu_p$, and ($iii$) the anticommutation relations of the Dirac matrices to obtain

$$\mathscr{T}_0^{\triangleright} = \bar{u}_{p'} \not{k}' u_p = \bar{u}_{p'} (\not{p} + s\not{k} - \not{p}') u_p = s\bar{u}_{p'} \not{k} u_p \,, \tag{D.5}$$

$$\mathscr{T}_{\pm}^{\triangleright} = \bar{u}_{p'} \Big[ d_{p'} \not{\epsilon}_{\pm} \not{k} (\not{p} - \not{p}') - d_p (\not{p}' - \not{p}) \not{k} \not{\epsilon}_{\pm} \Big] u_p = -\frac{\alpha_{\pm}}{2} \bar{u}_{p'} \not{k} u_p \,, \tag{D.6}$$

$$\mathscr{T}_2^{\triangleright} = \frac{m^2 a_0^2}{4} \frac{k \cdot k'}{k \cdot p \, k \cdot p'} \, \bar{u}_{p'} \not{k} u_p = -\beta \bar{u}_{p'} \not{k} u_p \,. \tag{D.7}$$

In summary, the transformed matrix element reads

$$\mathscr{M}^{\triangleright}(s) = \bar{u}_{p'} \not{k} u_p \left[ s\mathscr{A}_0(s) - \frac{\alpha_+}{2} \mathscr{A}_+(s) - \frac{\alpha_-}{2} \mathscr{A}_-(s) - \beta \mathscr{A}_2(s) \right] \overset{!}{=} 0 \tag{D.8}$$

and vanishes if and only if, for $s \neq 0$, the term in the square brackets vanishes. Thus, the phase integrals $\mathscr{A}_n(s)$ need to be related as

$$s\mathscr{A}_0(s) = \frac{\alpha_+}{2} \mathscr{A}_+(s) + \frac{\alpha_-}{2} \mathscr{A}_-(s) + \beta \mathscr{A}_2(s) \,, \tag{D.9}$$

which is precisely the relation (3.23). The requirement of gauge invariance leads to an unambiguous definition of the phase integral $\mathscr{A}_0$ in terms of the other phase integrals $\mathscr{A}_{\pm}$ and $\mathscr{A}_2$, thus reducing the number of independent integrals by one.

## D.2   Two-photon Compton scattering

The transformation will be considered only for photon "*2*"; for the other photon one proceeds analogously. In the following, the commutators

$$[\not{p}, X_p] = [\bar{X}_p, \not{p}] = ma_0 \not{\epsilon} - \alpha_p \not{k} \,, \tag{D.10}$$

$$[\bar{X}_p, \not{p}] X_{p'} = \bar{X}_{p'} [\not{p}, X_p] = 2\beta_{p'} \not{k} = \bar{X}_p \not{p} X_{p'} \,, \tag{D.11}$$

will be useful, where $\alpha_p = ma_0 (\epsilon \cdot p)/(k \cdot p)$, $\beta_p = m^2 a_0^2/(4 \, k \cdot p)$ and $X_p = \not{k} \not{\epsilon} \, ma_0/(2 \, k \cdot p)$ with the properties $\bar{X}_{p'} X_p = X_p \bar{X}_{p'} = 0$ and $\bar{X}_p = -X_p$. As an example, the transformation will be shown for the coefficient $\mathscr{U}_{00}$ of the direct channel (the left Feynman diagram in Figure 4.1), where the transformed quantities are again denoted as $\mathscr{U}_{00}^{\triangleright} \equiv \mathscr{U}_{00}(\epsilon_2 \to k_2)$ etc.,

$$\mathscr{U}_{00}^{\triangleright} = \bar{u}_{p'} \not{k}_2 G_1 \not{\epsilon}_1^* u_p = \bar{u}_{p'} (\not{Q}_1 - \not{p}' + (s - \ell_1)k) G_1 \not{\epsilon}_1^* u_p$$
$$= (s - \ell_1) \bar{u}_{p'} \not{k} G_1 \not{\epsilon}_1^* u_p \tag{D.12}$$

employing the energy momentum conservation $k_2 = p + sk - p' - k_1$ in the form $k_2 = Q_1 + (s - \ell_1)k - p'$ and introducing the abbreviation $Q_1 \equiv P_1 + \ell_1 k$ for the on-shell value of the propagator momentum, $\not{Q}_1^2 = Q_1^2 = m^2$, which has the property that $\not{Q}_1 G_1 = mG_1$, where $G_1 = \not{Q}_1 + m$. A more complicated example is the transformation of $\mathscr{U}_{20}$

$$\mathscr{U}_{20}^{\triangleright} = \bar{u}_{p'} \bar{X}_{p'} \not{k}_2 X_{P_1} G_1 \not{\epsilon}_1^* u_p$$
$$= \bar{u}_{p'} \bar{X}_{p'} (\not{P}_1 - \not{p}' + s\not{k}) X_{P_1} G_1 \not{\epsilon}_1^* u_p$$
$$= \bar{u}_{p'} \left( \bar{X}_{p'} \not{P}_1 X_{P_1} - \bar{X}_{p'} \not{p}' X_{P_1} \right) G_1 \not{\epsilon}_1^* u_p$$
$$= 2(\beta_{p'} - \beta_{P_1}) \bar{u}_{p'} \not{k} G_1 \not{\epsilon}_1^* u_p \,, \tag{D.13}$$

using the fact that $X_{P_1} = X_{Q_1}$, which can be verified by a direct evaluation. One notices that the Dirac structures which remain in $\mathscr{U}_{00}^\triangleright$ and $\mathscr{U}_{20}^\triangleright$, are equal, allowing for a possible mutual cancellation. The same statement holds true for $\mathscr{U}_{10}^\triangleright$. The coefficient $\mathscr{V}_0$ transforms as

$$
\begin{aligned}
\mathscr{V}_0^\triangleright &= \bar{u}_{p'} \slashed{k}_2 \slashed{k} \slashed{\epsilon}_1^* u_p \\
&= \bar{u}_{p'} (\slashed{Q}_1 + (s - \ell_1)\slashed{k} - \slashed{p}')\slashed{k} \slashed{\epsilon}_1^* u_p \\
&= \bar{u}_{p'} (\slashed{Q}_1 - m)\slashed{k} \slashed{\epsilon}_1^* u_p \\
&= -\bar{u}_{p'} \slashed{k} G_1 \slashed{\epsilon}_1^* u_p + 2k \cdot P_1 \bar{u}_{p'} \slashed{\epsilon}_1^* u_p \,.
\end{aligned}
\tag{D.14}
$$

This term transforms inhomogeneous, i.e. extra an term appears, which is not proportional to $\bar{u}_{p'} \slashed{k} G_1 \slashed{\epsilon}_1^* u_p$. With the definitions for the direct channel $\mathfrak{U}_n$ and the exchange channel $\mathfrak{U}_n^\times$

$$
\begin{aligned}
\mathfrak{U}_0 &= \bar{u}_{p'} \slashed{k} G_1 \slashed{\epsilon}_1^* u_p \,, & \mathfrak{U}_0^\times &= \bar{u}_{p'} \slashed{\epsilon}_1^* G_1 \slashed{k} u_p \,, \\
\mathfrak{U}_1 &= \bar{u}_{p'} \slashed{k} G_1 (\overline{X}_{P_1} \slashed{\epsilon}_1^* + \slashed{\epsilon}_1^* X_p) u_p \,, & \mathfrak{U}_1^\times &= \bar{u}_{p'} (\overline{X}_{P_1} \slashed{\epsilon}_1^* + \slashed{\epsilon}_1^* X_p) G_1 \slashed{k} u_p \,, \\
\mathfrak{U}_2 &= \bar{u}_{p'} \slashed{k} G_1 \overline{X}_{P_1} \slashed{\epsilon}_1^* X_p u_p \,, & \mathfrak{U}_2^\times &= \bar{u}_{p'} \overline{X}_{P_1} \slashed{\epsilon}_1^* X_p G_1 \slashed{k} u_p \,,
\end{aligned}
\tag{D.15}
$$

one can summarize the transformed coefficients

$$
\begin{aligned}
\mathscr{U}_{0n}^\triangleright &= (s - \ell_1)\mathfrak{U}_n \,, & \mathscr{U}_{0n}^{\triangleright\times} &= \ell_2 \mathfrak{U}_n^\times \,, \\
\mathscr{U}_{1n}^\triangleright &= (\alpha_{p'} - \alpha_{P_1})\mathfrak{U}_n \,, & \mathscr{U}_{1n}^{\triangleright\times} &= (\alpha_{P_2} - \alpha_p)\mathfrak{U}_n^\times \,, \\
\mathscr{U}_{2n}^\triangleright &= 2(\beta_{p'} - \beta_{P_1})\mathfrak{U}_n \,, & \mathscr{U}_{2n}^{\triangleright\times} &= 2(\beta_{P_2} - \beta_{p'})\mathfrak{U}_n^\times
\end{aligned}
\tag{D.16}
$$

and

$$
\begin{aligned}
\mathscr{V}_0^\triangleright &= -\mathfrak{U}_0 + 2k \cdot P_1 \bar{u}_{p'} \slashed{\epsilon}_1^* u_p \,, & \mathscr{V}_0^{\triangleright\times} &= \mathfrak{U}_n^\times - 2k \cdot P_2 \bar{u}_{p'} \slashed{\epsilon}_1^* u_p \,, \\
\mathscr{V}_1^\triangleright &= -\mathfrak{U}_1 + 2k \cdot P_1 \bar{u}_{p'} (\bar{X}_{p'} \slashed{\epsilon}_1^* + \slashed{\epsilon}_1^* X_p) u_p \,, & \mathscr{V}_1^{\triangleright\times} &= \mathfrak{U}_1^\times - 2k \cdot P_2 \bar{u}_{p'} (\bar{X}_{p'} \slashed{\epsilon}_1^* + \slashed{\epsilon}_1^* X_p) u_p \,, \\
\mathscr{V}_2^\triangleright &= -\mathfrak{U}_2 + 2k \cdot P_1 \bar{u}_{p'} \bar{X}_{p'} \slashed{\epsilon}_1^* X_p u_p \,, & \mathscr{V}_2^{\triangleright\times} &= \mathfrak{U}_2^\times - 2k \cdot P_2 \bar{u}_{p'} \bar{X}_{p'} \slashed{\epsilon}_1^* X_p u_p \,.
\end{aligned}
\tag{D.17}
$$

For the transformed matrix element (4.23), as the sum of the direct and the exchange channel one finds

$$
\begin{aligned}
\mathscr{M}^\triangleright = \; & \frac{1}{2k \cdot P_1} \sum_{n=0,1,2} \mathfrak{U}_n \Big[ -\mathscr{C}_n(s) - i\big\{ (s - \ell_1)\mathscr{B}_{0n}(s, \ell_1) + (\alpha_{p'} - \alpha_{P_1})\mathscr{B}_{1n}(s, \ell_1) \\
& \hspace{6cm} + 2(\beta_{p'} - \beta_{P_1})\mathscr{B}_{2n}(s, \ell_1) \big\} \Big] \\
& + \frac{1}{2k \cdot P_2} \sum_{n=0,1,2} \mathfrak{U}_n^\times \Big[ \mathscr{C}_n(s) - i\big\{ \ell_2 \mathscr{B}_{n0}(s, \ell_2) + (\alpha_{P_2} - \alpha_p)B_{n1}(s, \ell_2) \\
& \hspace{6cm} + 2(\beta_{P_2} - \beta_p )B_{n2}(s, \ell_2) \big\} \Big] \,,
\end{aligned}
\tag{D.18}
$$

where the inhomogeneous parts of the transformed coefficients $\mathscr{V}_n$ and $\mathscr{V}_n^\times$ have cancelled mutually between the direct and the exchange channel. The transformed matrix element is zero if and only if the all terms in square brackets vanish individually. With a similar result for the gauge transformation with respect to photon "*1*", one obtains the following relations between the phase integrals

$$
\begin{aligned}
(s - \ell_i)\mathscr{B}_{0n}(s, \ell_i) &= \;\; i\mathscr{C}_n(s) + (\alpha_{P_i} - \alpha_{p'})\mathscr{B}_{1n}(s, \ell_i) + 2(\beta_{P_i} - \beta_{p'})\mathscr{B}_{2n}(s, \ell_i) \,, \tag{D.19} \\
\ell_i \mathscr{B}_{n0}(s, \ell_i) &= -i\mathscr{C}_n(s) + (\alpha_p - \alpha_{P_i})\mathscr{B}_{n1}(s, \ell_i) + 2(\beta_p - \beta_{P_i})\mathscr{B}_{n2}(s, \ell_i) \,. \tag{D.20}
\end{aligned}
$$

This defines the non-convergent phase integrals which involve an index zero in a unique and gauge invariant way. In this way, the number of independent phase integrals is reduced from

12 to 6 in each channel. In particular, the definition of $\mathscr{B}_{00}$ requires two steps and is possible in two different ways, either $\mathscr{B}_{00} \to \mathscr{B}_{0l} \to \mathscr{B}_{nl}$ or $\mathscr{B}_{00} \to \mathscr{B}_{n0} \to \mathscr{B}_{nl}$, which are equivalent if additionally

$$s\mathscr{C}_0(s) = (\alpha_p - \alpha_{p'})\mathscr{C}_1(s) + 2(\beta_p - \beta_{p'})\mathscr{C}_2(s) \tag{D.21}$$

holds. It should be noted that a regularization in the spirit of [Boc09], where a convergence factor is introduced before the non-convergent integrals are integrated by parts to extract the divergence, gives exactly the same results (D.19) – (D.21).

# E
# The infrared behaviour of two-photon Compton scattering

IT is well known that the emission probabilities for soft photon Bremsstrahlung $\omega \to 0$ diverges logarithmically as [Jau76]

$$\int \frac{d\omega}{\omega} \sim \ln \omega \,. \tag{E.1}$$

The physical origin of this unfavourable behaviour of the perturbative iteration of the $S$ matrix is the separation of the emission of real Bremsstrahlung photons and soft virtual loop corrections to the same order in the coupling constant $\alpha$, which become indistinguishable in the long-wavelength limit. It is indeed the case that the infrared divergences in soft photon Bremsstrahlung and loop corrections cancel mutually. The Kinoshita-Lee-Nauenberg theorem [Mut87] states that the complete standard model is free of infrared divergences to arbitrary orders in perturbation theory. In quantum electrodynamics, the cancellations of infrared divergences are known as Bloch-Nordsieck theorem or Bloch-Nordsieck cancellations. (Note that the Bloch-Nordsieck cancellations fail in non-Abelian gauge theories due to additional collinear singularities [Mut87].) In the following it will be shown how these cancellations emerge in strong-field processes in the Furry picture when working with dressed electron states and propagators. In particular the two-photon Compton process will be discussed when one of the two emitted photons becomes soft. These soft photons have to be treated properly when calculating the inclusive two-photon spectra.

The general solution of the soft-photon divergence problem has been given by Bloch and Nordsieck very early [Blo37]: In any scattering process there is the possibility that a certain number of low energy photons escapes undetected, leading to an observable energy loss $\Delta E$. Typically, $\Delta E$ is identified with an experimental resolution scale or low-energy threshold of the detectors. The number of these low-energy photons is unobservable since real and virtual photons cannot be distinguished in the soft-photon limit. Rather it appears as a collective soft-photon effect, which vanishes as $\Delta E \to 0$. The method of Bloch and Nordsieck includes the emission of an arbitrary amount of low-energy photons of frequencies $\omega_r$ such that $\sum_r \omega_r \leq \Delta E$. They showed that the average number of emitted photons is infinite. So there is a reinterpretation of the divergent emission probability of a single low-frequency photon as the emission of infinitely many soft photons.

## E.1 Extracting the divergent part

In the following, the cancellation of infrared divergences will be exemplified for the two-photon Compton process. It is assumed that $\omega_1$ is the soft photon $\omega_1 \to 0$ and $\omega_2$ is the hard photon. Since it will be necessary to compare the $S$ matrix expression for two-photon Compton scattering and one-photon Compton scattering with radiative corrections, it will be useful to introduce the notation $S^{(m,n)}$, where $m$ denotes the number of emitted photons and $n$ stands for the number of loops. The $S$ matrix for the two-photon process reads [see Eq. (4.13)]

$$S^{(2,0)} = -ie^2(2\pi)^2 \int [ds][d\phi]\delta(p' + k_1 + k_2 - p - (s_1 + s_2)k)e^{is_1\phi_1 + is_2\phi_2}$$
$$\times \bar{u}_{p'}\mho^{\epsilon_2}_{p',P_1}(\phi_2)G_0(P_1 + s_1 k)\mho^{\epsilon_1}_{P_1 p}(\phi_1)u_p \; + \; (1 \leftrightarrow 2), \quad \text{(E.2)}$$

where the abbreviation $[ds]$ means integration over all remaining $s_j$; the same holds for $\phi$. The quantities $\mho^{\epsilon}_{P,p}(\phi)$ denote the dressed vertices, e.g.

$$\mho^{\epsilon_1}_{P_1,p}(\phi_1) = \bar{\Omega}_{P_1}(\phi_1)\slashed{\epsilon}_1^*\Omega_p(\phi_1). \quad \text{(E.3)}$$

In the soft photon limit, $\omega_1 \to 0$, one can safely take the limit $P_1 = p - k_1 \to p$ everywhere, except in the denominator of the propagator $G_0$. Thus, in the dressed vertex at which the soft-photon $\omega_1$ is emitted, the non-linear phases $f_{P_1} - f_p$ cancel exactly, yielding

$$e^{is_1\phi_1}\mho^{\epsilon_1}_{pp}(\phi_1) = (1 + \bar{X}_p a(\phi_1))\slashed{\epsilon}_1^*(1 + X_p a(\phi_1))e^{is_1\phi_1}$$
$$= e^{is_1\phi_1}\slashed{\epsilon}_1^* + e^{is_1\phi_1}a(\phi_1)[\bar{X}_p\slashed{\epsilon}_1^* + \slashed{\epsilon}_1^* X_p] + e^{is_1\phi_1}a^2(\phi_1)\bar{X}_p\slashed{\epsilon}X_p. \quad \text{(E.4)}$$

Upon integrating over $\phi_1$, a term $\propto \delta(s_1)$ is generated together with the Fourier transforms of $a$ and $a^2$, which have support in the vicinity of $s_1 = \pm 1$. The propagator has the structure

$$G_0(P_1 + s_1 k) \to \frac{\slashed{p} + s_1\slashed{k} + m}{-2p \cdot k_1 - 2s_1 k \cdot p + i\varepsilon}, \quad \text{(E.5)}$$

where one sees that the soft-photon divergence for $\omega_1 \to 0$ is screened by finite values of $s_1$. Hence, only for $s_1 = 0$ there is a contribute to the infrared-divergent part of the amplitude, singling out the delta contribution $\delta(s_1)$. The other contributions have vanishing measure at $s_1 = 0$. As a consequence, the dressed soft vertex turns into the free vertex

$$\mho^{\epsilon_1}_{P_1 p}(\phi_1) \to \slashed{\epsilon}_1^*. \quad \text{(E.6)}$$

As a result, the $S$ matrix for the emission of a soft photon with $\omega_1 \to 0$ reads

$$S^{(2,0)} = -ie^2(2\pi)^3 \int ds_2 d\phi_2\delta(p' + k_2 - p - s_2 k)e^{is_2\phi_2}$$
$$\times \bar{u}_{p'}\mho^{\epsilon_2}_{p',P_1}(\phi_2)\frac{\slashed{p} + m}{-2p \cdot k_1}\slashed{\epsilon}_1^* u_p \; + \; (1 \leftrightarrow 2). \quad \text{(E.7)}$$

With the (anti-)commutation relations for slashed expressions and the definitions of the spinors $u_p$ one finds $(\slashed{p}+m)\slashed{\epsilon}_1^* u_p = 2(p \cdot \epsilon_1^*)u_p$. With a similar result from the second Feynman diagram [denoted as $(1 \leftrightarrow 2)$], where the vertex with soft photon emission $\omega_1 \to 0$ is the second vertex next to the spinor $\bar{u}_{p'}$ (see Figure E.1), the total result for the $S$ matrix factorizes as

$$S^{(2,0)} = \beta(k_1)\, S^{(1,0)}(p \to p'k_2) \quad \text{(E.8)}$$
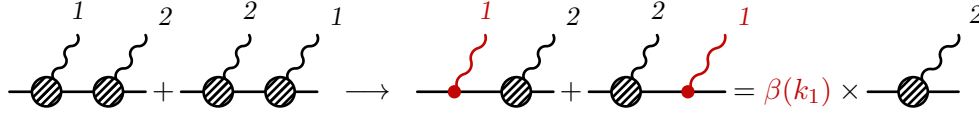
**Figure E.1:** Diagrammatic representation of the factorization of the soft-photon emission current. The label "*1*" is for the soft photon with momentum $k_1$ and $\omega_1 \to 0$. Soft virtual photon lines are depicted as red long-wavelength wavy lines. The dashed blobs denote the laser dressed vertices (cf. Figure 4.2)

with

$$\beta(k_1) = e\left(\frac{p' \cdot \epsilon_1^*}{p' \cdot k_1} - \frac{p \cdot \epsilon_1^*}{p \cdot k_1}\right) = \beta_\mu(k_1)\,\epsilon_1^{\mu*}\,, \tag{E.9}$$

and the $S$ matrix for one-photon Compton scattering $S^{(1,0)}$ using the above introduced notation. Thus, the infrared divergent part is factored out of the two-photon $S$ matrix as a gauge invariant classical current expression, which is quantified by the relation $k_1^\mu \beta_\mu(k_1) = 0$. A diagrammatic representation is given in Figure E.1. The appropriate emission probability diverges when one integrates over the phase space of $k_1$ with the Lorentz invariant measure $d^3\mathbf{k}_1/(2\pi)^2 2\omega_1$, yielding the logarithmic singularity of Eq. (E.1). The first and second term in the brackets of $\beta(k_1)$ in Eq. (E.9) can be interpreted [Pes95, Jau76] as final state and initial state Bremsstrahlung corrections to one-photon Compton scattering, respectively.

## E.2   Radiative corrections to one-photon Compton scattering

The infrared divergent parts encountered in the two-photon emission probability in the preceding subsection stemming from the divergent soft-photon phase space element are cancelled by soft virtual loop integrals, i.e. loop corrections of order $\alpha$ to one-photon Compton scattering. The corresponding Feynman diagrams are collected in Figure E.2. In particular, the vertex correction (a) and the external state self-energy corrections (b) and (c) contribute to the cancellation. In general, loop diagrams are infrared divergent if both ends of the photon line are attached to *external* charge lines [Yen61]. The vacuum polarization diagram of the outgoing hard photon does not contribute to the infrared divergence.

The vertex correction to the one-photon Compton scattering reads

$$S_{(a)}^{(1,1)} = e^3 \int d^4x d^4y d^4z\, \bar{\Psi}_{p'}(z)\gamma^\mu \mathcal{G}(z,y|A)\not\!\epsilon_2^* \mathcal{G}(y,x|A)\gamma^\nu \Psi_p(x)\mathcal{D}_{\mu\nu}(x-z)e^{ik_2 \cdot y} \tag{E.10}$$

with the free photon propagator

$$D_{\mu\nu}(x-z) = \int \frac{d^4k_1}{(2\pi)^4}\frac{g_{\mu\nu}}{k_1^2 + i0^+}e^{ik_1 \cdot (x-z)}\,. \tag{E.11}$$

Performing the spacetime and momentum integrations in the same manner as above one finds

$$S_{(a)}^{(1,1)} = e^3 \int \frac{d^4k_1}{k_1^2}\frac{[ds][d\phi]}{(2\pi)^3}\,\delta^4(p - p' - k_2 + (s_1 + s_2 + s_3)k)\,e^{i(s_1\phi_1 + s_2\phi_2 + s_3\phi_3)}$$
$$\times\, g_{\mu\nu}\,\bar{u}_{p'}\mathfrak{V}_{p',p'-k_1}^\nu(\phi_3)G_0(p' - k_1 - s_3 k)\mathfrak{V}_{p'-k_1,p-k_1}^{\epsilon_1}(\phi_2)$$
$$\times\, G_0(p - k_1 + s_1 k)\mathfrak{V}_{p-k_1,p}^\mu(\phi_1)u_p \tag{E.12}$$
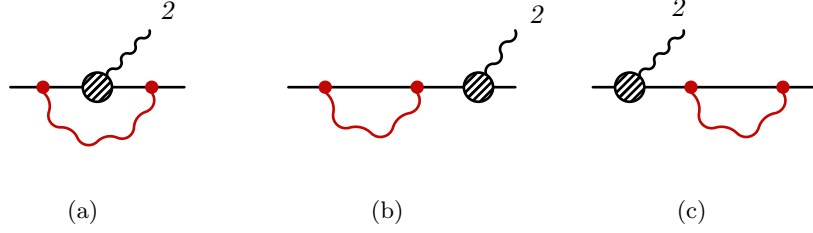
**Figure E.2:** Feynman diagrams for the radiative loop corrections of order $\alpha$ to one-photon Compton scattering which contribute to the cancellation of the infrared divergence in two-photon Compton scattering, namely the vertex correction (a) and the external state self-energy corrections (b) and (c). Soft virtual photon lines are depicted as red long-wavelength wavy lines.

with the dressed vertex functions

$$\mho^{\mu}_{p-k_1,p}(\phi_1) \equiv \bar{\Omega}_{p-k_1}(\phi_1)\gamma^{\mu}\Omega_p(\phi_1) \,, \tag{E.13}$$

etc. If one is only interested in the contributions from soft virtual photons with $\omega_1 \to 0$, then, as discussed above, one may neglect $k_1$ with respect to the electron momenta $p'$ and $p$ everywhere except for the denominators of the propagators. As a consequence (see discussion above), the two soft-photon dressed vertices turn into free vertices

$$\mho^{\mu}_{p-k_1,p}(\phi_1) \to \gamma^{\mu} \,, \tag{E.14}$$

$$\mho^{\nu}_{p',p'-k_1}(\phi_3) \to \gamma^{\nu} \,, \tag{E.15}$$

which are independent of $\phi_1$ and $\phi_3$, respectively, such that these integrations yield delta distributions $2\pi\delta(s_1)$ and $2\pi\delta(s_3)$. Using the equalities

$$G_0(p-k_1)\gamma^{\mu}u_p = -\frac{p^{\mu}}{k_1 \cdot p}u_p \,, \tag{E.16}$$

$$\bar{u}_{p'}\gamma_{\mu}G_0(p'-k_1) = -\frac{p'_{\mu}}{k_1 \cdot p'}\bar{u}_{p'} \tag{E.17}$$

the vertex correction factorizes as

$$S^{(1,1)}_{(a)} = \frac{ie^2}{(2\pi)^4}\int\frac{d^4k_1}{k_1^2+i0^+}\frac{p \cdot p'}{(k_1 \cdot p)(k_1 \cdot p')}S^{(1,0)} \,. \tag{E.18}$$

A direct calculation of the terms (b) and (c), which contribute to the wave function renormalization, would lead to undetermined expressions [Jau76]. These parts are calculated by using the cancellation of spurious charge renormalization [Yen61], that is

$$S^{(1,1)}_{(b)} = -\frac{1}{2}S^{(1,1)}_{(a)}(p' \to p) \,, \qquad\qquad S^{(1,1)}_{(c)} = -\frac{1}{2}S^{(1,1)}_{(a)}(p \to p') \,. \tag{E.19}$$

In the complete result for the one-loop one-photon Compton matrix element

$$S^{(1,1)} = V(k_1)\,S^{(1,0)} \tag{E.20}$$

one factors out the contribution from soft virtual photons

$$V(k_1) = -\frac{1}{2}\frac{ie^2}{(2\pi)^4}\int\frac{d^4k_1}{k_1^2+i0^+}\left(\frac{p'_{\mu}}{k_1 \cdot p'} - \frac{p_{\mu}}{k_1 \cdot p}\right)^2 \,. \tag{E.21}$$

Performing the integral over the time component $k_1^0$ first yields, by closing the contour in the lower half plane to pick up the pole at $k_1^0 = |\boldsymbol{k}_1| = \omega_1$ by means of the residue theorem

$$V(k_1) = \frac{1}{2} \frac{e^2}{(2\pi)^3} \int \frac{d^3\boldsymbol{k}_1}{2\omega_1} \left( \frac{p'_\mu}{k_1 \cdot p'} - \frac{p_\mu}{k_1 \cdot p} \right)^2 . \tag{E.22}$$

The cancellation of the infrared divergent parts occurs when taking into account the soft real and virtual photons together by calculating

$$\left| S^{(1,0)} + S^{(1,1)} \right|^2 + \sum_{\lambda_1} \int \frac{d^3\boldsymbol{k}_1}{(2\pi)^2 2\omega_1} \left| S^{(2,0)} \right|^2$$

$$= \left| S^{(1,0)} \right|^2 + 2\mathrm{Re}\left[ S^{*(1,1)} S^{(1,0)} \right] + \sum_{\lambda_1} \int \frac{d^3\boldsymbol{k}_1}{(2\pi)^3 2\omega_1} \left| S^{(2,0)} \right|^2$$

$$= \left| S^{(1,0)} \right|^2 \left[ 1 + 2V(k_1) - \int \frac{d^3\boldsymbol{k}_1}{(2\pi)^3 2\omega_1} \beta_\mu \beta^\mu \right] , \tag{E.23}$$

where the term in square brackets has exactly the same structure as in perturbative QED where the cancellation is ensured by the Bloch-Nordsieck theorem [Jau76]. It was shown that the laser dressed vertices of strong-field QED turn into the usual free vertices $\not{\epsilon}_i^*$, if the frequency of the photon emitted at that particular vertex goes to zero. This completes the discussion of the cancellation of infrared divergent parts of the two-photon Compton process in strong-field QED.

# Focused laser beams and finite electron distributions

I̲ᴛ is the objective of the present Appendix to evaluate the effects of realistic experimental set
ups, such as focused laser beams instead of plane waves, and electron distributions instead
of single electrons. This is necessary in view of a possible experimental verification of the
predicted short pulse effects in the non-linear Compton spectra. The aim is to study the
principal mechanisms due to the aforementioned non-ideal circumstances and their influence
on the spectra.

An important non-linear finite-size effect is the appearance of substructures in the one-
photon Compton frequency spectrum. An experimental verification of these substructures
would be of interest. Non-ideal conditions will lead to a reduction of the contrast of these
sub-peaks in the energy spectrum of non-linear Compton scattering. The parameters used
for numerical simulations are primarily for the combination ELBE linac [ELB] and DRACO
laser [Deb09] at the HZDR. This means, in all simulations the energy of the initial electrons
will be on the order of 40 MeV, thus, one is in the Thomson limit $\mathfrak{s} - m^2 \ll m^2$, where $\mathfrak{s}$
is the relevant centre-of-mass energy squared, and the study can be based on the classical
dynamics.

## F.1   Trajectories and optimized form of the current

The trajectories of electrons in plane electromagnetic waves have been discussed in Section 2.1,
where an analytical expression for the particle orbits has been given in Eqs. (2.7) and (2.8).
For general field configurations which are not plane waves, the trajectories are determined by
solving the eight coupled differential equations

$$\frac{dt}{d\tau} = \gamma(\tau)\,, \qquad\qquad \frac{d\gamma}{d\tau} = e\boldsymbol{u}(\tau) \cdot \boldsymbol{E}\big(\boldsymbol{x}(\tau), t(\tau)\big)\,,$$

$$\frac{d\boldsymbol{x}}{d\tau} = \boldsymbol{u}(\tau)\,, \qquad\qquad \frac{d\boldsymbol{u}}{d\tau} = e\Big[\gamma(\tau)\boldsymbol{E}\big(\boldsymbol{x}(\tau), t(\tau)\big) + \boldsymbol{u}(\tau) \times \boldsymbol{B}\big(\boldsymbol{x}(\tau), t(\tau)\big)\Big] \qquad \text{(F.1)}$$

with initial conditions $u^\mu(\tau = \tau_0) = u_0^\mu$, $x^\mu(\tau = \tau_0) = x_0^\mu$ yielding the particle orbits $x^\mu(\tau)$,
$u^\mu(\tau)$. These differential equations are solved numerically using the differential equation solver
`odeint` from the `scipy.integrate` package. The orbits are used afterwards to calculate the
photon spectral density (see Section 3.5)

$$\rho(k') = -\frac{\omega'}{16\pi^3} j^*(k') \cdot j(k') = \frac{\omega'}{16\pi^3} |\boldsymbol{n}' \times \boldsymbol{j}(k')|^2\,. \qquad\qquad \text{(F.2)}$$

For numerical evaluations of the radiation spectrum, the definition of the current (3.49) over the pre-exponential velocity is not the best choice. The constant velocity outside the interaction region contributes to the current and therefore also to the radiation spectrum, making the numeric integrations unstable.

An integration by parts, using a factor $e^{-\epsilon|\tau|}$ to ensure convergence at $\tau \to \pm\infty$ [Jac83], leads to a suitable form of the radiation integral, i.e. of the Fourier transformed current, which is proportional to the proper acceleration $\dot{u}^\mu$:

$$j^\mu(k') = ie \int d\tau \left( \frac{d}{d\tau} \frac{u^\mu}{k' \cdot u} \right) e^{ik' \cdot x} = ie \int d\tau \left[ \frac{\dot{u}^\mu}{k' \cdot u} - u^\mu \frac{k' \cdot \dot{u}}{(k' \cdot u)^2} \right] e^{ik' \cdot x} \,, \tag{F.3}$$

which is only non-zero if the electron acceleration is non-zero. The prefactor $i$ ensures the property $j^\mu(k')^* = j^\mu(-k')$; the transversality $k' \cdot j(k') = 0$ is manifest in this expression.

## F.2   Gaussian beams as model for focused laser beams

One is seeking a solution of the wave equation for the vector potential

$$\Box A_\mu(x) = 0 \,, \tag{F.4}$$

fulfilling the Lorenz gauge condition $\partial_\mu A^\mu = 0$, which incorporates a transverse profile describing a focused laser beam. This is taken into account by choosing the complex vector potential $A_\mu = (\Phi, \boldsymbol{A})$ with[1]

$$\boldsymbol{A} = A_0 \boldsymbol{\epsilon} \Psi(x_\perp, z) \, g(\phi) \, e^{i\phi} \,, \tag{F.5}$$

where the $z$-axis is designated as optical axis and the laser phase is $\phi = k \cdot x = \omega(t + z)$. The scalar potential $\Phi$ is determined via the Lorenz gauge condition $\partial_\mu A^\mu = 0$. Thus, the Lorenz gauge condition is fulfilled by construction [Dav79]. The polarization three-vectors are given by

$$\boldsymbol{\epsilon} \in \begin{cases} \{\boldsymbol{e}_x, \boldsymbol{e}_y\} & \text{for linear polarization}\,, \\ \{\boldsymbol{e}_+, \boldsymbol{e}_-\} = \{\frac{1}{\sqrt{2}}(\boldsymbol{e}_x + i\boldsymbol{e}_y), \frac{1}{\sqrt{2}}(\boldsymbol{e}_x - i\boldsymbol{e}_y)\} & \text{for circular polarization}\,, \end{cases} \tag{F.6}$$

and the transverse distance is $x_\perp \equiv (x^2 + y^2)^{1/2}$. Plugging the ansatz (F.5) in to the wave equation $\Box \boldsymbol{A}(x) = 0$ for the spatial parts of the vector potential, one obtains an equation for the transverse profile $\Psi(x_\perp, z)$

$$(\partial_z^2 + \triangle_\perp)\Psi + 2\omega(\partial_z\Psi)\left[i + \frac{g'}{g}\right] = 0 \tag{F.7}$$

with the transverse Laplacian $\triangle_\perp = \partial_x^2 + \partial_y^2$; primes denote derivatives with respect to the laser phase $\phi$. The paraxial approximation of this equation is obtained under the assumption that $\Psi$ changes only slowly along the $z$ direction, such that $|\partial_z^2\Psi| \ll |\partial_z\Psi|/\lambda$ [Trä07]. This assumption is equivalent to the assertion that all modes of the laser beam are propagating almost parallel, i.e. that the transverse momentum component ($k_\perp$, see below) is much smaller than the longitudinal momentum. One obtains the paraxial equation for the transverse profile $\Psi$ as [Trä07]

$$\triangle_\perp\Psi + 2i\omega(\partial_z\Psi)\left[1 - i\frac{g'}{g}\right] = 0\,. \tag{F.8}$$

---

[1]The physical fields are the real parts of the complex fields.

The standard Gaussian beam solution reads for $g = 1$, $g' = 0$ [Cha05, Dav79]

$$\Psi_0 = \frac{1}{1 + i\zeta} \exp\left\{ -\frac{x_\perp^2}{w_0^2(1 + i\zeta)} \right\} , \tag{F.9}$$

where a dimensionless longitudinal coordinate $\zeta = z/z_R$ is introduced. The Rayleigh length is defined as $z_R = w_0^2 \omega/2$ with focal spot radius ("waist") $w_0$. A more descriptive representation of the transverse profile reads

$$\Psi_0(x_\perp, z) = \frac{w_0}{w(z)} \exp\left\{ -\frac{x_\perp^2}{w(z)^2} \right\} \exp\left\{ i\phi_G - i\frac{\omega x_\perp^2}{2R(z)} \right\} , \tag{F.10}$$

when introducing the beam radius $w(z) = w_0\sqrt{1 + z^2/z_R^2}$, the curvature of the wave fronts $R(z) = z(1 + z_R^2/z^2)$ and the Guoy phase $\phi_G = \arctan z/z_R$. The Gaussian profiles $\Psi_0(x_\perp, z)$ (F.9) and (F.10) are solutions of the paraxial equation (F.8) supposed that the term containing the derivative of the pulse envelope is negligibly small [McD97]:

$$\left| \frac{g'}{g} \right| \ll 1 . \tag{F.11}$$

A Gaussian envelope function $g(\phi) = \exp(-\phi^2/2\Delta\phi^2)$ does not fulfil this condition, since $g'/g = -\phi/\Delta\phi^2$ is unbounded. For a hyperbolic secant pulse, $g(\phi) = 1/\cosh(\phi/\Delta\phi)$, the condition can be fulfilled for long pulses $\Delta\phi \gg 1$, as $|g'/g| = \Delta\phi^{-1}\tanh(\phi/\Delta\phi) < \Delta\phi^{-1}$ is bounded [Dav79, McD97]. But the situation is not as bad as suspected also for Gaussian envelopes, as $g'/g$ is small at the important centre of the pulse $|\phi| < \Delta\phi$, and the condition (F.11) is violated only at the periphery of the pulse which is rather insignificant. The Gaussian beam solution for $A_\mu$ can be derived in an alternative way, propagating the spectral field distribution $\tilde{A}_\mu(\omega, k_\perp, z = 0)$ from a given plane $z = 0$ to the whole spacetime [Har02]. In this approach, the vector potential at an arbitrary point $x^\mu$ is given by the application of the propagation operator

$$A_\mu(x) = \int \frac{dk_\perp d\omega}{(2\pi)^3} \tilde{A}_\mu(\omega, k_\perp, z = 0) e^{ik \cdot x} \tag{F.12}$$

with the photon mass shell condition $k^2 = k \cdot k = 0$ implying $k_z = \sqrt{\omega^2 - k_\perp^2}$. The spectral field distribution $\tilde{A}_\mu(\omega, k_\perp, z = 0)$ is obtained by Fourier transformation the local field distribution in the plane $z = 0$

$$\tilde{A}_\mu(\omega, k_\perp, z = 0) = \int dt dx_\perp e^{-i(\omega t - k_x x - k_y y)} A_\mu(t, x_\perp, z = 0) . \tag{F.13}$$

Equations (F.12) and (F.13) provide an exact solution for the wave equation (F.4) but the integral (F.12) is hard to solve in general.[2] The paraxial approximation in this formalism is implemented by approximating the mass shell condition $k^2 = 0$ as a Taylor expansion up to second order around $\boldsymbol{k}_\perp = 0$ (i.e. expanding around parallel modes), yielding $\sqrt{\omega^2 - k_\perp^2} \approx$

---

[2]To ensure the validity of a gauge condition in these calculations and the approximations done it must be implemented manifestly. For instance, for Coulomb gauge, $\boldsymbol{\nabla} \cdot \boldsymbol{A} = 0$, one should require $\boldsymbol{A} = \boldsymbol{\nabla} \times \boldsymbol{G}$ with an auxiliary field $\boldsymbol{G}$ such that the gauge condition is automatically fulfilled since $\boldsymbol{\nabla} \cdot (\boldsymbol{\nabla} \times \boldsymbol{G}) \equiv 0$. Since the wave operator $\Box$ commutes with the curl, it is clear that the vector potential $\boldsymbol{A}$ is a solution of the wave equation (F.7) if $\boldsymbol{G}$ satisfies the wave equation $\Box \boldsymbol{G} = 0$. The above mentioned evaluation of the propagation integral (F.12) and approximations thereof should be performed for the auxiliary field $\boldsymbol{G}$ [Har02]. For Lorenz gauge $\partial_\mu A^\mu = 0$, one should choose $A_\mu = \frac{1}{2}\epsilon_{\mu\nu\kappa\lambda}\partial^\nu G^{\kappa\lambda}$ with the auxiliary field $G^{\kappa\lambda}$.

$\omega - k_\perp^2/(2\omega)$. A decoupling of the $\omega$ and $k_\perp$ integrations is achieved upon approximating to leading order $\omega \simeq \omega_0$ in the denominator, where $\omega_0$ is the central frequency of the frequency distribution. With these approximations one obtains an equivalent Gaussian beam solution as provided in (F.9) and (F.10), but the condition $\omega \simeq \omega_0$ implies now $\Delta\phi \gg 1$, which is less restrictive than condition (F.11) since it only sets limits on frequency bandwidth of the pulse. A conclusion of these considerations is that ultra-short laser pulses in the single cycle regime with a large frequency bandwidth cannot be described appropriately within this paraxial approximation; more sophisticated approaches are needed.

The Gaussian beams $\Psi_0(x_\perp, z)$ in (F.9) and (F.10) represent the lowest order approximation in the diffraction angle $\theta_D \equiv w_0/z_R = 2\lambda/w_0$, for $\theta_D \ll 1$, where $\lambda = 1/\omega$ is the (reduced) laser wavelength. Making Eq. (F.7) dimensionless by introducing the scaled variables $z \to \zeta$ and $x_\perp \to \xi_\perp = x_\perp/w_0$ ($x \to \xi = x/w_0$, $y \to \nu = y/w_0$) one finds [Dav79]

$$\triangle_{\xi_\perp}\Psi + 4i\partial_\zeta + \theta_D^2 \partial_\zeta^2 \Psi = 0 \tag{F.14}$$

with the dimensionless transverse Laplacian $\triangle_{\xi_\perp} = \partial_\xi^2 + \partial_\nu^2$. The paraxial equation is obtained as leading order in the expansion in $\theta_D \ll 1$, i.e. for $w_0 \gg \lambda$. For a strongly focused beam, such that $\theta_D \sim \mathcal{O}(1)$, the intensity profile $\Psi_0$ has to be approximated by an expansion in powers of $\theta_D^2$ [Dav79, Sal02]

$$\Psi = \Psi_0 + \sum_{n=1}^{\infty} \theta_D^{2n}\Psi_{2n}\,, \tag{F.15}$$

which yields an iteration series

$$\triangle_{\xi_\perp}\Psi_{2n+2} + 4i\partial_\zeta\Psi_{2n+2} = -\partial_\zeta^2\Psi_{2n}\,, \qquad n = 0, 1, 2, \dots \tag{F.16}$$

if (F.15) is plugged into (F.14). Although the higher order terms $\Psi_2$, $\Psi_4$ are crucially important in some cases, such as for the vacuum acceleration of electrons [Sal02], no relevant corrections for the electron trajectories or the non-linear Compton photon spectrum associated with the (almost) head-on collisions of electrons with the laser pulse were found. Finally, the electric and magnetic fields are listed up to terms $\mathcal{O}(\theta_D^4)$ and the condition (F.11) imposed[3]

$$E_x/F = \epsilon_x + \theta_D^2\left[\epsilon_x\left(f^2\xi^2 - \frac{f^3\xi_\perp^2}{4}\right) + \epsilon_y f^2\nu\xi\right]\,, \tag{F.17}$$

$$E_y/F = \epsilon_y + \theta_D^2\left[\epsilon_y\left(f^2\nu^2 - \frac{f^3\xi_\perp^2}{4}\right) + \epsilon_x f^2\xi\nu\right]\,, \tag{F.18}$$

$$E_z/F = -i(\xi\epsilon_x + \nu\epsilon_y)\left(\theta_D f - \theta_D^3\left[\frac{f^2}{2} - f^3\xi_\perp^2 + \frac{f^4\xi_\perp^4}{4}\right]\right)\,, \tag{F.19}$$

$$B_x/F = \epsilon_y + \theta_D^2\epsilon_y\left[\frac{f^2\xi_\perp^2}{2} - \frac{f^3\xi_\perp^4}{4}\right]\,, \tag{F.20}$$

$$B_y/F = -\epsilon_x - \theta_D^2\epsilon_x\left[\frac{f^2\xi_\perp^2}{2} - \frac{f^3\xi_\perp^4}{4}\right]\,, \tag{F.21}$$

$$B_z/F = i(\epsilon_x\nu - \epsilon_y\xi)\left(\theta_D f + \theta_D^3\left[\frac{f^2}{2} + \frac{f^3\xi_\perp^2}{2} - \frac{f^4\xi_\perp^4}{4}\right]\right) \tag{F.22}$$

with $F = -i\omega A_0 g e^{i\phi}\Psi_0$, $f = (1 + i\zeta)^{-1}$ and the projections $\epsilon_{x,y} = \boldsymbol{\epsilon} \cdot \boldsymbol{e}_{x,y}$. This concludes the discussion of Gaussian beams as model for focused laser beams.

---

[3]These results have been obtained in collaboration with Thorger Sünert in 2009.
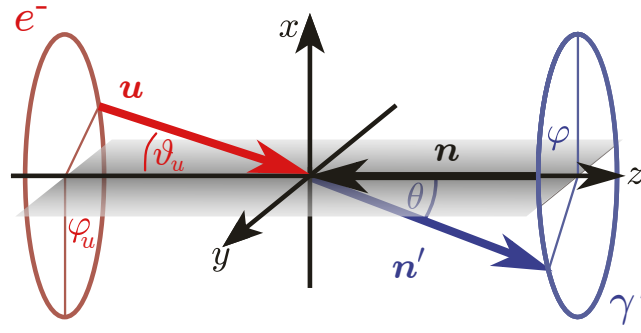
**Figure F.1:** Sketch of geometrical relations and the orientation of the coordinate system. The initial electron velocity is denoted by $\boldsymbol{u}$, while $\boldsymbol{n}$ is the direction of the laser and $\boldsymbol{n}'$ is the direction of the outgoing photon $\gamma'$.

## F.3  Electron phase space distributions

In collisions of a relativistic electron beams with the laser pulse, the frequency of a scattered photon reads $\omega'_\ell = \ell \chi \omega$, where

$$\chi(u, n', a_0) = \frac{n \cdot u}{n' \cdot u + \frac{a_0^2}{4 n \cdot u} n' \cdot n} \tag{F.23}$$

is the relativistic Doppler up-shift factor. It depends on three four-vectors: the laser propagation direction $n = (1, \boldsymbol{n})$, the direction of the outgoing photon $n' = (1, \boldsymbol{n}')$ and the four-velocity of the incoming electron $u = (\gamma, \boldsymbol{u})$, which can be parametrized as[4]

$$\boldsymbol{n} = (0, 0, -1), \tag{F.24}$$

$$\boldsymbol{n}' = (\sin\theta\cos\varphi \,, \sin\theta\sin\varphi \,, \cos\theta \,), \tag{F.25}$$

$$\boldsymbol{u} = \gamma v \,(\sin\vartheta_u \cos\varphi_u \,, \sin\vartheta_u \sin\varphi_u \,, \cos\vartheta_u \,), \tag{F.26}$$

where $\boldsymbol{n}$ is kept fixed and defines the orientation of the coordinate system. Here, the angles $(\vartheta_u, \varphi_u)$ and $(\theta, \varphi)$ measure the direction of incoming electrons and outgoing photons with respect to the $z$-axis, respectively. These geometric relations are exhibited in Figure F.1. With these definitions, the scalar products in (F.23) become

$$n \cdot n' = 1 + \cos\theta \,, \tag{F.27}$$

$$n \cdot u = \gamma(1 + v\cos\vartheta_u) = \kappa/\omega \,, \tag{F.28}$$

$$n' \cdot u = \gamma(1 - v\cos\bar\vartheta_u) \,, \tag{F.29}$$

$$\cos\bar\vartheta_u = \cos\vartheta_u \cos\theta + \sin\vartheta_u \sin\theta \cos(\varphi_u - \varphi) \,. \tag{F.30}$$

An electron bunch consists of $N_e$ electrons, associated with individual photon spectra $\rho_i(\omega', n'; \boldsymbol{x}^{(i)}, \boldsymbol{u}^{(i)})$, emitted by the $i$-th electron into the direction $n'$ with energy $\omega'$, which have to be added incoherently to obtain the total incoherent spectral density

$$\rho_W(\omega', n') = \sum_{i=1}^{N_e} \rho_i(\omega', n'; \boldsymbol{x}^{(i)}, \boldsymbol{u}^{(i)}) \,. \tag{F.31}$$

---

[4]With $v = \sqrt{\gamma^2 - 1}/\gamma$ being the electron velocity.

Following [Har02], this quantity is denoted "warm spectral density" $\rho_W$, referring to the finite energy distribution in an electron bunch.[5] The electrons of the bunch have a certain distribution in phase space $f(\boldsymbol{x}^{(i)}, \boldsymbol{u}^{(i)}, t_0)$, describing the distribution at a time $t_0$ prior to the interaction with the laser beam. The positions $\boldsymbol{x}^{(i)}$ and velocities $\boldsymbol{u}^{(i)}$ of the electron can be obtained as the output of an electron accelerator code (like PARMELA [You03, Har10] or TREDI [Gia99]) or can be modelled otherwise. Test particles or macroparticles can be used to sample the distribution functions, where the sum in Eq. (F.31) runs over an ensemble of macroparticles, each representing a certain number of real electrons [Fon09]. Assuming the factorization $f(\boldsymbol{x}^{(i)}, \boldsymbol{u}^{(i)}) = f_x(\boldsymbol{x}^{(i)}) f_u(\boldsymbol{u}^{(i)})$, i.e. neglecting intra-beam correlations, the spatial distribution $f_x(\boldsymbol{x}^{(i)})$ will be described by longitudinal and transverse distributions, e.g. by a Gaussian distribution with longitudinal ($L_b$) and transverse ($r_b$) beam size, respectively. The distribution in momentum space $f_u(\boldsymbol{u}^{(i)})$, however, is parametrized in terms of an energy spread and transverse emittance. According to [Har02] the former may be modelled by a distribution of the Lorentz factor $\gamma$ of width $\Delta\gamma$, centred at the nominal value $\gamma_0$, while the emittance measures the transverse phase space volume of the beam via the correlator

$$\varepsilon_x = \gamma_0 v_0 \sqrt{\langle x^2 \rangle \langle \pi_x^2 \rangle - \langle x\pi_x \rangle^2} \simeq \gamma_0 v_0 \, r_b \, \Delta\vartheta_u \tag{F.32}$$

for one transverse dimension. The expectation values $\langle \ldots \rangle$ refer to the transverse phase space distribution of the electron ensemble, usually taken to be as Gaussian as well. In addition, the normalized transverse momentum is defined as $\pi_x = |p_x/p_z| = \tan\vartheta_u \approx \vartheta_u$, which basically coincides with the injection angle $\vartheta_u$ with respect to the beam axis.

For a large number of electrons, it is more efficient to work with smooth electron phase space distribution functions [Har02]. The summation over an ensemble of test particles (F.31) is replaced by an integral over the distribution functions $f$ as

$$\rho_W(k') = N_e \int d^3x \, d\gamma \, d\vartheta_u \, d\varphi \, f_x(\boldsymbol{x}) f_u(\gamma, \vartheta_u, \varphi_u) \, \rho(k'; \boldsymbol{x}, \boldsymbol{u}(\gamma, \vartheta_u, \varphi_u)) \,. \tag{F.33}$$

Here, the normalized distribution functions in momentum space are parametrized in a factorized form as $f_u(\gamma, \vartheta_u, \varphi_u) = f_1(\gamma) \, f_2(\vartheta_u) \, f_3(\varphi_u)$, to be taken as a product of a Gaussian distribution being a function of $\gamma$, a $\chi$-distribution (with 2 degrees of freedom) for the $\vartheta_u$ dependence and a uniform distribution with respect to $\varphi_u$:

$$f_1(\gamma) = \frac{1}{\sqrt{2\pi}\Delta\gamma} \exp\left\{ -\frac{(\gamma - \gamma_0)^2}{2(\Delta\gamma)^2} \right\} \,,$$

$$f_2(\vartheta_u) = \frac{\vartheta_u}{(\Delta\vartheta_u)^2} \exp\left\{ -\frac{\vartheta_u^2}{2(\Delta\vartheta_u)^2} \right\} \,,$$

$$f_3(\varphi_u) = \frac{1}{2\pi} \,. \tag{F.34}$$

Hereby, the electron beam is assumed to be axially symmetric with both transverse components $u_{x0}$ and $u_{y0}$ being normally distributed and uncorrelated. For the distributions it is required that the inequalities $\gamma_0 \gg 1$, $\Delta\gamma \ll \gamma_0$ and $\Delta\vartheta_u \ll \pi/2$ hold; these constraints are usually fulfilled for relativistic electron beams.

## F.4   Ponderomotive scattering

An important effect of the transverse beam profile is the ponderomotive force $\boldsymbol{F}_p = -\boldsymbol{\nabla}U_p$ with the ponderomotive potential $U_p = e^2 \boldsymbol{A}^2/2m^2$ pushing the electrons away from regions of

---

[5]In [Har02], the warm and cold spectral brightness is discussed, which is proportional to the spectral density.
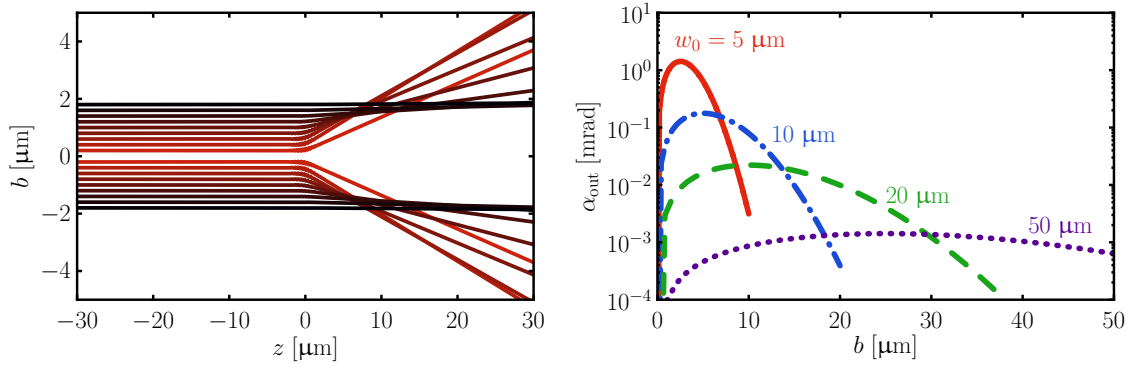
**Figure F.2:** Left panel: The effect of the ponderomotive force: A bunch of trajectories colliding head-on with the laser pulse, i.e. zero injection angle, are ejected with an angle $\alpha_{\text{out}}$ after the interaction with the laser pulse depending on the impact parameter $b$. Right panel: The scattering angle $\alpha_{\text{out}}$ as a function of $b$ for different focal waists $w_0$. For laser parameters see the text.

high intensity as they gain transverse momentum [McD86]. (For the theory of ponderomotive scattering in intense laser fields see also [Sal97, Nar00, Nar05].) For an estimate of the effect, the momentum space distribution is taken now as $f_u = \delta(\gamma - \gamma_0)\delta(\vartheta_u)\delta(\varphi_u)$. Accordingly, all electrons have velocities $\boldsymbol{u}_0 \parallel \boldsymbol{e}_z$ before the interaction with the laser beam. They will leave the interaction region under angles $\alpha_{\text{out}}$ with respect to the $z$ axis. For fixed total laser pulse energy $\mathcal{W}_{\text{tot}}$ and laser pulse length[6] $T_0$, the magnitude of the ponderomotive force scales as $|\boldsymbol{F}_p| \propto \mathcal{W}_{\text{tot}}/(T_0 w_0^3) \propto \max(\alpha_{\text{out}})$. This is since $\boldsymbol{A}^2$ is proportional to the energy density $\mathcal{W}_{\text{tot}}/V$ in the typical volume $V \propto T_0 w_0^2$, and the transverse gradient is $\propto 1/w_0$. That means, the ponderomotive force leads to significant effects only for small waist size $w_0$, with a dependence $\propto w_0^{-3}$.

To quantify the effect, electron trajectories corresponding to head-on collisions for different impact parameters $b = x_\perp$ have been simulated by solving numerically the system of differential equations (F.1). Several trajectories are exhibited in the left panel of Figure F.2, showing the dependence of the deflection angle $\alpha_{\text{out}}$ on the impact parameter $b$. In the right panel of Figure F.2, the deflection angle $\alpha_{\text{out}}$ is shown as a function of the impact parameter $b$ for different values of $w_0$. For $w_0 = 5$ μm the maximum deflection angle for 40 MeV electrons (total pulse energy $\mathcal{W}_{\text{tot}} = 3$ J, $T_0 = 20$ fs and laser frequency $\omega = 1.5$ eV) is about 1 mrad. For 10 μm the maximum of $\alpha_{\text{out}}$ is roughly one order of magnitude lower [Hei10b, DP12] and it further decreases for increasing values of $w_0$. This is small compared to the typical angular scale of the emitted radiation which is of order $1/\gamma_0 \sim 12$ mrad. The numerically calculated values of the maximum scattering angle agree well with the scaling $\max(\alpha_{\text{out}}) \propto w_0^{-3}$.

## F.5   Photon spectrum in pulsed focused laser fields: beam size effects

Now, the interplay of the spatial size of the electron bunch and laser focus is to be studied. Again, the laser pulse is taken to have a total energy of $\mathcal{W}_{\text{tot}} = 3$ J and pulse length of $T_0 = 20$ fs with a central frequency of $\omega = 1.5$ eV with different values of the focal waist $w_0$ determining the values of the parameter $a_0$. These parameters refer to the DRACO laser [Deb09] at the HZDR. The electron bunch — in this section the momentum space distribution

---

[6]In this Appendix the definition of $T_0$ is specified as $\omega T_0 \equiv \int_{-\infty}^{\infty} g(\phi)d\phi = \nu_1[g]\Delta\phi$, see Table A.1 for the explicit values of $\nu_1[g]$ for various pulse shapes.
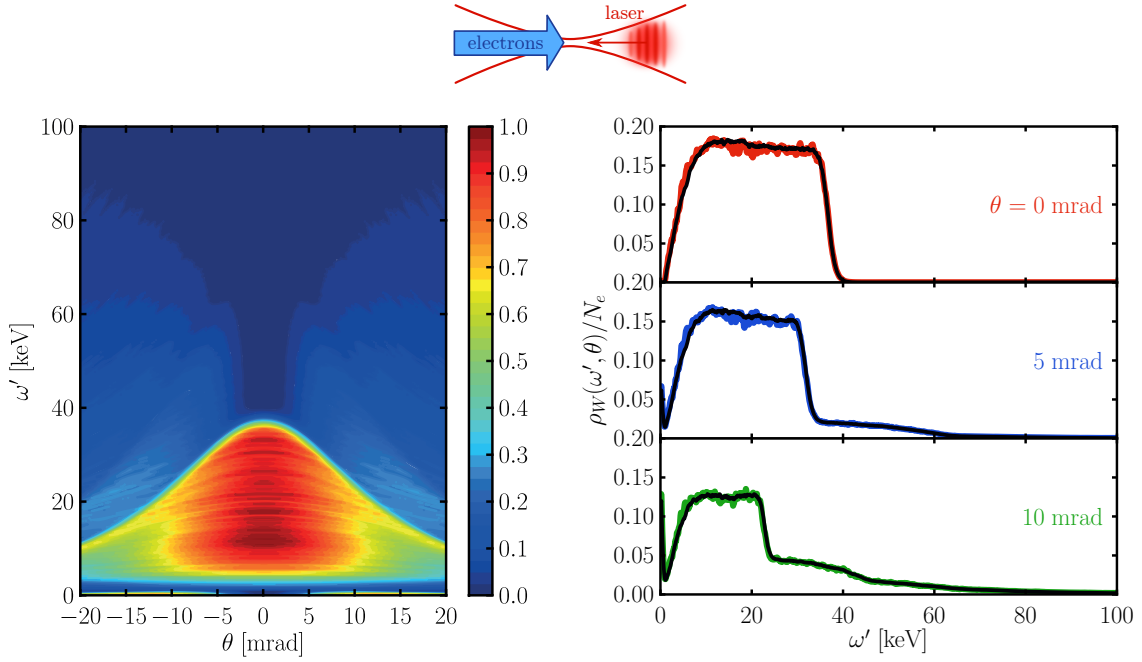
**Figure F.3:** Left: Contour plot of the normalized warm spectral density $\rho_W(\omega', \theta)/N_e$ as a function of the frequency $\omega'$ and scattering angle $\theta$. A dilute electron bunch (represented by $N_e = 1000$ test particles) collides head-on with a strongly focused ($w_0 = 5\,\mu\mathrm{m}$) and linearly polarized laser pulse. Right: The warm spectral density $\rho_W(\omega', \theta)/N_e$ as a function of $\omega'$ for constant values $\theta$. The coloured curves are cuts through the contour plot at the corresponding scattering angle. The black curves in each panel correspond to a second calculation with a larger set of $N_e = 10000$ test particles.
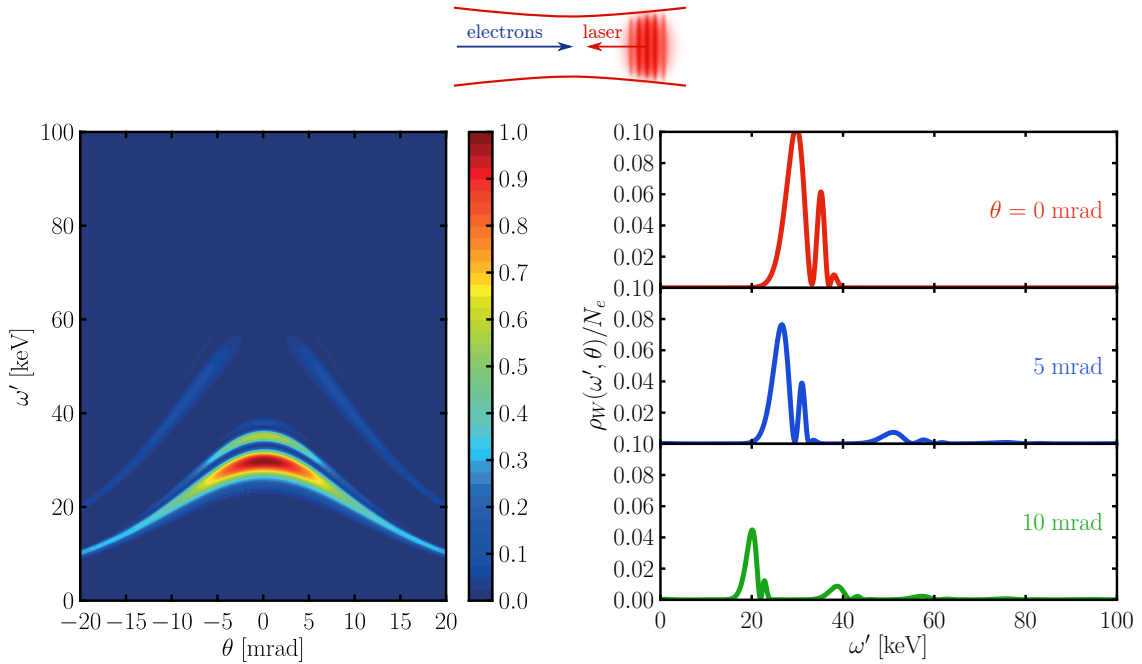


**Figure F.4:** Same as Figure F.3 but for $w_0 = 50\,\mu\mathrm{m}$.
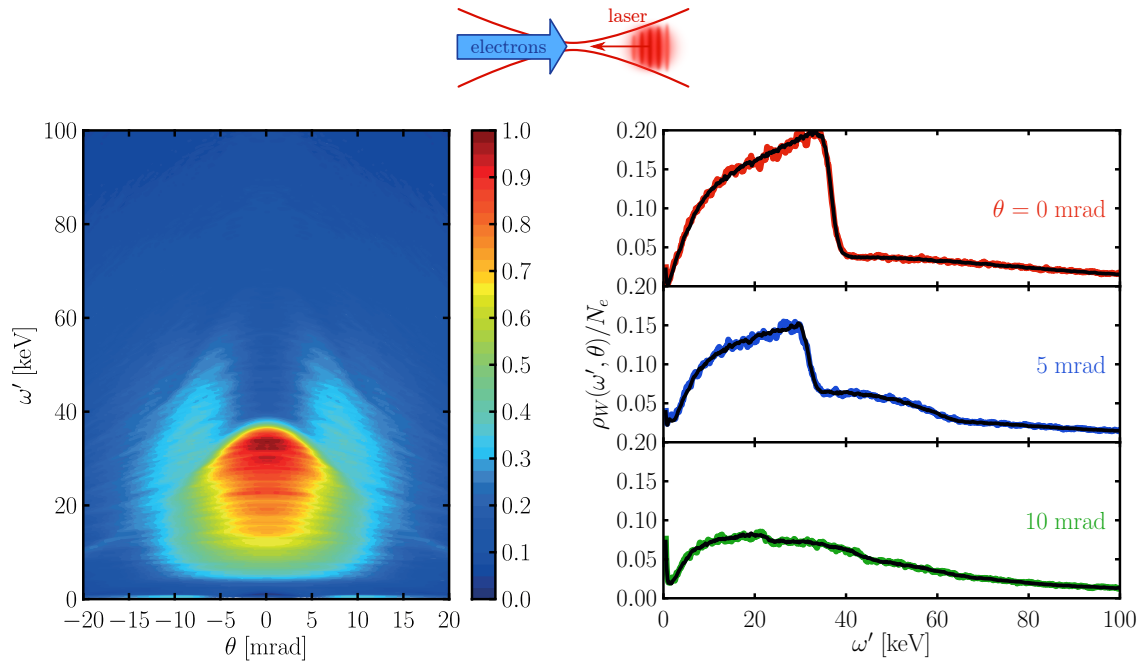
**Figure F.5:** Same as Figure F.3 but for linear laser polarization.
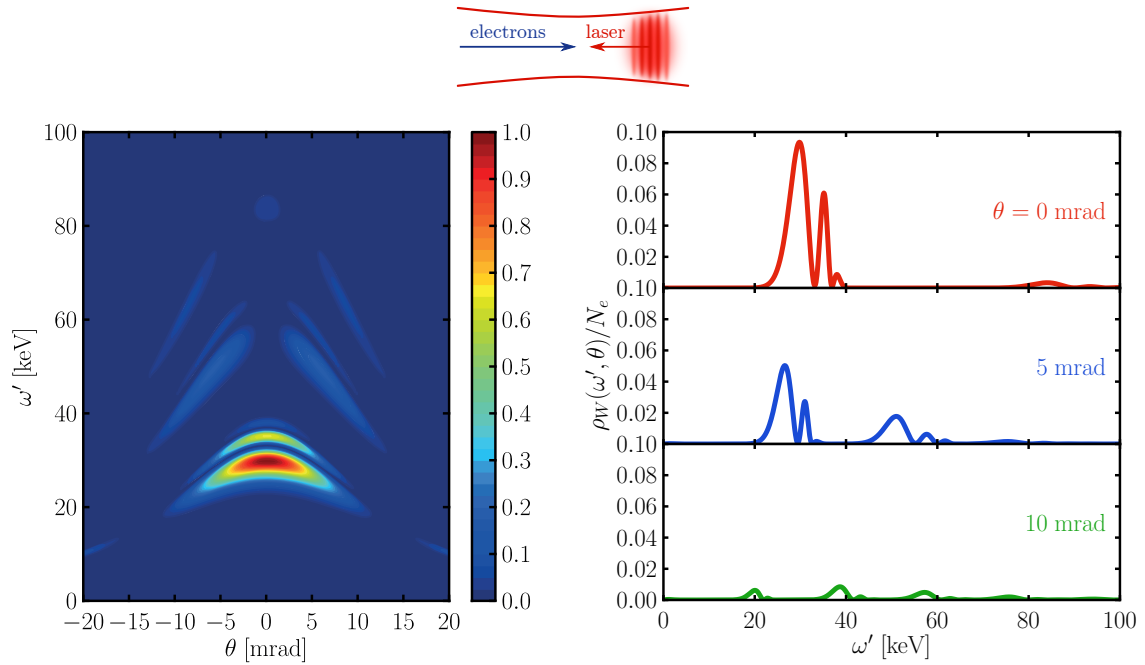


**Figure F.6:** Same as Figure F.3 but for linear laser polarization and $w_0 = 50\,\mu m$.

is taken to be $f = \delta(\gamma - \gamma_0)\delta(\vartheta_u)\delta(\varphi_u)$ as in the previous Section F.4 — is modelled by a Gaussian with a bunch length of $L_b = 300$ µm and a transverse beam size of $r_b = 5$ µm and energy $m\gamma_0 = 40$ MeV corresponding to the ELBE linac [ELB, Arn08, Deb09]. The bunch is approximated by $N_e = 1000$ test particles.

Figure F.3 (Figure F.5) shows the spectrum $\rho_W(\omega', \theta)$ of Compton scattered photons for $\varphi = 0$ for a circularly (linearly) polarized and tightly focused laser with $w_0 = 5$ µm and a corresponding Rayleigh length of $z_R \simeq 100$ µm. Given the total pulse energy $\mathcal{W}_{\text{tot}}$, pulse length $T_0$ and focus waist $w_0$, the peak value of the laser intensity is calculated as $I = 1.5 \times 10^{20}$ W/cm$^2$ yielding the normalized amplitude $a_0 = 8.6$, which is clearly in the non-linear regime. The associated red-shifted non-linear Compton edge is approximately at 1 keV, cf. (F.23). The normalized spectral density is shown as a function of the frequency $\omega'$ and scattering angle $\theta$ in the left panel. The dead cone for circular polarization, i.e. the lack of radiation in the backscattering direction $\theta = 0$ above 40 keV, is clearly visible in Figure F.3. In the right panels, cuts through the spectrum $\rho_W/N_e$ as a function of $\omega'$ are exhibited for various scattering angles $\theta = 0$ (top), 5 (middle) and 10 mrad (bottom). Due to the strong field gradients of the laser beam in both transverse and longitudinal directions, the spectrum is fairly broad for the parameter values chosen. The individual harmonics can not be recognized since the individual spectral lines are overlapping. It seems fair to describe the scattered photons as a broad continuum. The fluctuations are due to the rather small number of test particles; they would vanish upon increasing $N_e$. Indeed, the black curves in the right panels, corresponding to a larger set of $N_e = 10000$ test particles, are much smoother than the coloured curves for $N_e = 1000$ test particles.

In comparison, Figure F.4 (Figure F.6) shows the backscattered spectrum for the same pulse as before (3 J, $T_0 = 20$ fs) for circular (linear) polarization, but with a larger focal radius of $w_0 = 50$ µm corresponding to a Rayleigh length of $z_R \simeq 10$ mm. The maximum value of the normalized amplitude is $a_0 = 0.86$ in this case, which corresponds to a peak laser intensity of $I = 1.5 \times 10^{18}$ W/cm$^2$. The corresponding non-linear Compton edge is at 27.5 keV. The electron beam has the same transverse beam size $r_b$ and bunch length as above, so that the electron bunch exclusively probes the very centre of the focus where the laser intensity is almost constant. In fact, at $r_b = 5$ µm $= w_0/10$ the field intensity is only 1% lower than at the centre of the focus. In contrast to Figure F.3, the harmonics are now well-separated and clearly visible and also the sub-peaks in the harmonics are observable.

The result of this section is two-fold: To achieve a possible observation of the harmonics in non-linear Compton scattering in the energy spectra, ($i$) the spatial ponderomotive scattering must be minimized and ($ii$) all electrons in the bunch contributing to the radiation need to experience the same intensity. As a consequence, it is necessary to have a large focus with low field gradients which scale as $1/w_0$ [to fulfil condition ($i$)], and the transverse electron bunch radius $r_b$ should be much smaller than the laser beam waist $w_0$ to fulfil ($ii$). The possibility to fulfil ($i$) is directly limited by the available energy per laser pulse since $a_0^2 \sim \mathcal{W}_{\text{tot}}/(T_0 w_0^2)$, but in order to observe the harmonics and their sub-peaks one needs high intensity, i.e. $a_0 \sim 1$, and a suitable value for the ponderomotive phase shift determining the number of sub-peaks $N_{\text{S-P}} \propto T_0 a_0^2$. Condition ($ii$) implies that the radiation process can be described by a plane-wave model for the laser pulse.

## F.6   A scaling law for the spectral density

For the following it is assumed that the laser waist size $w_0$ is much larger than the electron beam radius, $w_0 \gg r_b$, so that the electron beam interacts only with the central part of the laser focus. In this case, the laser beam may be reasonably described by a pulsed plane

wave in the relevant interaction region [Tom05] and it is not necessary to model the spatial distribution of the electron bunch. One may thus concentrate on energy spread and emittance. In line with this, the momentum space distribution $f_u$ will be denoted simply by $f$ from now on.

According to (F.2) and (F.3) the one-particle spectral density $\rho(\omega'; n', u_0)$ depends on the initial conditions $u_0$ through the orbit $x^\mu(\tau; u_0)$ and the velocity $u^\mu(\tau; u_0)$. The posed problem is how the spectral density changes when changing the initial conditions $\boldsymbol{u}_0 = \boldsymbol{u}_0(\gamma_0, \vartheta_{u0}, \varphi_{u0})$ to different initial conditions, e.g. $\boldsymbol{u}(\gamma, \vartheta_u, \varphi_u)$. This change of initial conditions can be mediated by a Lorentz transformation $\Lambda$ applied to $u_0$ [Hei10b]. As a motivation, consider the most simple case first, namely backscattering and a head-on collision $\boldsymbol{u} \parallel \boldsymbol{u}_0 \parallel \boldsymbol{n}' \parallel \boldsymbol{n}$, implying a change only in the electron energy, $\gamma_0$ to $\gamma$ (as $\vartheta_u = \varphi_u = \theta = \varphi = 0$). This means that $u_0^\mu = (\gamma_0, 0, 0, v_0\gamma_0)$ changes to $u^\mu = (\gamma, 0, 0, v\gamma)$. In this case, the spectral density obeys the scaling relation

$$\rho(\omega', \gamma) = \rho(\omega'/h, \gamma_0) \tag{F.35}$$

with a rescaled frequency $\omega'/h$ where $h = \chi(u, n', a_0)/\chi(u_0, n', a_0)$ with the Doppler boost factor $\chi$ from Eq. (F.23).

If one also allows for a change of the direction of $\boldsymbol{u}$, the height of the spectral peak will certainly change, since the radiated intensity is peaked in the direction of $\boldsymbol{u}$. Thus, one has to use the modified scaling ansatz $\rho(\omega'; n', u) = \mathcal{M}(u, u_0)\rho(\omega'/h; n', u_0)$ with a transition function $\mathcal{M}(u, u_0)$ depending on both sets of initial conditions. The transition function $\mathcal{M}$ is derived from the electron current $\boldsymbol{j}$ in the limit $a_0 \ll 1$. Afterwards, the result is continued to arbitrary $a_0 \sim 1$ by substituting the appropriate Doppler shift factors $\chi$. The initial conditions enter the spectral density $\rho$ via the current

$$\boldsymbol{j}(k') = e \int d\tau\, \boldsymbol{u}(\tau; u_0) e^{ik' \cdot x(\tau; u_0)} \,. \tag{F.36}$$

Linearizing the orbit expressions $u^\mu(\tau)$ and $x^\mu(\tau)$ [cf. Eqs. (2.7) and (2.8)] in the gauge field $a_\mu = eA_\mu/m$,

$$u^\mu(\tau; u_0) = u_0^\mu - a^\mu + n^\mu \frac{a \cdot u_0}{n \cdot u_0} \,, \tag{F.37}$$

$$x^\mu(\tau; u_0) = x_0^\mu + u_0^\mu \tau - \int_0^\tau d\tau' a^\mu(\tau') + n^\mu \int_0^\tau d\tau' \frac{a(\tau') \cdot u_0}{n \cdot u_0} \,, \tag{F.38}$$

the linearized electron current (F.36) becomes, to $O(a)$,

$$\boldsymbol{j}(\omega', n', u_0) = e \int d\tau \left[ \frac{a(\tau) \cdot u_0}{n \cdot u_0} \boldsymbol{n} - \boldsymbol{a}(\tau) \right.$$

$$\left. + i\boldsymbol{u}_0 \left( k' \cdot n \int_0^\tau d\tau' \frac{a(\tau') \cdot u_0}{n \cdot u_0} - \int_0^\tau d\tau' a(\tau') \cdot k' \right) \right] e^{ik' \cdot u_0 \tau} \,. \tag{F.39}$$

Since this expression is linear in the vector potential $a_\mu$, one can work with a complex-valued vector potential with $a = (0, \boldsymbol{a})$ and $\boldsymbol{a} = a_0 \boldsymbol{\epsilon} e^{-i\phi} g(\phi)$ with polarization vectors $\boldsymbol{\epsilon}$ as in (F.6). The inner integral over $\tau'$ in (F.39) yields, after an integration by parts,

$$\int_0^\tau d\tau' a^\mu(\tau') = \frac{i}{\kappa} a^\mu(\tau) \left( 1 + \mathcal{O}(\Delta\phi^{-1}) \right), \tag{F.40}$$

where $\kappa = k \cdot u_0$ is the light-cone variable (see Section 2.1). For sufficiently long pulses, $\Delta\phi \gg 1$, the contribution $\mathcal{O}(\Delta\phi^{-1})$ can be neglected. Within these approximations, the result for the electron current reads

$$\boldsymbol{j}(\omega') = -\frac{ea_0}{n \cdot u_0} \tilde{g}\left(\omega - \frac{\omega'}{\chi(u_0, n', 0)}\right) \boldsymbol{j}_0 \tag{F.41}$$

with $\tilde{g}$ being the Fourier transform

$$\tilde{g} = \int d\phi\, g(\phi) e^{-i\phi\left(\omega - \omega' \frac{n' \cdot u_0}{n \cdot u_0}\right)}, \tag{F.42}$$

where the proper time integration has been replaced by an integration over the laser phase $\phi$ employing the relation $\phi = \kappa\tau = \omega(n \cdot u_0)\tau$. The constant vector part of the current reads

$$\boldsymbol{j}_0 = \boldsymbol{\epsilon} + \boldsymbol{n}\frac{\boldsymbol{\epsilon} \cdot \boldsymbol{u}_0}{n \cdot u_0} + t\boldsymbol{u}_0\big\{\boldsymbol{\epsilon} \cdot \boldsymbol{n}'(n \cdot u_0) - n \cdot n'(\boldsymbol{\epsilon} \cdot \boldsymbol{u}_0)\big\} \tag{F.43}$$

with $t = \frac{\omega'}{\omega(n \cdot u_0)^2}$. Using (F.2) the spectral density becomes

$$\rho(\omega', n'; u_0) = \frac{e^2 a_0^2}{16\pi^3} \frac{\omega'}{(n \cdot u_0)^2} \left|\tilde{g}\left(\chi(u_0, n', 0)\omega - \omega'\right)\right|^2 \left|\boldsymbol{n}' \times \boldsymbol{j}_0\right|^2. \tag{F.44}$$

Upon evaluating the two-fold cross product $|\boldsymbol{n}' \times \boldsymbol{j}_0|^2$ one arrives at an expression which is cumbersome and therefore not noted here explicitly for general geometries. One particularly interesting limit for $|\boldsymbol{n}' \times \boldsymbol{j}_0|^2$ is the backscattering geometry with $\boldsymbol{n}' \cdot \boldsymbol{n} = -1$ and $\boldsymbol{n}' \cdot \boldsymbol{\epsilon} = 0$, yielding, with $(\boldsymbol{n}' \times \boldsymbol{a}) \cdot (\boldsymbol{n}' \times \boldsymbol{b}) = \boldsymbol{a} \cdot \boldsymbol{b} - (\boldsymbol{n}' \cdot \boldsymbol{a})(\boldsymbol{n}' \cdot \boldsymbol{b})$,

$$\left|\boldsymbol{n}' \times \boldsymbol{j}_0\right|^2 = 1 + 4t^2|\boldsymbol{\epsilon} \cdot \boldsymbol{u}_0|^2(u_0^2 - (n \cdot u_0)^2) - 4t|\boldsymbol{\epsilon} \cdot \boldsymbol{u}_0|^2, \tag{F.45}$$

which is discussed also in [Hei10b]. Another limit is the case where the photon is scattered into the direction of the incoming electron, i.e. $\boldsymbol{n}' \parallel \boldsymbol{u}$. The latter case yields the particularly simple result

$$|\boldsymbol{n}' \times \boldsymbol{j}_0|^2 = 1 + |\boldsymbol{\epsilon} \cdot \boldsymbol{n}'|^2\big\{\nu^2 - (1 + \nu\boldsymbol{n} \cdot \boldsymbol{n}')^2\big\} \tag{F.46}$$

with

$$\nu = \frac{v}{1 + v\cos\vartheta_u}. \tag{F.47}$$

The high symmetry of this special case is the reason for this short expression. The form of $\tilde{g}$ in (F.44) lends support to the scaling behaviour of the frequency adopted in (F.35). On changing the geometry, $u_0 \to u$, $n_0' \to n'$ and simultaneously replacing the frequency, $\omega' \to h\omega'$, with $h = \chi(u, n', 0)/\chi(u_0, n_0', 0)$, the function $\tilde{g}$ remains invariant. With this, the scaling relation is found to be

$$\rho(\omega'; n', u) = \mathcal{M}(u, u_0; n', n_0')\rho(\omega'/h; n_0', u_0) \tag{F.48}$$

with the transition function

$$\mathcal{M}(u, u_0; n', n_0') = h\frac{(n \cdot u_0)^2}{(n \cdot u)^2} \frac{|\boldsymbol{n}' \times \boldsymbol{j}_0(h\omega', n'; u')|^2}{|\boldsymbol{n}_0' \times \boldsymbol{j}_0(\omega', n_0'; u_0)|^2}, \tag{F.49}$$

where $\boldsymbol{j}_0$ is given by the expression (F.43) and $h = \chi(u, n', 0)/\chi(u_0, n_0', 0)$. Equations (F.48) and (F.49), together with the definition of $\boldsymbol{j}_0$, represent a general formulation of the scaling

law for the spectral distribution of photons emitted by an electron in a plane electromagnetic wave, i.e. for Thomson/Compton scattering. In the form given in (F.48), the scaling law is strictly valid for $a_0 \ll 1$. To include the non-linear case, $a_0 \gtrsim 1$, one substitutes the Doppler factor $\chi(u, n', 0) \rightarrow \chi(u, n', a_0)$ in the definition of $h$, i.e. $h$ is modified to $h = \chi(u, n', a_0)/\chi(u_0, n'_0, a_0)$. In the non-linear regime where $a_0 \sim 1$, the scaling law perfectly accounts for changes in the electron's initial energy $\gamma_0 \rightarrow \gamma$. However, changes of the incidence angles, in particular $\vartheta_u$, are accurate only for $\vartheta_u \ll 1$. Nevertheless, for the present purposes, the scaling law is sufficiently accurate to account for the typical angular divergence of focused electron beams. The validity of the scaling law was demonstrated in [Sei11c] by comparing a direct numerical calculation of the spectral density $\rho(\omega', n', u')$ with an application of the scaling law where $\rho(\omega', n'_0, u'_0)$ was calculated numerically and $\rho(\omega', n', u')$ was determined by application of the scaling law. The special case of the head-on geometry characterized by $u_0 = (\gamma_0, 0, 0, \gamma_0 v_0)$ as a reference, and a second, different geometry characterized by $u(\gamma, \vartheta_u, \varphi)$ (cf. Figure F.1), and staying strictly in the backscattering geometry $n' = -n$, i.e. $n'_0 = n'$, was discussed in [Hei10b].

## F.7   Discussion of electron phase space distribution effects

To discuss the effects of the electron phase space distribution on the non-linear Compton spectra one has to fold the one-photon spectrum $\rho(\omega', n', u)$ with an electron phase space distribution $f(\gamma, \vartheta_u, \varphi_u)$

$$\rho_W(\omega', n') = N_e \int d\gamma d\vartheta_u d\varphi_u f(\gamma, \vartheta_u, \varphi_u) \, \rho(\omega', \boldsymbol{n}', u) \,. \tag{F.50}$$

Exploiting the scaling law (F.48), where the observation direction $n'$ is kept fixed, the warm spectral density $\rho_W$ can be reformulated as

$$\rho_W(\omega', n') = N_e \int d\gamma d\vartheta_u d\varphi_u f(\gamma, \vartheta_u, \varphi_u) \mathcal{M}(u, u_0) \rho(\omega'/h, n'; u_0) \,, \tag{F.51}$$

where the arguments $n'$ are omitted in the transition function, $\mathcal{M}(u, u_0) \equiv \mathcal{M}(u, u_0; n', n')$. Thus, instead of calculating the one-electron spectral density $\rho$ for all the different initial conditions $u$, it is sufficient to calculate $\rho$ for a single set of parameters $u_0$ for all relevant frequencies $\omega'$. To conveniently define the distribution functions $f$, a new coordinate system is introduced, which is aligned with the mean initial velocity $\boldsymbol{u}_0$. The unit vectors of this rotated system read

$$\begin{aligned}
\boldsymbol{e}_{x'} &= - \cos \vartheta_{u0} \cos \varphi_{u0} \boldsymbol{e}_x - \cos \vartheta_{u0} \sin \varphi_{u0} \boldsymbol{e}_y + \sin \vartheta_{u0} \boldsymbol{e}_z \,, \\
\boldsymbol{e}_{y'} &= \sin \varphi_{u0} \boldsymbol{e}_x - \cos \varphi_{u0} \boldsymbol{e}_y \,, \\
\boldsymbol{e}_{z'} &= \sin \vartheta_{u0} \cos \varphi_{u0} \boldsymbol{e}_x + \sin \vartheta_{u0} \sin \varphi_{u0} \boldsymbol{e}_y + \cos \vartheta_{u0} \boldsymbol{e}_z \,,
\end{aligned} \tag{F.52}$$

i.e. in the new coordinate system $\boldsymbol{u}'_0 = (0, 0, v_0 \gamma_0)$ and $\vartheta'_{u0} = \varphi'_{u0} = 0$. The distribution functions are defined in the primed coordinate system via $f(\gamma, \vartheta'_u, \varphi'_u) = f_1(\gamma) f_2(\vartheta'_u) f_3(\varphi'_u)$, where the $f_i$ are defined in (F.34).

As a first example, the results for the warm spectral density $\rho_W(\omega'; n')$ in the linear Thomson scattering regime are compared to the cold spectral density $\rho_C(\omega'; n') = \rho(\omega'; n', u_0)$, which is $N_e$ times the spectral density for a single electron with velocity $u_0$ [i.e. the corresponding phase space distribution would be $f_C = \delta(\gamma - \gamma_0)\delta(\vartheta_u - \vartheta_{u0})\delta(\varphi_u - \varphi_{u0})$] in Figure F.7 for different incidence angles of the electron in the linear regime, i.e. $a_0 = 0.01$. The observation direction is the mean direction of the incoming electron in each case, i.e. $\boldsymbol{n}' \parallel \boldsymbol{u}_0$. The
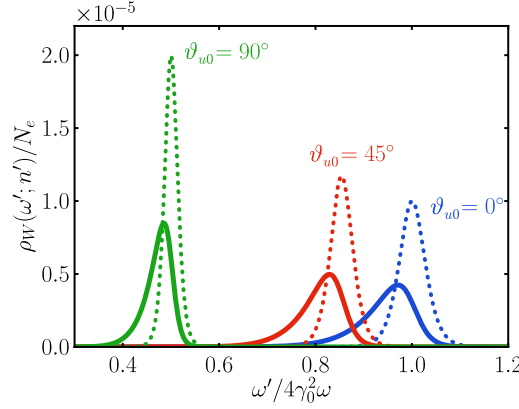
**Figure F.7:** Cold spectral density (dotted curves) vs. warm spectral density (solid curves) as a function of scaled frequency $\omega'/4\gamma_0^2\omega$ at low intensity, $a_0 = 0.01$, and a laser pulse length parameter of $\Delta\phi = 18$. The observation is assumed in the direction of the incoming electron bunch $\boldsymbol{n}' \parallel \boldsymbol{u}_0$, i.e. $\theta = \vartheta_{u0}$, $\varphi = \varphi_{u0}$, for various electron incidence angles $\vartheta_{u0}$, as depicted. The spectral densities have been calculated for an energy of $m\gamma_0 = 40$ MeV with an energy spread of $\Delta\gamma/\gamma_0 = 0.001$ and an angular spread of $\Delta\vartheta_u = 2.5$ mrad.

inherent width and shape of the peaks of the cold spectral density are determined by the width and shape of the laser envelope function $g(\phi)$. The effects of energy and angular spread of the incoming electron bunch are (*i*) a broadening of the peaks and (*ii*) a reduction of the peak heights. Dominantly, the peaks are shifted to the low-energy side due to the effects of angular spread. The relative bandwidth is the same for each geometry; also the integrated value $\int \rho(\omega')d\omega'$ is the same for the three spectra exhibited.

## F.8   Head-on backscattering geometries

In this section, some available sources of ultrarelativistic electron beams for the detection of the sub-peaks in non-linear Compton scattering are discussed, proposing optimal experimental parameters. A common source for ultrarelativistic electron beams are linacs, such as the ELBE accelerator at the HZDR [ELB, Arn08]. It is capable of producing electron bunches with a low energy spread of $\Delta\gamma/\gamma_0 = 10^{-3}$ and transverse emittance of about $\varepsilon_x = 1.5$ mm mrad. On the other hand, new laser based acceleration schemes like laser wake field acceleration (LWFA) report the production of electron bunches with $\Delta\gamma/\gamma_0 = 3.5\%$ and angular divergence of $\Delta\vartheta_u = 0.68$ mrad at $\gamma_0 = 400$ [Ost08]. The numerical results for the warm spectral densities using both ELBE and LWFA electron beam parameters are shown in Figure F.8 which also includes a comparison with the respective cold spectral densities for head-on backscattering set-ups. Clearly, the harmonic sub-peaks are smeared out for ELBE parameters and even more so for the LWFA set-up [Ost08]. For ELBE it is the emittance which is too high for the observation of the sub-peaks. A LWFA electron bunch, on the other hand, has too large an energy spread — despite of its low angular divergence. It is concluded that in order to resolve the sub-peaks both energy spread and emittance need to be sufficiently small. Very low values for both the energy and angular spread are needed for a possible observation of the sub-peaks. In Table F.1, a suitable set of parameters which allows to observe the harmonic sub-peaks with a 100 TW laser is listed. For petawatt lasers, the strong constraint on the emittance may be relaxed because they are capable to achieve non-linear peak intensities
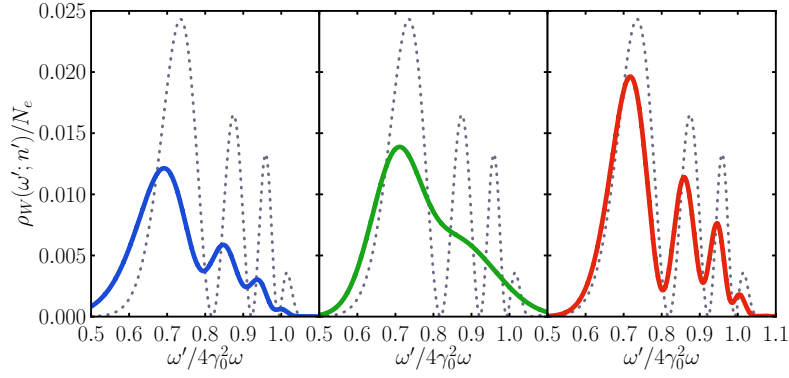
**Figure F.8:** The warm spectral density (solid curves) for ELBE parameters [Arn08] (left panel), LWFA electrons [Ost08] (centre panel) and optimal parameters (right panel, see Table F.1) in combination with a 100 TW laser. For comparison the cold spectral density is shown also in each plot as grey dotted curve.

$a_0^2 \gtrsim 1$ across larger spot sizes $w_0$ such that larger electron beam radii $r_b$ can be tolerated. The essential quantity in the integral (F.51) is $\Delta\vartheta_u \propto \varepsilon_x/r_b$ and not the emittance itself.

However, the emittance characterizes the transverse momentum distribution of an electron beam and is a conserved quantity. That means, when focusing an electron beam to smaller spot sizes the angular spread increases since $\varepsilon_x \propto r_b\Delta\vartheta_u = const$. Thus, the larger the laser spot size $w_0$, the easier the emittance constraints can be fulfilled with the present specifications of the ELBE accelerator. Therefore, the application of petawatt lasers for the observation of the sub-peaks seems advisable. Furthermore, the REGAE electron gun [REG] provides promising parameters for a detection of the harmonic peaks including their substructure in combination with a 200 TW laser [Har12].

**Table F.1:** Proposed optimal laser and electron beam parameters required for observing the sub-peaks in the fundamental harmonic of non-linear Thomson scattering employing a 100 TW laser or a 1 PW laser.

| parameter | | 100 TW | 1 PW |
|---|---|---|---|
| laser frequency | $\omega$ [eV] | 1.5 | 1.5 |
| laser amplitude | $a_0$ | 1.0 | 1.0 |
| laser pulse length | $T_0$ [fs] | 25 | 25 |
| laser focal radius | $w_0$ [µm] | 50 | 150 |
| electron beam radius | $r_b$ [µm] | 5 | 15 |
| electron energy | $\gamma_0$ | 80 | 80 |
| electron energy spread | $\Delta\gamma/\gamma_0$ | 0.001 | 0.001 |
| angular spread | $\Delta\theta_u$ [mrad] | 1.75 | 1.75 |
| electron transverse emittance | $\varepsilon_x$ [mm mrad] | 0.7 | 2.2 |
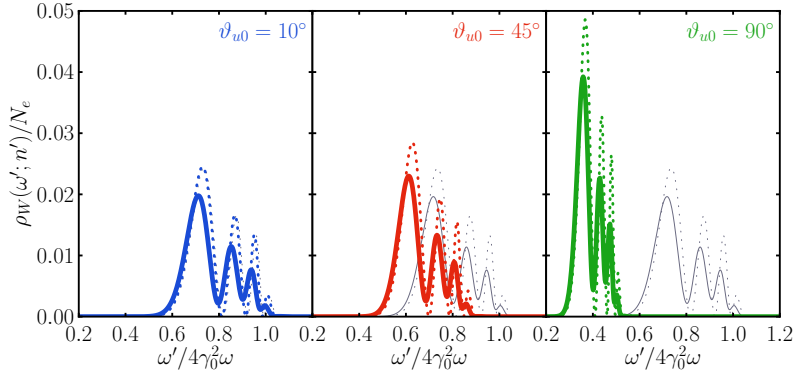
**Figure F.9:** Dependence of the warm spectral density (solid curves) on the scaled photon frequency for different electron incidence angles $\vartheta_{u0} = 10°, 45°$ and $90°$. The spectrum is observed in the direction of the primary electron bunch $\boldsymbol{n}' \parallel \boldsymbol{u}_0$ as in Figure F.7. For comparison, the respective cold spectral densities are also shown as fat dotted lines. The results for $\vartheta_{u0} = 0°$, which correspond to the right panel of Figure F.8, are also shown in each panel as thin grey solid and grey dotted curves. Parameters are $a_0 = 1.0$, $\Delta\phi = 18$, $\omega = 1.5$ eV, $m\gamma_0 = 40$ MeV, $\Delta\gamma/\gamma_0 = 10^{-3}$ and $\Delta\vartheta_u = 1.75$ mrad.

## F.9   Non-head-on scattering

The previous analysis is extended here to allow for non-head-on collisions of the electron beam with the laser pulse which is much closer to an actual experimental situation, e.g. the interaction angle in the SLAC E-144 experiment was $\vartheta_u = 17°$ [Bam99]. To uncover a large range of possible conditions, the incidence angles $\vartheta_{u0} = 10°, 45°$ and $90°$ are considered. (Thomson scattering with an incidence between $0° < \vartheta_u < 180°$ is discussed, e.g. in [Deb10].) The numerical results are exhibited in Figure F.9, where one observes a decrease in the frequency of the scattered radiation (e.g., for $\vartheta_{u0} = 90°$ the maximum Doppler shift reaches half the value of the Doppler shift at $\vartheta_{u0} = 0°$). The contrast of the minima and maxima, however, stays the same in all cases. Such geometries, where the spectrum is observed in the forward direction of the electron, turn out to be equally well suited for an experimental observation of the substructures with the beam parameters of Table F.1, as for head-on collisions.

Going one step further, the dependence of the warm spectral density on the observation direction $n'$ is considered, if $n'$ slightly deviates from the forward direction of the primary electrons. The radiation scattered off an ultrarelativistic electron forms a cone with its axis given by the direction of the electron velocity $\boldsymbol{u}$ with a typical opening angle $\bar{\vartheta}_u \sim 1/\gamma$ [cf. Eq. (F.30)], where $\bar{\vartheta}_u$ is the angle between $\boldsymbol{u}$ and $\boldsymbol{n}'$. Expanding the Doppler shift function $\chi(\bar{\vartheta}_u)$ for small opening angles, $\bar{\vartheta}_u \ll 1$, one obtains

$$\chi(\bar{\vartheta}_u) = \chi(0)\left(1 - \frac{\nu\chi(0)}{2}\bar{\vartheta}_u^2 + \mathcal{O}(\bar{\vartheta}_u^4)\right) \tag{F.53}$$

with $\nu$ defined in Eq. (F.47) and

$$\bar{\vartheta}_u \simeq \sqrt{(\vartheta_u - \theta)^2 + (\varphi_u - \varphi)^2 \sin^2\vartheta_u}\,, \tag{F.54}$$

where both $|\vartheta_u - \theta| \ll 1$ and $|\varphi_u - \varphi| \ll 1$. (Note that $\vartheta_u$ denotes the angle between $\boldsymbol{u}$ and $\boldsymbol{e}_z$, while $\theta$ is the angle between $\boldsymbol{n}'$ and $\boldsymbol{e}_z$.) This accounts for both the changes in the initial
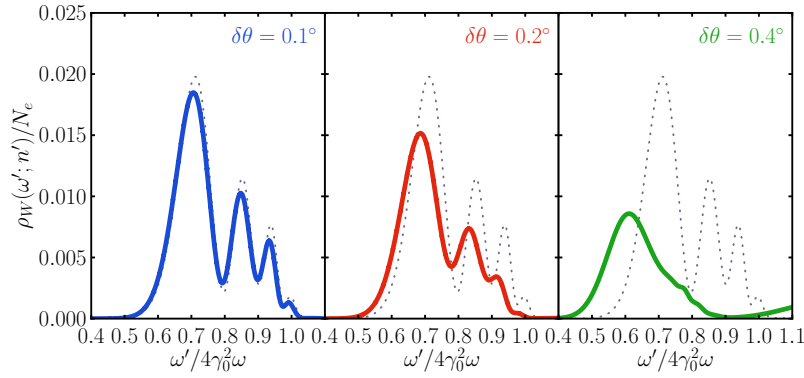
**Figure F.10:** Warm spectral density for an electron incidence angle $\vartheta_{u0} = 10°$ relative to the laser beam (cf. left panel of Figure F.8) for the observation direction given by the angles $\delta\theta = \theta - \vartheta_{u0}$ and $\varphi = \varphi_{u0} = 0$. The results for the respective cold spectral density are also shown as grey dotted curves in each panel for comparison. All other parameters are the same as in Figure F.9.

electron direction due to the emittance and the changes in the observation direction. The typical cone opening, where the Doppler factor changes its value significantly, is set by the scale $\bar{\vartheta}_u \sim 1/\gamma_0$, which is for the chosen ELBE parameters $\gamma_0 \approx 100$, $\bar{\vartheta}_u \sim 10$ mrad. For $\bar{\vartheta}_u \ll 1/\gamma_0$, the Doppler shift is almost constant. This explains the good visibility of the sub-peaks in the geometries studied so far (cf. Figures F.8 and F.9): Because the typical angular spread due to the beam emittance is much smaller than $1/\gamma_0$, all electrons of the bunch provide approximately the same Doppler up-shift for the spectrum observed in the direction of $\boldsymbol{u}_0$.

However, if the radiation is observed in a different direction, one cannot expect to have the same situation, since the Doppler up-shift strongly depends on the direction of each electron. Indeed, the numerical simulations show that the contrast of the sub-peaks vanishes rapidly for off-axis observation directions. The numerical results are exhibited in Figure F.10 for $\vartheta_{u0} = 10°$ and an observation direction $\theta = \vartheta_{u0} + \delta\theta$, which slightly deviates from the direction of the incoming electron by less than one degree. The contrast of the sub-peaks vanishes completely for $\delta\theta \geq 0.4°$.

## F.10   Finite detectors size

Until now, it was always assumed that the scattered radiation is observed at a fixed direction $n'$. However, any real detector will have a finite size spanning a certain range of observation directions or have a finite angular resolution. It has been shown in the previous section that the observed spectrum strongly depends on the observation direction, i.e. changes of the observation direction of the order of tenths of degrees drastically change the observed photon spectrum. Thus, it is necessary to consider the effect of a finite-size detector by integrating the spectrum over a certain range of angles $\theta$ and $\varphi$ of the direction of the outgoing photons. The detector should cover only a cone around the direction of $\boldsymbol{u}_0$ with an opening angle $\delta\theta \ll 1/\gamma_0$. One now has to allow a change in the direction of the outgoing photon $n'_0(\theta_0, \varphi_0) \to n'(\theta, \varphi)$ in the scaling law (F.48). Employing the general scaling, the spectrum
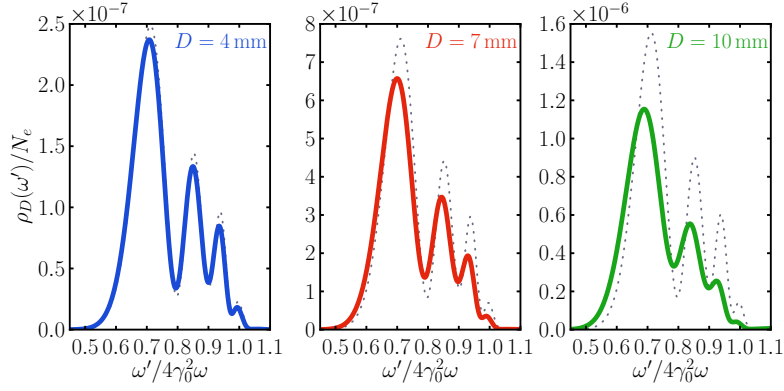
**Figure F.11:** Photon spectrum for a finite detector size. The solid curves correspond to a detector geometry as described below Eq. (F.55) with diameter $D = 4$ mm (left panel), 7 mm (centre panel) and 10 mm (right panel) at a distance of $L = 1$ m from the interaction point in the mean direction of the primary electron beam for an electron incidence angle $\vartheta_{u0} = 10°$. For comparison, the spectra of an idealized pointlike detector $\rho_{pD}$ normalized to the same effective size are also plotted as grey dotted curves in each panel.

measured by a finite detector reads

$$\rho_D(\omega') = N_e \int d\Omega d(\gamma, \vartheta_u, \varphi_u) f(\gamma, \vartheta_u, \varphi_u) S(\theta, \varphi) \mathcal{M}(u, u_0; n', n_0') \rho(\omega'/h; n_0', u_0),$$
(F.55)

where $S(\theta, \varphi)$ is the detector acceptance function, which is, in an ideal case, 1 on the surface of the detector and 0 otherwise, e.g. $S_D(\theta, \varphi) = \Theta(\theta_D - \theta)$ with $\tan \theta_D = D/2L$ for an active circular detector spot of diameter $D$ placed at a distance $L$ away from the interaction region in the direction of $\boldsymbol{u}_0$. Examples of photon distributions are exhibited in Figure F.11. There, the detector spectral density $\rho_D$ for an electron incidence angle $\vartheta_{u0} = 10°$ is contrasted with an approximation, where the spectrum of an idealized point-like detector is multiplied by the respective real detector size, i.e. $\rho_{pD} = \rho_W(\omega', n_0') \int d\Omega S(\theta, \phi)$, which is an integral mean value approximation of (F.55). Naturally, a larger detector collects more photons, but at the price that the contrast of the sub-peaks is also reduced. For $L = 1$ m and the parameters of Table F.1, the active detector area should be much smaller than 10 mm in diameter, corresponding to a cone opening angle $\delta\theta \ll 5$ mrad.

## F.11   Concluding remarks

In the strong-field domain $a_0 \sim 1$ two prominent effects appear in the frequency spectra of Compton backscattering of pulsed laser fields: (*i*) the emergence of broad higher harmonics and (*ii*) each harmonic itself is distributed into a sequence of sub-peaks (for certain parameters the harmonics are overlapping). There is still no clear-cut experimental verification of these effects, in particular with respect to (*ii*). In this section, the several realistic set-ups have been considered to find optimal experimental parameters for an experimental verification of these strong-field effects in the frequency spectra of non-linear Compton scattering, including focused laser pulses and electron phase space distributions. The effect of electron phase space distributions was incorporated by a folding of the single-electron spectral density with the electron distribution function using a scaling property of the spectral density. An electron

beam with parameters as in Table F.1 should be adequate to allow for an experimental verification of the substructures in combination with a petawatt laser. The petawatt laser should be weakly focused, such that $a_0 \sim 1$ is achieved in a large spatial volume, minimizing the ponderomotive scattering. High-quality electron beams such as the ones provided by ELBE or REGAE should probe the central region of the laser focus with the electron beam radius much smaller than the laser focal size. A detector should cover a sufficiently narrow cone around the direction of the incoming electron beam with an opening angle much smaller than the inverse Lorentz factor. In this analysis, opening angles of $2 - 3$ mrad (for a 40 MeV electron beam) yield good results with suitable contrast of minima and maxima, thus offering the conditions for an experimental set-up appropriate for verifying the predicted substructures in non-linear Compton scattering.

# List of Publications

Results obtained in the course of elaborating this thesis are published in

- T. HEINZL, D. SEIPT AND B. KÄMPFER:
  *Beam-shape effects in nonlinear Compton and Thomson scattering*,
  Phys. Rev. A **81**, 022125 (2010).

- D. SEIPT AND B. KÄMPFER:
  *Nonlinear Compton scattering of ultrashort intense laser pulses*,
  Phys. Rev. A **83**, 022101 (2011).

- D. SEIPT AND B. KÄMPFER:
  *Scaling law for the photon spectral density in the nonlinear Thomson-Compton scattering*,
  Phys. Rev. Special Topics AB **14**, 040704 (2011).

- D. SEIPT AND B. KÄMPFER:
  *Non-linear Compton scattering of ultrahigh-intensity laser pulses*,
  accepted in Laser Phys., arXiv:1111.0188 [hep-ph] (2011).

- D. SEIPT AND B. KÄMPFER:
  *Two-photon Compton process in pulsed intense laser fields*,
  Phys. Rev. D **85**, 101701(R) (2012).

- T. NOUSCH, D. SEIPT, B. KÄMPFER AND A. I. TITOV:
  *Pair production in short laser pulses near threshold*,
  Phys. Lett. B **715**, 246 (2012).

# Glossary

APOLLON     10 PW high-power laser project at the Institut de Lumière Extrême.

BNL-ATF     Brookhaven National Laboratory – Accelerator Test Facility, www.bnl.gov/atf.

BRST     Becchi-Rouet-Stora-Tyutin.

CODATA     Committee on Data for Science and Technology, physics.nist.gov/cuu/Constants.

CPA     chirped pulse amplification.

CUOS     Center for Ultrafast Optical Science, www.engin.umich.edu/research/cuos.

DESY     Deutsches Elektronen-Synchrotron, www.desy.de.

DRACO     Dresden laser acceleration source, www.hzdr.de.

ELBE     Electron Linac for beams with high Brilliance and low Emittance, www.hzdr.de.

ELI     Extreme Light Infrastructure, www.extreme-light-infrastructure.eu.

FACET     Facility for Advanced Accelerator Experimental Tests, facet.slac.stanford.edu.

FWHM     full width at half maximum.

HERCULES     high power laser at the CUOS.

HICS     high-intensity Compton scattering.

HiPER     High Power laser Energy Research, www.hiper-laser.org.

HZDR     Helmholtz-Zentrum Dresden-Rossendorf, www.hzdr.de.

IPW     infinite plane wave.

IZEST     International Zeta-Exawatt Science Technology, www.int-zest.com.

LLNL     Lawrence Livermore National Laboratory, www.llnl.gov.

LSZ     Lehmann-Symanzik-Zimmermann.

LWFA     laser wake field acceleration.

| | |
|---|---|
| MPQ | Max-Planck-Institut für Quantenoptik, www.mpq.mpg.de. |
| NIF | National Ignition Facility, lasers.llnl.gov. |
| PARMELA | Phase And Radial Motion in Electron Linear Accelerators. |
| PEnELOPE | Petawatt, Energy-Efficient Laser for Optical Plasma Experiments, www.hzdr.de. |
| PETRA III | Positron-Elektron-Tandem-Ring-Anlage, A brilliant X-ray synchrotron source at DESY, petra3.desy.de. |
| PFS | Petawatt Field Synthesizer. |
| PIC | particle in cell. |
| PPW | pulsed plane wave. |
| QED | quantum electrodynamics. |
| REGAE | Relativistic Electron Gun for Atomic Exploration, regae.desy.de. |
| SLAC | Stanford Linear Accelerator Center, slac.stanford.edu. |
| SPA | stationary phase approximation. |
| SPring-8 | Super Photon ring-8 GeV, www.spring8.or.jp/en. |
| SVEA | slowly varying envelope approximation. |
| TREDI | fully 3D beam dynamics simulation of RF guns, bendings and FELs. |
| XCELS | Exawatt Center for Extreme Light Studies, www.xcels.iapras.ru. |
| XFEL | X-ray free electron laser. |

# List of Figures

# List of Tables

# Bibliography

[Adl71]    S. L. Adler: *Photon Splitting and Photon Dispersion in a Strong Magnetic Field*, Annals of Physics **67**, 599 (1971).

[Ahl08]    M. Ahlers, H. Gies, J. Jaeckel, J. Redondo and A. Ringwald: *Laser experiments explore the hidden sector*, Phys. Rev. D **77**, 095001 (2008).

[Akh02]    S. Z. Akhmadaliev, G. Y. Kezerashvili, S. G. Klimenko, R. N. Lee, V. M. Malyshev, A. L. Maslennikov, A. M. Milov, A. I. Milstein, N. Y. Muchnoi, A. I. Naumenkov, V. S. Panin, S. V. Peleganchuk, G. E. Pospelov, I. Y. Protopopov, L. V. Romanov, A. G. Shamov, D. N. Shatilov, E. A. Simonov, V. M. Strakhovenko and Y. A. Tikhonov: *Experimental Investigation of High-Energy Photon Splitting in Atomic Fields*, Phys. Rev. Lett. **89**, 061802 (2002).

[Aoy07]    T. Aoyama, M. Hayakawa, T. Kinoshita and M. Nio: *Revised Value of the Eighth-Order Contribution to the Electron $g - 2$*, Phys. Rev. Lett. **99**, 110406 (2007).

[Arn08]    A. Arnold, H. Büttig, D. Janssen, T. Kamps, G. Klemz, W. D. Lehmann, U. Lehnert, D. Lipka, F. Marhauser, P. Michel, K. Möller, P. Murcek, C. Schneider, R. Schurig, F. Staufenbiel, J. Stephan, J. Teichert, V. Volkov, I. Will and R. Xiang: *A high-brightness SRF photoelectron injector for FEL light sources*, Nucl. Instrum. Methods Phys. Res., Sect. A **593**, 57 (2008).

[Atz09]    S. Atzeni: *Laser driven inertial fusion: the physical basis of current and recently proposed ignition experiments*, Plasma Phys. Controlled Fusion **51**, 124029 (2009).

[Bab06]    M. Babzien, I. Ben-Zvi, K. Kusche, I. V. Pavlishin, I. V. Pogorelsky, D. P. Siddons, V. Yakimenko, D. Cline, F. Zhou, T. H. Y. Kamiya, T. Kumita, T. Omori, J. Urakawa and K. Yokoya: *Observation of the Second Harmonic in Thomson Scattering from Relativistic Electrons*, Phys. Rev. Lett. **96**, 054802 (2006).

[Bag90]    V. G. Bagrov and D. M. Gitman: *Exact Solutions of Relativistic Wave Equations*, Kluwer Academic Publishers, Dordrecht, 1990.

[Bag05]    V. G. Bagrov and D. M. Gitman: *Non-Volkov solutions for a charge in a plane wave*, Ann. Phys. (Leipzig) **14**, 467 (2005), [8. Folge].

[Baĭ68]    V. N. Baĭer and V. M. Katkov: *Processes involved in the motion of high energy particles in a magnetic field*, Sov. Phys. J. Exp. Theor. Phys. **26**, 854 (1968).

[Baĭ69]    V. N. Baĭer and V. M. Katkov: *Quasiclassical theory of bremsstrahlung by relativistic particles*, Sov. Phys. J. Exp. Theor. Phys. **28**, 807 (1969).

[Baĭ75]   V. N. Baĭer, V. M. Katkov and V. M. Strakhovenko: *Operator approach to quantum electrodynamics in an external field. Electron loops*, Sov. Phys. J. Exp. Theor. Phys. **41**, 198 (1975).

[Baĭ76]   V. N. Baĭer, A. I. Mil'shteĭn and V. M. Strakhovenko: *Interaction between a photon and an intense electromagnetic wave*, Sov. Phys. J. Exp. Theor. Phys. **42**, 961 (1976).

[Bam99]  C. Bamber, S. J. Boege, T. Koffas, T. Kotseroglou, A. C. Melissinos, D. D. Meyerhofer, D. A. Reis, W. Ragg, C. Bula, K. T. McDonald, E. J. Prebys, D. L. Burke, R. C. Field, G. Horton-Smith, J. E. Spencer, D. Walz, S. C. Berridge, W. M. Bugg, K. Shmakov and A. W. Weidemann: *Studies of nonlinear QED in collisions of 46.6 GeV electrons with intense laser pulses*, Phys. Rev. D **60**, 092004 (1999).

[Bec75]   W. Becker and H. Mitter: *Vacuum polarization in laser fields*, J. Phys. A **8**, 1638 (1975).

[Bec76]   W. Becker and H. Mitter: *Modification of the quasi-levels of an electron in a laser field due to radiative corrections*, J. Phys. A **9**, 2171 (1976).

[Bel77]   I. V. Belousov: *On resonance compton scattering in the field of an intense electromagnetic wave*, Opt. Commun. **20**, 205 (1977).

[Bel08]   A. R. Bell and J. G. Kirk: *Possibility of Profilic Pair Production with High-Power Lasers*, Phys. Rev. Lett. **101**, 200403 (2008).

[Ber80]   W. B. Berestetzki, E. M. Lifschitz and L. P. Pitajewski: *Relativistische Qantentheorie*, volume IV of *Lehrbuch der Theoretischen Physik*, Akademie Verlag, Berlin, 1980.

[Bet46]   H. A. Bethe and J. R. Oppenheimer: *Reaction of Radiation on Electron Scattering and Heitler's Theory of Radiation Damping*, Phys. Rev. **70**, 451 (1946).

[Bla47]   J. M. Blatt: *On the Heitler Theory of Radiation Damping*, Phys. Rev. **72**, 466 (1947).

[Bla06]   D. B. Blaschke, A. V. Prozorkevich, C. D. Roberts, S. M. Schmidt and S. A. Smolyansky: *Pair production and optical lasers*, Phys. Rev. Lett. **96**, 140402 (2006).

[Bla09]   D. B. Blaschke, V. A. Prozorkevich, G. Köpke, C. D. Roberts, S. M. Schmidt, D. S. Shkirmanov and S. A. Smolyansky: *Dynamical Schwinger effect and high-intensity lasers. Realising nonperturbative QED*, Eur. Phys. J. D **55**, 341 (2009).

[Blo37]   F. Bloch and A. Nordsieck: *Note on the Radiation Field of the Electron*, Phys. Rev. **52**, 54 (1937).

[Boc09]   M. Boca and V. Florescu: *Nonlinear Compton scattering with a laser pulse*, Phys. Rev. A **80**, 053403 (2009), [Erratum in Phys. Rev. A **81**, 039901(E) (2010)].

[Boc11a] M. Boca: *On the properties of the Volkov solutions of the Klein–Gordon equation*, J. Phys. A **44**, 445303 (2011).

[Boc11b] M. Boca and V. Florescu: *Thomson and Compton scattering with an intense laser pulse*, Eur. Phys. J. D **61**, 449 (2011).

[Boc11c] M. Boca and A. Oprea: *Thomson scattering in the high intensity regime*, Phys. Scr. **83**, 055404 (2011).

[Boc12] M. Boca, V. Dinu and V. Florescu: *Electron distributions in nonlinear Compton scattering*, Phys. Rev. A **86** (2012), arXiv:1206.6971v1 [physics.atom-ph].

[Bou11] R. Bouchendira, P. Cladé, S. Guellati-Khélifa, F. Nez and F. Biraben: *New Determination of the Fine Structure Constant and Test of the Quantum Electrodynamics*, Phys. Rev. Lett. **106**, 080801 (2011).

[Bra56] A. Bracci, C. Coceva, L. Colli and E. Lonati: *Experimental measurements on double compton effect*, Nuovo Cimento **3**, 203 (1956).

[Bra09] T. Brabec (Editor): *Strong Field Laser Physics*, volume 134 of *Springer Series in Optical Sciences*, Springer, New York, 2009.

[Bre34] G. Breit and J. A. Wheeler: *Collision of Two Light Quanta*, Phys. Rev. **46**, 1087 (1934).

[Bro52] L. M. Brown and R. P. Feynman: *Radiative Corrections to Compton Scattering*, Phys. Rev. **85**, 231 (1952).

[Bro64] L. S. Brown and T. W. B. Kibble: *Interaction of intense laser beams with electrons*, Phys. Rev. **133**, A705 (1964).

[Bro83] R. W. Brown and K. L. Kowalski: *Volkov Solutions, Gauge-Poincaré Transformations, and Plane-Wave Decoupling*, Phys. Rev. Lett. **51**, 2355 (1983).

[Bro84] R. W. Brown and K. L. Kowalski: *Gauge couplings as local gauge and Poincaré transformations: Generalized Taub-Volkov solutions*, Phys. Rev. D **30**, 2602 (1984).

[Bul96] C. Bula, K. T. McDonald, E. J. Prebys, C. Bamber, S. Boege, T. Kotseroglou, A. C. Melissinos, D. D. Meyerhofer, W. Ragg, D. L. Burke, R. C. Field, G. Horton-Smith, A. C. Odian, J. E. Spencer, D. Walz, S. C. Berridge, W. M. Bugg, K. Shmakov and A. W. Weidemann: *Observation of Nonlinear Effects in Compton Scattering*, Phys. Rev. Lett. **76**, 3116 (1996).

[Bul09] S. V. Bulanov, T. Z. Esirkepov, D. Habs, F. Pegoraro and T. Tajima: *Relativistic laser-matter interaction and relativistic laboratory astrophysics*, Eur. Phys. J. D **55**, 438 (2009).

[Bur97] D. L. Burke, R. C. Field, G. Horton-Smith, J. E. Spencer, D. Walz, S. C. Berridge, W. M. Bugg, K. Shmakov, A. W. Weidemann, C. Bula, K. T. McDonald, E. J. Prebys, C. Bamber, S. J. Boege, T. Koffas, T. Kotseroglou, A. C. Melissinos, D. D. Meyerhofer, D. A. Reis and W. Ragg: *Positron Production in Multiphoton Light-by-Light Scattering*, Phys. Rev. Lett. **79**, 1626 (1997).

[Bur07] C. P. Burgess: *An Introduction to Effective Field Theory*, Annu. Rev. Nucl. Part. S. **57**, 329 (2007).

[Cha69] S.-J. Chang and M. Shang-Keng: *Feynman Rules and Quantum Electrodynamics at Infinite Momentum*, Phys. Rev. D **180**, 1506 (1969).

[Cha73a]  S.-J. CHANG, R. G. ROOT AND T.-M. YAN: *Quantum Field Theories in the Infinite-Momentum Frame. I. Quantization of Scalar and Dirac Fields*, Phys. Rev. D **7**, 1133 (1973).

[Cha73b]  S.-J. CHANG AND T.-M. YAN: *Quantum Field Theories in the Infinite-Momentum Frame. II. Scattering Matrices of Scalar and Dirac Fields*, Phys. Rev. D **7**, 1147 (1973).

[Cha05]  W. S. C. CHANG: *Principles of Lasers and Optics*, Cambridge University Press, 2005.

[Che98]  S.-Y. CHEN, A. MAKSIMCHUK AND D. UMSTADTER: *Experimental observation of relativistic nonlinear Thomson scattering*, Nature **396**, 653 (1998).

[Che99]  P. CHEN AND T. TAJIMA: *Testing Unruh Radiation with Ultraintense Lasers*, Phys. Rev. Lett. **83**, 256 (1999).

[Chl06]  J. CHLUBA, S. Y. SAZONOV AND R. A. SUNYAEV: *The double Compton emissivity in a mildly relativistic thermal plasma within the soft photon limit*, Astron. Astrophys. **468**, 785 (2006).

[Cor11a]  J. P. CORSON AND J. PEATROSS: *Quantum-electrodynamic treatment of photoemission by a single-electron wave packet*, Phys. Rev. A **84**, 053832 (2011).

[Cor11b]  J. P. CORSON, J. PEATROSS, C. MÜLLER AND K. Z. HATSAGORTSYAN: *Scattering of intense laser radiation by a single-electron wave packet*, Phys. Rev. A **84**, 053831 (2011).

[Cri08]  L. CRISPINO, A. HIGUCHI AND G. E. A. MATSAS: *The Unruh effect and its applications*, Rev. Mod. Phys. **80**, 787 (2008).

[Cro12]  B. J. B. CROWLEY, R. BINGHAM, R. G. EVANS, D. O. GERICKE, O. L. LANDEN, C. D. MURPHY, P. A. NORREYS, S. J. ROSE, T. TSCHENTSCHER, C. H.-T. WANG, J. S. WARK AND G. GREGORI: *Testing quantum mechanics in non-Minkowski space-time with high power lasers and 4th generation light sources*, Sci. Rep. **2**, 491 (2012).

[Dav79]  L. W. DAVIS: *Theory of electromagnetic beams*, Phys. Rev. A **19**, 1177 (1979).

[Daw83]  J. M. DAWSON: *Particle simulation of plasmas*, Rev. Mod. Phys. **55**, 403 (1983).

[Deb09]  A. DEBUS, S. BOCK, M. BUSSMANN, T. COWAN, A. JOCHMANN, T. KLUGE, S. KRAFT, R. SAUERBREY, K. ZEIL AND U. SCHRAMM: *Linear and Non-Linear Thomson-Scattering X-Ray Sources Driven by Conventionally and Laser Plasma Accelerated Electrons*, Proc. SPIE **7359**, 735908 (2009).

[Deb10]  A. DEBUS, M. BUSSMANN, M. SIEBOLD, A. JOCHMANN, U. SCHRAMM, T. COWAN AND R. SAUERBREY: *Traveling-wave Thomson scattering and optical undulators for high-yield EUV and X-ray sources*, Appl. Phys. B **100**, 61 (2010).

[Dic09]  D. A. DICUS, A. FARZINNIA, W. W. REPKO AND T. M. TINSLEY: *Muon decay in a laser field*, Phys. Rev. D **79**, 013004 (2009).

[Din12]  V. DINU, T. HEINZL AND A. ILDERTON: *Infra-red divergences in plane wave backgrounds* (2012), arXiv:1206.3957 [hep-ph].

[Dit00]   W. DITTRICH AND H. GIES: *Probing the Quantum Vacuum*, volume 166 of *Springer Tracts in Modern Physics*, Springer-Verlag, Berlin, Heidelberg, New York, 2000.

[DP07]   A. DI PIAZZA, A. I. MILSTEIN AND C. H. KEITEL: *Photon splitting in a laser field*, Phys. Rev. A **76**, 032103 (2007).

[DP08]   A. DI PIAZZA: *Exact solution of the Landau-Lifshitz equation in a plane wave*, Lett. Math. Phys. **83**, 305 (2008).

[DP09]   A. DI PIAZZA, K. Z. HATSAGORTSYAN AND C. H. KEITEL: *Strong signatures of radiation reaction below the radiation dominated regime*, Phys. Rev. Lett. **102**, 254802 (2009).

[DP10]   A. DI PIAZZA, K. Z. HATSAGORTSYAN AND C. H. KEITEL: *Quantum Radiation Reaction Effects in Multiphoton Compton Scattering*, Phys. Rev. Lett. **105**, 220403 (2010).

[DP12]   A. DI PIAZZA, C. MÜLLER, K. Z. HATSAGORTSYAN AND C. H. KEITEL: *Extremely high-intensity laser interactions with fundamental quantum systems*, Rev. Mod. Phys. **84**, 1177 (2012).

[Dun06]   G. V. DUNNE AND Q.-H. WANG: *Multidimensional Worldline Instantons*, Phys. Rev. D **74**, 065015 (2006).

[Ebe66]   J. H. EBERLY AND H. R. REISS: *Electron Self-Energy in Intense Plane-Wave Field*, Phys. Rev. **145**, 1035 (1966).

[Ebe69]   J. H. EBERLY: *Interaction of Very Intense Light with Free Electrons*, in E. WOLF (Editor), *Progress in Optics*, volume VII, page 359, North-Holland publishing company, Amsterdam - London, 1969.

[Ehl09]   F. EHLOTZKY, K. KRAJEWSKA AND J. Z. KAMIŃSKI: *Fundamental processes of quantum electrodynamics in laser fields of relativistic power*, Rep. Prog. Phys. **72**, 046401 (2009).

[Ein17]   A. EINSTEIN: *Zur Quantentheorie der Strahlung*, Phys. Z. **18**, 121 (1917).

[ELB]   *ELBE homepage*, http://www.hzdr.de/db/Cms?pNid=145.

[Elk11]   N. V. ELKINA, A. M. FEDOTOV, I. Y. KOSTYUKOV, M. V. LEGKOV, N. B. NAROZHNY, E. N. NERUSH AND H. RUHL: *QED cascades induced by circularly polarized laser fields*, Phys. Rev. ST Accel. Beams **14**, 054401 (2011).

[Eng83]   T. J. ENGLERT AND E. A. RINEHART: *Second-harmonic photons from the interaction of free electrons with intense laser radiation*, Phys. Rev. A **28**, 1539 (1983).

[Erd53]   A. ERDÉLYI, W. MAGNUS, F. OBERHETTINGER AND F. G. TRICOMI: *Higher Transcendental Functions*, volume II, McGraw-Hill, 1953.

[Esa93]   E. ESAREY, S. K. RIDE AND P. SPRANGLE: *Nonlinear Thomson scattering of intense laser pulses from beams and plasmas*, Phys. Rev. E **48**, 3003 (1993).

[FAC]   *The FACET project homepage*, http://facet.slac.stanford.edu.

[Fau04]   J. Faure, Y. Glinec, A. Pukhov, S. Kiselev, S. Gordienko, E. Lefebvre, J.-P. Rousseau, F. Burgy and V. Malka: *A laser–plasma accelerator producing monoenergetic electron beams*, Nature **431**, 541 (2004).

[Fau06]   J. Faure, C. Rechatin, A. Norlin, A. Lifschitz, Y. Glinec and V. Malka: *Controlled injection and acceleration of electrons in plasma wakefields by colliding laser pulses*, Nature **444**, 737 (2006).

[Fed10]   A. M. Fedotov, N. B. Narozhny, G. Mourou and G. Korn: *Limitations on the Attainable Intensity of High Power Lasers*, Phys. Rev. Lett. **105**, 080402 (2010).

[Fer89]   R. C. Fernow, H. G. Kirk, J. Rogers, I. J. Bigio, N. A. Kurnit, T. Shimada, K. T. McDonald, D. P. Russell and M. E. Wall: *Proposal for an experimental study of nonlinear Compton scattering* (1989), DOE/ER/3072-55.

[Flo83]   G. Floquet: *Sur les équations différentielles linéaires à coefficients périodiques*, Annales de l'École Normale Supérieure **12**, 47 (1883).

[Fon09]   R. Fonseca: *Computational Challenges in Laser-Plasma Interactions*, in D. A. Jaroszynski, R. Bingham and R. A. Cairns (Editors), *Laser-Plasma Interactions*, chapter 6, page 173, CRC press, 2009.

[Fra65]   L. M. Frantz: *Compton Scattering of an Intense Photon Beam*, Phys. Rev. **139**, B1326 (1965).

[Fra81]   E. S. Fradkin and D. M. Gitman: *Furry Picture for Quantum Electrodynamics with Pair-Creating External Field*, Fortsch. Phys. **29**, 281 (1981).

[Fra91]   E. S. Fradkin, D. M. Gitman and S. M. Shvartsman: *Quantum Electrodynamics with Unstable Vacuum*, Springer-Verlag, 1991.

[Fri64]   Z. Fried and J. H. Eberly: *Scattering of a High-Intensity, Low-Frequency Electromagnetic Wave by an Unbound Electron*, Phys. Rev. **136**, B 871 (1964).

[Fur51]   W. H. Furry: *On Bound States and Scattering in Positron Theory*, Phys. Rev. **81**, 115 (1951).

[Gao04]   J. Gao: *Thomson Scattering from Ultrashort and Ultraintense Laser Pulses*, Phys. Rev. Lett. **93**, 243001 (2004).

[Ghb12]   I. Ghbregziabher, B. Shadwick and D. Umstadter: *Spectral Bandwidth Reduction of Thomson Scattered Light by Pulse Chirping.* (2012), arXiv:1204.1068 [physics.optics].

[Gia99]   L. Giannessi, P. Musumeci and M. Quattromini: *TREDI: fully 3D beam dynamics simulation of RF guns, bendings and FELs*, Nucl. Instrum. Methods Phys. Res., Sect. A **436**, 443 (1999).

[Gie05]   H. Gies and K. Klingmüller: *Pair production in inhomogeneous fields*, Phys. Rev. D **72**, 065001 (2005).

[Gie09]   H. Gies: *Strong laser fields as a probe for fundamental physics*, Eur. Phys. J. D **55**, 311 (2009).

[Gla63a] R. J. Glauber: *Coherent and Incoherent States of the Radiation Field*, Phys. Rev. **131**, 2766 (1963).

[Gla63b] R. J. Glauber: *The Quantum Theory of Optical Coherence*, Phys. Rev. **130**, 2529 (1963).

[Gol64] I. I. Goldman: *Intensity effects in Compton scattering*, Phys. Lett. **8**, 103 (1964).

[Gre85] W. Greiner, B. Müller and J. Rafelski: *Quantum electrodynamics of strong fields*, Springer, 1985.

[Grü07] F. Grüner, S. Becker, U. Schramm, T. Eichner, M. Fuchs, R. Weingartner, D. Habs, J. Meyer-ter-Vehn, M. Geissler, M. Ferrario et al.: *Design considerations for table-top, laser-based VUV and X-ray free electron lasers*, Appl. Phys. B **86**, 431 (2007).

[Hal84] F. Halzen and A. D. Martin: *Quarks & Leptons: An Introductory Course in Modern Particle Physics*, John Wiley & Sons, 1984.

[Han08] D. Hanneke, S. Fogwell and G. Gabrielse: *New Measurement of the Electron Magnetic Moment and the Fine Structure Constant*, Phys. Rev. Lett. **100**, 120801 (2008).

[Har91] A. K. Harding: *The physics of gamma-ray bursts*, Phys. Rep. **206**, 327 (1991).

[Har96a] F. V. Hartemann and A. K. Kerman: *Classical Theory of Nonlinear Compton Scattering*, Phys. Rev. Lett. **76**, 624 (1996).

[Har96b] F. V. Hartemann, A. L. Troha, N. C. Luhmann Jr. and Z. Toffano: *Spectral analysis of the nonlinear relativistic Doppler shift in ultrahigh intensity Compton scattering*, Phys. Rev. E **54**, 2956 (1996).

[Har02] F. V. Hartemann: *High-field electrodynamics*, CRC press, 2002.

[Har05] F. V. Hartemann, D. J. Gibson and A. K. Kerman: *Classical theory of Compton scattering: Assessing the validity of the Dirac-Lorentz equation*, Phys. Rev. E **72**, 026502 (2005).

[Har07] F. V. Hartemann, D. J. Gibson, W. J. Brown, A. Rousse, K. Ta Phuoc, V. Mallka, J. Faure and A. Pukhov: *Compton scattering x-ray sources driven by laser wakefield acceleration*, Phys. Rev. ST Accel. Beams **10**, 011301 (2007).

[Har08] F. V. Hartemann, C. W. Siders and C. P. J. Barty: *Compton Scattering in Ignited Thermonuclear Plasmas*, Phys. Rev. Lett. **100**, 125001 (2008).

[Har09] C. Harvey, T. Heinzl and A. Ilderton: *Signatures of High-Intensity Compton Scattering*, Phys. Rev. A **79**, 063407 (2009).

[Har10] F. V. Hartemann, F. Albert, C. W. Siders and C. P. J. Barty: *Low-Intensity Nonlinear Sprectral Effects in Compton Scattering*, Phys. Rev. Lett. **105**, 130801 (2010).

[Har11a] C. Harvey, T. Heinzl, N. Iji and K. Langfeld: *Covariant Worldline Numerics for Charge Motion with Radiation Reaction*, Phys. Rev. D **83**, 076013 (2011).

[Har11b] C. HARVEY, T. HEINZL AND M. MARKLUND: *Symmetry breaking from radiation reaction in ultra-intense laser fields*, Phys. Rev. D **84**, 116005 (2011).

[Har12] C. HARVEY, T. HEINZL, A. ILDERTON AND M. MARKLUND: *The intensity dependent mass shift: existence, universality and detection* (2012), arXiv: 1203.6077 [hep-ph].

[Heb08] F. HEBENSTREIT, R. ALKOFER AND H. GIES: *Pair production beyond the Schwinger formula in time-dependent electric fields*, Phys. Rev. D **78**, 061701 (2008).

[Heb11a] F. HEBENSTREIT, A. ILDERTON AND M. MARKLUND: *Pair production: The view from the lightfront*, Phys. Rev. D **84**, 125022 (2011).

[Heb11b] F. HEBENSTREIT, A. ILDERTON, M. MARKLUND AND J. ZAMANIAN: *Strong field effects in laser pulses: The Wigner formalism*, Phys. Rev. D **83**, 065007 (2011).

[Heg06] B. M. HEGELICH, B. J. ALBRIGHT, J. COBBLE, K. FLIPPO, S. LETZRING, M. PAFFETT, H. RUHL, J. SCHREIBER, R. K. SCHULZE AND J. C. FERNÁNDEZ: *Laser acceleration of quasi-monoenergetic MeV ion beams*, Nature **439**, 441 (2006).

[Hei34] W. HEITLER AND L. NORDHEIM: *Über die Wahrscheinlichkeit von Mehrfach-prozessen bei sehr hohen Energieen*, Physica **1**, 1059 (1934).

[Hei36] W. HEISENBERG AND H. EULER: *Folgerungen aus der Diracschen Theorie des Positrons*, Z. Phys. **98**, 714 (1936).

[Hei41] W. HEITLER: *The Influence of Radiation Damping on the Scattering of Light and Mesons by Free Particles. I*, Math. Proc. Cambridge Philos. Soc. **37**, 291 (1941).

[Hei01] T. HEINZL: *Light-Cone Quantization: Foundations and Applications*, in H. LATAL AND W. SCHWEIGER (Editors), *Methods of Quantization*, volume 572 of *Lecture Notes in Physics*, page 55, Springer, Berlin, 2001.

[Hei07] T. HEINZL: *Alternative approach to light-front perturbation theory*, Phys. Rev. D **75**, 025013 (2007).

[Hei09a] T. HEINZL: *Exploring high-intensity QED at ELI*, Eur. Phys. J. D **55**, 359 (2009).

[Hei09b] T. HEINZL AND A. ILDERTON: *A Lorentz and gauge invariant measure of laser intensity*, Opt. Commun. **282**, 1879 (2009).

[Hei10a] T. HEINZL, A. ILDERTON AND M. MARKLUND: *Finite size effects in stimulated laser pair production*, Phys. Lett. B **692**, 250 (2010).

[Hei10b] T. HEINZL, D. SEIPT AND B. KÄMPFER: *Beam-shape effects in nonlinear Compton and Thomson scattering*, Phys. Rev. A **81**, 022125 (2010).

[Hei11] T. HEINZL: *Strong-Field QED and High Power Lasers* (2011), arXiv:1111.5192 [hep-ph].

[Her72] J. HERRMANN AND V. C. ZHUKOVSKII: *Compton Scattering and Induced Compton Scattering in a Constant Electromagnetic Field*, Ann. Phys. (Leipzig) **482**, 349 (1972).

[Her79]   H. Herold: *Compton and Thomson scattering in strong magnetic fields*, Phys. Rev. D **19**, 2868 (1979).

[Hew70]   A. Hewish: *Pulsars*, Annu. Rev. Astron. Astr. **8**, 265 (1970).

[HIP]   *HiPER project homepage*, http://www.hiper-laser.org.

[Hu10]   H. Hu, C. Müller and C. H. Keitel: *Complete QED Theory of Multiphoton Trident Pair Production in Strong Laser Fields*, Phys. Rev. Lett. **105**, 080401 (2010).

[Hu11]   H. Hu: *Multi-photon creation and single-photon annihilation of electron-positron pairs*, Ph.D. thesis, University of Heidelberg (2011).

[Ild10]   A. Ilderton, J. Lundin and M. Marklund: *Strong Field, Noncommutative QED*, SIGMA **6**, 41 (2010).

[Ild11a]   A. Ilderton: *Trident pair production in strong laser pulses*, Phys. Rev. Lett. **106**, 020404 (2011).

[Ild11b]   A. Ilderton, P. Johansson and M. Marklund: *Pair annihilation in laser pulses: optical vs. XFEL regimes*, Phys. Rev. A **84** (2011).

[Itz80]   C. Itzykson and J.-B. Zuber: *Quantum Field Theory*, McGraw-Hill, 1980.

[Iva04]   D. Y. Ivanov, G. L. Kotkin and V. G. Serbo: *Complete description of polarization effects in emission of a photon by an electron in the field of a strong laser wave*, Eur. Phys. J. C **36**, 127 (2004).

[Iva05]   D. Y. Ivanov, G. L. Kotkin and V. G. Serbo: *Complete description of polarization effects in $e^+e^-$ pair production by a photon in the field of a strong laser wave*, Eur. Phys. J. C **40**, 27 (2005).

[Jac83]   J. D. Jackson: *Klassische Elektrodynamik*, Walter de Gruyter, Berlin, New York, 1983, 2nd edition.

[Jau76]   J. M. Jauch and F. Rohrlich: *The Theory of Photons and Electrons*, Springer-Verlag, Berlin, Heidelberg, New York, 1976.

[Joh11]   P. Johansson: *Pair annihilation in laser pulses*, Master's thesis, Umeå University (2011).

[Kak93]   M. Kaku: *Quantum Field Theory*, Oxford University Press, 1993.

[Käm75]   B. Kämpfer: *Pulsare und Beeinflussung von Comptonstreuspektren durch Magnetfelder*, Ph.D. thesis, Universität Jena (1975).

[Kam06]   J. Z. Kamiński, K. Krajewska and F. Ehlotzky: *Monte Carlo analysis of electron-positron pair creation by powerful laser-ion impact*, Phys. Rev. A **74**, 033402 (2006).

[Kar12]   F. Karbstein, L. Roessler, B. Döbrich and H. Gies: *Optical probes of the quantum vacuum: The photon polarization tensor in external fields*, Int. J. Mod. Phys. Conf. Ser. **14**, 403 (2012).

[Kib65]   T. W. B. Kibble: *Frequency Shift in High-Intensity Compton Scattering*, Phys. Rev. **138**, B740 (1965).

[Kib68]    T. W. B. Kibble: *Coherent Soft-Photon States and Infrared Divergences. I. Classical Currents*, J. Math. Phys. **9**, 315 (1968).

[Kib75]    T. W. B. Kibble, A. Salam and J. Strathdee: *Intensity-dependent mass shift and symmetry breaking*, Nucl. Phys. B **96**, 255 (1975).

[Kin06]    T. Kinoshita and M. Nio: *Improved $\alpha^4$ term of the electron anomalous magnetic moment*, Phys. Rev. D **73**, 013003 (2006).

[Kin10a]   B. King, A. Di Piazza and C. H. Keitel: *Double-slit vacuum polarization effects in ultraintense laser fields*, Phys. Rev. A **82**, 032114 (2010).

[Kin10b]   B. King, A. Di Piazza and C. H. Keitel: *A matterless double slit*, Nature Photon. **4**, 92 (2010).

[Kin12]    B. King, H. Gies and A. Di Piazza: *Thermally-induced vacuum instability in a single plane wave* (2012), arXiv:1204.2442v1 [hep-ph].

[Koc04]    K. Koch: *Vakuumfluktuationen und nichtlineare Elektrodynamik* (2004), Diplomarbeit, Friedrich-Schiller-Universität Jena.

[Kog70]    J. B. Kogut and D. E. Soper: *Quantum Electrodynamics in the Infinite-Momentum Frame*, Phys. Rev. D **1**, 2901 (1970).

[Koh12]    M. C. Kohler, T. Pfeifer, K. Z. Hatsagortsyan and C. H. Keitel: *Frontiers of atomic high-harmonic generation* (2012), submitted to Advances In Atomic, Molecular, and Optical Physics, arXiv:1201.5094v1 [physics.atom-ph].

[Kor06]    H. J. Korsch, A. Klumpp and D. Witthaut: *On two-dimensional Bessel functions*, J. Phys. A **39**, 14947 (2006).

[Kor11]    A. V. Korzhimanov, A. A. Gonoskov, E. A. Khazanov and A. M. Sergeev: *Horizons of petawatt laser technology*, Phys. Usp. **54**, 9 (2011).

[Kou98]    C. Kouveliotou, S. Dieters, T. Strohmayer, J. van Paradijs, G. J. Fishman, C. A. Meegan, K. Hurley, J. Kommers, I. Smith, D. Frail and T. Murakami: *An X-ray pulsar with a superstrong magnetic field in the soft $\gamma$-ray repeater SGR1806–20*, Nature **393**, 235 (1998).

[Koz11]    V. V. Kozlov, N. N. Rosanov, C. D. Angelis and S. Wabnitz: *Generation of unipolar pulses from nonunipolar optical pulses in a nonlinear medium*, Phys. Rev. A **84**, 023818 (2011).

[Kra04]    G. A. Krafft: *Spectral Distributions of Thomson-Scattered Photons from High-Intensity Pulsed Lasers*, Phys. Rev. Lett. **92**, 204802 (2004).

[Kra05]    G. A. Krafft, A. Doyuran and J. B. Rosenzweig: *Pulsed-laser nonlinear Thomson scattering for general scattering geometries*, Phys. Rev. E **72**, 056502 (2005).

[Kra10]    K. Krajewska and J. Z. Kamiński: *Recoil effects in multiphoton electron-positron pair creation*, Phys. Rev. A **82**, 013420 (2010).

[Kra12]    K. Krajewska and J. Z. Kamiński: *Compton Process in Intense Short Laser Pulses*, Phys. Rev. A **85**, 062102 (2012).

[Kry94]   P. Kryukov, A. Nikishov, V. Ritus and V. Sergienko: *Feasibility of experimental investigation of nonlinear QED processes — photon emission by electrons and pair creation by photons in strong laser field*, J. Russ. Laser Res. **15**, 351 (1994).

[Kuc07]   M. Y. Kuchiev: *Production of High-Energy Particles in Laser and Coulomb Fields and the $e^+e^-$ Antenna*, Phys. Rev. Lett. **99**, 130404 (2007).

[Lab09]   L. Labzowsky, D. Solovyev and G. Plunien: *Two-photon decay of excited levels in hydrogen: The ambiguity of the separation of cascades and pure two-photon emission*, Phys. Rev. A **80**, 062514 (2009).

[Lan97]   G. Landi: *An Introduction to Noncommutative Spaces and their Geometry*, volume 51 of *Lecture Notes in Physics monographs*, Springer-Verlag, Berlin, 1997.

[Lau03]   Y. Y. Lau, F. He, D. Umstadter and R. Kowalczyk: *Nonlinear Thomson scattering: A tutorial*, Phys. Plasmas **10**, 2155 (2003).

[Led03]   K. W. D. Ledingham, P. McKenna and R. P. Singhal: *Applications for Nuclear Phenomena Generated by Ultra-Intense Lasers*, Science **300**, 1107 (2003).

[Led10]   K. W. D. Ledingham and W. Galster: *Laser-driven particle and photon beams and some applications*, New J. Phys. **12**, 045005 (2010).

[Lee06]   W. P. Leemans, B. Nagler, A. J. Gonsalves, C. Tóth, K. Nakamura, C. G. R. Geddes, E. Esarey, C. B. Schroeder and S. M. Hooker: *GeV electron beams from a centimetre-scale accelerator.*, Nature Phys. **2**, 696 (2006).

[Leu11]   C. Leubner: *Uniform asymptotic expansion of a class of generalized Bessel functions occurring in the study of fundamental scattering processes in intense laser fields*, Phys. Rev. A **23**, 2877 (2011).

[Lig81]   A. P. Lightman: *Double Compton emission in radiation dominated thermal plasmas*, Astrophys. J. **244**, 392 (1981).

[Löt07]   E. Lötstedt, U. D. Jentschura and C. H. Keitel: *Evaluation of Laser-Assisted Bremsstrahlung with Dirac-Volkov Propagators*, Phys. Rev. Lett. **98**, 043002 (2007).

[Löt08]   E. Lötstedt: *Laser-assisted second-order relativistic QED processes: Bremsstrahlung and pair creation modified by a strong electromagnetic wave field*, Ph.D. thesis, University of Heidelberg (2008).

[Löt09a]  E. Lötstedt and U. D. Jentschura: *Correlated two-photon emission by transitions of Dirac-Volkov states in intense laser fields: QED predictions*, Phys. Rev. A **80**, 053419 (2009).

[Löt09b]  E. Lötstedt and U. D. Jentschura: *Nonperturbative Treatment of Double Compton Backscattering in Intense Laser Fields*, Phys. Rev. Lett. **103**, 110404 (2009).

[Löt09c]  E. Lötstedt and U. D. Jentschura: *Recursive algorithm for arrays of generalized Bessel functions: Numerical access to Dirac-Volkov solutions*, Phys. Rev. E **79**, 026707 (2009).

[Löt12]   E. Lötstedt and U. D. Jentschura: *Triple Compton Effect: A Photon Splitting into Three upon Collision with a Free Electron*, Phys. Rev. Lett. **108**, 233201 (2012).

[Mac09]   K. F. MACKENROTH: *Multiphoton Compton scattering in ultra-short laser pulses* (2009), Diplomarbeit.

[Mac10]   F. MACKENROTH, A. DI PIAZZA AND C. H. KEITEL: *Determining the Carrier-Envelope Phase of Intense Few-Cycle Laser Pulses*, Phys. Rev. Lett. **105**, 063903 (2010).

[Mac11]   F. MACKENROTH AND A. DI PIAZZA: *Nonlinear Compton scattering in ultra-short laser pulses*, Phys. Rev. A **83**, 032106 (2011).

[Mac12]   F. MACKENROTH AND A. DI PIAZZA: *Nonlinear double Compton scattering in the full quantum regime* (2012), arXiv:1208.3424v1 [hep-ph].

[Mai60]   T. H. MAIMAN: *Stimulated Optical Radiation in Ruby*, Nature **187**, 493 (1960).

[Mai86]   L. MAIANI, R. PETRONZIO AND E. ZAVATTINI: *Effects of nearly massless, spin-zero particles on light propagation in a magnetic field*, Phys. Lett. B **175**, 359 (1986).

[Man52]   F. MANDL AND T. H. R. SKYRME: *The Theory of the Double Compton Effect*, Proc. R. Soc. London, Ser. A **215**, 497 (1952).

[Man95]   L. MANDEL AND E. WOLF: *Optical coherence and quantum optics*, Cambridge university press, 1995.

[Mar06]   M. MARKLUND AND P. K. SHUKLA: *Nonlinear collective effects in photon-photon and photon-plasma interactions*, Rev. Mod. Phys. **78**, 591 (2006).

[Mar09]   M. MARKLUND AND J. LUNDIN: *Quantum vacuum experiments using high intensity lasers*, Eur. Phys. J. D **55**, 319 (2009).

[McD86]   K. T. MCDONALD: *PROPOSAL FOR EXPERIMENTAL STUDIES OF NON-LINEAR QUANTUM ELECTRODYNAMICS* (1986), preprint DOE/ER/3072-38, www.hep.princeton.edu/~mcdonald/e144/prop.pdf.

[McD97]   K. T. MCDONALD: *A Relativistic Electron Can't Extract Net Energy from a 'Long' Laser Pulse* (1997), www.hep.princeton.edu/~mcdonald/accel/gaussian2.pdf.

[Mer08]   S. MEREGHETTI: *The strongest cosmic magnets: soft gamma-ray repeaters and anomalous X-ray pulsars*, Astron. Astrophys. Rev. **15**, 225 (2008).

[Meu11]   S. MEUREN AND A. DI PIAZZA: *Quantum electron self-interaction in a strong laser field*, Phys. Rev. Lett. **107**, 260401 (2011), arXiv:1107.4531 [hep-ph].

[Mey71]   J. W. MEYER: *Covariant Classical Motion of Electron in a Laser Beam*, Phys. Rev. D **3**, 621 (1971).

[Mil06a]  D. B. MILOŠEVIĆ, G. G. PAULUS, D. BAUER AND W. BECKER: *Above-threshold ionization by few-cycle pulses*, J. Phys. B **39**, R203 (2006).

[Mil06b]  A. I. MILSTEIN, C. MÜLLER, K. Z. HATSAGORTSYAN, U. D. JENTSCHURA AND C. H. KEITEL: *Polarization-operator approach to electron-positron pair production in combined laser and Coulomb fields*, Phys. Rev. A **73**, 062106 (2006).

[Mit75]   H. MITTER: *Quantum Electrodynamics in Laser Fields*, Acta Physica Austriaca, Suppl. XIV pages 397–468 (1975).

[Mit87]    M. H. Mittleman: *Multiphoton pair creation*, Phys. Rev. A **35**, 4624 (1987).

[Mit98]    H. Mitter: *unpublished lecture notes on electrodynamics (in German)* (1998), available at http://physik.uni-graz.at/∼hem/.

[Moc09]    G. R. Mocken, Y. I. Salamin and C. H. Keitel: *Relativistic Quantum Dynamics in Intense Laser Fields*, in K. Yamanouchi, A. Becker, R. Li and S. L. Chin (Editors), *Progress in Ultrafast Intense Laser Science*, volume IV, chapter 15, Springer, 2009.

[Moh12]    P. J. Mohr, B. N. Taylor and D. B. Newell: *CODATA Recommended Values of the Fundamental Physical Constants: 2010* (2012), arXiv:1203.5425v1 [physics.atom-ph].

[Mor75]    D. A. Morozov and V. I. Ritus: *Elastic electron scattering in an intense field and two-photon emission*, Nucl. Phys. B **86**, 309 (1975).

[Mou06]    G. A. Mourou, T. Tajima and S. V. Bulanov: *Optics in the relativistic regime*, Rev. Mod. Phys. **78**, 309 (2006).

[MP09]     G. Moortgat-Pick: *The Furry Picure*, J. Phys.: Conf. Series **198**, 012002 (2009).

[Mül03]    C. Müller, A. B. Voitkiv and N. Grün: *Differential rates for multiphoton pair production by an ultrarelativistic nucleus colliding with an intense laser beam*, Phys. Rev. A **67**, 063407 (2003).

[Mut87]    T. Muta: *Foundations Of Quantum Chromodynamics*, World Scientific Publishing, 1987.

[Nak04]    S. Nakai and K. Mima: *Laser driven inertial fusion energy: present and prospective*, Rep. Prog. Phys. **67**, 321 (2004).

[Nak10]    K. Nakamura et al.: *2011 Review of Particle Physics*, J. Phys. G **37**, 075021 (2010).

[Nar65]    N. B. Narozhnyi, A. I. Nikishov and V. I. Ritus: *Quantum processes in the field of a circularly polarized electromagnetic wave*, Sov. Phys. J. Exp. Theor. Phys. **20**, 622 (1965).

[Nar80]    N. B. Narozhny: *Expansion parameter of perturbation theory in intense-field quantum electrodynamics*, Phys. Rev. D **21**, 1176 (1980).

[Nar96a]   N. B. Narozhnyi and M. S. Fofanov: *Creation of a Pair by a Photon Colliding with a Short Focused Laser Pulse*, Laser Phys. **7**, 141 (1996).

[Nar96b]   N. B. Narozhnyǐ and M. S. Fofanov: *Photon emission by an electron in a collision with a short focused laser pulse*, J. Exp. Theor. Phys. **83**, 14 (1996).

[Nar00]    N. B. Narozhny and M. Fofanov: *Scattering of relativistic electrons by a focused laser pulse*, J. Exp. Theor. Phys. **90**, 753 (2000).

[Nar05]    N. B. Narozhny: *A Relativistic Electron in a Focused Laser Pulse*, Laser Phys. **15**, 1458 (2005).

[Ner11]    E. N. Nerush, I. Y. Kostyukov, A. M. Fedotov, N. B. Narozhny, N. V. Elkina and H. Ruhl: *Laser Field Absorption in Self-Generated Electron-Positron Pair Plasma*, Phys. Rev. Lett. **106**, 035001 (2011).

[Nev71a]  R. A. NEVILLE AND F. ROHRLICH: *Quantum Electrodynamics on Null Planes and Applications to Lasers*, Phys. Rev. D **3**, 1692 (1971).

[Nev71b]  R. A. NEVILLE AND F. ROHRLICH: *Quantum Field Theory off Null Planes*, Nuovo Cimento A **1**, 625 (1971).

[Nev76]  R. A. NEVILLE: *Null-plane quantum electrodynamics in an external radiation field*, Can. J. Phys. **54**, 2246 (1976).

[NIF]  *National Ignition Facility project homepge*, http://lasers.llnl.gov.

[Nik64a]  A. I. NIKISHOV AND V. I. RITUS: *Quantum processes in the field of a plane electromagnetic wave and in a constant field*, Sov. Phys. J. Exp. Theor. Phys. **19**, 1191 (1964).

[Nik64b]  A. I. NIKISHOV AND V. I. RITUS: *Quantum processes in the field of a plane electromagnetic wave and in a constant field. I*, Sov. Phys. J. Exp. Theor. Phys. **19**, 529 (1964).

[Nik65]  A. I. NIKISHOV AND V. I. RITUS: *Nonlinear effects in Compton scattering and pair production owing to absorption of several photons*, Sov. Phys. J. Exp. Theor. Phys. **20**, 757 (1965).

[Nou11]  T. NOUSCH: *Multiphotonen Paarerzeugung in starken gepulsten Laserfeldern* (2011), Diplomarbeit, Technische Universität Dresden.

[Nou12]  T. NOUSCH, D. SEIPT, B. KÄMPFER AND A. I. TITOV: *Subthreshold pair production in short laser pulses*, Phys. Lett. B **715**, 246 (2012).

[Ole67]  V. P. OLEĬNIK: *Resonance effects in the field of an intense laser beam*, Sov. Phys. J. Exp. Theor. Phys. **25**, 697 (1967).

[Ole68]  V. P. OLEĬNIK: *Resonance effects in the field of an intense laser ray II*, Sov. Phys. J. Exp. Theor. Phys. **26**, 1132 (1968).

[Ost08]  J. OSTERHOFF, A. POPP, Z. MAJOR, B. MARX, T. P. ROWLANDS-REES, M. FUCHS, M. GEISSLER, R. HÖRLEIN, B. HIDDING, S. BECKER, E. A. PERALTA, U. SCHRAMM, F. GRÜNER, D. HABS, F. KRAUSZ, S. M. HOOKER AND S. KARSCH: *Generation of Stable, Low-Divergence Electron Beams by Laser-Wakefield Acceleration in a Steady-State-Flow Gas Cell*, Phys. Rev. Lett. **101**, 085002 (2008).

[Pan02a]  P. PANEK, J. Z. KAMIŃSKI AND F. EHLOTZKY: *Relativistic electron-atom scattering in an extremely powerful laser field: Relevance of spin effects*, Phys. Rev. A **65**, 033408 (2002).

[Pan02b]  P. PANEK, J. Z. KAMIŃSKI AND F. EHLOTZKY: *X-ray generation by Compton scattering of elliptically polarized laser light at relativistic radiation powers*, Opt. Commun. **213** (2002).

[Pan04]  P. PANEK, J. Z. KAMIŃSKI AND F. EHLOTZKY: *Analysis of resonances in Møller scattering in a laser field of relativistic radiation power*, Phys. Rev. A **69**, 013404 (2004).

[Pea08]    J. Peatross, C. Müller, K. Z. Hatsagortsyan and C. H. Keitel: *Photoemission of a Single-Electron Wave Packet in a Strong Laser Field*, Phys. Rev. Lett. **100**, 153601 (2008).

[PEN]    *PEnELOPE homepage*, https://www.hzdr.de/db/Cms?pOid=30472&pNid=2098.

[Per99]    M. D. Perry, D. Pennington, B. C. Stuart, G. Tietbohl, J. A. Britten, C. Brown, S. Herman, B. Golick, M. Kartz, J. Miller, H. T. Powell, M. Vergino and V. Yanovsky: *Petawatt laser pulses*, Opt. Lett. **24**, 160 (1999).

[Pes95]    M. E. Peskin and D. V. Schroeder: *An Introduction to Quantum Field Theory*, Addison-Wesley Publishing Company, 1995.

[PET]    *PETRA III homepage*, http://petra3.desy.de/.

[Pop04]    V. S. Popov: *Tunnel and multiphoton ionization of atoms and ions in a strong laser field (Keldysh theory)*, Phys. Usp. **47**, 855 (2004).

[Puk03]    A. Pukhov: *Strong field interaction of laser radiation*, Rep. Prog. Phys. **66**, 47 (2003).

[Ram71]    M. Ram and P. Y. Wang: *Calculation of the Total Cross Section for Double Compton Scattering*, Phys. Rev. Lett. **26**, 476 (1971).

[REG]    *REGAE homepage*, http://regae.desy.de/.

[Rei62]    H. R. Reiss: *Absorption of Light by Light*, J. Math. Phys. **3**, 59 (1962).

[Rei05]    H. R. Reiss: *Strong-Field Physics Viewed as a Paradigm Shift*, Laser Phys. **15**, 1486 (2005).

[Rid95]    S. K. Ride, E. Esarey and M. Baine: *Thomson scattering of intense lasers from electron beams at arbitrary interaction angles*, Phys. Rev. E **52**, 5425 (1995).

[Rin01]    A. Ringwald: *Pair production from vacuum at the focus of an X-ray free electron laser*, Phys. Lett. B **510**, 107 (2001).

[Rit72]    V. I. Ritus: *Radiative Corrections in Quantum Electrodynamics with Intense Field and Their Analytical Properties*, Annals of Physics **69**, 555 (1972).

[Rit85]    V. I. Ritus: *Quantum effects of the interaction of elementary particles with an intense electromagnetic field*, J. Sov. Laser Res. **6**, 497 (1985).

[Roh73]    F. Rohrlich and J. H. Ten Eyck: *Null plane quantum electrodynamics*, Phys. Lett. B **46**, 102 (1973).

[Rom69]    P. Roman: *Introduction to Quantum Field Theory*, John Wiley & Sons, Inc., New York, 1969.

[Ros96]    S. P. Roshchupkin: *Resonant Effects in Collisions of Relativistic Electrons in the Field of a Light Wave*, Laser Phys. **6**, 837 (1996).

[Ruf09]    M. Ruf, G. R. Mocken, C. Müller, K. Z. Hatsagortsyan and C. H. Keitel: *Pair Production in Laser Fields Oscillating in Space and Time*, Phys. Rev. Lett. **102**, 080402 (2009).

[Ryd94]    L. H. Ryder: *Quantum Field Theory*, Cambridge University Press, 1994.

[Rys57]   I. M. Ryshik and I. S. Gradstein: *Summen-, Produkt- und Integraltafeln*, VEB Deutscher Verlag der Wissenschaften, Berlin, 1957.

[Sal97]   Y. I. Salamin and F. H. M. Faisal: *Ponderomotive scattering of electrons in intense laser fields*, Phys. Rev. A **55**, 3678 (1997).

[Sal02]   Y. I. Salamin and C. H. Keitel: *Electron Acceleration by a Tightly Focused Laser Beam*, Phys. Rev. Lett. **88**, 095005 (2002).

[Sal06]   Y. I. Salamin, S. X. Hu, K. Z. Hatsagortsyan and C. H. Keitel: *Relativistic high-power laser-matter interactions*, Phys. Rep. **427**, 41 (2006).

[San00]   B. S. Sandhu, R. Dewan, M. B. Saddi, B. Singh and B. S. Ghumman: *Experimental study of angular dependence in double photon Compton scattering*, Nucl. Instrum. Methods Phys. Res., Sect. B **168**, 329 (2000).

[Sar70]   E. S. Sarachik and G. T. Schappert: *Classical Theory of the Scattering of Intense Laser Radiation by Free Electrons*, Phys. Rev. D **1**, 2738 (1970).

[Sau31]   F. Sauter: *Über das Verhalten eines Elektrons im homogenen elektrischen Feld nach der relativistischen Theorie Diracs*, Z. Phys. **69**, 742 (1931).

[Sau07]   R. Sauerbrey and J. Hein: *Generation of Ultrahigh Light Intensities and Relativistic Laser-Matter Interaction*, in F. Träger (Editor), *Springer Handbook of Lasers and Optics*, chapter 11.13, pages 827–841, Springer, New York, 2007.

[Sch26]   E. Schrödinger: *Der stetige Übergang von der Mikro- zur Makromechanik*, Naturwissenschaften **14**, 664 (1926).

[Sch51]   J. Schwinger: *On Gauge Invariance and Vacuum Polarization*, Phys. Rev. **82**, 664 (1951).

[Sch68]   E. Schmutzer: *Relativistische Physik*, B. G. Teubner Verlagsgesellschaft, 1968.

[Sch96]   R. W. Schoenlein, W. P. Leemans, A. H. Chin, P. Volfbeyn, T. E. Glover, P. Balling, M. Zolotorev, K.-J. Kim, S. Chattopadhyay and C. V. Shank: *Femtosecond X-ray Pulses at 0.4 Å Generated by 90° Thomson Scattering: A Tool for Probing the Structural Dynamics of Materials*, Science **274**, 236 (1996).

[Sch06a]  R. Schützhold, G. Schaller and D. Habs: *Signatures of the Unruh Effect from Electrons Accelerated by Ultrastrong Laser Fields*, Phys. Rev. Lett. **97**, 121302 (2006).

[Sch06b]  H. Schwoerer, B. Liesfeld, H.-P. Schlenvoigt, K.-U. Amthor and R. Sauerbrey: *Thomson-Backscattered X Rays From Laser-Accelerated Electrons*, Phys. Rev. Lett. **96**, 014802 (2006).

[Sch06c]  H. Schwoerer, S. Pfotenhauer, O. Jäckel, K.-U. Amthor, B. Liesfeld, W. Ziegler, R. Sauerbrey, K. W. D. Ledingham and T. Esirkepov: *Laser-plasma acceleration of quasi-monoenergetic protons from microstructured targets*, Nature **439**, 445 (2006).

[Sch07]   S. Schnez, E. Lötstedt, U. D. Jentschura and C. H. Keitel: *Laser-assisted bremsstrahlung for circular and linear polarization*, Phys. Rev. A **75**, 053412 (2007).

[Sch08]   R. Schützhold, G. Schaller and D. Habs: *Tabletop Creation of Entangled Multi-keV Photon Pairs and the Unruh Effect*, Phys. Rev. Lett. **100**, 091301 (2008).

[Sch09]   R. Schützhold and C. Maia: *Quantum radiation by electrons in lasers and the Unruh effect*, Eur. Phys. J. D **55**, 375 (2009).

[Sch12]   B. Schnizer: *Analytische Methoden der Theoretischen Physik, Kapitel 13: Ergänzungen zur Funktionentheorie* (2012), unpublished lecture notes, available at http://itp.tugraz.at/∼schnizer/AnalyticalMethods/AnMe13.pdf.

[Sei11a]  D. Seipt and B. Kämpfer: *Non-linear Compton scattering of ultrahigh-intensity laser pulses* (2011), arXiv:1111.0188v1 [hep-ph].

[Sei11b]  D. Seipt and B. Kämpfer: *Non-Linear Compton Scattering of Ultrashort and Intense Laser Pulses*, Phys. Rev. A **83**, 022101 (2011).

[Sei11c]  D. Seipt and B. Kämpfer: *Scaling law for the photon spectral density in the nonlinear Thomson-Compton scattering*, Phys. Rev. ST Accel. Beams **14**, 040704 (2011).

[Sei12]   D. Seipt and B. Kämpfer: *Two-photon Compton process in pulsed intense laser fields*, Phys. Rev. D **85**, 101701 (2012).

[Sek88]   G. S. Sekhon, B. S. Sandhu, B. Singh and B. S. Ghumman: *Double-Photon Compton Scattering of 662 keV Gamma-Rays*, Nuovo Cimento A **100**, 789 (1988).

[Sen52]   N. D. Sengupta: *On the Scattering of Electromagnetic Waves by A Free Electron - II Wave Mechanical Theory*, Bull. Math. Soc. (Calcutta) **44**, 175 (1952).

[Shi91a]  G. V. Shishkin: *Some generalizations of Volkov's problem*, Nuovo Cimento B **106**, 1137 (1991).

[Shi91b]  G. V. Shishkin and Y. M. Ali: *Exact description of a Dirac particle in the presence of wave fields (generalization of the Volkov problem)*, Sov. J. Nucl. Phys. **53**, 536 (1991).

[Sok76]   A. A. Sokolov, A. M. Voloshchenko, V. C. Zhukovskii and Y. G. Pavlenko: *Two-photon synchrotron emission*, Russ. Phys. J. **19**, 1139 (1976).

[Sok10]   I. V. Sokolov, N. M. Naumova, J. A. Nees and G. A. Mourou: *Pair Creation in QED-Strong Pulsed Laser Fields Interacting with Electron Beams*, Phys. Rev. Lett. **105**, 195005 (2010).

[Som78]   A. Sommerfeld: *Atombau und Spektrallinien – II. Band*, Verlag Harri Deutsch, 1978, 4th edition, chapter IV, § 11, p. 329.

[Spo00]   H. Spohn: *The critical manifold of the Lorentz-Dirac equation*, Europhys. Lett. **50**, 287 (2000).

[SPR]     *SPring-8 homepage,*, http://www.spring8.or.jp/en.

[SR00]    J. San Roman, L. Roso and H. R. Reiss: *Evolution of a relativistic wavepacket describing a free electron in a very intense laser field*, J. Phys. B **33**, 1869 (2000).

[Str85]   D. Strickland and G. Mourou: *Compression of amplified chirped optical pulses*, Opt. Commun. **56**, 219 (1985).

[Szy97]  C. Szymanowski, V. Véniard, R. Taïeb and A. Maquet: *Mott scattering in strong laser fields*, Phys. Rev. A **56**, 3846 (1997).

[Tam11]  M. Tamburini, F. Pegoraro, A. Di Piazza, C. H. Keitel, T. V. Liseykina and A. Macchi: *Radiation reaction effects on electron nonlinear dynamics and ion acceleration in laser–solid interaction*, Nucl. Instrum. Methods Phys. Res., Sect. A **653**, 181 (2011).

[TE74]  J. H. Ten Eyck and F. Rohrlich: *Equivalence of null-plane and conventional quantum electrodynamics*, Phys. Rev. D **9**, 2237 (1974).

[Thi09]  P. G. Thirolf, D. Habs, A. Henig, D. Jung, D. Kiefer, C. Lang, J. Schreiber, C. Maia, G. Schaller, R. Schützhold and T. Tajima: *Signatures of the Unruh effect via high-power, short-pulse lasers*, Eur. Phys. J. D **55**, 379 (2009).

[Tit11]  A. I. Titov, B. Kämpfer, H. Takabe and A. Hosaka: *Neutrino pair emission off electrons in a strong electromagnetic wave field*, Phys. Rev. D **83**, 053008 (2011).

[Tit12]  A. I. Titov, H. Takabe, B. Kämpfer and A. Hosaka: *Enhanced Subthreshold $e^+e^-$ Production in Short Laser Pulses*, Phys. Rev. Lett. **108**, 240406 (2012).

[Tom05]  P. Tomassini, A. Giulietti, D. Giulietti and L. A. Gizzi: *Thomson backscattering X-rays from ultra-relativistic electron bunches and temporally shaped laser pulses*, Appl. Phys. B **80**, 419 (2005).

[Trä07]  F. Träger (Editor): *Springer Handbook of Lasers and Optics*, Springer, 2007.

[Unr76]  W. G. Unruh: *Notes on black-hole evaporation*, Phys. Rev. D **14**, 870 (1976).

[Unr84]  W. G. Unruh and R. M. Wald: *What happens when an accelerating observer detects a Rindler particle*, Phys. Rev. D **29**, 1047 (1984).

[Vai92]  A. Vaidya, C. Farina and M. Hott: *Furry's Picture in the Path Integral Framework*, Nuovo Cimento A **105**, 925 (1992).

[Vol35]  D. M. Volkov: *Über eine Klasse von Lösungen der Diracschen Gleichung*, Z. Phys. **94**, 250 (1935).

[Wat22]  G. N. Watson: *A treatise on the theory of Bessel functions*, Cambridge University Press, 1922.

[Wei95]  S. Weinberg: *The Quantum Theory of Fields*, Cambridge University Press, 1995.

[WFS]  *The Wolfram Function Site*, http://functions.wolfram.com.

[Wil41]  A. H. Wilson: *The Quantum Theory of Radiation Damping*, Math. Proc. Cambridge Philos. Soc. **37**, 301 (1941).

[XFE]  *The European XFEL project*, http://www.xfel.eu/.

[Yan73a]  T.-M. Yan: *Quantum Field Theories in the Infinite-Momentum Frame III. Quantization of Coupled Spin-One Fields*, Phys. Rev. D **7**, 1760 (1973).

[Yan73b]  T.-M. Yan: *Quantum Field Theories in the Infinite-Momentum Frame. IV. Scattering Matrix of Vector and Dirac Fields and Perturbation Theory*, Phys. Rev. D **7**, 1780 (1973).

[Yan08]  V. Yanovsky, V. Chvykov, G. Kalinchenko, P. Rousseau, T. Planchon, T. Matsuoka, A. Maksimchuk, J. Nees, G. Cheriaux, G. Mourou and K. Krushelnick: *Ultra-high intensity- 300-TW laser at 0.1 Hz repetition rate*, Opt. Express **16**, 2109 (2008).

[Yen61]  D. R. Yennie, S. C. Frautschi and H. Suura: *The infrared divergence phenomena and high-energy processes*, Annals of Physics **13**, 379 (1961).

[You03]  L. M. Young and J. Billen: *The Particle Tracking Code PARMELA*, in *Proceedings of the 2003 IEEE Particle Accelerator Conference (PAC 03)*, page 3521, 2003.

[Zak05]  S. Zakowicz: *Square-integrable wave packets from the Volkov solutions*, J. Math. Phys. **46**, 032304 (2005).

[Zel67]  Y. B. Zel'dovich: *The Quasienergy of a Quantum-Mechanical System Subjected to a Periodic Action*, Sov. Phys. J. Exp. Theor. Phys. **24**, 1006 (1967).

[Zhi02]  A. Zhidkov, J. Koga, A. Sasaki and M. Uesaka: *Radiation Damping Effects on the Interaction of Ultraintense Laser Pulses with an Overdense Plasma*, Phys. Rev. Lett. **88**, 185002 (2002).

# Acknowledgement

# Erklärung

Hiermit versichere ich, dass ich die vorliegende Arbeit ohne unzulässige Hilfe Dritter und ohne Benutzung anderer als der angegebenen Hilfsmittel angefertigt habe; die aus fremden Quellen direkt oder indirekt übernommenen Gedanken sind als solche kenntlich gemacht. Die Arbeit wurde bisher weder im Inland noch im Ausland in gleicher oder ähnlicher Form einer anderen Prüfungsbehörde vorgelegt.

Diese Dissertation wurde am Helmholtz-Zentrum Dresden-Rossendorf e.V. unter der wissenschaftlichen Betreuung von Herrn Prof. Dr. Burkhard Kämpfer angefertigt. Ich habe bisher an keiner Institution, weder im Inland noch im Ausland, einen Antrag auf die Eröffnung eines Promotionsverfahrens gestellt. Ich erkläre ferner, dass ich die Promotionsordnung der Fakultät Mathematik und Naturwissenschaften der Technischen Universität Dresden vom 23. Februar 2011 anerkenne.

Daniel Seipt
Dresden, September 2012